DESIGN, SYNTHESIS AND APPLICATION OF VISIBLE AND NEAR INFRARED LUMINESCENT LANTHANIDE COMPLEXES: FROM SMALL MOLECULES TO MACROMOLECULES

by

Hyounsoo Uh

B.S., Yonsei University, 1995

M.S., Yonsei University, 2001

Submitted to the Graduate Faculty of

The Dietrich School of Arts & Sciences in partial fulfillment

of the requirements for the degree of

Doctor of Philosophy

University of Pittsburgh

2012

UNIVERSITY OF PITTSBURGH

THE DIETRICH SCHOOL OF ARTS AND SCIENCES

This dissertation was presented

by

Hyounsoo Uh

It was defended on

August 7th, 2012

and approved by

Toby Chapman, PhD, Department of Chemistry, The Dietrich School of Arts and Sciences

Nathaniel Rosi, PhD, Department of Chemistry, The Dietrich School of Arts and Sciences

Catalina Achim, PhD, Departmet of Chemistry, Carnegie Mellon University

Dissertation Advisor: Stéphane Petoud, PhD, Department of Chemistry, The Dietrich School

of Arts and Sciences

DESIGN, SYNTHESIS AND APPLICATION OF VISIBLE AND NEAR INFRARED LUMINESCENT LANTHANIDE COMPLEXES: FROM SMALL MOLECULES TO MACROMOLECULES

Hyounsoo Uh, PhD

University of Pittsburgh, 2012

Luminescent lanthanide complexes have great potential for practical applications such as fluoroimmunoassay, polymer-based optical signal amplifiers, active materials in lasers and bio-imaging. Interest in the lanthanide cations as luminescent probes stems from their unique photophysical properties such as sharp emission bands, photostability and long luminescence lifetimes. In order to generate a sufficient number of photons allowing sensitive detection, lanthanide cations must be sensitized with suitable antennae that possess the appropriate electronic structure and that can sufficiently protect the cation from high energy vibrations to prevent the non-radiative deactivation of the lanthanide luminescence. In this thesis, it has been demonstrated that a series of salophen derivatives can be used as an efficient sensitizer for near-infrared emitting lanthanide cations, and derivatives of naphthalimide-attached polyamidoamine (PAMAM) dendrimers can be used as suitable ligands for visible and near infrared emitting lanthanide cations. These systems fulfill the requirements for lanthanide luminescence by forming stable coordination with lanthanide cations, protecting lanthanide cations from non-radiative deactivation and having suitable energy levels for efficient energy transfer to specific lanthanide cations. By introducing functional groups on the surface of dendrimer complex, the physical and photophysical properties of the complex can be controlled. It has been demonstrated that the versatility of dendrimer-lanthanide complexes as backbones for a broad variety of applications.

TABLE OF CONTENTS

LIST OF TABLES

LIST OF FIGURES

xiii

xviii

injection of CC531 tumor cells. No dendrimer was infused into this liver. The second image shows the absence of luminescence in the nodules. (b) Arrows show metastatic lesions in another liver of a rat from a splenic injection of CC531 tumor cells. The liver was infused with Eu-G3P4A18N (300 µL of a 60 µM solution in 10%DMSO/H$_2$O). Luminescence image were taken with a CCD camera (excitation light of 450 nm and emission filter of 610 nm with a 30 nm bandpass filter). 104

Figure 3.17. Gross and luminescent photographs of tumors in the livers of rats with analysis of the tumor luminescence. Gross (top row) and luminescent (bottom row) images of the livers containing tumors (arrows) that were implanted 20 – 30 days prior to infusion and excised at 0 h, 4 h, 24 h and 72 h time points after hepatic infusion with Eu-G3P4A18N. Average signals obtained from the tumors were compared to that of tissue autofluorescence and displayed in the resulting graph. Asterisks represent specular reflection. 105

Figure 3.18. *In vivo* colorectal hepatic tumor localization after the infusion of Eu-G3P4A18N and histological imaging using confocal and multi-photon scanning microscopy. (left) White light photograph of an in vivo rat liver containing a tumor; Luminescent images of the abdominal cavity of the rat before (center) and after (right) Eu-G3P4A18N infusion (excitation 450 nm and emission filter of 610 nm with a 30 nm bandpass). 106

Figure 3.19. (a) 20x confocal microscopic image of a section of liver without the tumor after Eu-G3P4A18N infusion, no luminescence of the dendrimer is seen. The excitation wavelength was 488 nm and emission wavelength was 567 nm. Vessels are labeled with CD-31 (red), nuclei of hepatocytes with dapi (blue) and dendrimer (green); (b) Eu-G3P4A18N can be seen in green (arrows) with the 40x magnification of a confocal microscopic image of tumor in the liver after infusion. The same colored labels are used; (c) 25x magnification of a tumor section in a rat liver

ACKNOWLEDGEMENT

I would like to express my gratitude to my research advisor, Prof. Stéphane Petoud, for his guidance, support and patience throughout the years. It has been a great pleasure for me to work under his supervision. I would also like to thank my thesis committee, Prof. Toby Chapman, Prof. Nathaniel Rosi and Prof. Catalina Achim, for all of their time and helpful suggestions.

I am grateful to the excellent members of Petoud group, for their support and help – Paul Badger, Jason Cross, Grzegorz Filipczyk, Demetra Chengelis Czegan, Jian Zhang, Adrienne Yingling Oxley, Samuel Oxley, Chad Shade, Kristy Gogick, Lijuan Su, Patrick Calinao, Anthony Otero, Zachary Thompson and Alexandra Foucault.

I still remember the great German friends who spent memorable time together – Sebastian Blanck, Florian Wallerstein, Benedikt Huber, Matthias Bischof and Daniela Stöckel.

I would like to thank to my collaborators who were essential to complete this work – Douglas Kauffman, Alexander Star, Ruth Modzelewski, Marco Alcala, Charles Brown, Per Basse, Yong Lee, Anna Powolny, Silvia Stan, Shivendra Singh, Claudette St.Croix, Simon Watkins, Adam Meier, Timothy Strein and Shu Ying Kwan.

I also appreciate the staff of the chemistry department office, machine shop, electronics shop, glass shop, NMR, MS, X-ray facility and stockroom for their help.

I must thank my dear parents, sister and brother. They have been always there to support me. Many thanks to my son, Subin, for always making me smile. Finally, the biggest thanks to my wife, Eun Shin, for her sacrifice, support, encouragement and endless love.

1.0   INTRODUCTION TO LUMINESCENT LANTHANIDE COMPLEXES

1.1   LANTHANIDE LUMINESCENCE

Lanthanides (Ln) are the elements located in the first row of the *f*-block of the periodic table, ranging from cerium (Z = 58) to lutetium (Z = 71). The lanthanides are usually present as cations with (+3) charge. Though f orbitals are higher in energy than 5*s* and 5*p* orbitals, they are spatially shielded by the outer 5*s* and 5*p* orbitals. This special electronic configuration gives them unique photophysical properties.[1] The *f*→*f* transitions are Laporte or parity forbidden, which leads to low molar absorption coefficients (in the order of 10 cm^{-1}mol^{-1}) and long luminescence lifetimes up to several ms. Unlike the *d* block elements, the 4*f* orbitals of the lanthanides are almost not involved in bonding since they are shielded by the 5*s* and 5*p* orbitals. Thus the emission bands resulting from lanthanide cations appear as relatively sharp atom-like bands located at fixed wavelengths. The energy levels of the Ln^{3+} ions are shown in Figure 1.1.

Luminescent lanthanides can have emission bands ranging from UV to NIR regions, controlled by the nature of lanthanide cations. As shown in Figure 1.2, Nd^{3+}, Er^{3+}, Ho^{3+}, Tm^{3+} and Yb^{3+} have NIR emission, while Tb^{3+} and Dy^{3+} have visible emission. The emission bands from Sm^{3+} and Eu^{3+} are located in both of visible and NIR regions. Since interactions between lanthanide cations and ligands are predominately electrostatic,[2, 3] the emission of lanthanide complexes appear as atom-like, sharp emission bands,[4, 5] and the wavelength position of these

bands do not vary significantly with change of ligands or experimental condition such as temperature, pressure, pH or biological environment. The bandwidths are significantly narrower than those of organic fluorophores[6] and luminescent semiconductor nanocrystals (quantum dots)[7-10] and carbon nanotubes.[11, 12] As these emission bands do not overlap significantly, it is possible to monitor the emission of several different lanthanide cations during the same experiment for multiplex detection.

Since the energy is absorbed by a chromophore (or "antenna", see below) and the emission originates from the lanthanide cations, there is a large energy gap between the absorption and emission bands of lanthanide complexes, minimizing luminescence re-absorption and corresponding quantification artifacts. Due to their electronic properties, luminescence signals of the lanthanide cations can be spectrally discriminated from other signals, allowing enhanced detection sensitivity in complex mixtures such as biological media.

Most lanthanide compounds are photostable.[13] Trivalent electron-deficient lanthanide cations stabilize the excited states of bound organic sensitizers, preventing irreversible photoreactions when the complex is irradiated. Therefore, protection from light is not required, yielding a long shelf life and easy manipulation in ambient laboratory conditions. Most importantly, this photostability allows for long exposure times and repeated experiments.

The luminescence lifetimes of lanthanide cations are in the range of micro- to milliseconds,[14, 15] which is much longer than the pico- to nanosecond lifetimes that are typical for fluorescent organic molecules and proteins. The long luminescence lifetimes allow simple and accurate discrimination of the lanthanide complex signal from autofluorescence (background fluorescence) through time-resolved measurements, providing enhanced detection sensitivity.[16-18]

2
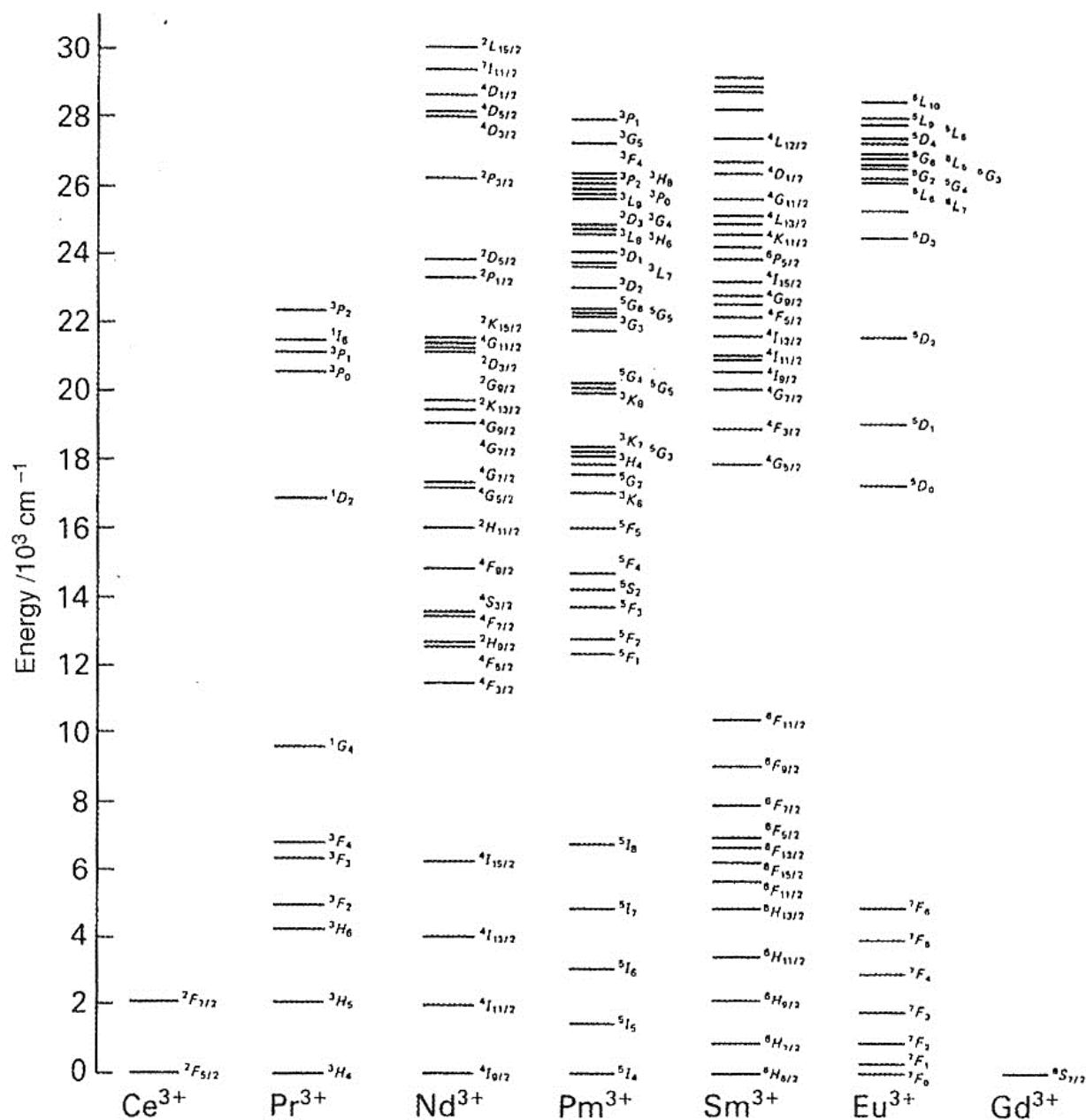
Figure 1.1. Energy levels of the trivalent lanthanide cations[19]
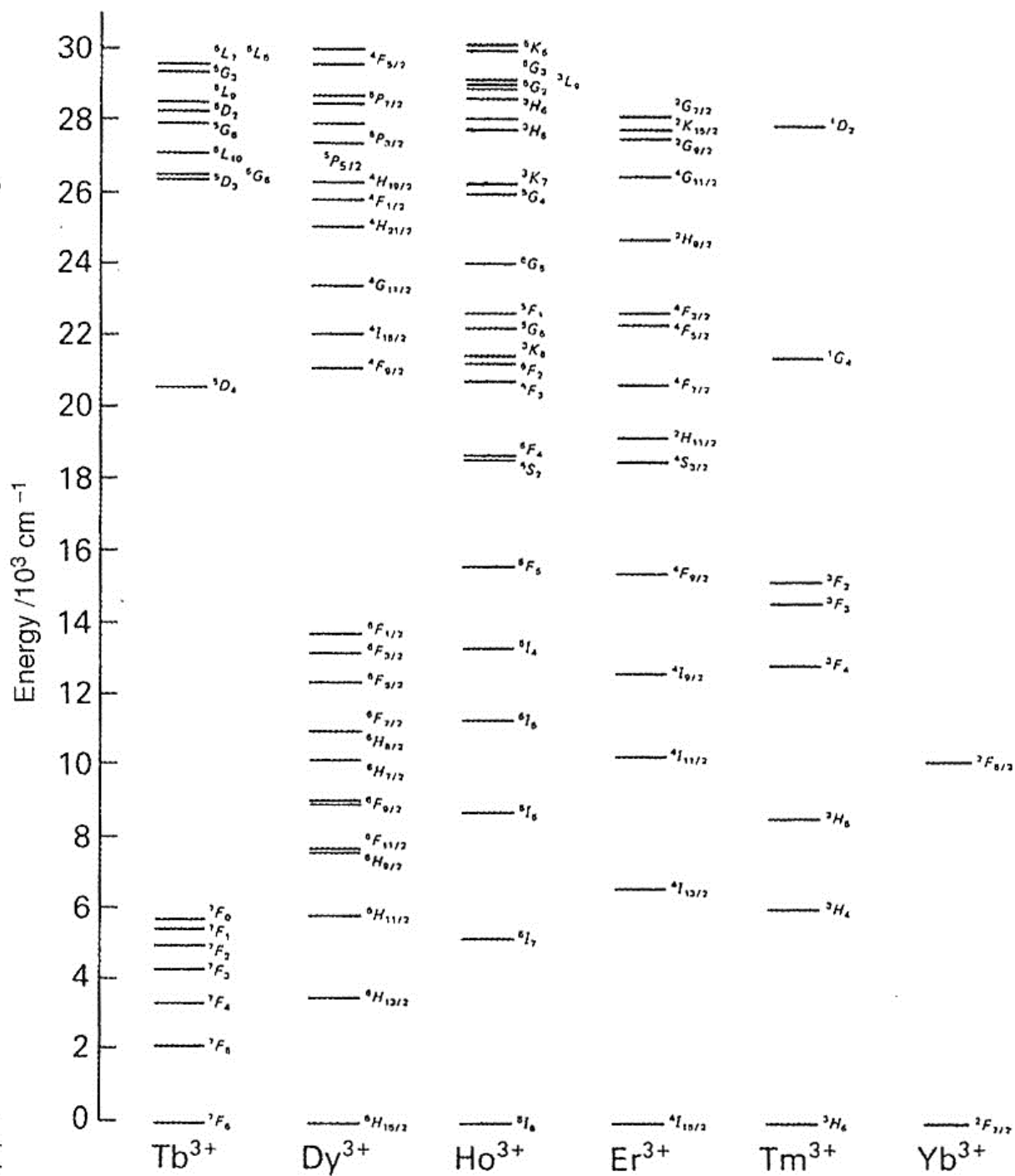
Figure 1.1. (continued) Energy levels of the trivalent lanthanide cations

4
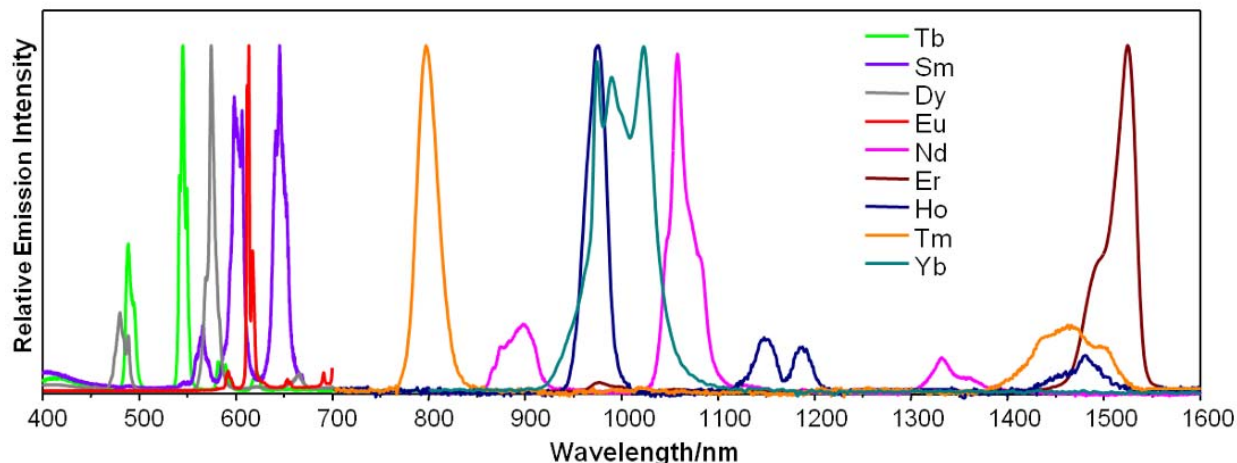
Figure 1.2. Normalized emission spectra of luminescent lanthanide complexes in solution, illustrating the sharp emission bands and minimal overlap of lanthanide luminescence.[4, 5]

Since *f*→*f* transitions are forbidden by the Laporte rule, free lanthanide cations have low extinction coefficients and can therefore not be excited directly with a good efficiency.[2, 3] As a result, the number of emitted photons will be small which will result in low detection sensitivity. A strategy to overcome this limitation that has been initially disclosed by Weissman in 1942[20] consist to locate a sensitizer at a controlled distance to the lanthanide cation. This sensitizer must fulfill the double function of absorbing as many photons as possible and to convert the resulting energy to the lanthanide metal ion. This combination of processes is known under the name of "antenna effect" [21] (Figure 1.3).
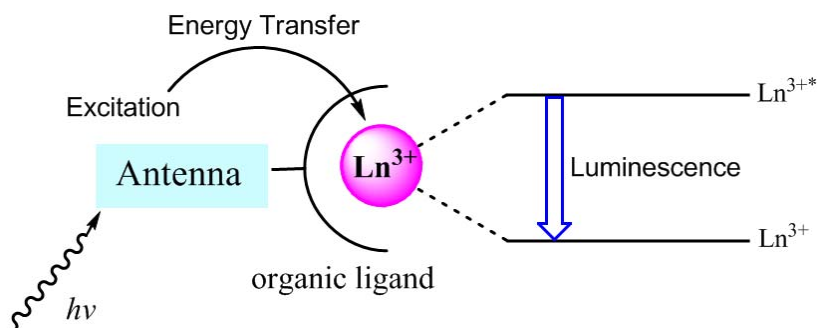
Figure 1.3. Schematic diagram of photosensitization of lanthanide ion by organic ligand.

A Jablonski diagram is commonly used to illustrate the energy transfer path between an organic ligand and the lanthanide ion (Figure 1.4). A transition from the ground singlet state, S_0 to the excited singlet state, S_1 is followed by intersystem crossing (ISC) which results in population of the antenna's triplet state, T_1. From the triplet excited antenna, the energy migrates to the lanthanide ion. There are number of competing pathways from the excited singlet and triplet states, such as fluorescence ($S_1 \rightarrow S_0$), phosphorescence ($T_1 \rightarrow S_0$) and non-radiative deactivation.
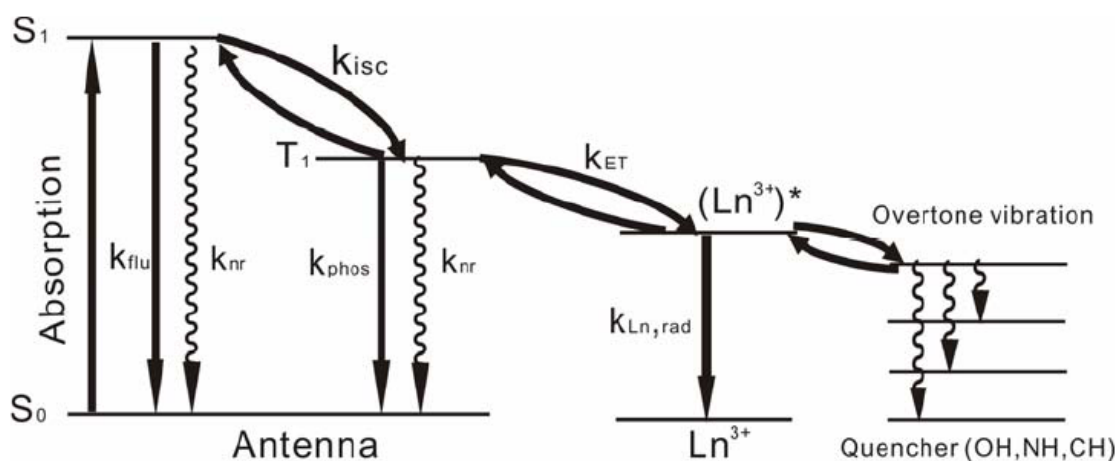
Figure 1.4. Jablonski diagram for sensitized Ln^{3+} emission (k_{flu}, rate of fluorescence; k_{ISC}, intersystem crossing rate; k_{phos}, phosphorescence rate; k_q, triplet quenching rate; k_{nr}, non-adiative decay rate; k_{ET}, energy transfer rate; and $k_{Ln,rad}$, radiative decay rate.).

Three possible mechanisms have been proposed for the energy transfer process from the donating electronic states of the sensitizer to the accepting energy levels of the metal center. The Förster mechanism is a dipole-dipole type of interaction between the donor and acceptor. This mechanism requires spectral overlap between absorption of the acceptor and emission of the donor. This mechanism takes place through space, the efficiency is dependent on r^{-6}, where r is the distance between the donor and acceptor.[22] The Dexter mechanism is a concerted electron-

exchange mechanism. It requires electron exchange between the donor and acceptor, therefore orbital overlap between the donor and acceptor is necessary. The efficiency is proportional to e^{-r}, where r is the distance between the donor and acceptor.[23] Electron transfer mechanism is a process which dependent upon orbital overlap and the oxidation and reduction potentials of the donor and metal ion respectively. It is limited to NIR emitting Yb^{3+} that has sufficiently low potential to be reduced ($E^0(Yb^{III}/Yb^{II}) = -1.05$ V).[19, 24-29] Through this mechanism, even non-fluorescent electron rich chromophores can still sensitize Yb^{3+} emission.[27]

The excited state of the lanthanide ion can be deactivated by the overtones of high frequency vibrations of C-H, N-H and O-H.[15] The efficiency of this quenching process is dependent on the energy gap between the ground state and the excited state of the lanthanide ion. This effect is much more pronounced in NIR-emitting lanthanide ions, because of their smaller energy gap (Figure 1.5).
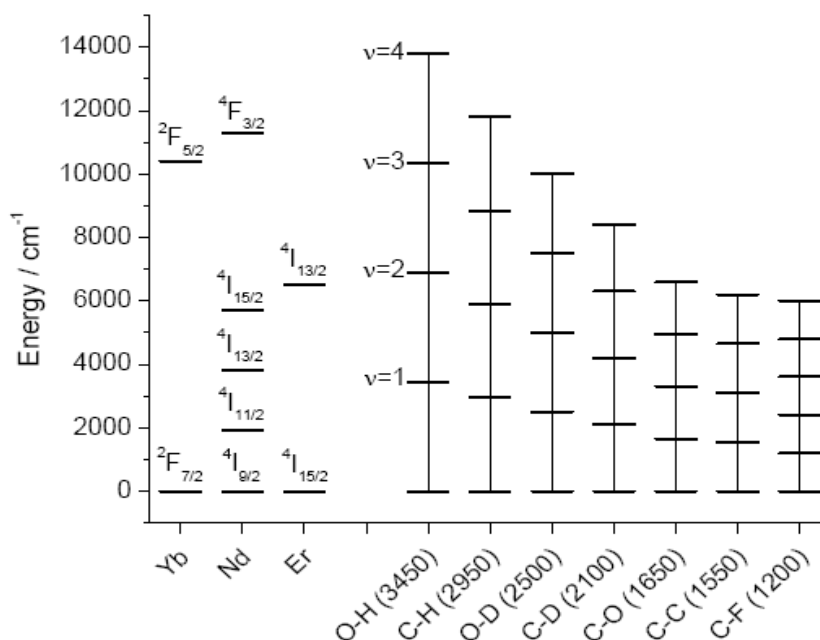
Figure 1.5. Radiative transition energies of Yb^{3+}, Nd^{3+} and Er^{3+} and the vibrational energies of common bonds found in organic systems.

7

Considering factors that affect the lanthanide luminescence, ligands must fulfill the following requirements: (1) The ligands have to form a stable complex with lanthanide ions, which typically have a high coordination number of 8 to 10 in solution. (2) The energy levels of the singlet state and the triplet state must match the accepting energy level of the lanthanide ions to achieve a good energy transfer. (3) The ligand has to provide good protection for lanthanide ions from non-radiative deactivation through solvent molecule vibrations. In addition, a ligand that is easily modified can allow the control of chemical or photophysical properties of the luminescent lanthanide complex.

1.2   NEAR-INFRARED LUMINESCENT LANTHANIDE COMPLEXES AND THEIR APPLICATION

In electromagnetic radiation, near-infrared (NIR) region ranges approximately from 650 nm to 1500 nm. There are constantly growing interests for NIR luminescence in the last decade because of their potentials for bioanalytical applications and biological imaging as well as for technological applications. The use of NIR luminescence is a promising approach for biological imaging and bioanalytical applications for three main reasons: (1) NIR photons have less interference with biological materials as they are mostly not absorbed by biological tissues (Figure 1.6).[30] Therefore, photons can penetrate deeply into tissues allowing non-invasive detection of biological molecules or events. (2) Since the autofluorescence arising from biological tissue is mainly located in the violet–blue region,[31] imaging in the NIR region also provides the advantage of improved detection sensitivity due to enhanced signal to noise ratio as

the background emission ("autofluorescence") of biological material in the NIR is almost inexistent (Figure 1.7).[30] (3) An additional advantage of NIR photons for biological imaging is the limited scattering of such photons in comparison to visible photons that result in improved image resolution. As the intensity of scattered light is proportional to $1/\lambda^{SP}$ (SP = scattering power), the longer wavelength of NIR light has reduced scattering, which results in the higher resolution of the obtained image.[32]
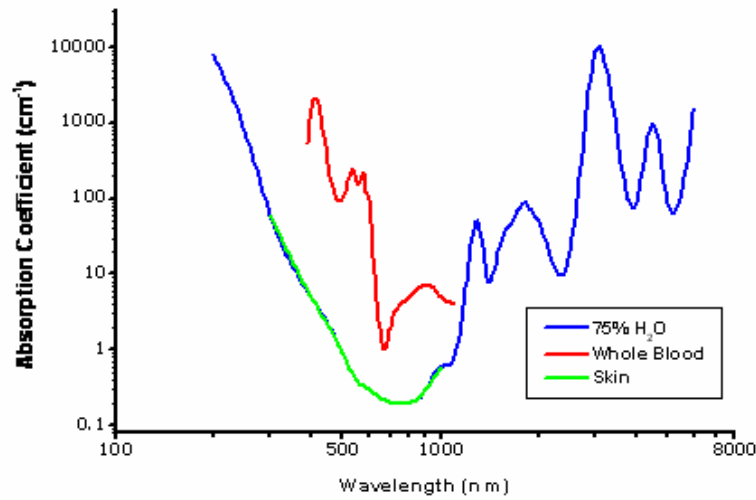
Figure 1.6. Absorption spectra of skin and whole blood.
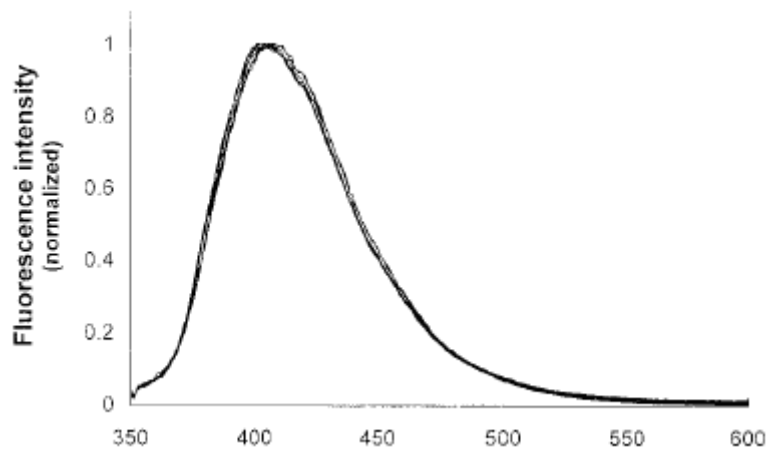
Figure 1.7. Fluorescence spectra of physical tissue model.

9

Besides the biological imaging, NIR luminescence is useful for NIR organic light-emitting diode technology,[33, 34] telecommunication where the electronic structure of lanthanide ions such as Er^{3+}, Nd^{3+} and Ho^{3+} can be used as the active material for optical amplification of NIR signal,[35, 36] and encrypted tags ("barcodes") to recognize the identity of chemical or biological entity or of an object.[37]

The field of development of sensitizers for NIR emitting lanthanide cations is currently booming. A large number of examples can be found in the literature. Several sensitizers or antennae have been described for the sensitization of NIR emitting lanthanide cations.[2, 5, 28, 29, 38-77] Nevertheless, the number of antennae for NIR emitting lanthanides is still limited and deserved more investigations as only a few lanthanide compounds match the requirements for practical applications in biological media. One of the strongest limitations for applications remains the ability to emit a sufficiently large number of photons per unit volume that will allow obtaining good detection sensitivity. Typically, the actual complexes formed with NIR emitting lanthanide cations have low quantum yields in comparison to visible emitting lanthanide compounds limiting the number of emitted photons per discrete molecule.

2.0   STRUCTURAL AND NEAR INFRARED LUMINESCENCE PROPERTIES OF

SALOPHEN-LANTHANIDE COMPLEXES

Parts of the work presented here have been completed in collaboration with Paul D. Badger (Stéphane Petoud Research Group, Department of Chemistry, University of Pittsburgh) and Steve J. Geib (Department of Chemistry, University of Pittsburgh). A portion of the results presented here have been published in Helvetica Chimica Acta, Vol. 92, No. 11, p 2313, 2009: "Synthesis and Solid-State, Solution, and Luminescence Properties of Near-Infrared-Emitting Neodymium(3+) Complexes Formed with Ligands Derived from Salophen."[78]

2.1   INTRODUCTION

There is a continuously growing interest for the properties of near infrared (NIR) luminescent lanthanide complexes.[2, 5, 28, 29, 38-77] The number of antennae for NIR emitting lanthanides is still moderate and it is interesting to test additional systems in order to broaden our understanding of the relationship between electronic structure of the antenna and luminescence properties of the resulting complexes.

In this work, we have investigated a system based on salophen to which different substituents can be rapidly attached in order to evaluate their effect on the solution behavior, solid state structure and luminescence properties of these complexes.

Metal complexes formed with Schiff ligands have occupied an important role in coordination chemistry for over half a century.[79] Salen, ethylenediamine-bridged salicylaldehydes and salophen, o-phenylenediamine-bridged salicylaldehydes have been extensively employed because of their stability resulting from the conjugated structure, the pre-organized tetradentate coordination geometry, the simplicity of synthesis and the facile modification of their structures. Salophen derivatives can act as good sensitizer-ligands for luminescent lanthanide cations, because this family of ligands can fulfill the specific requirements for lanthanide luminescence. The planar and rigid ligands have tetradentate coordination geometry which can be hypothesized to lead to the formation of ML_2 complexes with lanthanide ions to fulfill their coordination number requirements. The energy of the triplet state of the unsubstituted salophen chromophoric ligand has been reported to be located at 17,510 cm^{-1}.[80] This energy is suitable for a rapid and irreversible intramolecular energy transfer to NIR-emitting lanthanide ions such as Nd^{3+} that has one main accepting level located at 11,300 cm^{-1}. Another advantage of the salophen moiety is the easy and versatile modification of its structure. A large number of derived ligands possessing different substituents can be rapidly synthesized in few steps. A family of ligands possessing a variety of substituents is important for the systematic study and control of the photophysical properties of lanthanide complexes.

2.2 EXPERIMENTAL

2.2.1 Reagents

All reagents were used as received, unless otherwise stated. 5-Bromosalicylic acid, 4-methyl-1,2-phenylenediamine and paraformaldehyde were purchased from Acros Organics. 5-Bromosalicylaldehyde, 4,5-dimethyl-1,2-phenylenediamine, hexamethylenetetramine, magnesium sulfate and sodium bromate were purchased from Aldrich. 3,5-Dibromosalicylaldehyde and trifluoroacetic acid were purchased from Alfa Aesar. 2,4-Dihydroxybenzaldehyde was purchased from Avocado Research Chemiclas Ltd. 1,2-Phenylenediamine was purchased from Eastman. CH_2Cl_2, CH_3CN, ethyl acetate, MeOH, THF and Na_2CO_3 were purchased from EMD Chemicals Inc. Et_3N was purchased from Fisher Scientific. Benzyltrimethylammonium chloride was purchased from Fluka. Acetic acid, DMSO, Et_2O, HCl, hexanes, NaOH and $MgSO_4$ were purchased from Mallinckordt Baker, Inc. Salicylaldehyde was purchased from Matheson. Absolute EtOH was purchased from Pharmco Products, Inc. 2-Bromophenol was purchased from TCI. $Nd(OTf)_3 \cdot 6H_2O$ and $Yb(OTf)_3 \cdot 6H_2O$ were purchased from Strem Chemicals. All deuterated NMR solvents were purchased from Cambridge Isotope Labs and used as received.

2.2.2 Instrumental Information

Melting points were measured on a Fisher-Johns melting point apparatus and were uncorrected. Infrared spectra were recorded on a Perkin-Elmer Spectrum BX FT-IR. Polystyrene film was

used as the external standard (1601 cm^{-1} peak). Elemental analyses were performed by Atlantic Microlab, Inc. ^{1}H-NMR spectra were recorded on a Bruker DPX-300 at 300 MHz. EI-MS and ESI-MS were measured on a Micromass Autospec and Agilent HP 1100 series LC-MSD respectively. Absorption spectra were recorded on a PerkinElmer Lamda 9 spectrophotometer. Metal cation luminescence emission and excitation spectra were measured using a modified Jobin Yvon-Spex Fluorolog-322 spectrofluorometer equipped for both room temperature (RT) and 77 K measurements. Luminescence and excitation spectra were corrected for the instrumental function. Metal cation luminescence quantum yield were measured using the ^{4}F$_{3/2}$ → ^{4}I$_{11/2}$ transition of a K[Nd(tropolone)$_4$] previously reported (Φ = 2.1×10^{-3} in DMSO) as reference.[5] The use of a Nd^{3+} complex allows for a simple method of cross calibrating the visible detector with the NIR detector of the Fluorolog-322. The quantum yields were calculated using the following equation:

$$\frac{\Phi_x}{\Phi_r} = \frac{A_r(\lambda_r)}{A_x(\lambda_x)} \cdot \frac{I(\lambda_x)}{I(\lambda_r)} \left[\frac{\eta_x}{\eta_r}\right]^2 \cdot \frac{D_x}{D_r}$$

where subscript r stands for the reference and x for the sample; A is the absorbance at the excitation wavelength, I is the intensity of the excitation light at the same wavelength, η is the refractive index (η = 1.479 in DMSO), and D is the measured integrated luminescence intensity.

The luminescence lifetime measurements were performed by excitation of solutions in 1 cm quartz cells using a nitrogen laser (Oriel model 79110, wavelength 337.1 nm, pulse width at half-height 15 ns, 5-30 Hz repetition rate). Emission from the sample was collected at a right angle to the excitation beam by a 3" plano-convex lens. Emission wavelengths were selected by means of quartz filters. The signal was monitored by a cooled photomultiplier (Hamamatsu R316) coupled to a 500 MHz bandpass digital oscilloscope (Tektronix TDS 754D). The signals

(15,000 points each trace) from at least 500 flashes were collected and averaged. Background signals were similarly collected and subtracted from sample signals. Lifetimes are averages of at least three independent determinations. Data were fitted with exponential decay curves by OriginPro (V7 SP4) data analysis and linefitting software. Ligand-centered triplet state lifetimes were performed by excitation of solid samples in a quartz tube at 77 K using the nitrogen laser described previously. Emission from the samples was collected at a right angle to the excitation beam, and the emission wavelengths were selected by means of a Spex FL1005 double monochromator. The signal was monitored by a Hamamatsu R928 photomultiplier coupled to a 500 MHz bandpass digital oscilloscope (Tektronics TDS 620B). The signals (15,000 points each trace) from at least 500 flashes were collected and averaged. Background signals were similarly collected and subtracted from sample signals.

Crystals suitable for X-ray crystallographic study were coated with Fluorolube[®] then mounted on a glass fiber and coated with epoxy cement. X-ray data were collected on a Bruker Apex diffractometer using graphite monochromatized Mo Kα radiation ($\lambda = 0.71073$ Å). Data collection was controlled using the Bruker SMART program, and the data processing was done with the SHELXTL program package,[81] and the graphics were done by using Ortep-3,[82] Mercury 1.2.1[83] and Ortex.[84] All hydrogen atoms were calculated and placed in idealized positions ($d_{C-H} = 0.96$ Å). The diffraction studies were carried out by Dr. Steven Geib, Department of Chemistry, University of Pittsburgh.

2.2.3 Synthesis of Ligands and Complexes

N,N'-disalicylidene-4-methyl-1,2-phenylenediamine (**2**) was synthesized as follows: 1.01 g (8.26 mmol) of 4-methyl-1,2-phenylenediamine were added to a solution of 2.02 g (16.5 mmol) of salicylaldehyde in 20 mL EtOH. The mixture was heated and sonicated for 20 min. A yellow precipitate formed. The mixture was filtered, washed with hexanes and dried under vacuum (1.53 g, 56%). mp: 117–120 $^{\circ}$C. IR (selected absorbances only, KBr, cm^{-1}): 1617(C=N), 1278(Ph-O). ^{1}H-NMR (300 MHz, CD$_3$CN, δ): 13.18 (s, 1H, –OH), 13.10 (s, 1H, –OH), 8.77 (s, 1H, –N=C–H), 8.75 (s, 1H, –N=C–H), 7.52–7.49 (m, 2H, Ar H), 7.38 (m, 2H, Ar H), 7.27 (m, 1H, Ar H), 7.22–7.20 (m, 2H, Ar H), 7.00–6.94 (m, 4H, Ar H), 2.40 (s, 3H, –CH$_3$).

N,N'-disalicylidene-4,5-dimethyl-1,2-phenylenediamine (**3**) was synthesized as follows: 1.14 g (8.40 mmol) of 4,5-dimethyl-1,2-phenylenediamine were added to a solution of 2.05 g (16.8 mmol) of salicylaldehyde in 20 mL EtOH. The mixture was heated and sonicated for 15 min. A yellow precipitate formed. The mixture was filtered, washed with hexanes and dried under vacuum (2.54 g, 88%). mp: 144–146 $^{\circ}$C. IR (selected absorbances only, KBr, cm^{-1}): 1617(C=N), 1278(Ph-O). ^{1}H-NMR (300 MHz, CD$_3$CN, δ): 13.22 (s, 2H, –OH), 8.76 (s, 2H, –N=C–H), 7.50 (dd, *J* = 1.6 Hz, 7.6 Hz, 2H, Ar H), 7.47–7.36 (m, 2H, Ar H), 7.19 (s, 2H, Ar H), 6.99–6.92 (m, 4H, Ar H), 2.32 (s, 6H, –CH$_3$).

N,N'-bis(5-bromosalicylidene)-1,2-phenylenediamine (**4**) was synthesized as follows: 0.554 g (5.12 mmol) of 1,2-phenylenediamine were added to a solution of 2.06 g (10.3 mmol) of 5-bromosalicylaldehyde in 30 mL EtOH. The mixture was heated and sonicated for 20 min. A yellow precipitate formed. The mixture was filtered, washed with hexanes and dried under vacuum (0.813 g, 33%). mp: 206–212 $^{\circ}$C. IR (selected absorbances only, KBr, cm^{-1}):

1611(C=N), 1276(Ph-O). ^{1}H-NMR (300 MHz, CD$_3$CN, δ): 8.91 (s, 2H, –N=C–H), 7.88 (d, J = 2.5 Hz, 2H, Ar H), 7.54 (dd, J = 2.6 Hz, J = 8.9 Hz, 2H, Ar H), 7.45–7.43 (m, 4H, Ar H), 6.93 (d, J = 8.8 Hz, 2H, Ar H).

N,N'-bis(5-bromosalicylidene)-4-methyl-1,2-phenylenediamine (**5**) was synthesized as follows: 0.906 g (7.42 mmol) of 4-methyl-1,2-phenylenediamine were added to a solution of 3.00 g (14.9 mmol) of 5-bromosalicylaldehyde in 30 mL EtOH. The mixture was heated and sonicated for 30 min. A yellow precipitate formed. The mixture was filtered, washed with a small amount of EtOH and dried under vacuum (1.01 g, 38%). EI-MS: *m/z* [M$^+$] 488 (calcd. 487.96 for C$_{21}$H$_{16}$Br$_2$N$_2$O$_2$). ^{1}H-NMR (300 MHz, DMSO-d_6, δ): 8.91 (s, 1H, –N=C–H), 8.90 (s, 1H, –N=C–H), 7.89–7.86 (m, 2H, Ar H), 7.56–7.50 (m, 2H, Ar H), 7.38 (m, 1H, Ar H), 7.27–7.23 (m, 2H, Ar H), 6.95–6.91 (m, 2H, Ar), 2.38 (s, 3H, –CH$_3$).

N,N'-bis(5-bromosalicylidene)-4,5-dimethyl-1,2-phenylenediamine (**6**) was synthesized as follows: 0.160 g (1.18 mmol) of 4,5-dimethyl-1,2-phenylenediamine were dissolved in 4 mL of EtOH and added to a solution of 0.486 g (2.42 mmol) of 5-bromosalicylaldehyde in 7 mL EtOH. The mixture was refluxed overnight. An orange-yellow precipitate formed. The mixture was filtered, washed with EtOH and Et$_2$O and dried under vacuum (0.506 g, 85%). mp: 241–245 ^{o}C. IR (KBr, cm^{-1}): 1616(C=N), 1277(Ph-O). ^{1}H-NMR (300 MHz, DMSO-d_6, δ): 8.90 (s, 2H, –N=C–H), 7.86 (d, J = 2.5 Hz, 2H, Ar H), 7.52 (dd, J = 2.5 Hz, J = 8.8 Hz, 2H, Ar H), 7.28 (s, 2H, Ar H), 6.92 (d, J = 8.8 Hz, 2H, Ar H), 2.29 (s, 6H, –CH$_3$).

3-Bromosalicylaldehyde was synthesized by a reported method[85] with slight modification as follows: 1.60 mL (2.39 g; 13.8 mmol) of 2-bromophenol were added to a solution of 2.38 g (25.0 mmol) of MgCl$_2$, 2.61 g (86.8 mmol) of paraformaldehyde and 5.00 mL (3.63 g; 35.9 mmol) of Et$_3$N in 50 mL CH$_3$CN. The reaction mixture was refluxed for 2.5 days and then

17

allowed to cool. The solution was diluted with 80 mL of 1 M HCl and extracted with Et_2O (3×50mL). The organic layer was washed with 50 mL of brine, dried over $MgSO_4$, filtered and concentrated under reduced pressure. The crude product was purified by column chromatography over silica gel eluting 20% EtOAc in hexanes to give 3-bromosalicylaldehyde (0.961 g, 35%) EI-MS: m/z [M$^+$] 200 (calcd. 199.95 for $C_7H_5BrO_2$). ^{1}H-NMR (300 MHz, CDCl$_3$, δ): 11.62 (s, 1H, –OH), 9.88 (s, 1H, –C(=O)–H), 7.79 (dd, J = 1.5 Hz, J = 7.8 Hz, 1H, Ar H), 7.55 (dd, J = 1.4 Hz, J = 7.7 Hz, 1H, Ar H), 6.96 (t, J = 7.7 Hz, 1H, Ar H).

N,N'-bis(3-bromosalicylidene)-1,2-phenylenediamine (**7**) was synthesized as follows: 0.0535 g (0.495 mmol) of 1,2-phenylenediamine were added to a solution of 0.209 g (1.04 mmol) of 3-bromosalicylaldehyde in 5 mL EtOH. The mixture was then refluxed for 11 h. An orange precipitate formed. The mixture was filtered, washed with Et_2O and dried under vacuum (0.137 g, 58%). EI-MS: m/z [M$^+$] 474 (calcd. 473.94 for $C_{20}H_{14}Br_2N_2O_2$). ^{1}H-NMR (300 MHz, CD$_3$CN, δ): 8.76 (s, 2H, –N=C–H), 7.68 (dd, J = 1.5 Hz, J = 7.9 Hz, 2H, Ar H), 7.55 (dd, J = 1.5 Hz, J = 7.9 Hz, 2H, Ar H), 7.46–7.35 (m, 2H, Ar H), 6.92 (t, J = 7.8 Hz, 2H, Ar H).

N,N'-bis(3-bromosalicylidene)-4-methyl-1,2-phenylenediamine (**8**) was synthesized as follows: 0.0604 g (0.494 mmol) of 4-methyl-1,2-phenylenediamine were added to a solution of 0.205 g (1.02 mmol) of 3-bromosalicylaldehyde in 5 mL EtOH. The mixture refluxed for 11 h. An orange precipitate formed. The mixture was filtered, washed with Et_2O and dried under vacuum (0.0947 g, 39%). EI-MS: m/z [MH$^+$] 489 (calcd. 487.96 for $C_{21}H_{16}Br_2N_2O_2$). ^{1}H-NMR (300 MHz, CD$_3$CN, δ): 8.75 (s, 1H, –N=C–H), 8.74 (s, 1H, –N=C–H), 7.68–7.65 (m, 2H, Ar H), 7.55–7.52 (m 2H, Ar H), 7.31–7.23 (m, 2H, Ar H), 6.92 (t, J = 7.8 Hz, 1H, Ar H), 6.91 (t, J = 7.8 Hz, 1H, Ar H), 2.41 (s, 3H, –CH$_3$).

N,N'-bis(3-bromosalicylidene)-4,5-dimethyl-1,2-phenylenediamine (**9**) was synthesized as follows: 0.0654 g (0.480 mmol) of 4,5-dimethyl-1,2-phenylenediamine were added to a solution of 0.197 g (0.981 mmol) of 3,5-dibromosalicylaldehyde in 5 mL EtOH. The mixture refluxed for 12 h. An orange precipitate formed. The mixture was filtered, washed with Et_2O and dried under vacuum (0.124 g, 51%). EI-MS: *m/z* [M^+] 499.974113 (calcd. 499.973500 for $C_{22}H_{18}Br_2N_2O_2$). ^{1}H-NMR (300 MHz, CD_3CN, δ): 8.75 (s, 2H, –N=C–H), 7.67 (dd, J = 1.6, J = 7.9, 2H, Ar H), 7.53 (dd, J = 1.5, J = 7.7, 2H, Ar H), 7.21 (s, 1H, Ar H), 6.91 (t, J = 7.8, 2H, Ar H), 2.33 (s, 6H, –CH_3).

N,N'-bis(3,5-dibromosalicylidene)-1,2-phenylenediamine (**10**) was synthesized as follows: 0.300 g (2.78 mmol) of 1,2-phenylenediamine were added to a solution of 1.56 g (5.57 mmol) of 3,5-dibromosalicylaldehyde in 20 mL EtOH. The mixture was refluxed for 2 h. An orange precipitate formed. The mixture was filtered, washed with Et_2O and dried under vacuum (1.66 g, 94%). mp: 213–216 ^{o}C. IR (KBr, cm^{-1}): 1612(C=N), 1270(Ph-O). ESI-MS: *m/z* [MH^+] 632.8 (calcd. 631.76 for $C_{20}H_{12}Br_4N_2O_2$). ^{1}H-NMR (300 MHz, $CDCl_3$, δ): 8.53 (s, 2H, –N=C–H), 7.77 (d, J = 2.3 Hz, 2H, Ar H), 7.49 (d, J = 2.3 Hz, 2H, Ar H), 7.41 (dd, J = 3.4 Hz, J = 5.9 Hz,2H, Ar H), 7.23 (dd, J = 3.4 Hz, J = 5.9 Hz,2H, Ar H).

N,N'-bis(3,5-dibromosalicylidene)-4-methyl-1,2-phenylenediamine (**11**) was synthesized as follows: 0.213 g (1.74 mmol) of 4-methyl-1,2-phenylenediamine were added to a solution of 0.985 g (3.52 mmol) of 3,5-dibromosalicylaldehyde in 15 mL EtOH. The mixture was heated and sonicated for 30 min. An orange precipitate formed. The mixture was filtered, washed with hexanes and dried under vacuum (0.944 g, 84%). EI-MS: *m/z* [M^+] 646 (calcd. 635.96 for $C_{21}H_{14}Br_4N_2O_2$). ^{1}H-NMR (300 MHz, DMSO-d_6, δ): 8.97 (s, 2H, –N=C–H), 7.93–7.92 (m, 4H, Ar H), 7.47–7.44 (m, 1H, Ar H) 7.36 (s, 1H, Ar H), 7.31 (m, 1H, Ar H), 2.40 (s, 3H, –CH_3).

N,N'-bis(3,5-bromosalicylidene)-4,5-dimethyl-1,2-phenylenediamine **(12)** was synthesized as follows: 0.242 g (1.78 mmol) of 4,5-dimethyl-1,2-phenylenediamine were added to a solution of 1.02 g (3.66 mmol) of 3,5-dibromosalicylaldehyde in 15 mL EtOH. The mixture was heated and sonicated for 30 min. An orange precipitate formed. The mixture was filtered, washed with hexanes and dried under vacuum (1.02 g, 87%). EI-MS: *m/z* [M$^+$] 660 (calcd. 659.79 for $C_{22}H_{16}Br_4N_2O_2$). ^{1}H-NMR (300 MHz, DMSO-d_6, δ): 8.97 (s, 2H, –N=C–H), 7.93–7.91 (m, 4H, Ar H), 7.36 (s, 2H, Ar H), 2.31 (s, 6H, –CH$_3$).

Na[Nd(*N,N'*-disalicylidene-4,5-dimethyl-1,2-phenylenediamine)$_2$] was synthesized as follows: 0.115 g (0.333 mmol) of 4,5-dimethylsalophen (**3**) were dissolved in 7 mL of CH$_3$CN. 0.117 g (0.167 mmol) of Nd(OTf)·6H$_2$O were dissolved in 5 mL of CH$_3$CN and slowly added to the solution of ligand. 4.6 mL of 0.1078 M NaOH in MeOH solution (0.496 mmol) was then slowly added to the stirring solution. The reaction mixture was refluxed for 2 h. The yellow precipitate was centrifuged, washed with Et$_2$O and dried under vacuum (0.103 g, 72%). IR (selected absorbances only, KBr, cm^{-1}): 1618(C=N), 1544(C=C); 1385(Ph-O).

Na[Nd(*N,N'*-bis(5-bromosalicylidene)-4,5-dimethyl-1,2-phenylenediamine)$_2$] was synthesized as follows: 0.0699 g (0.139 mmol) of 5,5'-dibromo-4,5-dimethylsalophen (**6**) were dissolved in 15 mL of THF. 0.0487 g (0.0696 mmol) of Nd(OTf)·6H$_2$O were dissolved in 7.5 mL of CH$_3$CN and slowly added to the solution of ligand. 1.9 mL of 0.1078 M NaOH in MeOH solution (0.209 mmol) was then slowly added to the stirring solution. The reaction mixture was refluxed for 6 h. The solvents were removed under reduced pressure. The residue was triturated with Et$_2$O, centrifuged and dried under vacuum (0.064 g, 78%). IR (selected absorbances only, KBr, cm^{-1}): 1616(C=N), 1522(C=C); 1373(Ph-O).

Na[Nd(*N,N'*-bis(3-bromosalicylidene)-4,5-dimethyl-1,2-phenylenediamine)$_2$] was synthesized as follows: 0.0504 g (0.100 mmol) of 3,3'-dibromo-4,5-dimethylsalophen (**9**) were dissolved in 20 mL of THF. 0.0351 g (0.0502 mmol) of Nd(OTf)·6H$_2$O were dissolved in 7 mL of CH$_3$CN and slowly added to the solution of ligand. 1.5 mL of 0.1078 M NaOH in MeOH solution (0.151 mmol) was then slowly added to the stirring solution. The reaction mixture was refluxed overnight. The solvents were removed under reduced pressure. The yellow solid was centrifuged, washed with Et$_2$O and dried under vacuum (0.038 g, 65%).

Na[Nd(*N,N'*-bis(3,5-dibromosalicylidene)-4,5-dimethyl-1,2-phenylenediamine)$_2$] was synthesized as follows: 0.0534 g (0.0809 mmol) of tetrabromo-4,5-dimethylsalophen (**12**) were dissolved in 12 mL of a 2:1 (v/v) mixture of THF and CH$_3$CN. 0.0283 g (0.0405 mmol) of Nd(OTf)·6H$_2$O was then dissolved in 3 mL of CH$_3$CN and slowly added to the solution of ligand. 1.13 mL of 0.1078 M NaOH in MeOH solution (0.121 mmol) were slowly added to the stirring solution. The reaction mixture was refluxed overnight. The solvents were removed under reduced pressure. The yellow solid was centrifuged, washed with Et$_2$O and dried under vacuum (0.0346 g, 58%).

2.3   RESULTS AND DISCUSSION
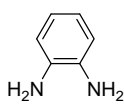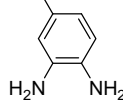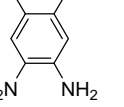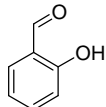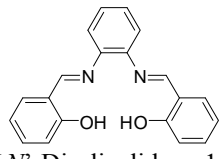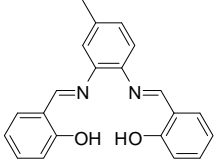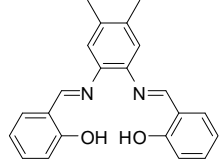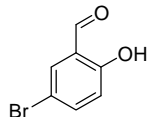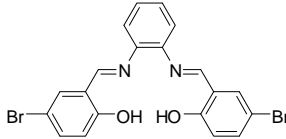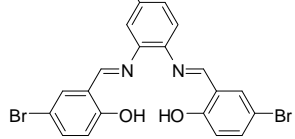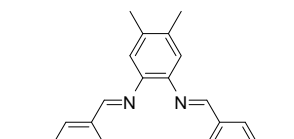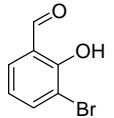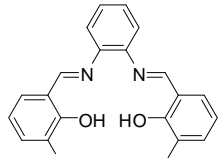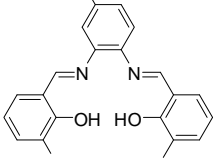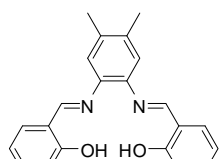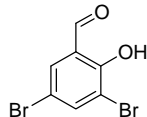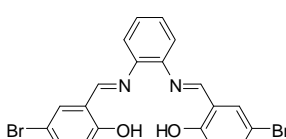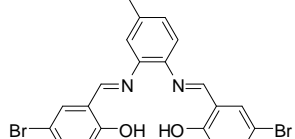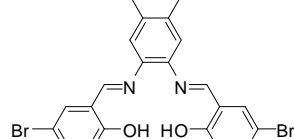
2.3.1   Design and Syntheses of Ligands Derived from Salophen

In a previous study,[86] the bromo-substituted salophen showed superior photophysical properties, such as higher quantum yield and longer luminescence lifetimes than other salophen

derivatives.[86] This can be explained by (1) the heavy atom effect and/or (2) the removal of one C–H vibration from the ligand responsible for the quenching. A methyl group on the phenylenediamine backbone also enhances the photophysical properties, as this electron donating group increase the electron density of the π system.

The salophen derivatives in Table 2.1 were designed and have been synthesized in order to systematically monitor the effects of the substituents. To investigate the electron donating effect of methyl groups on backbone, three types of phenylenediamine backbones with different numbers of methyl groups were used: phenylenediamine, methylphenylene-diamine and dimethylphenylenediamine. For the chelating arms, four types of salicyl-aldehyde were used: salicylaldehyde, 5-bromosalicylaldehyde, 3-bromosalicylaldehyde and 3,5-dibromo-salicylaldehyde. By comparing the chemical, physical and photophysical properties of the ligands made with different numbers of bromo groups and their corresponding lanthanide complexes, a relationship between the number of heavy atoms and their effects on the intramolecular energy transfer has been evaluated. In order to determine if the heavy atom effect or the removal of C–H vibration dominates in enhancing photophysical properties in bromo-substituted salophen, the ligands and their complexes made with 5- and 3-bromosalicylaldehyde have been compared.

Table 2.1. Structures of the synthesized salophen derivatives. Abbreviation is shown in the parentheses

Salicyl-aldehyde arms	Phenylenediamine backbones		
	 Phenylenediamine	 Methylphenylenediamine	 Dimethylphenylene-diamine
Salicyl-aldehyde 	 *N,N'*-Disalicylidene-1,2-phenylenediamine (Salophen; Sal; **1**)	 *N,N'*-Disalicylidene-4-methyl-1,2-phenylenediamine (Methylsalophen; MSal; **2**)	 *N,N'*-Disalicylidene-4,5-dimethyl-1,2-phenylenediamine (Dimethylsalophen; DMSal; **3**)
5-Bromo-salicyl-aldehyde 	 *N,N'*-Bis(5-bromo-salicylidene)-1,2-phenylenediamine (5,5'-Dibromosalophen; 5BSal; **4**)	 *N,N'*-Bis(5-bromosalicylidene)-4-methyl-1,2-phenylenediamine (5,5'-Dibromomethyl salophen; 5BMSal; **5**)	 *N,N'*-Bis(5-bromosalicylidene)-4,5-dimethyl-1,2-phenylenediamine (5,5'-Dibromodimethyl salophen; 5BDMSal; **6**)
3-Bromo-salicyl-aldehyde (**13**) 	 *N,N'*-Bis(3-bromosalicylidene)-1,2-phenylenediamine (3,3'-Dibromosalophen; 3BSal; **7**)	 *N,N'*-Bis(3-bromosalicylidene)-4-methyl-1,2-phenylenediamine (3,3'-Dibromomethyl-salophen; 3BMSal; **8**)	 *N,N'*-Bis(3-bromosalicylidene)-4,5-dimethyl-1,2-phenylenediamine (3,3'-Dibromodimethyl-salophen; 3BDMSal; **9**)
3,5-Dibromo-salicyl-aldehyde 	 *N,N'*-Bis(3,5-dibromosalicylidene)-1,2-phenylenediamine (Tetrabromosalophen; TBSal; **10**)	 *N,N'*-Bis(3,5-dibromosalicylidene)-4-methyl-1,2-phenylenediamine (Tetrabromomethyl-salophen; TBMSal; **11**)	 *N,N'*-Bis(3,5-dibromosalicylidene)-4,5-dimethyl-1,2-phenylenediamine (Tetrabromodimethyl-salophen; TBDMSal; **12**)

The salophen ligands can be easily synthesized by condensation of two equivalents of salicylaldehyde and one equivalent of phenylenediamine in refluxing ethanol (Figure 2.1(a)). This reaction is very fast and, in most cases, quantitative, with heating of the reaction mixture being essential. Without heating, the major product obtained was a Schiff base with only one amine condensed with the salicylaldehyde (Figure 2.1(b)). The ratio of the products was calculated from the integration of ^{1}H NMR peaks.
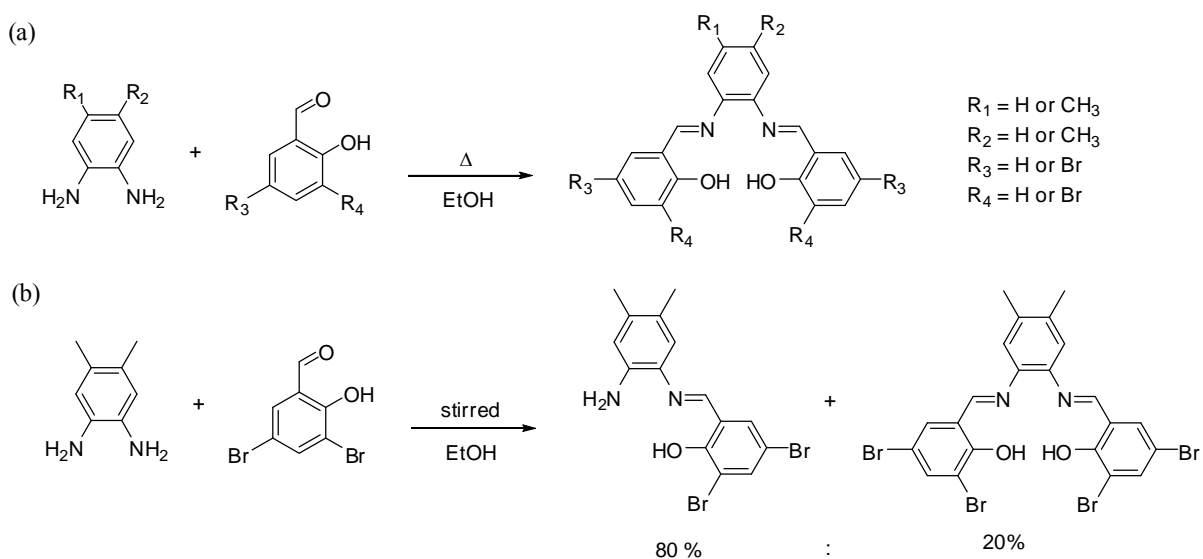
Figure 2.1. Depicting condensation of the phenylenediamine and salicylaldehyde

The formation of Schiff bases can be controlled by the temperature and the number of equivalents of aldehydes and amines. MacLachlan et al. reported the syntheses of Schiff bases with various ratios of aldehyde/amine from same dialdehyde and diamine.[87, 88] All the diamines and aldehydes were commercially available except 3-bromosalicylaldehyde. 3-Bromosalicylaldehyde was synthesized from bromophenol using paraformaldehyde in presence of magnesium chloride.[85]

2.3.2 Formation of NdL$_2$ Complexes

The syntheses of the NdL$_2$ complexes were carried out by the reaction of two equivalent of salophen ligand and one equivalent of Nd(OTf)$_3$·6H$_2$O. Depending on the solubility of the ligand, CH$_3$CN or the mixture of THF and CH$_3$CN were used as solvents. 1.5 equivalents of NaOH in MeOH was used as base to ensure complete deprotonation of the ligand. The Nd complex can be isolated by solvent evaporation and precipitation.

2.3.3 Nd-ligand Stoichiometry in Solution

To confirm the nature of the complexes formed between metal and ligand in solution, which is hypothesized to be ML$_2$, spectrophotometric titrations were performed in DMSO. There are two possible methods for titrations: dynamic and batch. In a dynamic titration, a ligand solution is prepared and increasing amounts of metal solution are added to the ligand solution. The absorbance of this mixture is recorded at each aliquot of metal. This method can be used only if the reaction between the metal and ligand is rapid. In a batch titration method, on the other hand, there is a longer time for the formation of the complex to reach equilibrium. In this method, samples with various ratios of metal and ligand are prepared and incubated, and the absorbance of each sample is recorded at a later time.

To ensure the formation of the complexes during the titration process, two methods were employed to completely deprotonate the ligands. In the first method, two equivalents of KOH for each ligand were added to a suspension of ligand in MeOH. The solution becomes clear indicating the deprotonation of the ligand. After evaporation of the solvent, the potassium salt of

the ligand was used to generate the solutions for the titration. The other method is mixing organic bases into the titration solutions. The deprotonation of the ligand can take place *in situ*. With this method, the instability of the potassium salt of the ligand and the undesirable re-protonation of the ligand can be avoided.

2.3.3.1 Nd-ligand stoichiometry in solution

One equivalent of Nd(OTf)$_3$·6H$_2$O and two equivalent of the potassium salt of dimethylsalophen (**3**) were mixed in DMSO, and the absorbance was recorded. The spectra of the complex continue to vary, indicating that the equilibrium of the metal and ligand cannot be reached in a short period of time. Therefore, a batch titration was carried out. Total 31 batches of solution were prepared in DMSO with the concentration of the ligand maintained at 3.00×10^{-5} M and the metal/ligand ratio were varied from 0:1 to 2:1 equivalents.
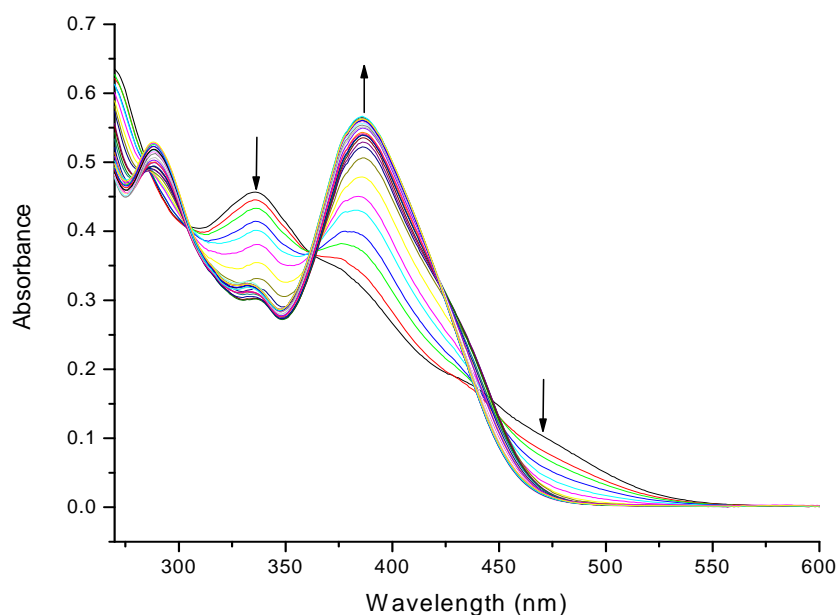
Figure 2.2. Absorption spectra of the batch titration of dimethylsalophen with Nd(OTf)$_3$·6H$_2$O.

26

An isosbestic point is present at 360 nm. As the metal/ligand ratio varied from 0.0 to 0.5, the spectra changed significantly. After the metal/ligand ratio reached 0.5, the change was diminished. The change of absorbance at 386 nm has a breaking point at the metal/ligand ratio of ~1:2, indicating the formation of the ML_2 complex (Figure 2.3).
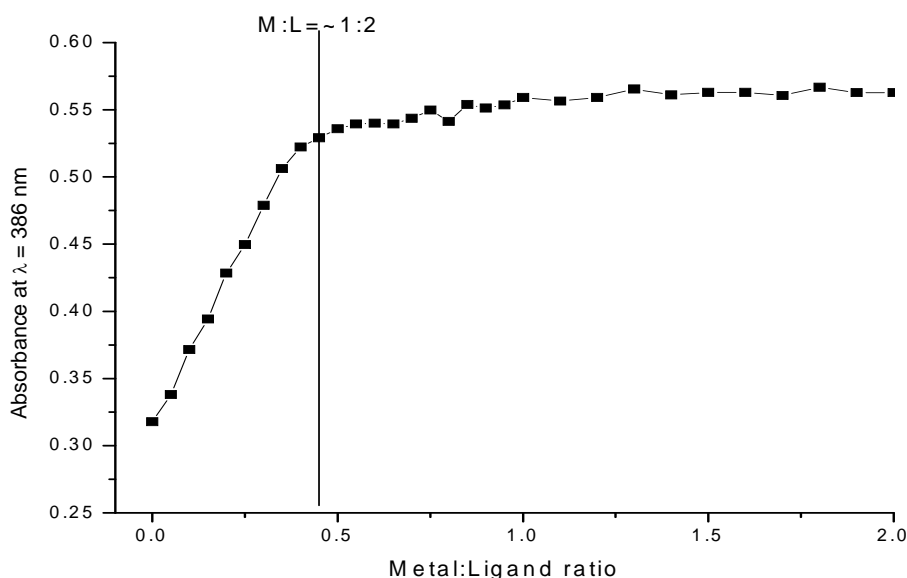
Figure 2.3. Absorbance at selected wavelength (386 nm) vs. metal/ligand ratio.

This titration data was analyzed using SPECFIT[89] program (Figure 2.4). Experimental data fitted best with ML and ML_2 model, and stability constants were obtained. The logarithm of the stability constants were $\log\beta_1 = 10\pm1$ and $\log\beta_2 = 17\pm1$, respectively. β_n is the overall equilibrium constant and K_n is the successive equilibrium constant.

$$M + L \rightarrow ML \qquad K_1 = \frac{[ML]}{[M][L]}; \qquad\qquad ML + L \rightarrow ML_2 \qquad K_2 = \frac{[ML_2]}{[ML][L]}$$

$$M + L \rightarrow ML \qquad \beta_1 = \frac{[ML]}{[M][L]} = K_1 \qquad M + 2L \rightarrow ML_2 \qquad \beta_2 = \frac{[ML_2]}{[M][L]^2} = K_1 \times K_2$$

(a)

(b)
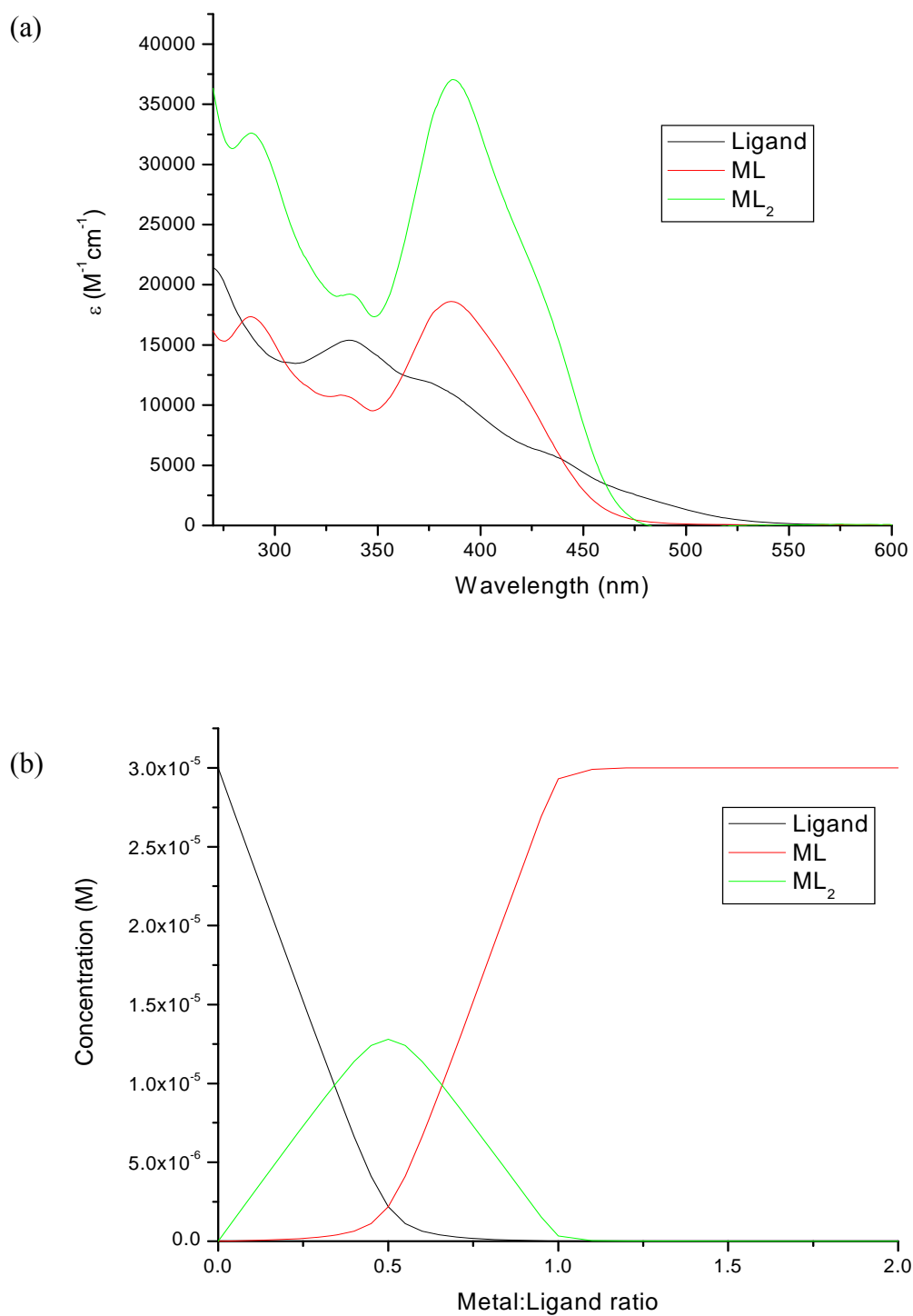
Figure 2.4. Results of the spectrophotometric titration of dimethylsalophen with Nd^{3+} (a) Calculated spectra for the three individual colored species; (b) Calculated concentrations of different species versus metal/ligand ratio.

2.3.3.2 Nd-tetrabromodimethylsalophen (12)

One equivalent of $Nd(OTf)_3 \cdot 6H_2O$ and two equivalents of the potassium salt of tetrabromodimethylsalophen were mixed in DMSO, and the absorbance was recorded over 120 minutes. The spectra did not change significantly (Figure 2.5), which indicated fast kinetics and allowed a dynamic titration to be carried out.
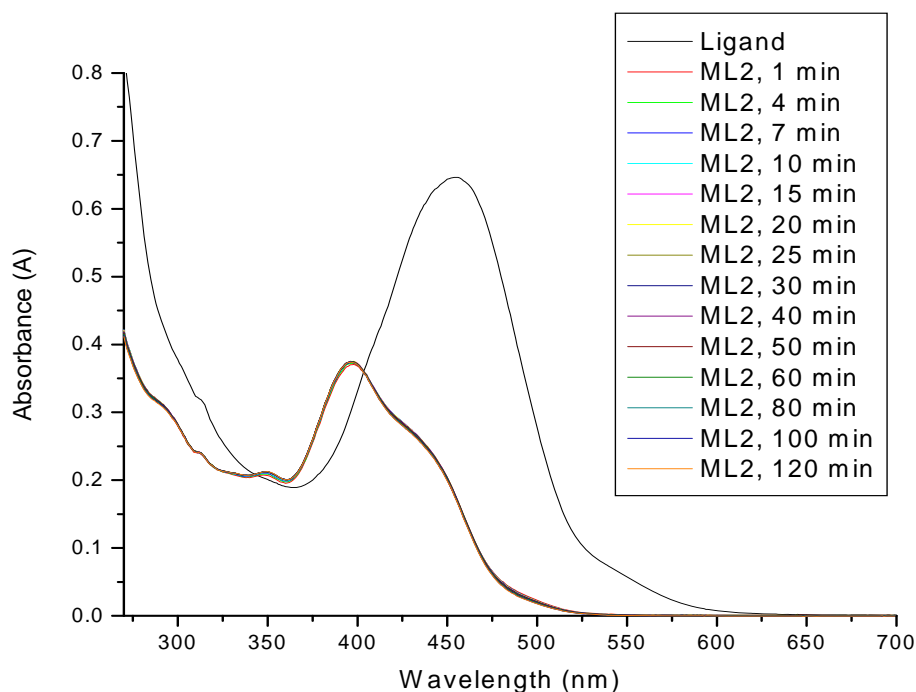
Figure 2.5. UV-Vis absorbance of a 1:2 mixture of Nd^{3+} and tetrabromodimethylsalophen.

A dynamic titration of the potassium salt of tetrabromodimethylsalophen with $Nd(OTf)_3 \cdot 6H_2O$ were performed in DMSO (Figure 2.6). The change of the absorbance at 398 nm and 498 nm indicate a breaking point at metal/ligand ratio of 1:4, which is different from the expected position of 1:2. Data analysis with SPECFIT program also gave similar result. The titration data were best fitted with ML, ML_2 and ML_4 model.

29

(a)

(b)
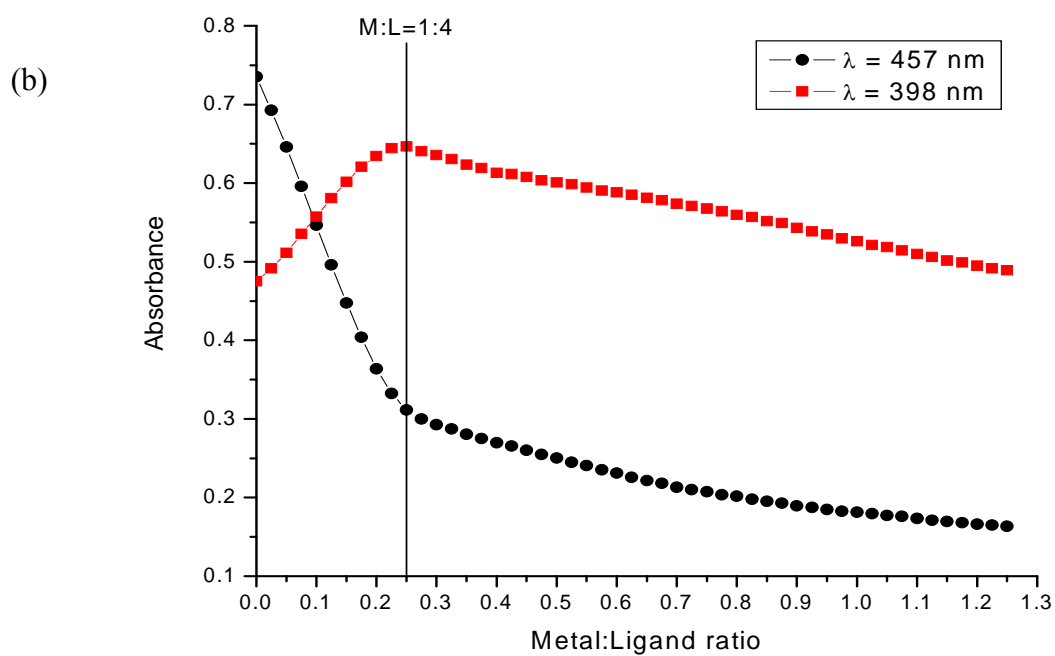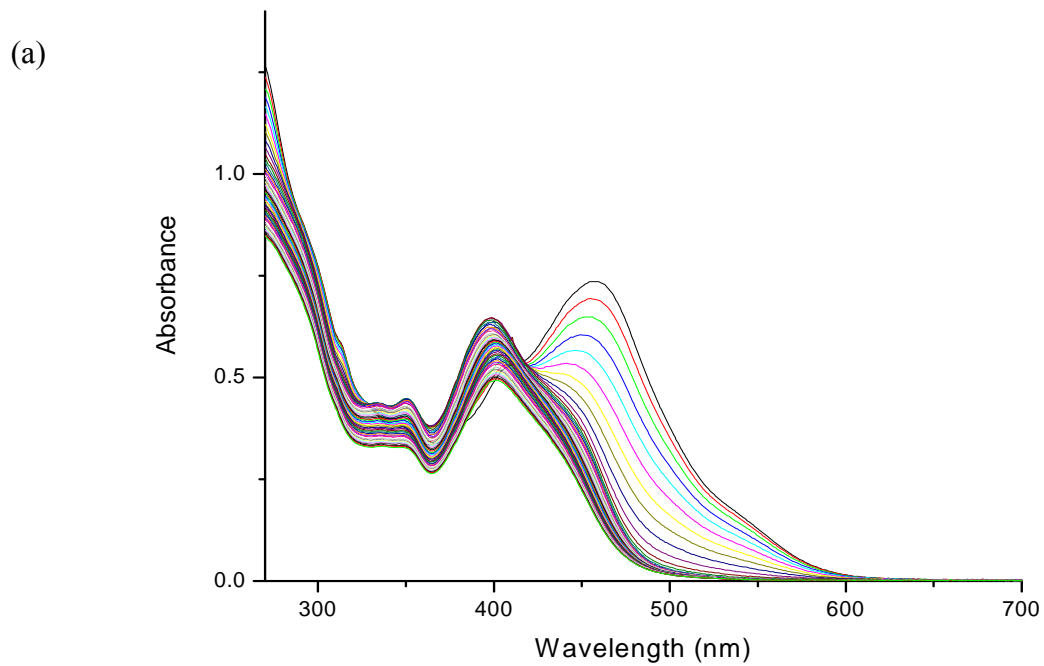
Figure 2.6. Dynamic titration of tetrabromodimethylsalophen with $Nd(OTf)_3 \cdot 6H_2O$ (a) Absorbance spectra;

(b) Absorbance at selected wavelengths vs. metal/ligand ratio.

30

Though there was little change of the spectra in the kinetic study (Figure 2.5), it is possible that the formed complex is not the most thermodynamically stable species in a dynamic titration. The titration of tetrabromodimethylsalophen was repeated in the batch titration method, expecting the most stable form of the complex can be present in solution. Total 31 batches of solution were prepared in DMSO with the concentration of the ligand maintained at 2.50×10^{-5} M and the metal/ligand ratio were varied from 0:1 to 1.5:1 equivalents (Figure 2.7).
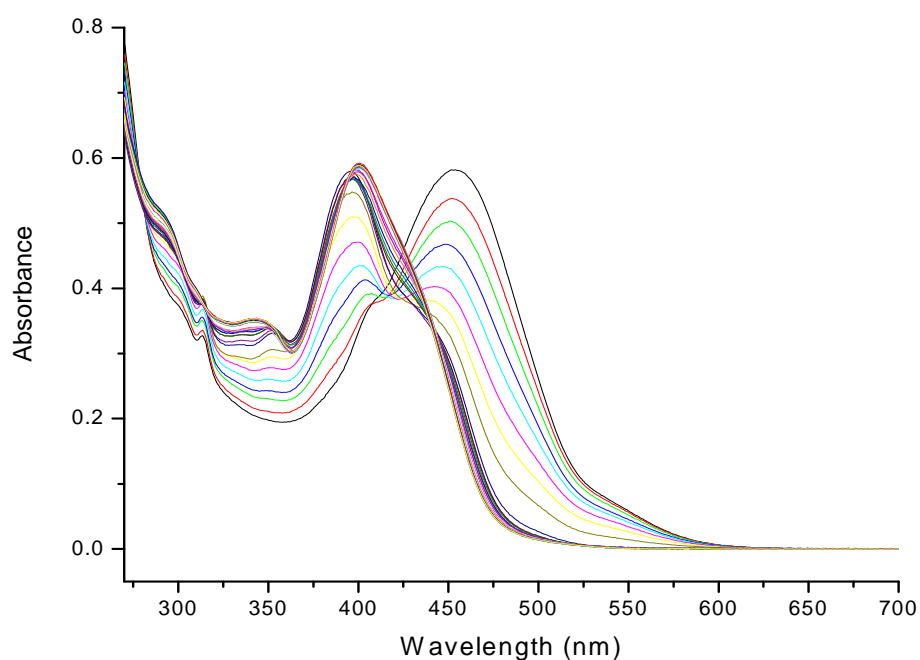
Figure 2.7. Absorbance spectra of the batch titration of tetrabromodimethylsalophen with $Nd(OTf)_3 \cdot 6H_2O$.

The change of the absorbance at 485 nm has a breaking point at metal/ligand ratio of 2:5 (Figure 2.8). The titration data were best fitted with ML, ML_2, ML_3 and ML_4 model in the data analysis with SPECFIT program. A repeated batch titration with another 36 batches of solution gave identical results.
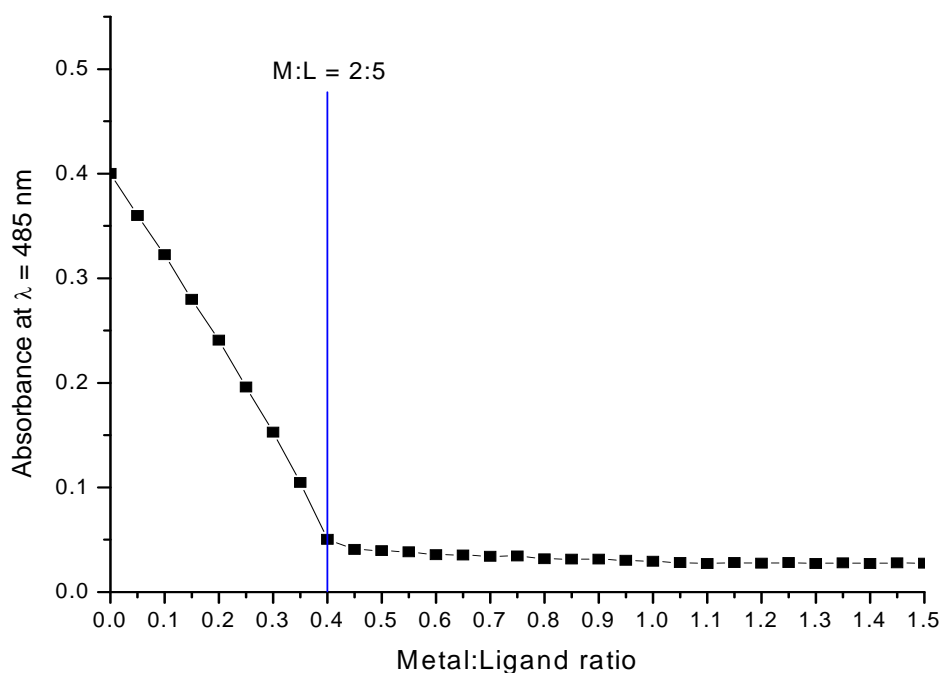
Figure 2.8. Absorbance at selected wavelength vs. metal/ligand ratio of the batch titration of tetrabromo-dimethylsalophen with $Nd(OTf)_3 \cdot 6H_2O$.

The breaking points in the dynamic titration and in the batch titration appeared at different positions, 1:4 metal/ligand ratio and 1:2.5 metal/ligand ratios, respectively. However, it seems that the ML_4 complex is formed in both cases, according to the SPECFIT analysis of the experimental data. Since it is sterically challenging to form ML_4 complex with four salophen ligands, a different binding mode can be involved. A possible explanation of this result is the cyclization of the ligand (Figure 2.9). It is well-known that salophen can rearrange to form 2-substituted benzimidazole, the cyclized structure.[90] In some cases, 2-substituted benzimidazole is the major product from the reaction between *o*-phenylenediamine and aldehydes.[91] Since 2-substituted benzimidazole coordinates to the metal with nitrogen on imidazole, the ML_4 complex

32

can be formed. As shown in the mechanism (Figure 2.9), the rearrangement from salophen to benzimidazole is accelerated in presence of acidic proton. In order to prevent the protonation to the salophen, excess organic bases were added to the solution and a batch titration was repeated.
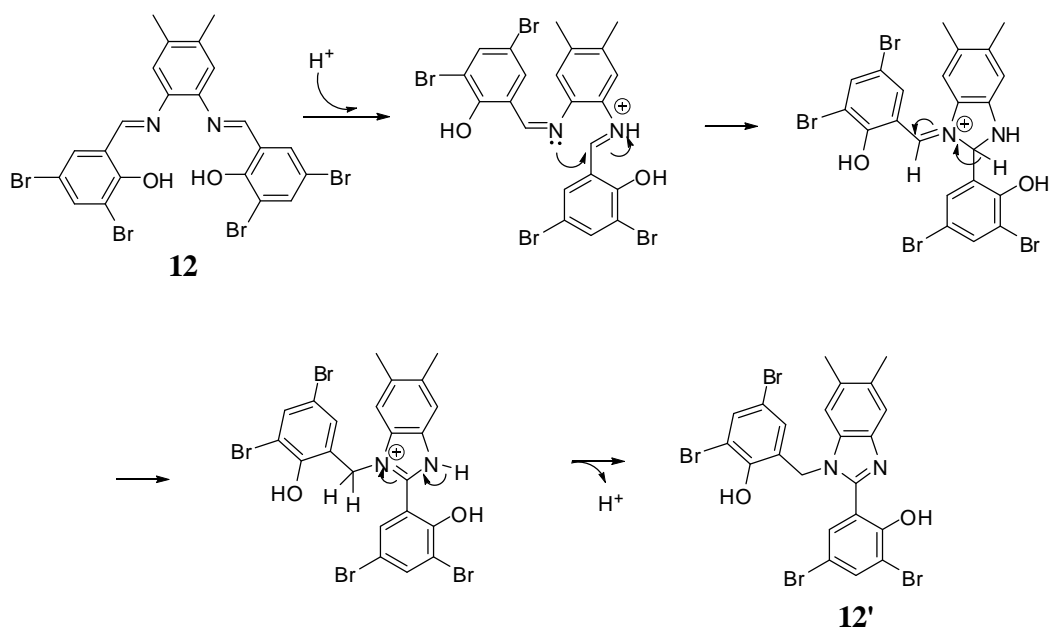
Figure 2.9. Proposed mechanism of cyclization of the salophen ligand.

2,4,6-Collidine (2,4,6-trimethylpyridine), whose pKa is 7.45, was chosen as the base. Total 22 batches of solution were made using 0.00117 M of 2,4,6-collidine in DMSO solution as the solvent. The concentration of the ligand was maintained at 2.50×10^{-5} M and the metal/ligand ratio were varied from 0:1 to 1.2:1 equivalents. The result of the titration is shown in Figure 2.10. No breaking points were apparent (Figure 2.10(b)) and the spectra continue to change throughout the whole titration process.
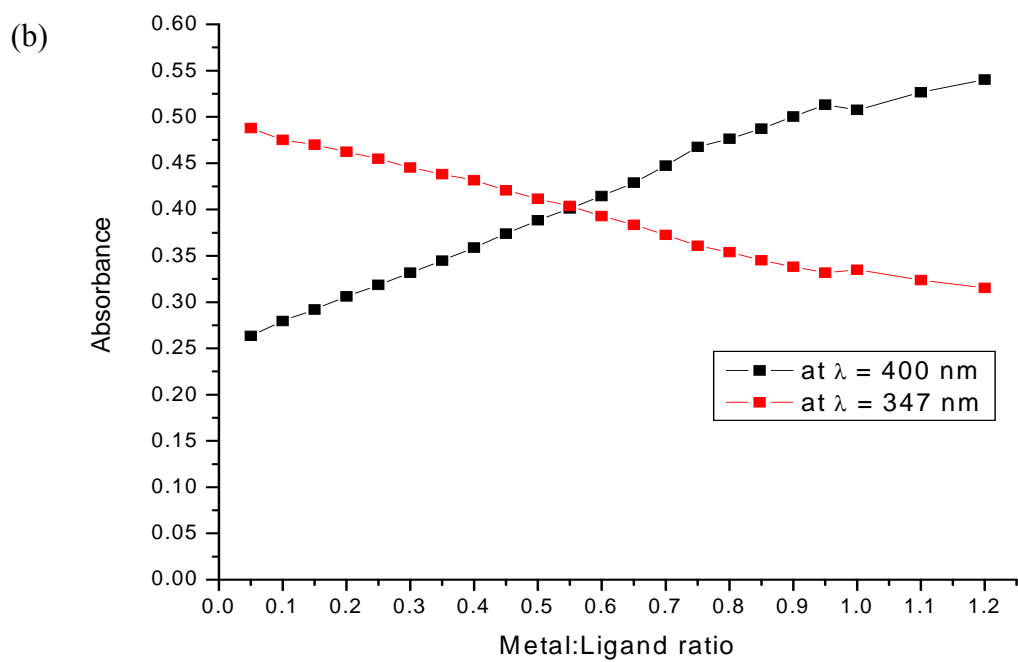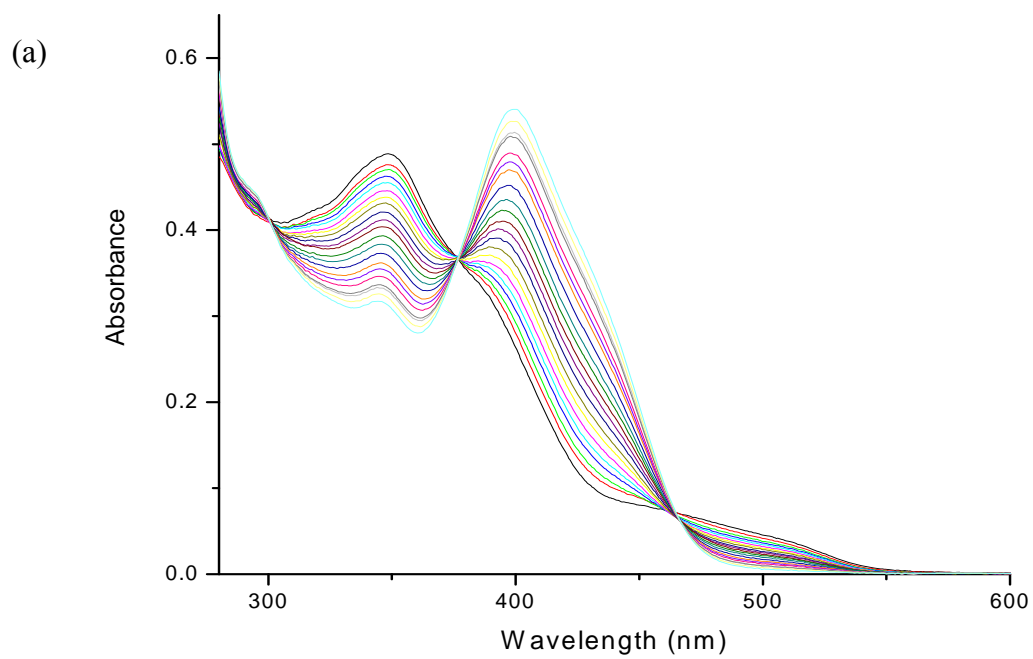
Figure 2.10. Batch titration of tetrabromodimethylsalophen with Nd(OTf)$_3$·6H$_2$O, using collidine as a base (a)
Absorbance spectra; (b) Absorbance at selected wavelengths vs. metal/ligand ratio.

When KOH or K_2CO_3 was used as a base, the ^1H-NMR spectrum of the ligand changed. With 2,4,6-collidine, there is no change in the spectrum of the ligand (Figure 2.11), indicating 2,4,6-collidine is not basic enough to deprotonate the ligand.
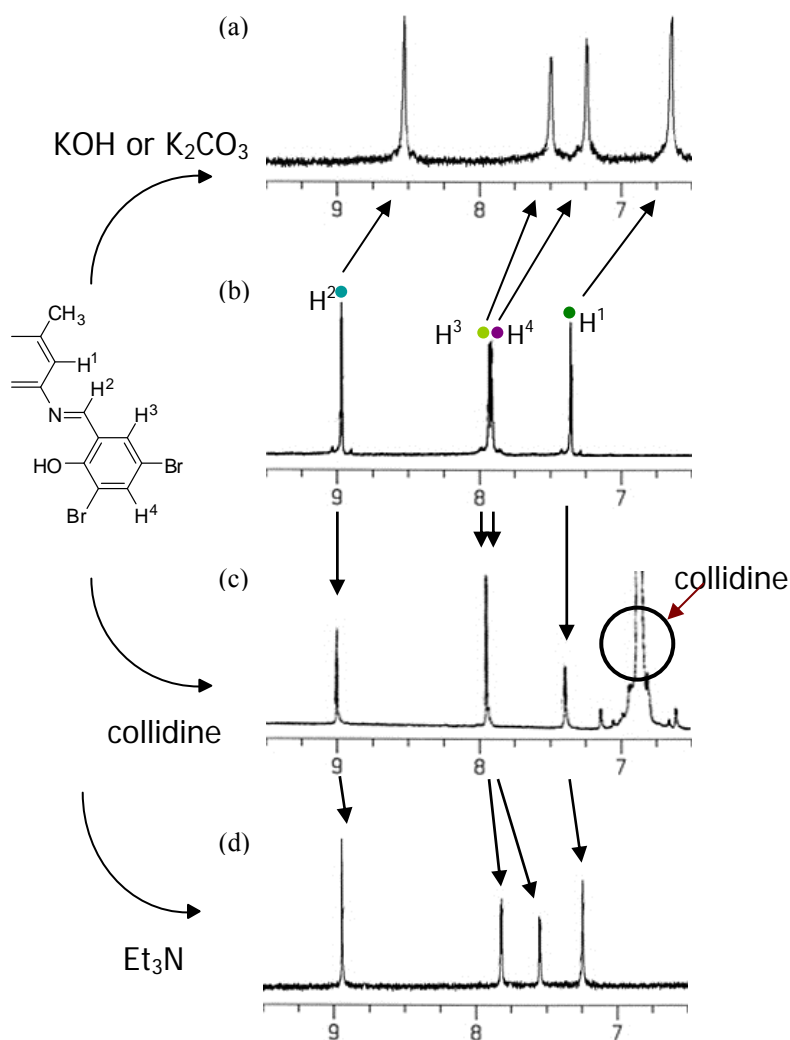
Figure 2.11. Partial ^1H-NMR spectra of (a) Tetrabromodimethylsalophen + KOH or K_2CO_3; (b) Tetrabromo-dimethylsalophen; (c) Tetrabromodimethylsalophen + 2,4,6-collidine; (d) Tetrabromodimethyl-salophen + Et$_3$N.

35

Triethylamine, Et$_3$N, whose pKa is 10.78, is a stronger base than collidine. The ^{1}H-NMR spectrum of the ligand with Et$_3$N looks similar to those of the ligand with KOH or K$_2$CO$_3$, which is showing that the basicity of Et$_3$N is sufficient to deprotonate the ligand (Figure 2.11(d)). The batch titration was repeated with Et$_3$N as a base. Total 22 batches of solution were made using DMSO as a solvent. Due to the volatility of Et$_3$N, Et$_3$N solution in DMSO cannot be made. Instead, 5 μL of Et$_3$N were added to the each batch solutions before the titration. The concentration of the ligand maintained at 2.50×10^{-5} M and the metal/ligand ratio were varied from 0:1 to 1.2:1 equivalents.
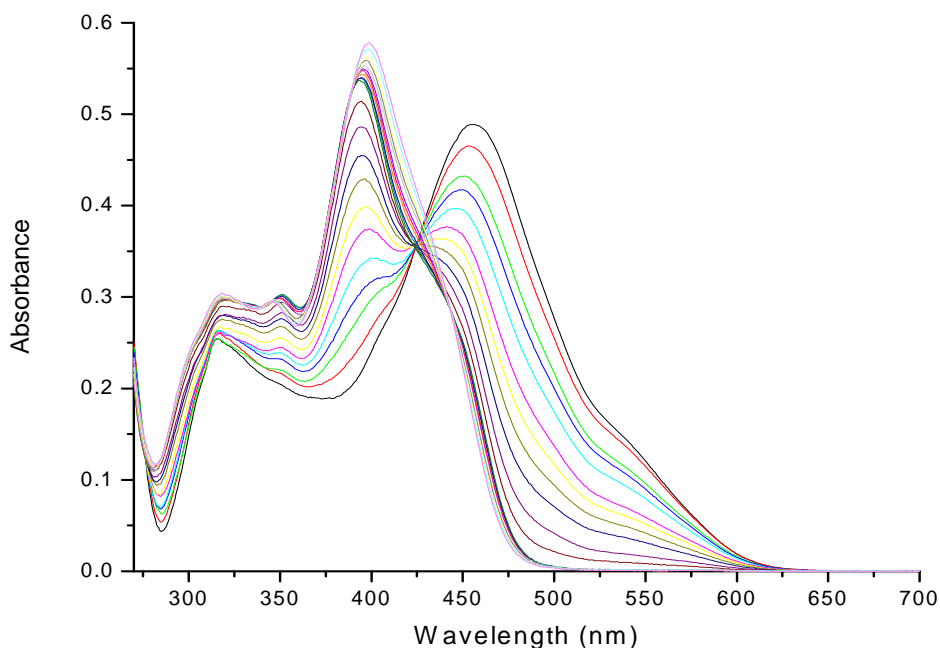
Figure 2.12. Absorbance spectra of the batch titration of tetrabromodimethylsalophen with Nd(OTf)$_3$·6H$_2$O using Et$_3$N as a base.
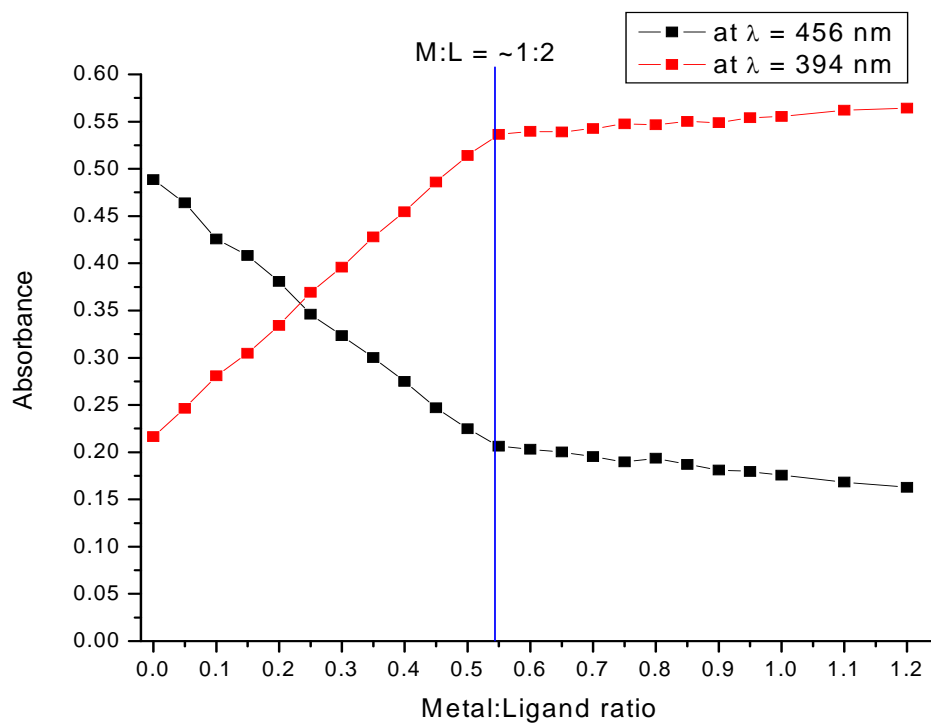
Figure 2.13. Absorbance at selected wavelength vs. metal/ligand ratio of the batch titration of tetrabromo-dimethylsalophen with $Nd(OTf)_3 \cdot 6H_2O$ using Et_3N as a base.

The change of absorbance at selected wavelengths has breaking points at metal/ligand ratio of ~1:2, indicating the formation of ML_2 complex (Figure 2.13). This titration data was analyzed using SPECFIT program (Figure 2.14). The data were well fitted with ML and ML_2 model. The logarithm of the stability constants were $\log\beta_1 = 9.1 \pm 0.5$ and $\log\beta_2 = 16.2 \pm 0.6$, respectively.

(a)

(b)
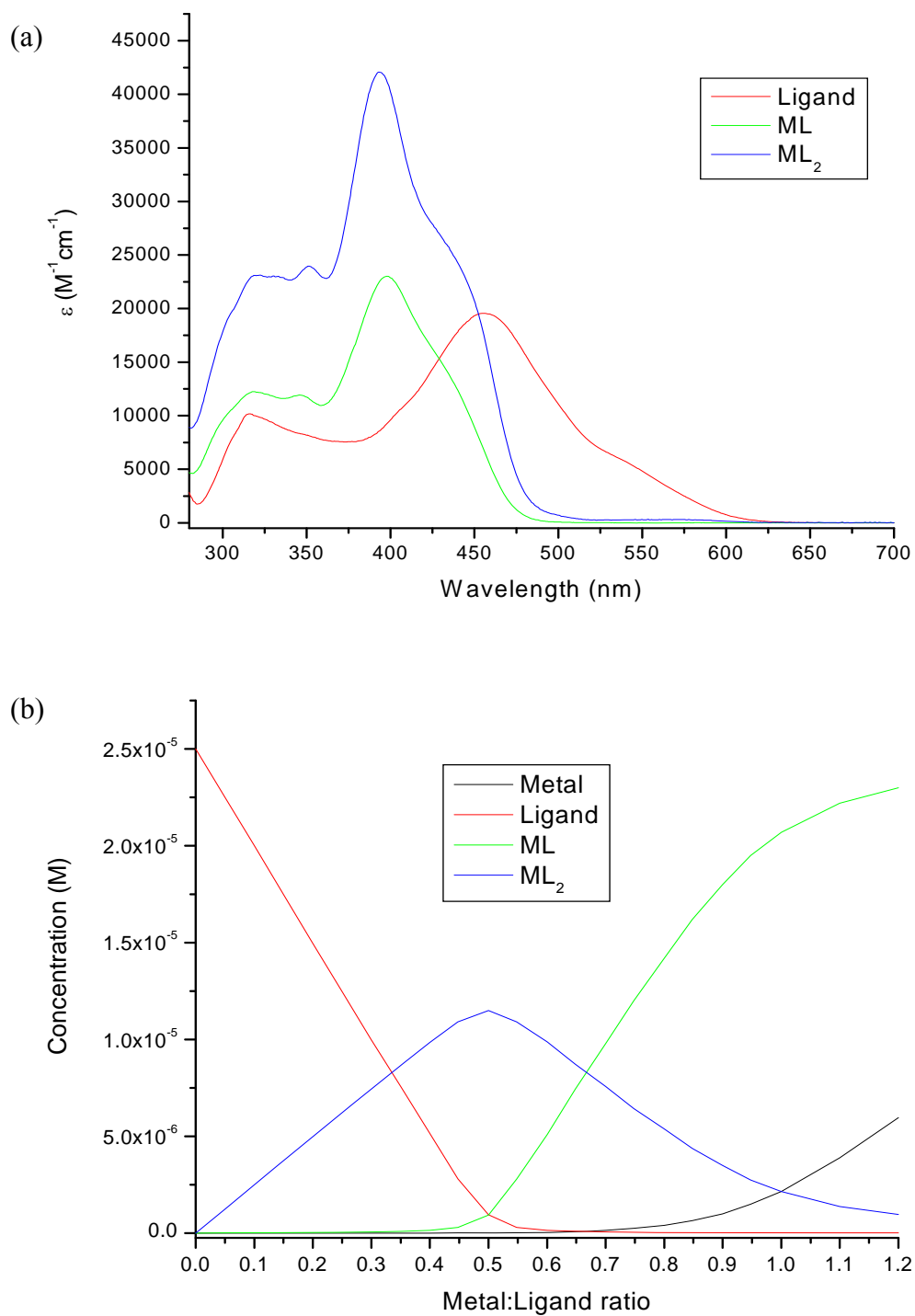
Figure 2.14 Results of spectrophotometric titration of dimethylsalophen with Nd^{3+} (a) Calculated spectra for the three individual species; (b) Calculated concentrations of different species versus metal/ligand ratio.

38

2.3.3.3 3,3'-dibromodimethylsalophen (9)

A batch titration of 3,3'-dibromodimethylsalophen (**9**) with $Nd(OTf)_3 \cdot 6H_2O$ was carried out with the same method used for tetrabromodimethylsalophen. Total 22 batches of solution were made using DMSO as a solvent. An amount of 5 μL of Et_3N was added to each batch solutions before the titration. The concentration of the ligand was maintained at 2.50×10^{-5} M and the metal/ligand ratio were varied from 0:1 to 1.2:1 equivalents.

The changes of absorbance at selected wavelengths have breaking points at metal/ligand ratio of ~1:2, indicating the formation of ML_2 complex (Figure 2.16). Experimental data obtained from this titration were analyzed using SPECFIT program. The data were well fitted with ML and ML_2 model. The logarithm of the stability constants were $\log\beta_1 = 6.0 \pm 0.6$ and $\log\beta_2 = 12.9 \pm 0.5$, respectively.
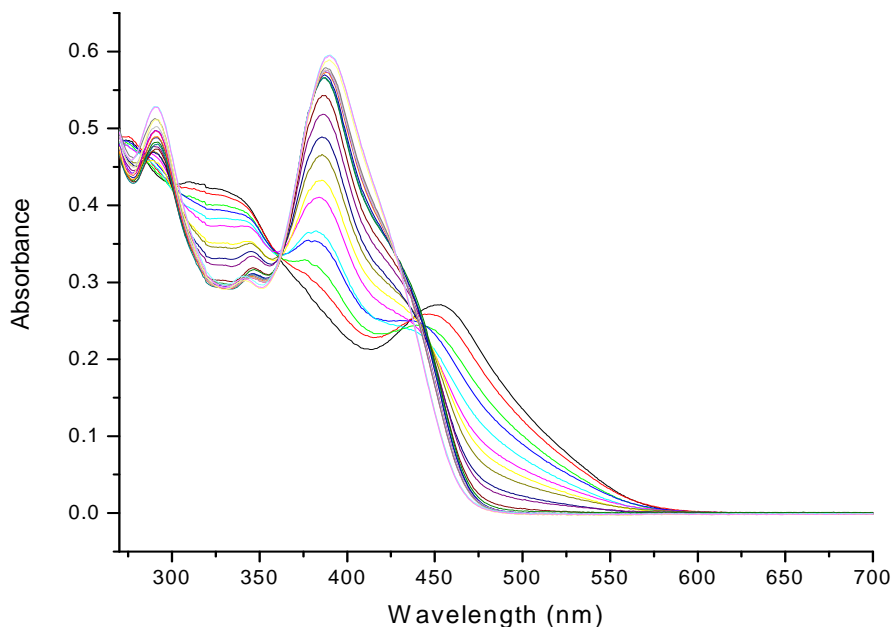
Figure 2.15. Absorbance spectra of the batch titration of 3,3'-dibromodimethylsalophen with $Nd(OTf)_3 \cdot 6H_2O$ using Et_3N as a base.
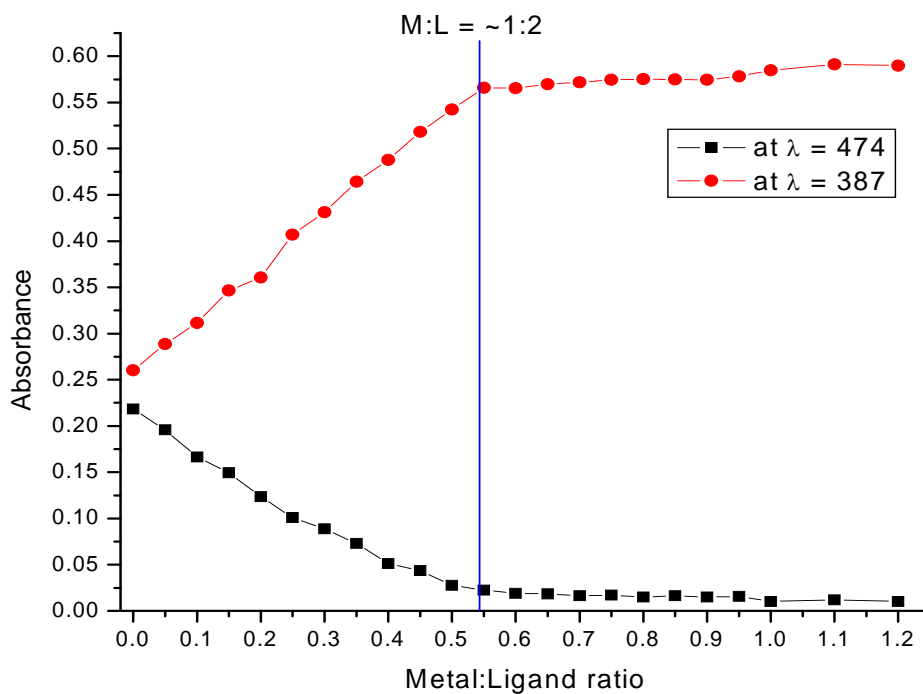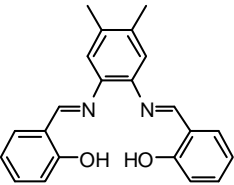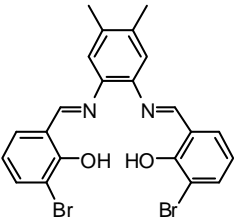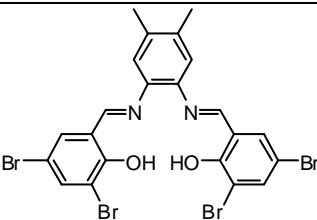
Figure 2.16. Absorbance at selected wavelength vs. metal/ligand ratio of the batch titration of 3,3'-dibromodimethylsalophen with $Nd(OTf)_3 \cdot 6H_2O$ using Et_3N as a base.

2.3.3.4 Summary of the stability constant measurements

The stability constants for three salophen ligands and Nd^{3+}, obtained from the data analysis using SPECFIT program, are summarized in table 3.2. For dimethylsalophen (**3**), KOH was used as a base, and Et_3N was used as a base for tetrabromodimethylsalophen (**12**) and 3,3'-dibromodimethylsalophen (**9**). The titration of dimethylsalophen (**3**) with Nd^{3+} using Et_3N as a base was also tested, but due to the nature of the ligand and Et_3N, no meaningful results could be obtained. This will be discussed in Section 2.3.4.

When stability constants for **9** and **12** are compared, it is evident that the more bromo groups are on the ligand, the higher the stability constant is. The attached bromo groups can provide electrons to the salophen molecule, which make the ligand more electron-rich, acting as stronger ligand for the Nd^{3+} metal. Due to the difference in natures of the counter cations, it is not possible to compare the stability constant for **3** and those for **9** or **12** directly. The first stability constant, K_1 is related to the dissociation of the ion pair of counter cation and anion of the ligand. However, in the second step of the complexation, $ML + L \rightarrow ML_2$, the effect of the counter cation is less important than for the first step, because the ligand is already bound to Nd^{3+} ion.

Table 2.2. Stability constants for the Nd^{3+} complexes of salophen ligands. All values were calculated with SPECFIT program using titration data of the ligand with Nd^{3+}.

Ligand	Counter Cation	$\log\beta_1$ $(\log K_1)$	$\log\beta_2$	$\log K_2$ $(\log\beta_2\text{-}\log\beta_1)$
3	K^+	10	16	6
9	Et_3NH^+	6.0	12.9	6.9
12	Et_3NH^+	9.1	16.2	7.1

The stability constant for the second step, K_2 can be calculated from β_2 and β_1. The values are 6, 6.9 and 7.1 for **3**, **9** and **12**, respectively. This result leads to the same conclusion stated above, that more bromo groups on the ligand leads to stable complexes.

2.3.4 Crystal structures of the complexes

2.3.4.1 Crystal structure of Nd-tetrabromodimethylsalophen (12)

Crystallographic grade sample of Nd-tetrabromodimethylsalophen (**12**) was prepared by following method: to a suspension of a ligand in MeOH, excess Et_3N was added. A half equivalent of $Nd(OTf)_3\cdot 6H_2O$ was added to the ligand solution. Hexane was slowly diffused to the solution.

The crystal was formed as $Et_3NH[Nd(TBDMSal)_2]$. The molecular structure of the complex is shown in Figure 2.17, and the selected bond lengths and angles for this complex are listed in Table 2.3. Complete data and parameters are available in Appendix A. The molecular structure of the obtained crystals can be described as a double-decker sandwich. There is one previous example of lanthanide complex with salophen derivative ligand, which adopts such a double-decker sandwich conformation.[92] This complex is formed by the coordination of one Ce^{4+} as metal cation with two salophen as ligand. It is interesting to note that the lanthanide cation coordinated in this complex has a different oxidation state and therefore cannot be considered as similar. In addition to the difference in charge, Ce^{4+} has a significantly different effective ionic radius: 0.97Å for Ce^{4+} versus 1.109 Å for Nd^{3+} (both calculated according to Shannon for eight coordinated cations).[93]
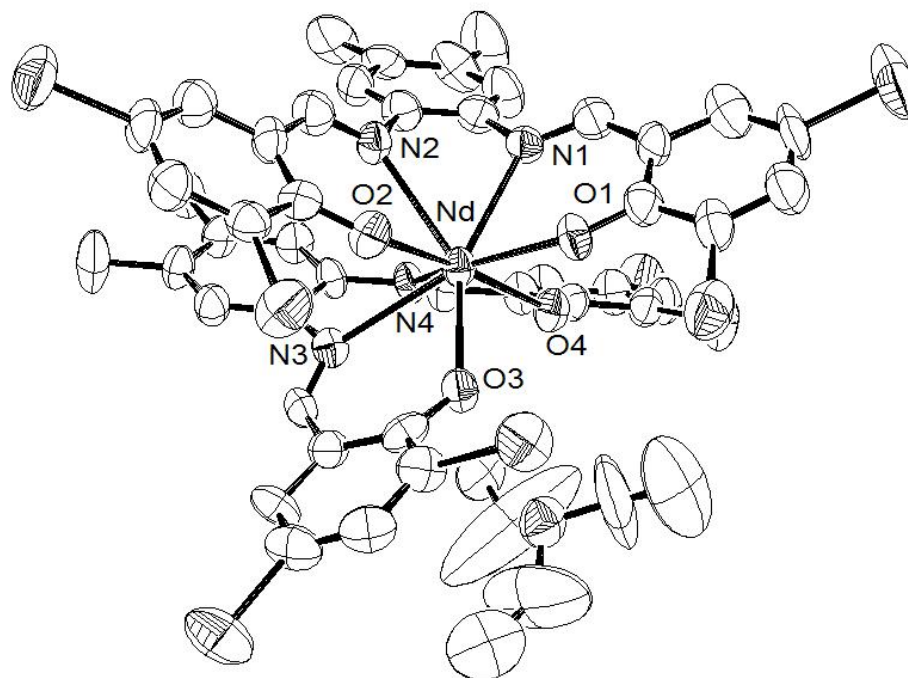
Figure 2.17. Molecular structure of $Et_3NH[Nd(TBDMSal)_2]$.

Table 2.3. Selected bond lengths (Å) and angles (°) in $Et_3NH[Nd(TBDMSal)_2]$

Nd-O(1)	2.327(6)	O(1)-Nd-O(2)	94.9(2)
Nd-O(2)	2.353(6)	O(2)-Nd-N(2)	68.0(2)
Nd-O(3)	2.367(6)	N(2)-Nd-N(1)	60.6(2)
Nd-O(4)	2.345(6)	N(1)-Nd-O(1)	69.6(2)
Nd-N(1)	2.629(7)	O(3)-Nd-O(4)	91.3(2)
Nd-N(2)	2.672(8)	O(4)-Nd-N(4)	66.8(2)
Nd-N(3)	2.678(7)	N(4)-Nd-N(3)	60.4(2)
Nd-N(4)	2.689(8)	N(3)-Nd-O(3)	68.6(2)

Two salophen ligands coordinate to the metal center in a tetradentate mode. The salicylidene arms are bent toward the exterior of the molecule. When a salophen ligand

coordinate to Nd^{3+}, one 5-membered ring, Nd-N(1)-C(8)-C(13)-N(2) and two six-membered

rings, Nd-N(1)-C(7)-C(6)-C(1)-O(1) and Nd-N(2)-C(14)-C(15)-C(20)-O(2) are formed (Figure

2.18). The salicylidene arms are bent to make these rings as planar as possible.
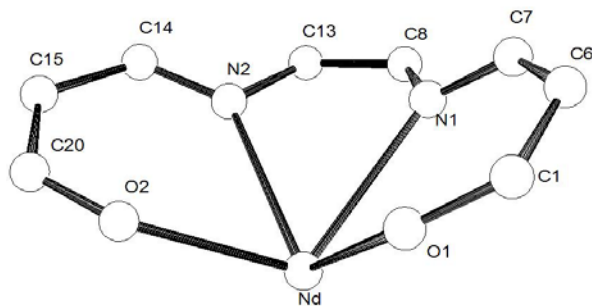
Figure 2.18. 5- and 6-membered rings formed by coordination of ligand to Nd^{3+}.

Since $[Nd(TBDMSal)_2]^-$ complex has net (−1) charge, Et_3NH^+ acts as a counter cation. In

the crystal packing structure (Figure 2.19), Et_3NH^+ is located in the space between two

$[Nd(TBDMSal)_2]^-$. Et_3NH^+ is another factor that may cause bending of the salophen ligand.

Molecules and ions are closely packed together to have minimal energy in a crystal. The bent

salicylidene arms can provide the space to accommodate the relatively larger Et_3NH^+ cation in

the crystal packing structure of $Et_3NH[Nd(TBDMSal)_2]$. The effect of the cation on the crystal

structure will be verified by growth and analysis of the crystal of TBDMSal complex with

smaller cations, such as Li^+.

When viewed from the orthogonal to the salophen plane, two salophen ligands are

located in staggered fashion. The coordination environment around Nd^{3+} cation is close to a

square antiprism geometry (Figure 2.20). Atoms O(1), O(2), N(2) and N(1) form a nearly planar

coordination ring, and atoms O(3), O(4), N(4) and N(3) also form a nearly planar coordination

ring. However, these coordination rings are trapezoids: O–O segments are longer than N–N

segments. Because two nitrogens, N(1) and N(2) (or N(3) and N(4)), are on the same phenylene ring, there is no flexibility around nitrogens, but relatively flexible oxygens can be widened. The Nd-O bonds are shorter than Nd-N bonds. This make the two planes, O(1)-O(2)-N(2)-N(1) and O(3)-O(4)-N(4)-N(3), not perfectly parallel.
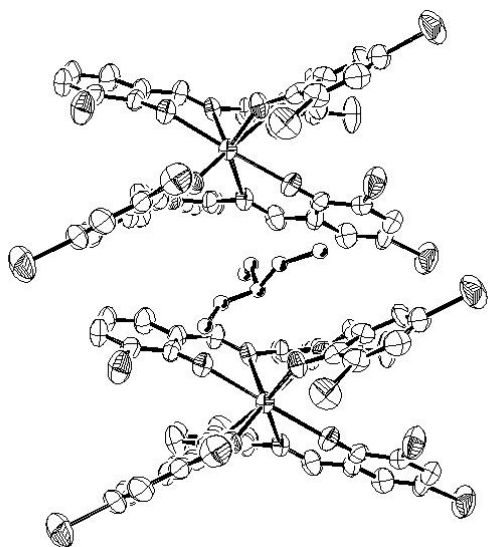
Figure 2.19. Et_3NH^+ in crystal packing structure of $Et_3NH[Nd(TBDMSal)_2]$.
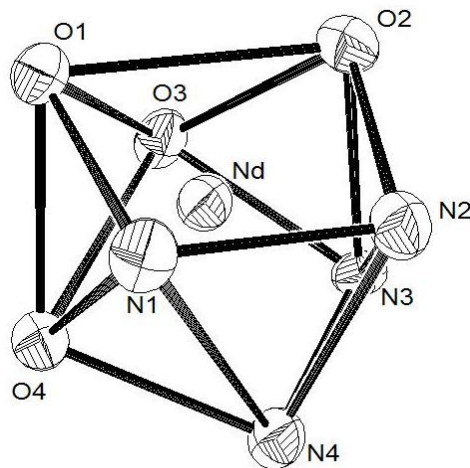
Figure 2.20. Coordination polyhedron of Nd in $Et_3NH[Nd(TBDMSal)_2]$.

2.3.4.2 Crystal structure of Nd-dimethylsalophen (3)

Crystallographic grade sample of Nd-DMSal (**3**) was obtained by same method applied to that of Nd-TBDMSal, mixing one equivalent of Nd^{3+} and two equivalents of DMSal in MeOH with excess Et_3N. An M_2L_3 structure, i.e. $Nd_2(DMSal)_3 \cdot MeOH$ was isolated. An almost identical structure was obtained for $Eu_2(Sal)_3 \cdot MeOH$ in our group.[86] The molecular structure of the complex is shown in Figure 2.21, and the selected bond lengths and angles for this complex are listed in Table 2.4. Complete data and parameters are available in Appendix A.

DMSal2 acts as a bridging ligand connecting two Nd^{3+} ions. This structure was postulated (but not characterized) by Archer *et. al.* for the similar structure of Ln^{3+}.[94] It is interesting that three ligands are not located on the same axis. DMSal1 and Nd(1) is out of the line formed by [the center of DMSal2] − Nd(2) − [the center of DMSal3]. Two nitrogens of DMSal2 are only coordinated to Nd(2) not to Nd(1). Because nitrogen has only one lone pair to coordinate to the metal ion, while oxygen has two or three lone pairs, nitrogen can bind only one metal ion. Thus Nd(1) cannot be located on the center of DMSal2. It is coordinated to two oxygens of DMSal2 and two oxygens and two nitrogens of DMSal1. To fill the empty coordination site, solvent MeOH is bound to Nd(1). The same coordination patterns, two salophen ligands form an eight-coordinated metal complex and additional metal ions and salophen ligands are located out of the axis forming 7- or 8-coordination with one or two solvent molecules, are observed in triple-decker or tetra-decker structures of Ln^{3+} complexes reported.[86, 95-97]
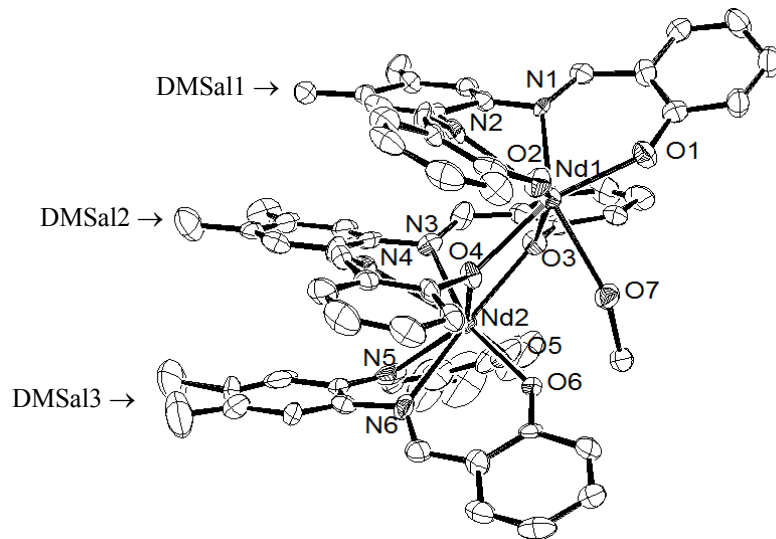
Figure 2.21. Molecular structure of $Nd_2(DMSal)_3 \cdot MeOH$.
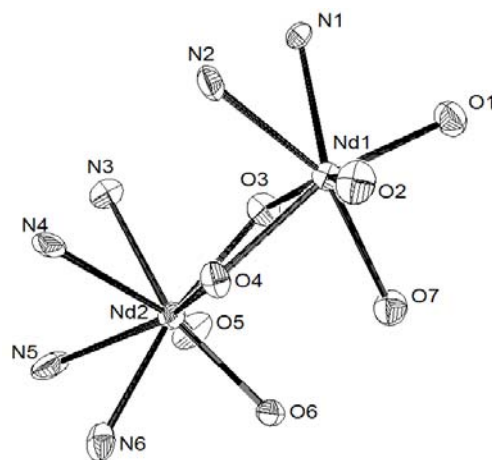
Figure 2.22. Coordination environment around two Nd^{3+} ions in $Nd_2(DMSal)_3 \cdot MeOH$.
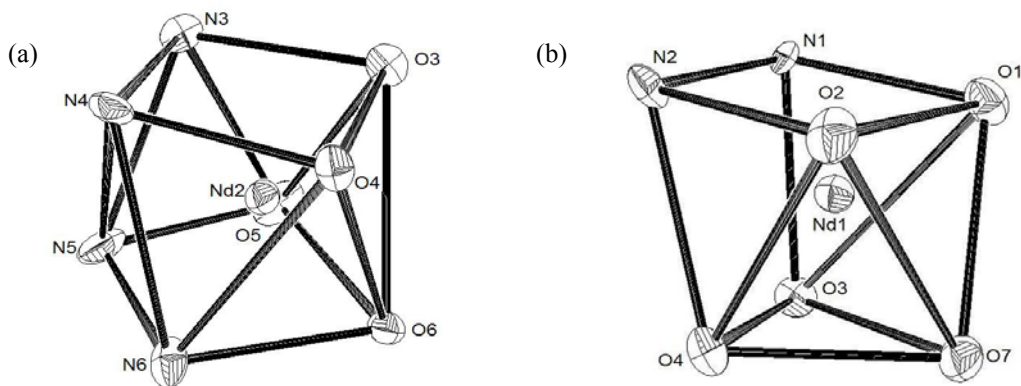
Figure 2.23. Coordination polyhedron of (a) Nd(2); (b) Nd(1).

47

Table 2.4. Selected bond lengths (Å) and angles (°) in $Nd_2(DMSal)_3 \cdot MeOH$.

Nd(1)-O(1)	2.271(8)	O(1)-Nd(1)-O(2)	97.2(3)
Nd(1)-O(2)	2.253(8)	O(2)-Nd(1)-N(2)	72.1(3)
Nd(1)-N(1)	2.545(9)	N(2)-Nd(1)-N(1)	63.4(3)
Nd(1)-N(2)	2.552(10)	N(1)-Nd(1)-O(1)	71.6(3)
Nd(1)-O(3)	2.476(8)	O(3)-Nd(1)-O(4)	69.7(3)
Nd(1)-O(4)	2.409(8)	O(3)-Nd(1)-O(7)	75.8(3)
Nd(1)-O(7)	2.459(10)	O(7)-Nd(1)-O(4)	75.8(3)
Nd(2)-O(3)	2.409(8)	O(3)-Nd(2)-O(4)	70.8(3)
Nd(2)-O(4)	2.410(8)	O(4)-Nd(2)-N(4)	68.1(3)
Nd(2)-N(3)	2.598(10)	N(4)-Nd(2)-N(3)	60.4(3)
Nd(2)-N(4)	2.679(10)	N(3)-Nd(2)-O(3)	69.4(3)
Nd(2)-O(5)	2.313(8)	O(5)-Nd(2)-O(6)	90.9(3)
Nd(2)-O(6)	2.365(8)	O(6)-Nd(2)-N(6)	71.2(3)
Nd(2)-N(5)	2.573(11)	N(6)-Nd(2)-N(5)	62.3(3)
Nd(2)-N(6)	2.575(10)	N(5)-Nd(2)-O(5)	70.0(4)
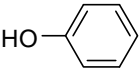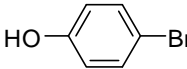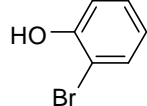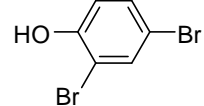
The stoichiometry of this complex is 1:2 in solution, but a different stoichiometry is observed in solid phase. Because the net charge of ML_2 complex is (−1), there must be a counter cation to form ML_2 structure. There is no counter cation in the structure of $Nd_2(DMSal)_3$, while Et_3NH^+ exists as counter cation in the structure of $Nd(TBDMSal)_2$. Without counter cation, trivalent Nd^{3+} and divalent $DMSal^{2-}$ forms M_2L_3 complex. This indicates that Et_3N can not act as a base in the solution of Nd^{3+} and DMSal during the crystal growing process. Investigation of the acidities of salophen ligands can provide information of whether Et_3N is basic enough to deprotonate salophen ligands. Since the pK_a values of these salophen derivatives are unknown,

two types of tests were carried out to compare the relative acidities of the salophen ligands: ^{1}H-NMR and UV-Vis absorbance.

^{1}H-NMR spectra of four salophen ligands, DMSal (**3**), 5BDMSal (**6**), 3BDMSal (**9**) and TBDMSal (**12**) were recorded in DMSO-d_6 with and without an excess of Et$_3$N. The chemical shifts of TBDMSal was changed after addition of Et$_3$N as mentioned in section 2.3.3, but no or very small changes were observed in those of DMSal, 5BDMSal and 3BDMSal. This result supports that TBDMSal can be ionized by Et$_3$N, but DMSal cannot be ionized.

UV-Vis absorbances of four salophen were recorded in DMSO, and after excess Et$_3$N was added the absorbances were recorded again (Figure 2.24). The absorbances of 3BDMSal and TBDMSal showed a significant change after Et$_3$N was added indicating the deprotonation of the ligands, while those of DMSal and 5BDMSal do not change after addition of Et$_3$N. From this result, it can be concluded that Et$_3$N can deprotonate more acidic 3BDMSal and TBDMSal ligands, but it is not sufficiently basic to deprotonate less acidic DMSal and 5BDMSal ligands. This trend of the acidities of salophen derivatives is consistent with that of acidities of phenol derivatives (Table 2.5). In order to obtain ML$_2$ structure of Nd-DMSal, crystal growth was attempted using more basic KOH as base, but it was not possible to isolate any crystals.

Table 2.5. pK_a of phenol derivatives[98]

Phenol derivatives	HO⟨⟩	HO⟨⟩—Br	HO—⟨⟩ (Br)	HO—⟨⟩—Br (Br)
pK_a	9.994	9.366	8.452	7.790

Figure 2.24. UV-Vis absorbance of salophen ligands without Et$_3$N (solid line) and with excess Et$_3$N (dashed line). (a) DMSal, c = 3.77×10^{-5} M in DMSO; (b) 5BDMSal, c = 4.08×10^{-5} M in DMSO; (c) 3BDMSal, c = 3.92×10^{-5} M in DMSO; (d) TBDMSal, c = 3.84×10^{-5} M in DMSO.

2.3.4.3 Crystal structure of Yb-3,3'-dibromodimethylsalophen (9)

There are two major coordination environments around the Ln^{3+} cation in the ML$_2$ complexes with a coordination number of eight: square antiprism (sandwich) and dodecahedron (interlock).[99] Though there are many reported sandwich structures of the complexes of salophen ligands and lanthanides,[92] the example of dodecahedral structures is limited. Kubono *et. al.*

50

reported a dodecahedral structure of Ce^{4+} complex with dibromo-salophen ligand.[100] The factors that determine the orientation of the ligands are the size of metal and the flexibility of the ligand. The reported dodecahedral structures of metal complexes of Schiff base ligands have either (1) small metal ion such as Zr^{4+} or Ce^{4+} or (2) flexible ligand such as salen.[92]

Because of the highly conjugated structure, it is hard to modify the flexibility of salophen ligand. In order to obtain a dodecahedral structure of Ln^{3+}–salophen complex, the smallest NIR-emitting lanthanide, Yb^{3+} was chosen and a crystal of the complex was grown with a series of salophen ligands by the same method applied to other Nd complexes. An interlock structure of $Et_3NH[Yb(3BDMSal)_2]$ was successfully isolated (Figure 2.25). Selected bond lengths and angles are listed in Table 2.6. As discussed in section 2.3.3.1, the salophen ligands were bent to minimize strains of the 5- and 6-membered rings formed around the Yb^{3+} ion. The counter cation Et_3NH is located in the widened space between two salophen ligands (Figure 2.25(b)). The coordination environment around the Yb^{3+} cation is a dodecahedral structure with D_{2d} symmetry (Figure 2.26). The bond lengths and angles are also very symmetrical. This Yb^{3+} complex confirms that the main structure controlling parameter can be attributed to the size of metal ion.
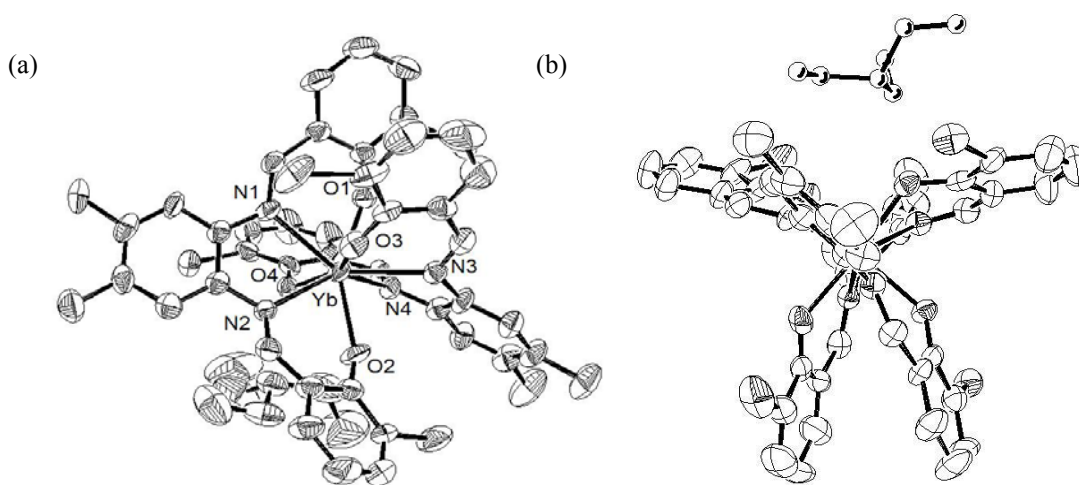
Figure 2.25. Molecular structure of $Et_3NH[Yb(3BDMSal)_2]$.

Table 2.6. Selected bond lengths (Å) and angles (°) in Et₃NH[Yb(3BDMSal)₂]

Yb-O(1)	2.208(5)	O(1)-Yb-O(2)	148.5(2)
Yb-O(2)	2.228(5)	O(2)-Yb-N(2)	71.2(2)
Yb-O(3)	2.216(5)	N(2)-Yb-N(1)	66.7(2)
Yb-O(4)	2.261(6)	N(1)-Yb-O(1)	72.9(2)
Yb-N(1)	2.495(6)	O(3)-Yb-O(4)	152.50(19)
Yb-N(2)	2.480(6)	O(4)-Yb-N(4)	71.1(2)
Yb-N(3)	2.509(6)	N(4)-Yb-N(3)	65.0(2)
Yb-N(4)	2.491(6)	N(3)-Yb-O(3)	71.5(2)
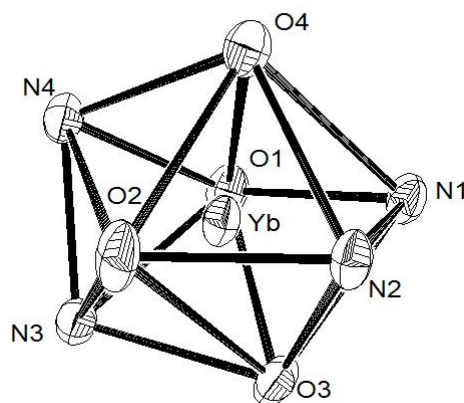
Figure 2.26. Coordination polyhedron around Yb^{3+} in Et₃NH[Yb(3BDMSal)₂].

2.3.5 Photophysical Properties of Nd^{3+} Complexes in Solution

2.3.5.1 Absorption, excitation and emission spectra of the complexes

The absorption, excitation and emission spectra of the Nd^{3+} complexes formed with DMSal, 5DMSal, 3DMSal and TBDMSal have been recorded in DMSO solution. For the deprotonation of ligands, NaOH was used as a base for the creation of these solutions.

The absorption, excitation and emission spectra of complexes are depicted in Figure 2.27. The apparent maximum of the absorption bands appears around 385 nm. The energy positions of the bands present in the excitation spectra recorded under Nd^{3+} signal match closely the position of the bands of the absorption spectra. This result suggests that NIR emitting lanthanide cations are sensitized through the electronic levels of the chromophoric ligand and that the ligand is providing an antenna effect. On the basis of their epsilon, we can assess the nature of the electronic bands resulting in the sensitization of Nd^{3+} as being $\pi-\pi^*$. The NIR emission spectra reveal the presence of three typical sharp bands arising from the electronic states of Nd^{3+}. These bands are located at 900 nm, 1060 nm and 1330 nm in NIR region and are attributed to the ${}^4F_{3/2}$ $\rightarrow {}^4I_{9/2}$, ${}^4F_{3/2} \rightarrow {}^4I_{11/2}$, and ${}^4F_{3/2} \rightarrow {}^4I_{13/2}$, f–f transitions respectively.
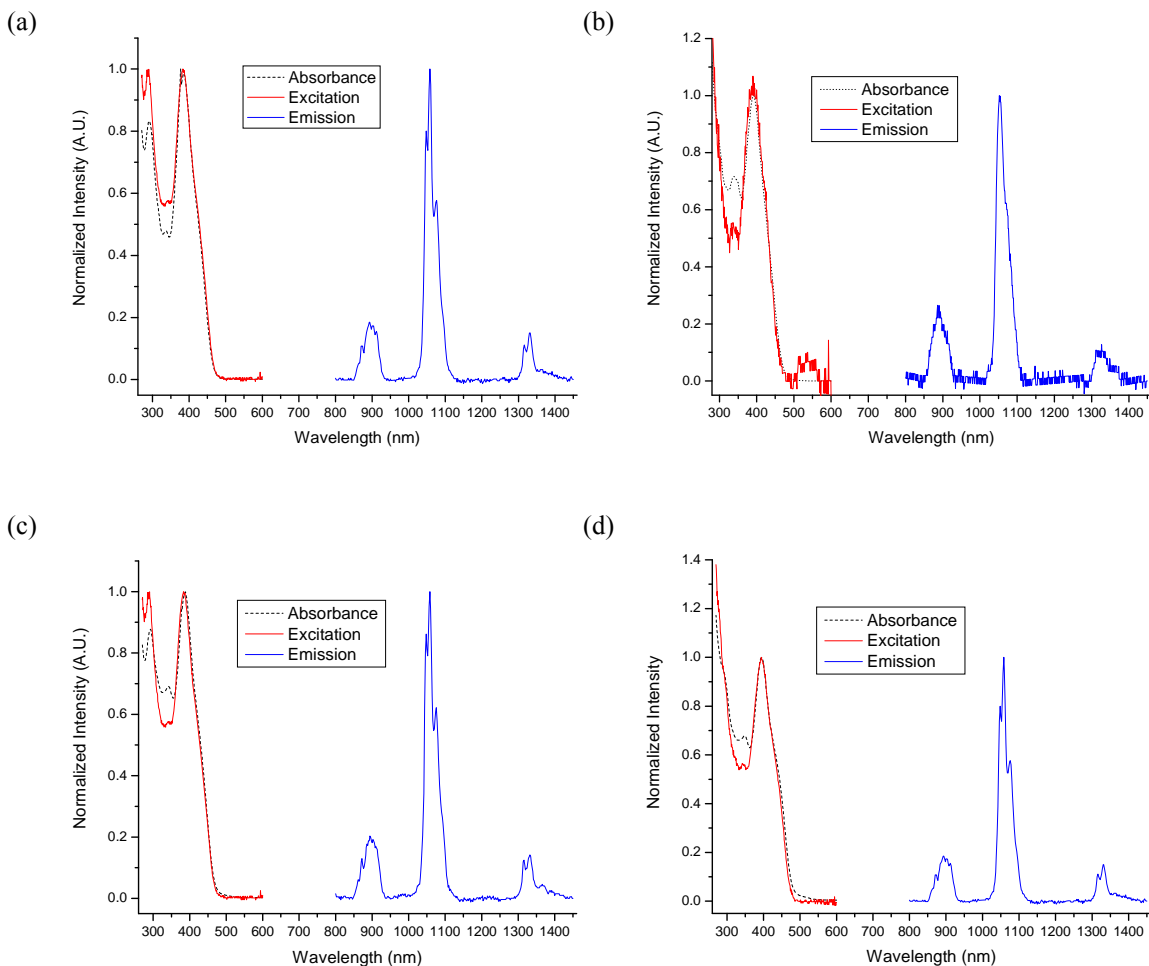
Figure 2.27. Absorption, Excitation and Emission spectra of (a) Na[Nd(DMSal)$_2$], at 4.64×10^{-5} M in DMSO at RT. λ_{ex} = 395 nm, λ_{em} = 1058 nm; (b) Na[Nd(5BDMSal)$_2$], at 4.65×10^{-5} M in DMSO at RT. λ_{ex} = 395 nm, λ_{em} = 1058 nm; (c) Na[Nd(3BDMSal)$_2$], at 4.54×10^{-5} M in DMSO at RT. λ_{ex} = 385 nm, λ_{em} = 1058 nm; (d) Na[Nd(TBDMSal)$_2$], at 3.51×10^{-5} M in DMSO at RT. λ_{ex} = 395 nm, λ_{em} = 1058 nm.

The four complexes also show similar absorption, excitation and emission spectra, which indicate that all these ligands sensitize Nd^{3+}. However, when the absorption spectra of four complexes are compared to one another, red shifts of the maxima of the electronic bands were observed, in the following order: Nd(DMSal)$_2$ → Nd(3BDMSal)$_2$ → Nd(5BDMSal)$_2$ →

Nd(TBDMSal)$_2$ (Figure 2.28). The excitation spectra also show the same trend of red shift. These results indicate that the more the ligand is substituted by bromide substituents the more that electronic state is shifted toward lower energy.
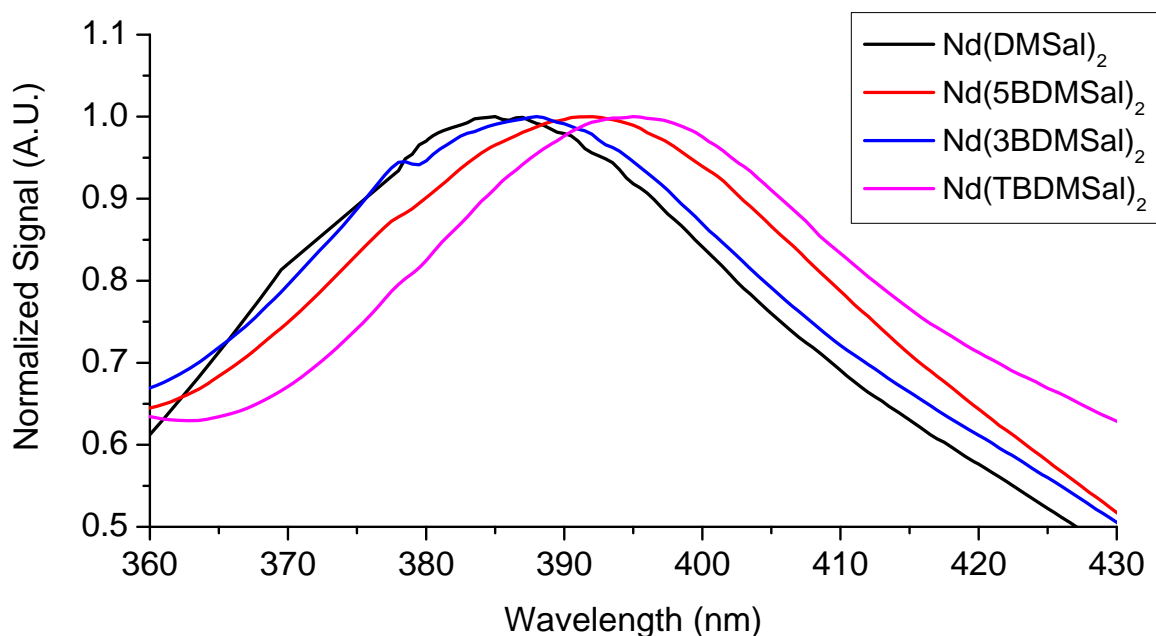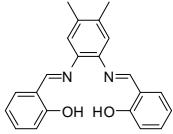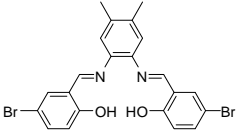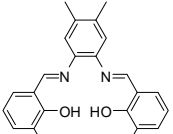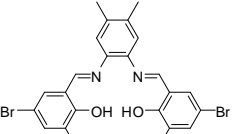
Figure 2.28. Comparison of selected ranges of the absorption spectra of the four complexes

2.3.5.2 Quantum yields and luminescence lifetimes of the complexes

To evaluate the efficiency of energy transfer from the ligand to lanthanide and the presence of quenching processes deactivating Nd^{3+} excited states, the quantum yields of the Nd^{3+} complexes formed with DMSal, 5DMSal, 3DMSal and TBDMSal were measured in DMSO using K[Nd(tropolonate)$_4$] ($\Phi = 2.1 \times 10^{-3}$)[5] as a reference. The results are listed in Table 2.7. These quantum yields are not superior to the typical values obtained for other Nd^{3+} complexes reported in the literature, which are comprised between $2 \times 10^{-3} - 3 \times 10^{-2}$ (Figure 2.29; Table 2.8), but are still comparable. These relatively low quantum yield values indicate that the energy transfer from the ligand to the lanthanide ion is not highly efficient and there is a quenching process present.

This drawback can be compensated for by modification of the salophen ligands. The introduction of heavier atom such as iodine can enhance the energy transfer process by increasing population of the triplet state of the ligand. A highly pre-organized ligand structure is an important parameter for protection of the metal ion.

Table 2.7. Quantum yield (Φ) of Nd^{3+} complexes in DMSO at r.t.

Complex	Na[Nd(DMSal)$_2$][a]	Na[Nd(5BDMSal)$_2$][b]	Na[Nd(3BDMSal)$_2$][c]	Na[Nd(TBDMSal)$_2$][d]
Absolute Φ_{tot}	$1.18 \pm 0.04 \times 10^{-3}$	$1.23 \pm 0.08 \times 10^{-3}$	$1.6 \pm 0.1 \times 10^{-3}$	$2.01 \pm 0.07 \times 10^{-3}$

(a) c = 4.95×10^{-5} M, λ_{ex} = 385 nm; (b) c = 8.70×10^{-5} M, λ_{ex} = 392 nm; (c) c = 4.89×10^{-5} M, λ_{ex} = 388 nm; (d) c = 4.95×10^{-3} M, λ_{ex} = 385 nm;

When quantum yields of the complexes are compared, it is evident that the presence of bromo groups on the salophen ligands enhances the efficiency of the energy transfer to the Nd^{3+}, which can be attributed to an increase in the population of the triplet state due to the heavy atom effect.[101] Na[Nd(3BDMSal)$_2$] has higher quantum yield than Na[Nd(5BDMSal)$_2$] has, though they have same number of bromo groups. Being located at the 3-position, a bromo group can (1) remove C–H from that position which may cause a non-radiative deactivation of lanthanide luminescence, and (2) have an increased heavy atom effect by the proximity factor.
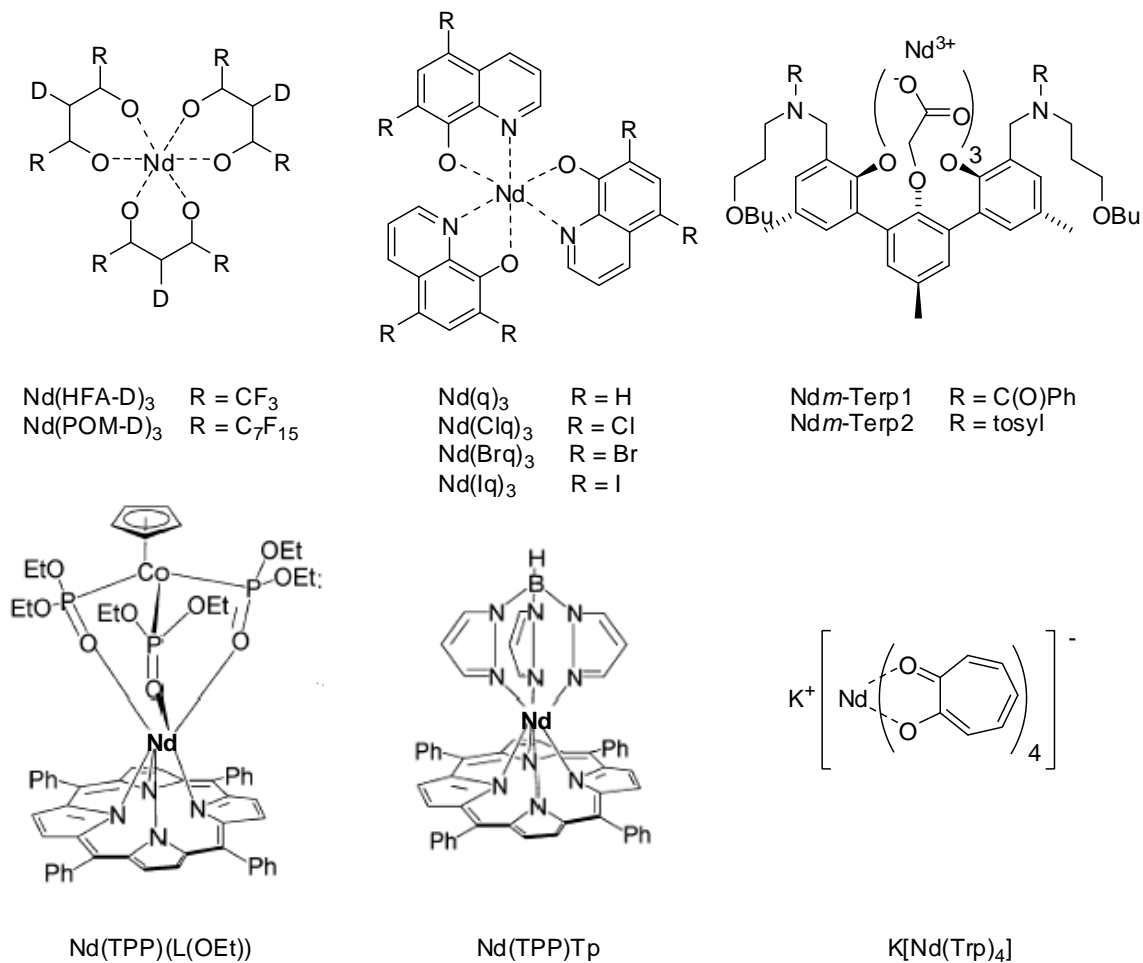
Figure 2.29. Structures and abbreviations of Nd^{3+} complexes reported in the literature.[5, 53, 60, 61, 65]
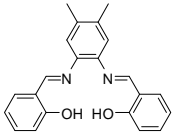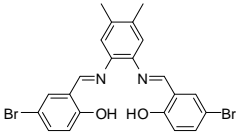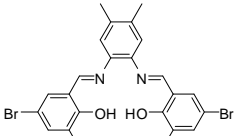
Table 2.8. Quantum yields (Φ_{tot}) and luminescence lifetimes (τ) of significant examples of Nd^{3+} complexes reported in the literature.

Complex	Φ_{tot}	τ (μs)	solvent
Nd(HFA-D)$_3$[60]	0.013	6.3	DMSO
Nd(POM-D)$_3$[60]	0.032	13.5	DMSO
Nd(q)$_3$[61]	0.004	2	DMSO-d_6
Nd(Clq)$_3$[61]	0.010	3	DMSO-d_6
Nd(Brq)$_3$[61]	0.010	3	DMSO-d_6

Nd(Iq)$_3$[61]	0.009	3	DMSO-d_6
Ndm-Terp1[53]	—	1.2	DMSO
Ndm-Terp2[53]	—	1.2	DMSO
Nd(TPP)(L(OEt))[65]	0.002	—	CH$_2$Cl$_2$
Nd(TPP)Tp[65]	0.0024	—	CH$_2$Cl$_2$
K[Nd(Trp)$_4$][5]	0.0021	1.10	DMSO

The luminescence lifetimes of Nd^{3+} in Na[Nd(DMSal)$_2$], Na[Nd(5BDMSal)$_2$] and Na[Nd(TBDMSal)$_2$] were measured in DMSO upon ligand excitation (Table 2.9). The values obtained are all close to 1.00 µs. These close lifetime values indicate that the Nd^{3+} are all in fairly similar coordination environments in the three different complexes: a similar degree of protection of Nd^{3+} is therefore provided by the organization of the ligand around the lanthanide ion. These lifetimes compare well with the luminescence lifetimes previously reported for Nd^{3+} complexes (1.10 – 13.5 µs, Table 2.8).]. From this experiment, we could not obtain quantitative data showing that the differences in quantum yields cannot be explained by differences in the protection of the NIR-emitting cations.

Table 2.9. Luminescence lifetime (τ) of Nd^{3+} complexes in DMSO at r.t. The samples were excited at 337 nm with a nitrogen laser, and the signals were collected at 1060 nm.

Complex	Na[Nd(DMSal)$_2$]	Na[Nd(5BDMSal)$_2$]	Na[Nd(TBDMSal)$_2$]
τ (µs)	1.00 ± 0.01	1.01 ± 0.01	0.998 ± 0.001

2.4   CONCLUSIONS

The coordination chemistry and photophysical properties of the Nd^{3+} and Yb^{3+} complexes formed with a series of ligands derived from salophen were systematically studied. All these pre-organized rigid tetradentate ligands form well-defined $[ML_2]^-$ complexes in solution. The stoichiometry of this complex in solution was identified via spectrophotometric titrations of a series of ligands with Nd^{3+} ion. The stability constants indicate that the stability of the complex can be controlled by the appropriate choice of ligand substituents. Three crystal structures were isolated and analyzed. The structures of the complexes in the solid phase can be significantly different from the structures in solution. The morphology of the crystal structure can be controlled by the size of lanthanide metal ion as well as the proper choice of base which itself controls the presence or absence of counter cations. The spectroscopy studies of the properties of the chromophoric groups of these systems indicate that the different substituents on the ligand do not affect significantly the energies of the different electronic levels. It was established that all four chromophoric ligand systems are able to sensitize Nd^{3+}, a NIR-emitting cation, through intramolecular energy transfer from the electronic states of the ligand to the metal ion. The luminescence properties of the complexes can be enhanced by modification of the ligand with Br-substituents.

3.0   LANTHANIDE-DENDRIMER COMPLEX FOR BIOLOGICAL IMAGING

accumulation within tumors and in vivo imaging by functionalized luminescent dendrimer lanthanide complexes".[103]

3.1   INTRODUCTION

Luminescent lanthanide reporters are useful for applications such as drug delivery, medical diagnostics and biological imaging due to the unique properties such as long luminescence lifetimes, photostability and sharp emission bands. To take advantage of these properties, it is crucial to have lanthanide complexes' strong absorption and emission signals which can be detected in biological matrices. A promising strategy to maximize the number of absorbed and emitted photos is the development of reporters that possess more than one luminescent metal ion combined with large number of sensitizer molecules. Polymetallic lanthanide-dendrimer complexes were demonstrated by incorporating eight equivalents of europium cations into 2,3-naphthalimide attached PAMAM (polyamidoamine) dendrimer.[104]

In this work, we have developed polymetallic lanthanide-dendrimer complexes utilizing functionalized 1,8-naphthalimide. The energy level of the triplet states of 1,8-naphthalimide is 18,519 cm^{-1}, which is compatible with the accepting energy levels of several lanthanide cations emitting in the visible and near-infrared domains. This sensitizer also have highly populated triplet states, a favorable feature for lanthanide sensitizers since it is globally hypothesized that energy transfer occurs mainly from the ligand triplet state to the accepting levels of the lanthanide cations. Therefore, high populations of the triplet state should favor efficient intramolecular ligand to lanthanide energy transfer.

The goal of this research is the utilization of lanthanide-dendrimer complexes as scaffolds for versatile applications. Functionalized lanthanide-dendrimer complexes can be used for detection technique for a large variety of biological problems and applications. By introducing functional groups on the surface of dendrimer complex, the physical and photophysical properties of the complex can be modified and controlled. Dendrimer complex with functional groups at their periphery lead to desirable properties for practical applications: improved solubility in water, ability to cross cell membranes for biological imaging and displacement of the excitation wavelengths to higher values. A schematic diagram of functionalized lanthanide-dendrimer complex is depicted in Figure 3.1.
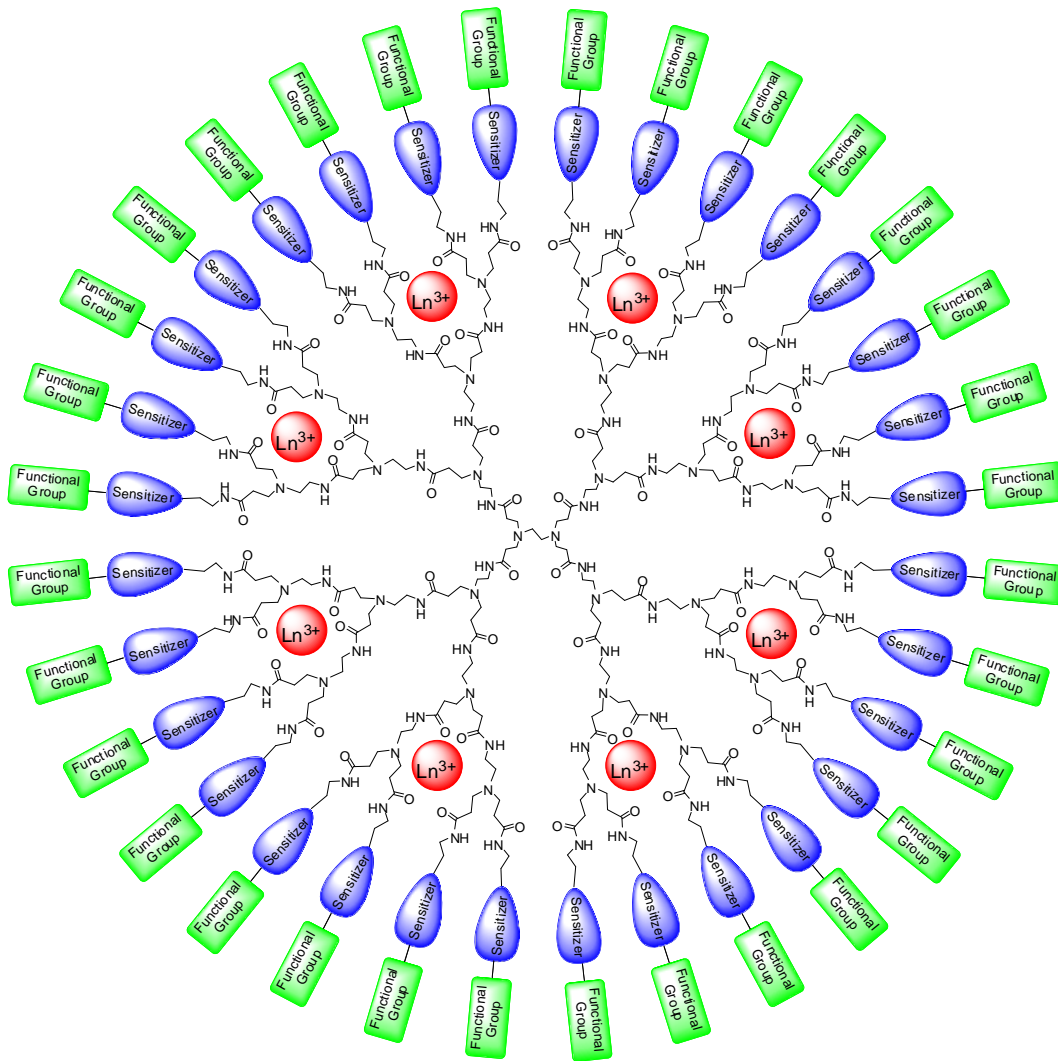
Figure 3.1. Schematic model of functionalized lanthanide-dendrimer complex

3.2   EXPERIMENTAL

3.2.1   Syntheses of Lanthanide-Dendrimer Complexes

3.2.1.1 Synthesis of the generation-3 PAMAM dendrimer with 3-isothiocyanato-1,8-naphthalimide containing europium ions (Eu-ITC)

3-Amino-1,8-naphthalimide was synthesized by a reported method.[105] 3-Isothiocyanato-1,8-naphthalimide-attached dendrimer was synthesized by adapting a reported method[104] with slight modification followed by conversion of amino group to isothiocyanto group: 181 mg (0.0262 mmol) of NH_2-terminated G3 PAMAM dendrimer (Dendritech, Inc.) and 250 mg (1.17 mmol) of 3-amino-1,8-naphthalic anhydride were suspended in 15 mL of DMF (J. T. Baker) and stirred at 90 °C for 48 hours under a nitrogen atmosphere, monitoring for the disappearance of the naphthalic anhydride by TLC. The compound was purified by dialysis using a regenerated cellulose membrane (Fisher; nominal MWCO 12,000−14,000) in DMSO for three days. The solution in the dialysis membrane was dried in a vacuum oven to yield 3-amino-1,8-naphthalimide-modified dendrimer as a brown solid (125 mg, 36%). This dendrimer was redissolved in 20 mL of DMF (J. T. Baker) and 0.25 g (1.81 mmol) of K_2CO_3 (J. T. Baker) was added to the solution. 0.1 mL (0.15g; 1.30 mmol) of thiophosgene (Aldrich) was slowly added to the solution at 0 °C. The mixture was stirred at 0 °C for 2.5 hrs, then at room temperature for 1 day. The compound was purified by dialysis using a regenerated cellulose membrane (nominal MWCO 12,000-14,000; Fisher Scientific) in DMSO for three days. The solution in the dialysis membrane was dried in a vacuum oven (40 °C, 50 mbar) to yield 3-isothiocyanato-1,8-naphthalimide-modified dendrimer as brown solid (34.3 mg, 25%). Anal. Calcd for

$C_{718}H_{704}N_{154}O_{124}S_{32}\cdot 32DMSO$: C, 55.25; H, 5.31; N 12.69. Found: C, 55.60; H 5.15; N 12.73.

The Eu^{3+} complex of 3-isothiocyanato-1,8-naphthalimide-modified dendrimer was synthesized by the following method: 0.51 mg (3.51×10^{-8} mol) of 3-isothiocyanato-1,8-naphthalimide-modified dendrimer was dissolved in 6 mL of DMSO (J. T. Baker). 129.7 μL of 2.17 mM $Eu(NO_3)_3$ solution in DMSO (2.81×10^{-7} mol of Eu^{3+}) was added to the dendrimer solution. The mixture was incubated at room temperature for seven days. The resulting solution (conc. = 5.74 μM) was used as obtained.

3.2.1.2 Synthesis of the generation-3 PAMAM dendrimer with 4-amino-1,8-naphthalimide containing europium ions (Eu-G3P4A18N)

Glycine-conjugated 4-amino-1,8-naphthalimide was synthesized by a reported method.[106] Glycine-conjugated 4-amino-1,8-naphthalimide was attached on the amine-terminated G3 PAMAM dendrimer by a standard amide coupling condition: 54.1 mg (2.00×10^{-4} mol) of glycine-naphthalimide conjugate was added to a solution of 29.4 mg (4.26×10^{-6} mol) of G3 PAMAM dendrimer (Dendritech Inc.) in 5 mL of DMF (Sigma-Aldrich). 92.1 mg (2.42×10^{-4} mol) of HATU (Aldrich) and 70 μL (52 mg; 4.0×10^{-4} mol) of DIPEA (Sigma-Aldrich) were added. The reaction mixture was stirred at room temperature for two days under nitrogen atmosphere while monitoring for the disappearance of G3 PAMAM dendrimer by TLC. The compound was purified by dialysis using a regenerated cellulose membrane (nominal MWCO 12,000-14,000; Fisher Scientific) in DMSO for three days. The solution recovered from the dialysis membrane was dried in a vacuum oven (40 °C, 50 mbar) to yield G3P4A18N as brown solid (52.5 mg, 82%). ^{1}H-NMR (300 MHz, DMSO-d_6): δ 8.54 p.p.m. (br s, 32 H), 8.32 (br s, 32 H), 8.15 (br s, 32 H), 8.10 (br s, 32 H), 7.90 (br s, 32 H), 7.76 (m, 28 H), 7.56 (br s, 32 H), 7.40

(br s, 64 H), 6.78 (br s, 32 H), 4.56 (br s, 64 H), 3.08 (m, 184 H), 2.61 (m, 120 H), 2.39 (m, 60 H

), 2.16 (m, 120 H); analysis (% calcd, % found for $C_{750}H_{864}N_{186}O_{156} \cdot 32DMSO \cdot 64H_2O$): C

(52.47, 51.74), H (6.40,6.29), N (13.98, 13.76). The Eu^{3+} complex of G3P4A18N (Eu-

G3P4A18N) was synthesized by the following method adapted from the methods developed in

our group[104]: 22.67 mg (1.513 × 10^{-6} mol) of G3P4A18N was dissolved in 10 mL of DMSO.

647.5 µL of 18.7 mM $Eu(NO_3)_3$ solution in DMSO (1.21 × 10^{-5} mol) was added to the dendrimer

solution. The mixture was diluted to 25.00 mL, incubated at room temperature for seven days.

The resulting solution (conc. = 60.5 µM) was used as obtained.

3.2.1.3 Synthesis of the generation-3 PAMAM dendrimer with naphthalimide and biotin
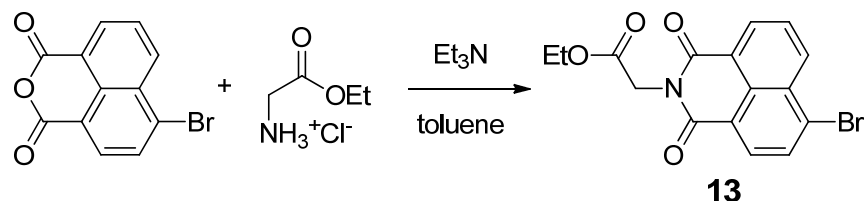
6-Bromo-1,3-dioxo-1H-benz[de]isoquinoline-2(3H)-acetic acid ethyl ester (**13**) was synthesized

as follows: 4-Bromo-1,8-naphthalic anhydride (3.00 g, 10.8 mmol) and glycine ethyl ester

hydrochloride (1.52 g, 10.9 mmol) were suspended in toluene (120 mL) and triethyl amine (2.2

g, 22 mmol) was added. The mixture was refluxed for 15 h. The precipitate was filtered off and

the residual solution was concentrated *in vacuo* to afford **13** as light yellow solid (3.87 g, 10.7

mmol, 99%): ^1H NMR (CDCl$_3$, 300 MHz, δ): 8.68 (dd, J = 7.2, 0.9 Hz, 1H, Ar H), 8.62 (dd, J =

8.4, 0.9 Hz, 1H, Ar H), 8.44 (d, J = 7.8 Hz, 1H, Ar H), 8.07 (d, J = 7.8 Hz, 1H, Ar H), 7.87 (dd, J

= 8.4, 7.2 Hz, 1H, Ar H), 4.93 (s, 2H, -CH_2COO-), 4.25 (q, J = 7.2 Hz, 2H,-CH_2CH$_3$), 1.30 (t, J

= 7.2 Hz, 3H, -CH$_2$CH_3); ^{13}C NMR (CDCl$_3$, 75 MHz, δ): 167.99 (1C), 163.35 (1C), 163.32 (1C),

133.79 (1C), 132.50 (1C), 131.64 (1C), 131.24 (1C), 130.88 (1C), 130.74 (1C), 129.18 (1C),

128.21 (1C), 122.65 (1C), 121.79 (1C), 61.79 (1C), 41.54 (1C), 14.27 (1C); HRMS-EI (m/z): [M]$^+$ calcd for $C_{16}H_{12}NO_4Br$, 360.9950; found, 360.9926.
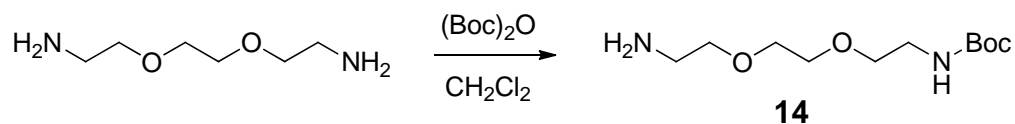
N-Boc-1,8-diamino-3,6-dioxaoctane (**14**) was synthesized by a reported method[107] with slight modification as follows: A solution of (Boc)$_2$O (2.25 g, 10.3 mmol) in CH$_2$Cl$_2$ (50 mL) was added dropwise to a solution of 1,8-diamino-3,6-dioxaoctane (10.3 g, 69.7 mmol) in CH$_2$Cl$_2$ (70 mL) at 0 °C for 3 h. The reaction mixture was stirred at room temperature for 4 h. The organic layer was successively washed with sat. NaHCO$_3$ solution (60 mL), water (2 × 60 mL) and brine (80 mL), dried over anhydrous MgSO$_4$ and concentrated *in vacuo* to afford **14** as a colorless oil (2.26 g, 9.10 mmol, 88%). ^{1}H NMR (300 MHz, CDCl$_3$, δ): 5.15 (br s, 1H, NH), 3.61 (s, 4H, -OC*H$_2$*C*H$_2$*O-), 3.54 (t, 2H, *J* = 5.1 Hz, -OC*H$_2$*-), 3.52 (t, 2H, *J* = 5.1 Hz, -OC*H$_2$*-), 3.31 (m, 2H, -C*H$_2$*NHBoc), 2.88 (m, 2H, -C*H$_2$*NH$_2$), 1.73 (br s, 2H, NH$_2$), 1.43 (s, 9H, *tert*-Bu); ^{13}C NMR (CDCl$_3$, 75 MHz, δ): 155.63 (1C), 78.37 (1C), 72.60 (1C), 69.70 (3C), 41.08 (1C), 39.83 (1C), 27.97 (3C); HRMS-ESI (m/z): [M+Na]$^+$ calcd for $C_{11}H_{24}N_2O_4Na$, 271.1634; found, 271.1617.
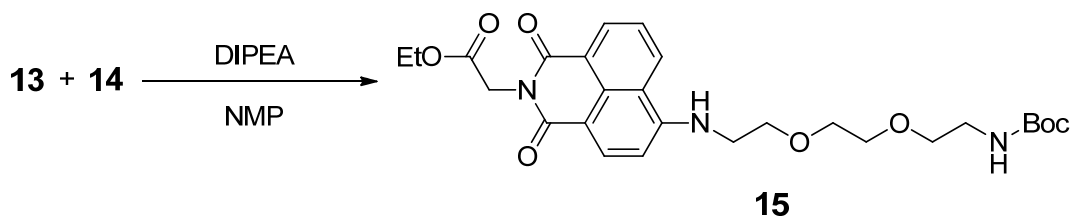
Compound **15** was synthesized as follows: Imide **13** (1.41 g, 3.89 mmol) and amine 14 (1.96 g, 7.91 mmol) were dissolved in *N*-methylpyrrolidone (NMP, 40 mL). *N,N*-diisopropylethylamine (DIPEA, 1.04 g, 8.04 mmol) was added and the mixture was stirred for one day at 120 °C. Then water (50 mL) was added and extracted with EtOAc (2 × 100 mL). The organic layer was washed with brine (2 × 75 mL), dried over anhydrous MgSO$_4$, and concentrated *in vacuo*. The mixture was purified by column chromatography on silica using EtOAc as an eluent to afford **15** as brown solid (1.70 g, 3.21 mmol, 82%): ^{1}H NMR (300 MHz, CDCl$_3$, δ): 8.18 (d, *J* = 7.2 Hz, 1H, Ar H), 8.10 (d, *J* = 8.4 Hz, 1H, Ar H), 7.99 (d, *J* = 8.1 Hz, 1H, Ar H), 7.28 (t, *J* = 7.8 Hz, 1H, Ar H), 6.36 (d, *J* = 8.4 Hz, 1H, Ar H), 6.18 (br s, 1H, NH), 5.15 (br s, 1H, NH), 4.83 (s, 2H, -C*H$_2$*COO-), 4.21 (q, *J* = 7.2 Hz, 2H, -C*H$_2$*CH$_3$), 3.74 (t, *J* = 7.2 Hz, 2H, -OC*H$_2$*-), 3.60 (m, 4H, -OCH$_2$CH$_2$O-), 3.49 (t, *J* = 7.2 Hz, 2H, -OC*H$_2$*-), 3.41 (m, 2H, -C*H$_2$*NH-), 3.25 (m, 2H, -C*H$_2$*NH-), 1.34 (s, 9H, *tert*-Bu), 1.27 (t, *J* = 7.2 Hz, 3H, -CH$_2$C*H$_3$*); ^{13}C NMR (CDCl$_3$, 75 MHz, δ): 169.20 (1C), 164.17 (1C), 163.39 (1C), 156.02 (1C), 150.07 (1C), 134.42 (1C), 131.06 (1C), 129.37 (1C), 127.06 (1C), 124.29 (1C), 121.58 (1C), 119.96 (1C), 108.67 (1C), 103.85 (1C), 79.21 (1C), 70.27 (1C), 70.22 (1C), 70.07 (1C), 68.62 (1C), 61.50 (1C), 43.03 (1C), 41.10 (1C), 40.23 (1C), 28.33 (3C), 14.15 (1C); HRMS-EI (m/z): [M]$^+$ calcd for C$_{27}$H$_{35}$N$_3$O$_8$, 529.2424; found, 529.2432.
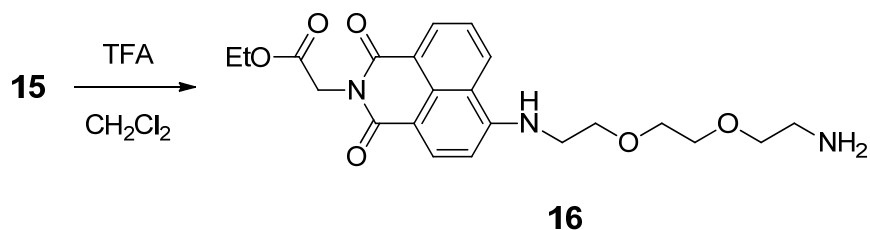
Compound **16** was synthesized as follows: Boc-protected amine **15** (0.202 g, 0.382 mmol) was dissolved in 5 mL of CH_2Cl_2 and 5 mL of trifluoroacetic acid was added. The solution was stirred at 0 °C for 30 min and then at r.t. for 30 min. The solvent and trifluoroacetic acid were removed under reduced pressure. The residue was dissolved in 5 mL of CH_2Cl_2 and washed with sat. Na_2CO_3 solution (5 mL) and brine (5 mL), dried over anhydrous $MgSO_4$, and concentrated *in vacuo* to afford **16** as brownish yellow solid (0.139 g, 0.325 mmol, 85%): ^{1}H NMR (300 MHz, CDCl$_3$, δ): 8.52 (d, J = 7.2 Hz, 1H, Ar H), 8.40 (d, J = 8.4 Hz, 1H, Ar H), 8.26 (d, J = 8.4 Hz, 1H, Ar H), 7.57 (t, J = 7.8 Hz, 1H, Ar H), 6.65 (d, J = 8.4 Hz, 1H, Ar H), 6.20 (br s, 1H, NH), 4.92 (s, 2H, -CH_2COO-), 4.24 (q, J = 7.2 Hz, 2H, -CH_2CH$_3$), 3.88 (t, J = 5.0 Hz, 2H, -OCH_2-), 3.73-3.66 (m, 4H, -OCH_2CH_2O-), 3.61-3.53 (m, 4H, -OCH_2- and -CH_2NH-), 2.90 (br s, 2H, -CH_2NH$_2$), 2.15 (br s, 2H, NH$_2$), 1.30 (t, J = 7.2 Hz, 3H, -CH$_2$CH_3); ^{13}C NMR (CDCl$_3$, 100 MHz, δ): 169.15 (1C), 164.15 (1C), 163.35 (1C), 150.09 (1C), 134.40 (1C), 131.04 (1C), 129.43 (1C), 127.09 (1C), 124.27 (1C), 121.68 (1C), 120.02 (1C), 108.76 (1C), 103.92 (1C), 72.91 (1C), 70.34 (1C), 70.09 (1C), 68.63 (1C), 61.47 (1C), 43.03 (1C), 41.47 (1C), 41.10 (1C), 14.16 (1C); HRMS-ESI (m/z): [M+Na]$^+$ calcd for $C_{22}H_{27}N_3O_6Na$, 452.1798; found, 452.1760.
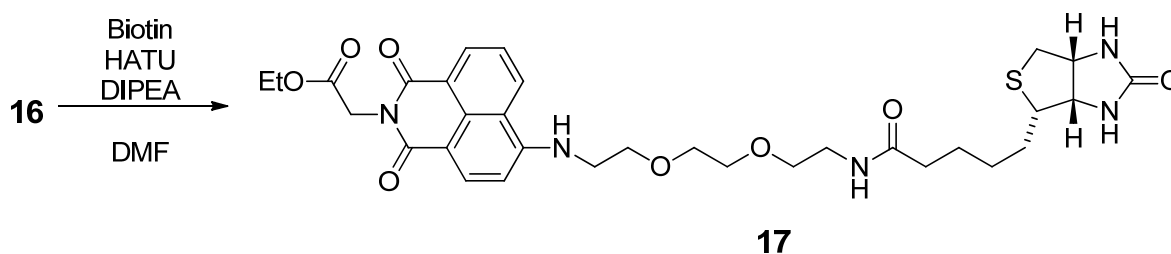
Compound **17** was synthesized as follows: Amine **16** (0.0520 g, 0.121 mmol), D-biotin (0.0297 g, 0.122 mmol), HATU (0.0538 g, 0.141 mmol) and DIPEA (0.0371 g, 0.287 mmol) were dissolved in 5.0 mL of DMF. The mixture was stirred at room temperature under N_2 atmosphere for 20 h. DMF was removed in vacuo, then the residual solid was triturated to afford

17 as yellow solid (0.0539 g, 0.0822 mmol, 68%): ^{1}H NMR (300 MHz, DMSO-d_6, δ): 8.76 (d, J = 8.1 Hz, 1H, Ar H), 8.46 (d, J = 6.9 Hz, 1H, Ar H), 8.28 (d, J = 8.4 Hz, 1H, Ar H), 7.93 (br t, 1H, NH), 7.81 (br t, 1H, NH), 7.73 (t, J = 8.1 Hz, 1H, Ar H), 6.88 (d, J = 8.7 Hz, 1H, Ar H), 6.41 (s, 1H, NH of biotin), 6.36 (s, 1H, NH of biotin), 4.77 (s, 2H, -CH_2COO-), 4.28 (m, 1H, -NHCH(CH)CH$_2$-), 4.14 (q, J = 7.2 Hz, 2H, -CH_2CH$_3$), 4.12 (m, 1H, -NHCH(CH)CH-), 3.73 (m, 2H, -OCH_2-), 3.59 (m, 4H, -OCH_2CH_2O-), 3.53 (m, 2H, -OCH_2-), 3.38 (m, 2H, -CH_2NH-), 3.16 (m, 2H, -CH_2NH-), 3.06 (m, 1H, -CHCH(CH$_2$)S-), 2.80 (dd, J = 12.5, 5.1 Hz, 1H, -CHCH_2S-), 2.56 (d, J = 12.0 Hz, 1H, -CHCH_2S-), 2.04 (t, J = 7.5 Hz, 2H, -NHC(=O)CH_2CH$_2$-), 1.65-1.40 (m, 4H, -NHC(=O)CH$_2$CH_2CH_2CH$_2$-), 1.27 (m, 2H, -NHC(=O)CH$_2$CH$_2$CH_2CH$_2$-), 1.21 (t, J = 7.2 Hz, 3H, -CH$_2$CH_3); ^{13}C NMR (CDCl$_3$, 75 MHz, δ): 172.12 (1C), 168.37 (1C), 163.52 (1C), 162.70 (1C), 162.46 (1C), 151.10 (1C), 134.61 (1C), 131.11 (1C), 129.63 (1C), 129.16 (1C), 124.50 (1C), 121.34 (1C), 120.22 (1C), 107.02 (1C), 104.19 (1C), 69.81 (1C), 69.57 (1C), 69.18 (1C), 68.13 (1C), 61.02 (1C), 60.94 (1C), 59.18 (1C), 55.43 (1C), 42.80 (1C), 40.88 (1C), 40.66 (1C), 38.40 (1C), 35.09 (1C), 28.19 (1C), 28.03 (1C), 25.26 (1C), 14.07 (1C); HRMS-ESI (m/z): [M+Na]$^+$ calcd for C$_{32}$H$_{41}$N$_5$O$_8$SNa, 678.2574; found, 678.2632.
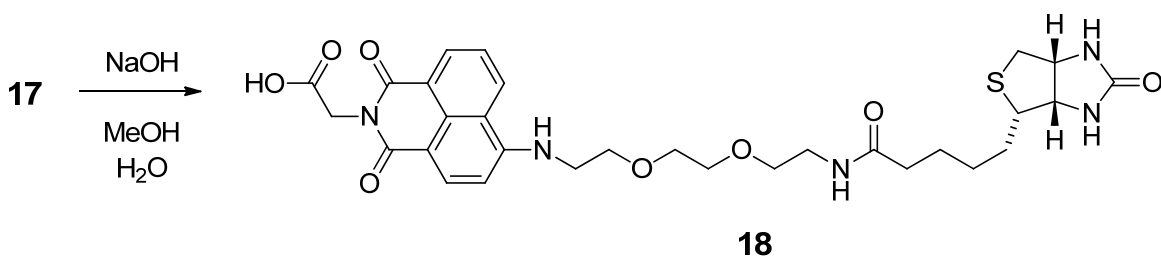
Compound **18** was synthesized as follows:: Ester **17** (0.355 g, 0.541 mmol) was suspended in 20 mL of MeOH. NaOH (0.266 g, 6.65 mmol) was dissolved in 10 mL of water and added to the suspension in MeOH. Upon addition of NaOH, the suspension changed to clear solution. The mixture was stirred at 40 °C for 5 h. The solution was acidified with 7 mL of 1 M

HCl at 0 °C, and yellow solid was formed. The solid was filtered, washed with cold water, and dried in vacuo to afford **18** (0.286 g, 0.4562 mmol, 84%): ^{1}H NMR (300 MHz, DMSO-d_6, δ): 12.94 (br s, 1H, -COO*H*), 8.76 (d, *J* = 8.7 Hz, 1H, Ar H), 8.46 (d, *J* = 7.2 Hz, 1H, Ar H), 8.28 (d, *J* = 8.7 Hz, 1H, Ar H), 7.91 (br t, 1H, NH), 7.82 (br t, 1H, NH), 7.72 (t, *J* = 7.8 Hz, 1H, Ar H), 6.87 (d, *J* = 8.7 Hz, 1H, Ar H), 6.41 (s, 1H, NH of biotin), 6.36 (s, 1H, NH of biotin), 4.69 (s, 2H, -C*H₂*COO-), 4.28 (m, 1H, -NHC*H*(CH)CH₂-), 4.11 (m, 1H, -NHC*H*(CH)CH-), 3.79 (m, 2H, -OC*H₂*-), 3.59 (m, 4H, -OC*H₂*C*H₂*O-), 3.53 (m, 2H, -OC*H₂*-), 3.39 (m, 2H, -C*H₂*NH-), 3.16 (m, 2H, -C*H₂*NH-), 3.06 (m, 1H, -CHC*H*(CH₂)S-), 2.80 (dd, *J* = 12.3, 5.1 Hz, 1H, -CHC*H₂*S-), 2.56 (d, *J* = 12.3 Hz, 1H, -CHC*H₂*S-), 2.04 (t, *J* = 7.4 Hz, 2H, -NHC(=O)C*H₂*CH₂-), 1.65-1.40 (m, 4H, -NHC(=O)CH₂C*H₂*CH₂C*H₂*-), 1.27 (m, 2H, -NHC(=O)CH₂CH₂C*H₂*CH₂-); ^{13}C NMR (CDCl₃, 75 MHz, δ): 172.14 (1C), 169.75 (1C), 163.56 (1C), 162.72 (1C), 162.55 (1C), 151.02 (1C), 134.53 (1C), 131.03 (1C), 129.62 (1C), 129.10 (1C), 124.48 (1C), 121.48 (1C), 120.22 (1C), 107.18 (1C), 104.14 (1C), 69.81 (1C), 69.59 (1C), 69.18 (1C), 68.13 (1C), 61.03 (1C), 59.18 (1C), 55.45 (1C), 42.79 (1C), 40.87 (1C), 40.51 (1C), 38.41 (1C), 35.11 (1C), 28.21 (1C), 28.05 (1C), 25.28 (1C); HRMS-ESI (m/z): [M+Na]$^+$ calcd for C₃₀H₃₇N₅O₈SNa, 650.2261; found 650.2259.

19
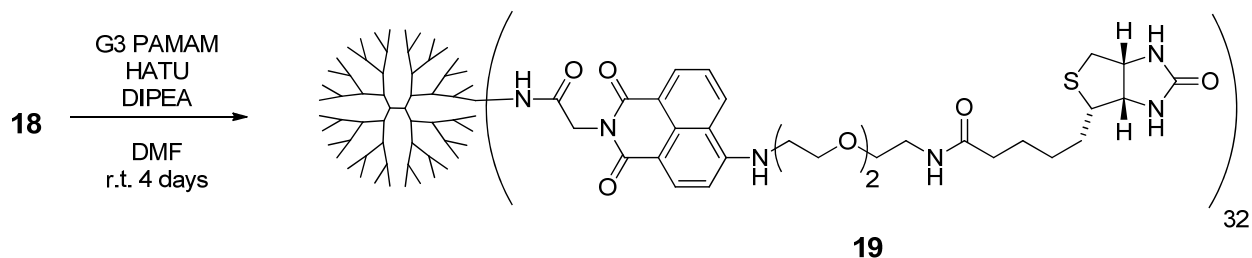
Biotin conjugated dendrimer **19** was synthesized as follows: 283.5 mg (4.516 × 10^{-4} mol) of **18** was added to a solution of 78.90 mg (1.142 × 10^{-5} mol) of G3 PAMAM dendrimer in 25

mL of DMF. 197.9 mg (5.205×10^{-4} mol) of HATU and 300 µL (223 mg; 1.72×10^{-3} mol) of DIPEA were added. The reaction mixture was stirred at room temperature for two days under nitrogen atmosphere while monitoring for the disappearance of G3 PAMAM dendrimer by TLC. The compound was purified by dialysis using a regenerated cellulose membrane (nominal MWCO 12,000-14,000) in DMSO for four days. The solution recovered from the dialysis membrane was dried in a vacuum oven (40 °C, 50 mbar) to yield dendrimer **19** as brown solid (144 mg, 48%).

3.2.2 Spectroscopic Characterization of of Lanthanide-Dendrimer Complexes

Absorption spectra were recorded on samples in a Perkin-Elmer Lambda 9 BX Spectrometer, coupled with a personal computer using software supplied by Perkin-Elmer (Waltham, MA).

Steady-state emission and excitation spectra were analyzed using a modified Horiba Jobin Yvon Spex Fluorolog-322 Spectrofluorometer, coupled to a personal computer with software supplied by Horiba Jobin Yvon Inc. (Edison, NJ). Emission and excitation spectra were corrected for the instrumental function. Samples were placed in 1 mm quartz fluorescence cells purchased from NSG Precision Cells, Inc. (Farmingdale, NY).

The Eu^{3+} luminescence lifetime measurements were performed using a Nd:YAG Continuum Powerlite 8010 laser (354 nm, third harmonic) as the excitation source. Emission was collected at a right angle to the excitation beam, and signals arising from the $^5D_0 \rightarrow {}^7F_2$ Eu^{3+} transition (615 nm) were selected by a Spectral Products CM 110 1/8 meter monochromator. The signal was monitored using a Hamamatsu R928 photomultiplier coupled to a 500 MHz band pass digital oscilloscope (Tektronix TDS 754D). For each flash, the experimental decay was recorded

with a resolution of 50,000 points. To minimize experimental contribution, signals from >1000 flashes were collected and averaged. Luminescence decay curves were analyzed with Origin 7.0 software. The experimental decay curves were fitted to single, double, and triple exponential models using the Chi-squared criteria to discriminate the best exponential fit. Four independent decay curves were collected for the sample.

For the photobleaching experiments, approximately 0.9 mL of each solution (0.2 µM in 30% DMSO/H_2O) was transferred into a 0.9 mL semimicro absorbance cuvette supplied by Varian (catalog number 66-100127-00). The cuvette was stoppered and parafilmed at the beginning of each trial to prevent solvent evaporation. Photobleaching was quantified with a Perkin-Elmer UV/Vis, collecting at 240 λ/nm scan rates. Samples were exposed to white light from the Xenon lamp of the Horiba Jobin Yvon Spex Fluorolog-322 Spectrofluorometer in-between scans. A water circulator was used to maintain constant room temperature (23 °C) within the fluorimeter during long periods of exposure.

For the quantum yield experiments, spectra were collected and analyzed using the Horiba Jobin Yvon Spex Fluorolog-322 fitted with an integrating sphere[108] using quartz tubes as sample holders. A 20 µM solution of Eu-G3P4A18N in 30% DMSO/H_2O was used for this analysis, and all spectra were corrected for the response of the lamp before integrating. Integrated values were used to determine the quantum yield by calculating the ratio of the photons into the sample to the photons emitted by the sample.

3.2.3   Mobility Determination by Capillary Zone Electrophoresis

The Eu-G3P4A18N dendrimer samples were characterized with electrophoretic analysis by CZE with diode array UV absorbance detection with an Agilent CE system (Agilent Technologies, Palo Alto, CA). A 75.0 μm i.d. unmodified fused silica capillary (Polymicro Technologies, Phoenix, AZ) 34.0 cm in total length, and 8.5 cm to the detector (short end) was employed. The background electrolyte was 40 mM phosphoric acid in 30% DMSO and 70% 18MΩ-cm water at pH of 2.3. Each day prior to use, the capillary was preconditioned with 1 M NaOH for 5 min, 18 MΩ-cm water for 15 min and running buffer for 15 min. The capillary was flushed with running buffer for 2 min in between analysis. A separation potential of 17.0 kV was employed and a co-flow pressure of 10 mbar was also applied during the electrophoresis. Dendrimer samples were at a concentration of 3 mg/mL in DMSO. Hydrodynamic injection (50 mbar, 1.5 sec) was employed, and the capillary was maintained at 25 °C. Detection was performed at 450 nm and 280 nm, and UV-vis spectra were collected in each peak. A small co-flow pressure of 10 mbar during electrophoresis was needed to reliably detect the neutral zone corresponding to the DMSO from the injection plug, and the migration time for this solvent zone was used to calculate the electroosmotic mobility of the system.

3.2.4   Methods for Imaging with Eu- ITC

3.2.4.1 Cell culture and cell viability assay

The human breast cancer cell line MDA-MB-231 and normal mammary epithelial cell line MCF-10A was purchased from American Type Culture Collection (Manassas, VA). Monolayer

cultures of MDA-MB-231 were maintained in RPMI 1640 supplemented with 10% fetal bovine serum and antibiotics. The nontumorigenic human mammary epithelial cell line MCF-10A was cultured in serum-free Mammary Epithelial Growth Medium (Clonetics, San Diego, CA) supplemented with 100 ng/mL cholera toxin (Calbiochem, La Jolla, CA). Each cell line was maintained at 37 °C in an atmosphere of 95% air and 5% CO_2. Stock solution of Eu-Dendrimer (Eu) and Eu-Dendrimer conjugated with an active agent, the isothiocyanite group (Eu-ITC), was prepared in dimethyl sulfoxide (DMSO) and stored at -20ºC. Each molecule of dendrimer was, on average, conjugated to 30 molecules of ITC therefore all concentrations presented refer to the concentrations of the active ITC molecule ([dendrimer] x 30 ITC attached = [Eu-ITC]). The NITC was reconstituted in DMSO and used as a positive control for ITC. An equal volume of DMSO (final concentration <0.1%) was added to the controls. Effect of Eu-ITC and Eu (dendrimer without the active ITC group) on cell viability was determined by trypan blue dye exclusion assay. 5 x 103 MDA-MB-231 cells and 2 x 104 MCF-10A cells were plated in 24-well plate and allowed to attach overnight. The medium was replaced with fresh complete medium containing desired concentrations of Eu-ITC, Eu NITC and DMSO (control), and the plates were incubated for 24 and 48 hrs at 37 °C in a humidified atmosphere of 95% air and 5% CO_2. Both floating and adherent cells were collected by trypsinization and pelleted by centrifugation at 700 g for 5 min. The cells were re-suspended in 25 µl phosphate buffered saline (PBS), mixed with 5 µl of 0.4% trypan blue solution and counted using a hemocytometer.

3.2.4.2 Determination of apoptosis

The Cell Death Detection kit was purchased from Roche Applied Science (Indianapolis, IN). This ELISA-based method detects apoptotic cell death in cellular systems by measuring

cytoplasmic histone-associated DNA fragments. Briefly, 4 x 104 MDA-MB-231 cells and 1.2 x 104 MCF-10A cells were seeded in 48-well plates, allowed to attach overnight and then treated with desired concentrations of Eu, Eu-ITC, NITC or DMSO for 24 and 48 h. Both floating and adherent cells were collected, and processed for quantification of cytoplasmic histone-associated DNA fragments according to the manufacturer's instructions.

3.2.4.3 Western blot analyses

The MDA-MB-231 cells were plated in at 1x 106 in 100 mm plates and exposed to desired concentrations of Eu-ITC, NITC and DMSO-control for 48 hrs. The cells were then harvested by scraping, washed with ice-cold PBS, lysed on ice with a solution containing 50 mM Tris, 1% Triton X-100, 0.1% sodium dodecyl sulfate, 150 mM NaCl, 2 mM Na_3VO_4, 2 mM EGTA, 12 mM ß-glycerol phosphate, 10 mM NaF, 16 µg/ml benzamidine hydrochloride, 10 µg/ml phenanthroline, 10 µg/ml aprotinin, 10 µg/ml leupeptin, 10 µg/ml pepstatin and 1 nM phenyl methyl sulfonyl fluoride. The cell lysate was cleared by centrifugation at 14 000 g for 30 min. Supernatant was then collected and saved as protein lysate. Protein content in each sample was determined using the Bradford method. 60 µg of protein lysate was resolved by 10-12.5% sodium dodecyl sulfate-polyacrylamide gel electrophoresis and the proteins were transferred onto polyvinylidene fluoride membrane. The membranes were then blocked by incubation in solution containing Tris-buffered saline, 0.05% Tween-20, and 5% (w/v) nonfat dry milk. The membrane was treated with the desired primary antibody (anti-Caspase-9, anti- PARP, anti-β-actin) for 1 h at room temperature or overnight at 4 °C. Following treatment with appropriate secondary antibody, the immunoreactive bands were visualized by enhanced chemiluminescence method. The blots were stripped and re-probed with anti-actin antibody to correct for differences

in protein loading. Immunoblotting for each protein was performed at least twice using independently prepared lysates to ensure reproducibility of the results.

3.2.4.4 Immunofluorescence and confocal microscopy

The MDA-MB-231 cells (5x104) were plated on coverslips and allowed to attach by overnight incubation. The cells were then exposed to DMSO (control) or Eu-ITC dendrimer complex (5, 10, or 20 μmol/L, as ITC) for 24 h at 37 °C, washed with PBS, and fixed with 2% paraformaldehyde at 4 °C overnight. The cells were permeabilized with 0.5% Triton X-100 for 15 min at room temperature. Subsequently, the cells were washed with PBS, and counterstained with 100 ng/ml DAPI for 5 min. Slides were mounted and examined under a Leica fluorescence microscope at x100 (objective lens) magnification or under a FluoView 1000 confocal microscope at x100 (objective lens) magnification and a 1.4 zoom.

For lysosomal labeling, cells were treated as described above, washed with PBS, and incubated with LysoTracker green DND-26 (50nM) for 30 min. The cells were then washed with PBS, and examined under a Leica fluorescence microscope at x100 magnification (objective lens).

3.2.5   Methods for Imaging with Eu-G3P4A18N

3.2.5.1 Animal model

Four to six week old male WAG/RijHsd rats were purchased from Harlan, Netherlands. Rats were fed ad libitum and maintained in environments with controlled temperature of 22–24 °C and 12 hours light and dark cycles. All procedures involving the rats were in accordance with the Guide for the Care and Use of Laboratory Animals (National Research Council, 1996) and on a

protocol approved by the Institutional Animal Care and Use Committee of the University of Pittsburgh.

3.2.5.2 Generation of colorectal metastasis by single tumor implantation

While others have initiated colorectal metastasis by injecting cancer cells via the portal vein, superior mesenteric vein[109] or spleen,[110] these approaches lead to small diffuse lesions, which are difficult to study.[111] We generated the isolated hepatic colorectal metastasis model by way of implanting CC531 tumor pieces into rat livers. Fourteen twenty-to-thirty-week-old WAG/RijHsd rats were anesthetized with a single intraperitoneal injection of 70 mg/kg of Ketamine (Bedford Labs) and 2.5 mg/kg of Acepromazine (Boehringer Ingleheim Vetmedica, Inc.). An intramuscular injection of 0.1 mg/kg of Buprenorphine (Bedford Labs) was also administered for analgesia prior to incision. Following midline incision, CC531 tumor nodules (1 × 2 mm weighing 25 mg) were implanted in the subcapsular area of the left lateral lobe (LLL) of the rat. These implanted tumor nodules were isolated from CC531 tumors grown hepatic implants in WAG/RijHsd rats. The tumors were placed about 5 mm deep to the subcapsular area of the LLL of the liver where it was easily found 20 – 30 days later when the rat underwent a second laparotomy for GDA cannulation and hepatic infusion of the Eu-G3P4A18N solution.

3.2.5.3 Anesthesia

Rats were anesthetized with a single intraperitoneal injection of 70 mg/kg of Ketamine (Bedford Labs, OH) and 2.5 mg/kg of Acepromazine (Boehringer Ingleheim Vetmedica, Inc., MO). An intramuscular injection of 0.1 mg/kg of buprenorphine (Bedford Labs, OH) was also

administered for analgesia prior to incision and 12-24 hours later if rats displayed any sign of distress.

3.2.5.4 GDA cannulation procedure with Eu-G3P4A18N

Once anesthetized, the rat was placed in the supine position on a heating pad (Deltaphase Isothermal Pad, Braintree Scientific, MA) to maintain body temperature. The abdomen was shaved and sterilely prepared; all subsequent steps were performed aseptically; non-glare bright lighting was obtained with a fiber optic light source (Ehrenreich Photo Optical Industries, NY). A 5 cm midline incision was made using a #10 scalpel and carried down into the peritoneal cavity and hemostasis was achieved with sterile gauze and pressure. The bowel was then brought to the surface and flipped to the left of the abdomen revealing the hepaticoduodenal ligament, portal vein, hepatic artery, bile duct and inferior aspect of the liver. The portal vein was isolated using a 6-0 silk suture and fine tipped tweezers (Miltex, PA) were used to reveal the vein, allowing clear visualization of the hepatic artery running posterior and adherent to it. After the hepatic artery was separated from the portal vein, the artery was then isolated with a 6-0 silk suture. The hepatic artery was traced inferiorly to the branching point where it meets with the GDA. The GDA was also isolated using a 6-0 silk suture at the most inferior point and skeletonized using fine tipped tweezers. Two 6-0 silk sutures were placed about 3 mm apart at the superior portion of the GDA and tied on loosely for control of the catheter after placement. Fine tipped 4.5 inch curved iris scissors (Miltex, A) were used to make a 0.5 mm arteriotomy into the middle of the GDA without bisecting it. Hemostasis was achieved with the superiorly placed 6-0 silk sutures. A 30 gauge needle bent halfway was used as a "hook" to help guide a polyethylene (PE-10) catheter (Becton, Dickinson and Company, NJ) retrograde into the GDA

and placed just before the bifurcation of the hepatic artery and the GDA. The catheter was inserted into the arteriotomy and placed approximately 4 mm into the GDA, stopping before the GDA-hepatic artery junction. The superiorly placed suture along with a second one placed 1 mm next to it was tied down to secure the catheter.

To prevent inflow of blood into the liver, micro vessel clamps were placed on the portal vein and the hepatic artery. Catheter placement was confirmed by visualizing blood return in the catheter upon drawing back on the syringe and patency was confirmed with an infusion of 1-2 ml of normal saline. Complete isolation of the liver was achieved through occlusion of the suprahepatic inferior vena cava (IVC) with cotton swabs during infusion of Eu-G3P4A18N.

3.2.5.5 Cell Culture and generation of colorectal metastasis by splenic injection

CC531 cell line is a moderately differentiated colon adenocarcinoma syngeneic to WAG/RijHsd rats.[112] Tumor cells were tested and found to be virus- and mycoplasma-free. CC531 cells were cultured in Dulbecco's modified eagle medium (DMEM) (Gibco; Grand Island, NY) supplemented with 10% fetal bovine serum. Cells were maintained by serial passage. Tumor cells were harvested with a solution of 0.25% trypsin (Sigma; St. Louis, MO), washed three times in 0.9% NaCl solution buffered with 1.4 mM phosphate (PBS) and adjusted to a suspension containing 2×10^6 viable (trypan blue exclusion test) tumor cells per 200 µL of PBS, which were then injected into the spleen to generate metastatic tumor nodules in the liver. Metastatic lesions to the liver were revealed 20–25 days later after a midline incision was performed.

3.2.5.6 Luminescence imaging of hepatic tumors

In vivo administration of the Eu-G3P4A18N (300μL of a 60 μM solution in 10% DMSO/H_2O) was captured as it was being infused and selectively associating with the liver tumor. The imaging system used to detect the luminescence of the dendrimer is custom-made, combining either a Andor DU 434-BR-DD cooled charge coupled device (CCD) camera (Andor Technology, South Windsor, CT) or Rolera XR fast digital CCD camera (QImaging; Surrey, Canada) fitted with a 50 mm AF Nikkor lens containing a minimum aperture of F16 and maximum aperture of F1.4. The emission filters used were 610 / 30 nm and a 740 / 140 nm cutoff in wavelength (Chroma Technologies; VT). The rat livers on living animals were excited using four, 5 Watt LEDs, emitting at 450 nm (Lumileds Lighting; CA). Qcapture software (QImaging, Surrey, Canada) was used for the data acquisition.

Luminescence imaging of 10 μm tumor sections following hepatic arterial infusion of functionalized dendrimers was accomplished with an Olympus FV1000MPE multi photon laser-scanning unit fitted to an IX81 microscope (Olympus Corp.; Tokyo, Japan). Illumination for two-photon excitation at 820 nm was provided by a mode-locked Chameleon Ultra Ti:Sapphire laser (Coherent Inc.; Santa Clara, CA). An Olympus 25x objective with N.A. of 1.05 was used to acquire images. Luminescence emission was collected with an external photomultiplier tube using a 570 – 625 nm bandpass filter. Scan resolution was set to 1024×1024 pixels at 4096 grey scales.

3.2.5.7 Histopathology of liver tumors sections

Tissue sections (10 microns) from dendrimer-infused livers were also processed for routine hematoxylin and eosin (H&E) and immunohistochemistry staining. Tissues were fixed with 2%

paraformaldehyde for 2 h at 4 °C, and then left overnight in 30% sucrose at 4 °C. The samples were frozen in a liquid nitrogen-cooled bath of 2-methyl-butane and cryosectioned. Sections were labeled with monoclonal CD31 (ABR MA1-26196) and Alexa Fluor 647 phalloidin (Invitrogen A22287). Goat anti mouse Cy3 secondary antibody for CD31 and DAPI followed. Images were then taken on the Olympus FV1000 confocal microscope.

3.2.6   Methods for Imaging with Ln-G3P-NB

3.2.6.1 Cytotoxicity test

The cells were seeded 2 days before the experiment in a 96 well plate at a rate of 1,104 cells per well. The next day, cells were incubated with different concentrations of dendrimer diluted in OptiMEM medium + 2% FCS. After 24 h of incubation at 37 °C, the Alamar Blue (Invitrogen) was added at 10% volume of culture medium from each well and the cells are at 37 °C for about 4h. Fluorescence was measured using a fluorimetric plate reader (Victor, Perkin-Elmer). The wavelengths of excitation and emission are 560nm and 605nm respectively. The fluorescence intensity of the medium is in connection with the cellular respiration. The percentage of toxicity was calculated based on the fluorescence of untreated control cells.

3.2.6.2 Imaging of HeLa cell with Yb-G3P-NB

HeLa cells were seeded at 7104 cells per well in a LabTek 4-well 24 hours before being incubated with the dendrimer-Yb-G3P NB 1μM at 37 °C.The cells were observed using a Zeiss Axiovert 200M ® video microscope coupled to a cooled Evolve EMCCD camera 512 (Roper Scientific) to work in the near infrared. The objective used was a Zeiss Plan Apochromat 40x

and the excitation source is a lamp 120W-HXP. The chromophore is excited at 485/20nm, the emission of the chromophore is collected 525/50nm (4ms exposure) and that of Yb^{3+} with a 770nm Long Pass (1.6s exposure). The acquisition and image processing are made with Zeiss AxioVision software 3.1.

3.3   RESULTS AND DICUSSION

3.3.1   Imaging with the generation-3 PAMAM dendrimer with 3-isothiocyanato-1,8-naphthalimide containing europium ions (Eu-ITC)

3.3.1.1 Design and synthesis of the compound

A luminescent lanthanide-dendrimer system based on a generation-3 dendrimer (Figure 3.2) was designed and synthesized. The use of this dendrimer allows a high density of naphthalimide emitting groups, resulting in a large number of emitted photons and a large number of attached therapeutic ITC units. We also have formulated the hypothesis that the dendrimer impacts the retention time of the imaging modalities and therapeutic units. Naphthalimides also offer the opportunity to be covalently attached to therapeutic units. Therapeutic agents may include antibody moieties which could target specific tissue or active treatment agents. We selected isothiocyantes (ITC) as an interesting group of compounds for several reasons: 1) organic ITC has been identified as the active components of cruciferous vegetables,[113, 114] whose dietary intake is known to be correlated with reduced risk of a variety of malignancies, including breast cancer;[115-120] 2) ITC can be relatively easily attached covalently to the naphthalimides; 3)

previous *in vitro* and *in vivo* studies demonstrated that ITC selectively inhibits growth of cancer cells without significant impact on normal tissues;[121-125] 4) based on pharmacokinetics and pharmacodynamic studies ITC can be readily removed from the body (half-life of 5 h),[13, 126-128] thus covalently attaching them to naphthalimides could extend their bioavailability and therapeutic efficiency.

The ITC groups were covalently attached on the surface of dendrimer, i.e. on the chromophore (1,8-naphthalimide). With this design, a large number of ITC units per unit volume can be delivered to the cells, and the bio-distribution as well as the water-solubility of dendrimer can be increased. Since ITC groups readily react with primary amines, ITC groups were introduced at the final step of the synthesis. 3-Amino-1,8-naphthalimide was used as a precursor for the ITC-compound, which can be easily converted to an ITC group by reaction with thiophosgene. 3-Amino-1,8-naphthalic anhydride was reacted with NH_2-terminated generation-3 PAMAM dendrimers, inspired by a previously reported method. In order to ensure the complete substitution of each dendrimer arms, 1.5 equivalent (in respect to each arm) of 3-amino-1,8-naphthalic anhydride was used. After conversion of amino groups to ITC groups, the compound was characterized using elemental analysis. The result indicates complete substitution and conversion of each arm to 3-isocyanato-1,8-naphthalimide. Interestingly, the analytical data show that this molecule still contains 32 molecules of DMSO that corresponds to one solvent molecule for each of the 32 arms (final molecular weight = 17204.14 g/mol). This result indicates that despite the extensive vacuum drying of the compound, some solvent molecules remain strongly bound by the dendrimer arms. We have previously observed a comparable phenomenon for a dendrimer of the same family (2,3-naphthalimide substituted generation-3 PAMAM) that contains 32 molecules of a different solvent, H_2O.

84
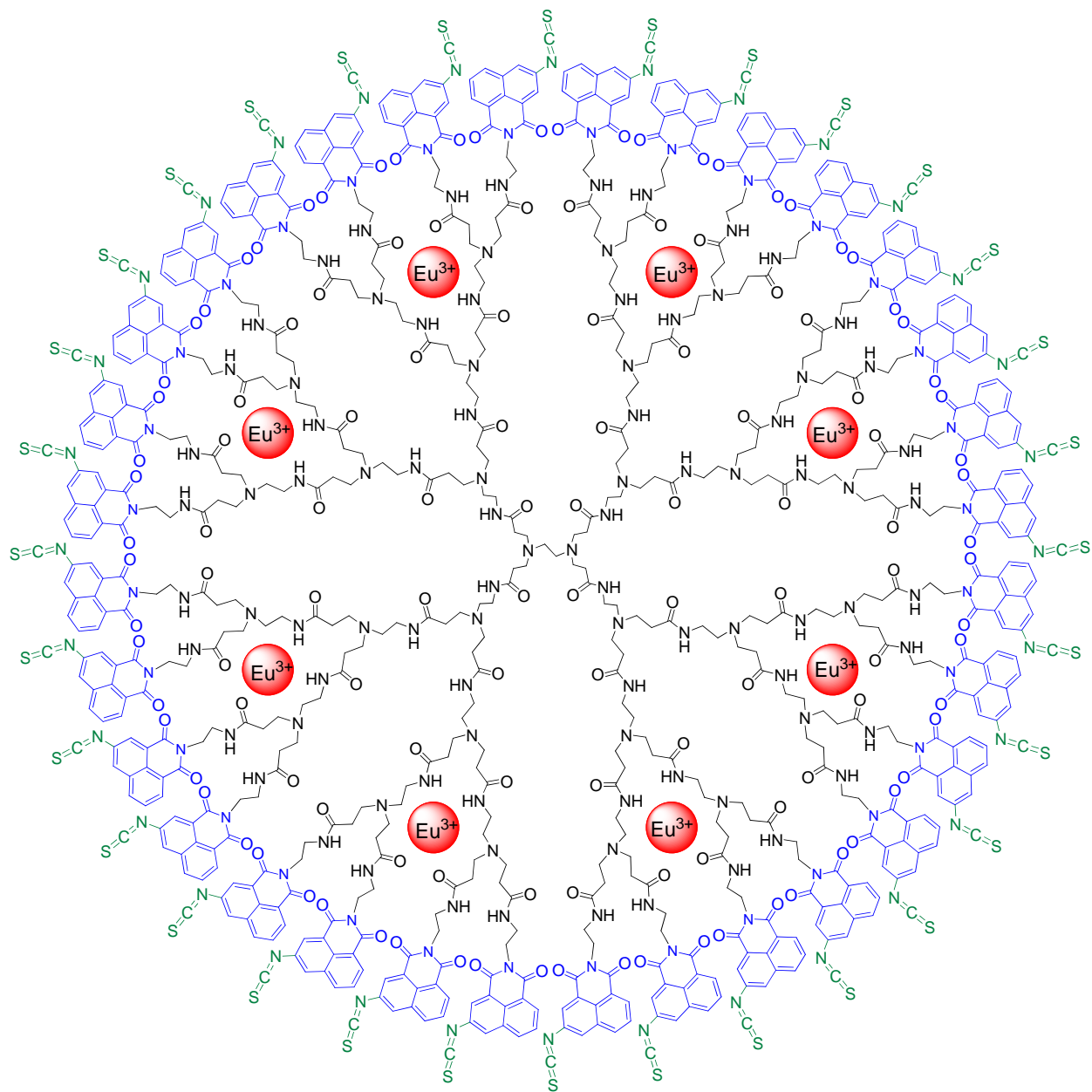
Figure 3.2. Molecular structure of the generation-3 PAMAM dendrimer with 3-isothiocyanato-1,8-naphthalimide containing europium ions (Eu-ITC)
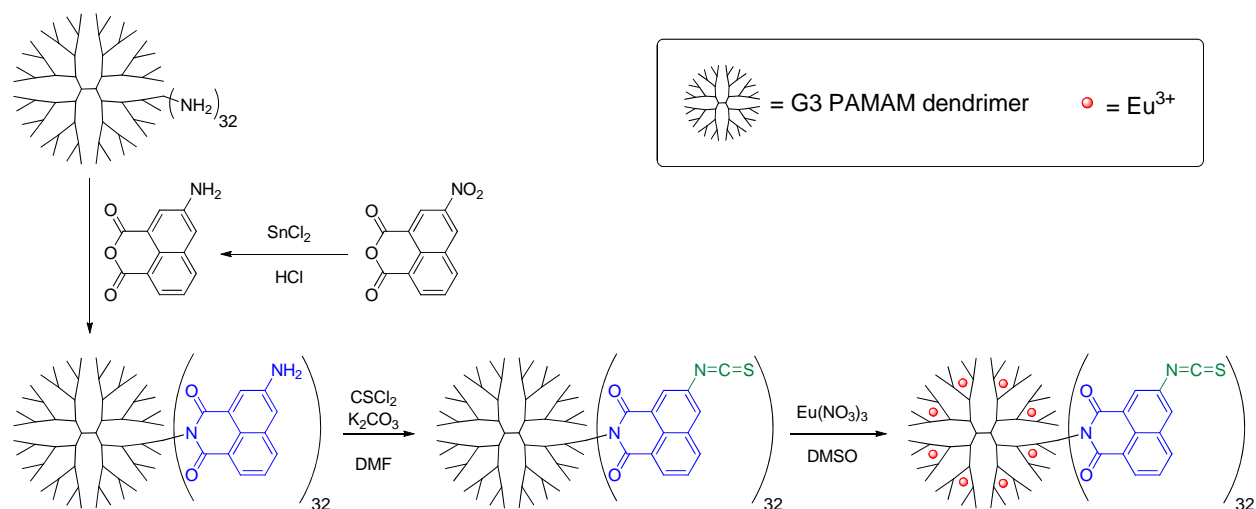
Figure 3.3. Synthesis of the generation-3 PAMAM dendrimer with 3-isothiocyanato-1,8-naphthalimide containing europium ions

3.3.1.2 Photophysical properties

The absorption spectrum of the Eu-ITC compound is depicted in Figure 3.4(a) (blue) and compared to that of the precursor system which does not contain ITC (red). The overall absorption cross-section is broadened as a result of ITC conjugation, with significantly increased epsilon values at longer wavelengths. The increased epsilon values in the red domain of the absorption profile are an advantage of ITC conjugation. Photons in the red/near-infrared region interact less with biological media and allow better detection sensitivity due to the absence of native biological emission in region of the electromagnetic spectrum. Fluorescence spectra of both compounds obtained upon excitation at 347 nm are presented in Figure 3.4(b). The apparent fluorescence maximum of Eu-ITC appears to be blue-shifted in respect to the precursor. In order to quantify the efficiency of the fluorescent system, quantum yields were collected for the ITC compound upon 347 nm excitation using a quinine sulfate reference. A value of 4.33 ± 0.03% was calculated. The red-edge tail of Eu-ITC emission extends further than that of the precursor

system, offering an area of detection which is favorable for biologic applications. Time-resolved emission spectroscopy was utilized to confirm the nature of Eu-ITC emission. In addition to observing the characteristically sharp Eu^{3+} bands at 614 nm and 698 nm ($^5D_0{\rightarrow}^7F_2$ and $^5D_0{\rightarrow}^7F_4$ transitions, respectively), the apparent emission maximum shifts from approximately 425 nm to 500 nm after a 0.1 ms delay time is applied to detection acquisition. This noted shift is consistent with the time-resolved emission signal being partly due to phosphorescence. The steady-state signal, however, was used to monitor the emission arising from the compound in the cells, providing good detection sensitivity.
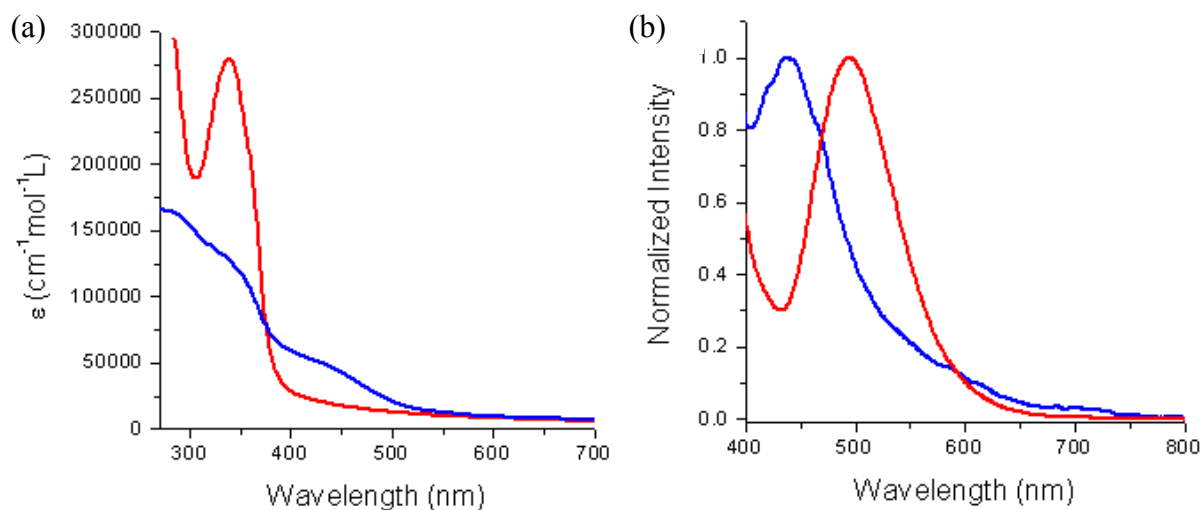
Figure 3.4. Photophysical properties of the Eu-ITC dendrimer versus control compound Eu-G3P18N-G3-(1,8-naphthalimide)$_{32}$ (that does not contains the ITC groups) 7×10^{-6} M solutions in a mixture of 10% DMSO/H$_2$O: (a) Absorption spectra for both ITC (blue) and control (red) compounds in solution, b) Fluorescence profiles for ITC (blue) and control (red) solutions upon excitation at 347 nm

3.3.1.3 Eu-ITC inhibits proliferation of MDA-MB-231 breast cancer cells

To examine the effects of Eu-ITC on cell growth and viability we treated breast cancer cells and normal breast cells with Eu-ITC, NITC (naphthyl isothiocyanate), Eu (dendrimer without the

ITC moieties attached), or DMSO (control) for 24 hours and evaluated cell viability by trypan blue exclusion assay. Previous experimental data shows that ITC can inhibit cancer cell growth at concentrations as low as 2.5-10 μM.[122, 129, 130] As observed in Figure 3.5(a), treatment with Eu-ITC resulted in significant reduction in cell viability (by 30-40% for 5 and 10 μM Eu-ITC, respectively) in MDA-MB-231 cells. However, the same treatment of normal breast MCF-10A cells did not result in reduction of their viability (Figure 3.5(a) lower panel). Exposure to NITC (positive control) produced reduction in viability that was similar to that observed with Eu-ITC in MDA-MB-231 cancer cells (Figure 3.5(a)). However it was not selective for cancer cells, as NITC treatment reduced the viability of normal breast MCF-10A cells as well. Interestingly, the presence of Eu-dendrimer alone was not able to induce any changes in cell viability in either normal breast cells or the cancerous ones, which indicates that the activity of the compound can be attributed to the ITC moiety of the Eu-ITC compound and that the Eu-ITC is selectively affecting cancer cells without having a toxic effect on normal breast cells.

3.3.1.4 Eu-ITC treatment induces apoptosis in MDA-MB-231 cells

Reduced cell viability may be a result of apoptosis or reduced proliferation. In order to determine whether Eu-ITC induced apoptosis, we quantified cytoplasmic histone-associated DNA fragmentation. Exposure of MDA-MB-231 breast cancer cells to 10 μM Eu-ITC resulted in an over two-fold increase in cytoplasmic histone-associated DNA fragments as compared to control cells, which is indicative of apoptosis (Figure 3.5(b)). A similar increase was observed in response to NITC treatment in the cancer cells. When MCF-10A normal breast cells were exposed to Eu-ITC, it did not result in a significant increase in the levels of cytosolic histone-associated DNA fragments, while NITC treatment increased the cytosolic histone-associated

DNA by over three fold (Figure 3.5(b)). It is important to note that the Eu dendrimer alone did not have an appreciable effect on either the normal or the breast cancer cells. To confirm our initial observation, expression of caspase-9 and PARP cleavage were examined as markers of apoptosis. We observed that a 24 hour treatment with Eu-ITC induced PARP cleavage in a dose dependent manner in MDA-MB-231 cells (Figure 3.5(c)). We have also detected a noticeable increase in the cleaved caspase 9 form with simultaneous decrease in the pro-caspase 9 form in MDA-MB-231 breast cancer cells in response to the Eu-ITC treatment (Figure 3.5(c)). All together these results indicate that Eu-ITC is affecting breast cancer cells by inducing apoptosis. Our results clearly indicate that Eu-ITC dendrimers retain the selectivity for the cancer cells that was previously observed for naturally occurring organic ITC.[122, 131] At this time, it is not fully clear yet what mechanisms are responsible for induction of cell death. It is possible that just like in case of other ITC, the mechanism is related to the presence of an electrophilic substance that can be reacting with nucleophilic compounds in the cell such as glutathione.[132] In such a case, the redox status of the cell would be changed leading to apoptosis.[129, 130] We should also consider other possibilities as the size of the dendrimer molecule may induce changes in the ITC activities. Elucidation of the mechanism behind Eu-ITC pro-apoptotic activity will require further evaluations.
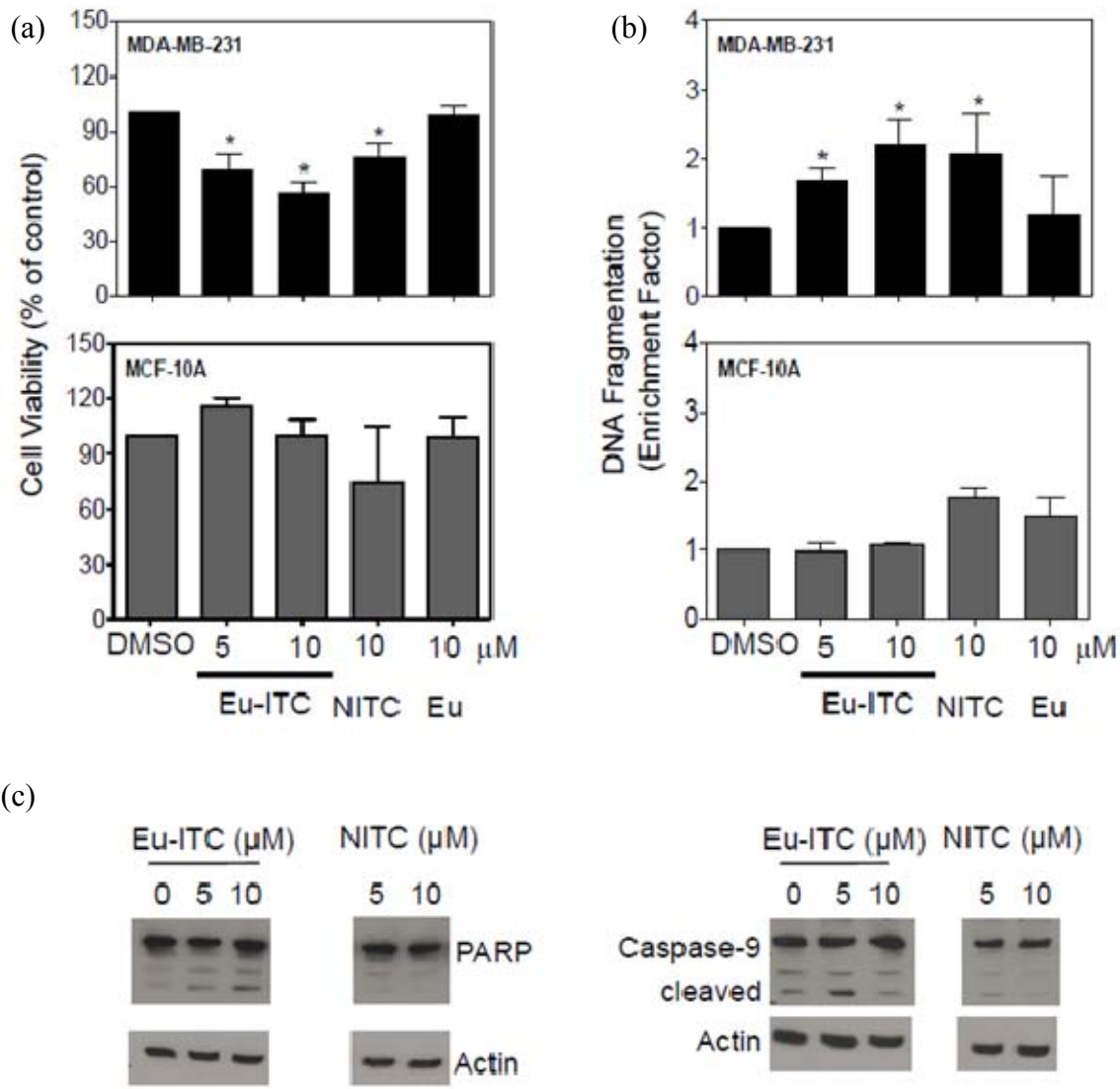
Figure 3.5. Differential response of MDA-MB-231 breast cancer cells and normal epithelial breast cells MCF-10A to treatment with europium dendrimer (Eu), europium dendrimer with isothiocyanate moieties (Eu-ITC), and NITC. (a) Cell viability of MDA-MB-231 and MCF-10A cells after 48 hrs of treatment with Eu, Eu-ITC, NITC or DMSO (control); (b) Induction of apoptosis in MDA-MB-231 and MCF-10A cells in response to Eu, Eu-ITC, NITC, or DMSO (control) (48hrs); (c) Immunoblotting for PARP and Caspase-9 using protein lysates from MDA-MB-231 cells treated with Eu-ITC, NITC or DMSO-control for 48 hrs. Blots were stripped and re-probed with an anti-actin antibody to ensure protein loading.

3.3.1.5 Cellular uptake and localization of Eu-ITC dendrimer in MDA-MB-231 breast cancer cells

Thanks to the fluorescence of the Eu-ITC dendrimer, we were able to evaluate cellular uptake and localization of Eu-ITC dendrimer in MDA-MB-231 breast cancer cells by using fluorescent and confocal microscopy. Fluorescent microscopy showed a dose-dependent cellular uptake of Eu-ITC dendrimer in breast cancer cells (Figure 3.6). Cellular distribution of red fluorescence showed that Eu-ITC dendrimer was mainly localized in the cytoplasm, and revealed a punctuate pattern, indicating that Eu-ITC dendrimer may be sequestered into vesicles. At higher concentrations (>20 μmol/L), a low level of red fluorescence was observed throughout the cell, suggesting a slow diffusion of Eu-ITC dendrimer throughout the cell. The control (DMSO-treated) cells showed no red fluorescence (Figure 3.6).
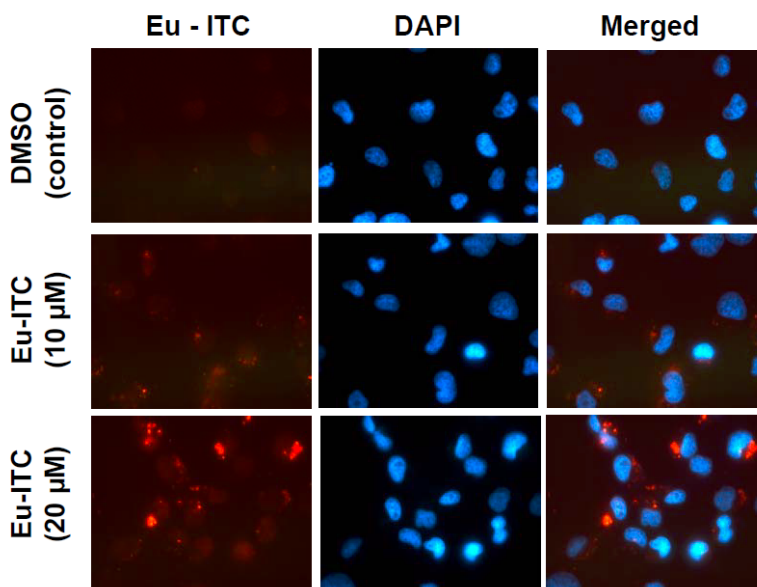
Figure 3.6. Fluorescence microscopy images showing a dose-dependent cellular uptake of Eu-ITC dendrimer in MDA-MB-231 cells. Fluorescent microscopy images depicting Eu-ITC dendrimer (red), DAPI (blue), and merged images of MDA-MB-231 cells treated with DMSO (control) or Eu-ITC dendrimer (10, and 20μmol/L, as ITC) for 24 h. 100x objective lens magnification.

91

The cellular delivery of Eu-ITC dendrimer inside the cells was also confirmed using confocal microscopy (Figure 3.7(a)), which clearly shows presence of the Eu-ITC within the cell and in the vicinity of the nucleus. Finally, to elucidate the origin of the punctuate pattern we observed in our initial microscopic analysis, LysoTracker green probes were used for labeling and tracking acidic organelles such as lysosomes in MDA-MB-231 live cells. Lyosomal fluorescence was co-localized with Eu-ITC dendrimer fluorescence indicating the uptake of dendrimer into the acidic vesicles (Figure 3.7(b)). It is hypothesized that accumulation of nanoparticles in lysosomes could lead to disruption of the lysosomal membrane (due to increased osmotic pressure) thus leading to the release of the nanoparticles into the cytoplasm.[133-135] Lysosomal localization of nanoparticles was previously reported in several models. For example, Bottini et al[134] showed that in Jurkat T leukemia cells exposed to silica nanobeads functionalized with antihuman CD2 and CD28 were able to uptake them via endocytosis and encapsulate them in lysosomal compartment. In this case, the endocytosis was mediated by receptor interaction.[134] However this interaction is not necessary for the uptake of dendrimer nanoparticles. Specifically, Ottaviani et al[133] indicated that PAMAM dendrimers may be able to interact with cellular membranes via electrostatic interactions between cationic polymer and anionic cell surface. The presence of eight Eu^{3+} in the Eu-ITC compound may further augment these electrostatic interactions. Use of the dendrimer as a mode of delivering ITC to the cells could also have other advantages: 1) increase in the local concentration of ITC and thus potentially increasing their activity, and 2) improvement of the bioavailability of the ITC by increasing the half-life of these molecules.
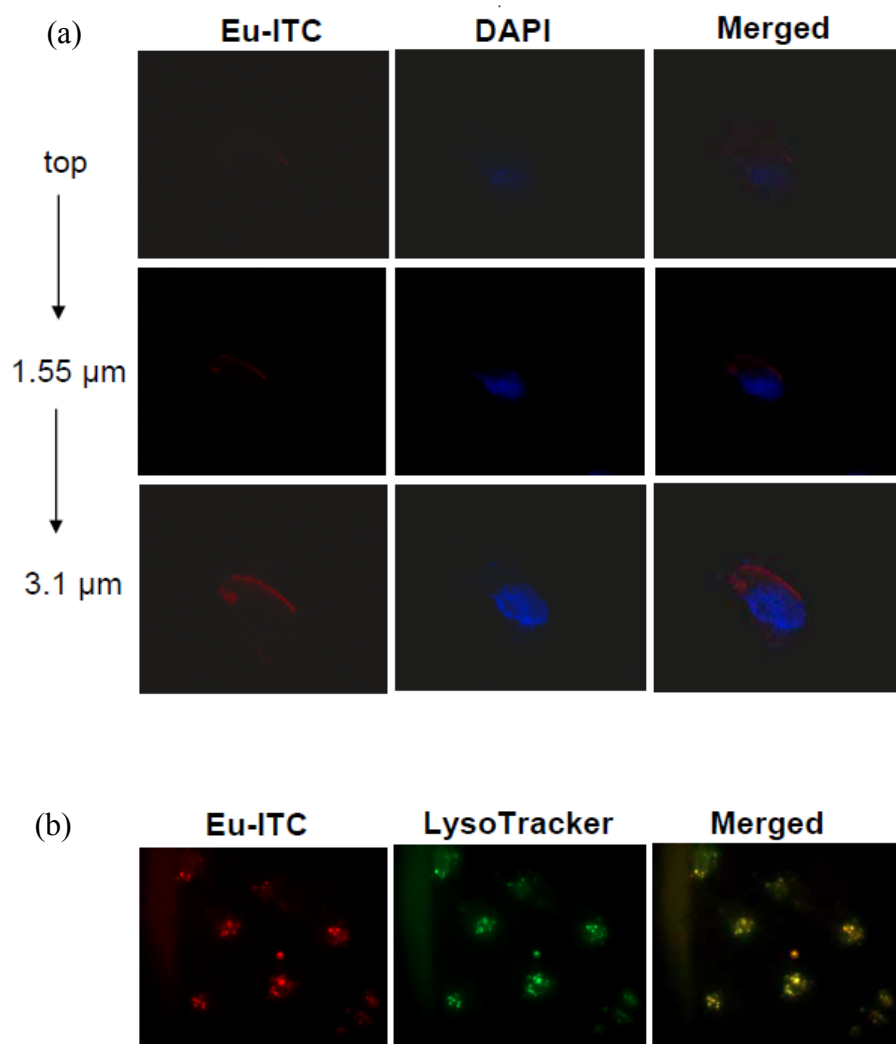
Figure 3.7. Confocal microscopy images showing Eu-ITC dendrimer internalization in MDA-MB-231 cells. (a) Confocal microscopy images depicting Eu-ITC dendrimer (red), DAPI (blue), and merged images of MDA-MB-231 cells treated with DMSO (control) or Eu-ITC dendrimer (20 μmol/L, as ITC) for 24 h. 100x objective lens magnification, 1.4 zoom; (b) Fluorescence microscopy images showing retention of Eu-ITC dendrimer in acidic organelles. Fluorescent microscopy images depicting Eu-ITC dendrimer (red), acidic organelles (green), and merged images of MDA-MB-231 cells treated with Eu-ITC dendrimer (20 μmol/L, as ITC) for 24 h. 100x objective lens magnification.

3.3.2 Imaging with the generation-3 PAMAM dendrimer with 4-amino-1,8-naphthalimide containing europium ions (Eu-G3P4A18N)

3.3.2.1 Dendrimer with 4-amino-1,8-naphthalimide and europium

We have designed and synthesized a nanoscale dendrimer complex that achieves site-specificity requirements and tested its use in live animal imaging. The dendrimer provides a versatile organic framework to which multiple fluorophores have been covalently attached. Covalently attaching organic fluorophores to the surface of the dendrimer can drastically improve the stability of the association when compared to occupying the interior cavities and being secured by secondary interactions. As a luminescent moiety, we have chosen 4-amino-1,8-naphthalimide since this molecule is hypothesized to emit a significant amount of photons in the red/near-infrared region of the electromagnetic spectrum. Such emission wavelengths allow for sensitive detection due to the absence of native fluorescence of biological systems in this spectral region (improvement of the signal-to-noise ratio). Higher generation dendrimers have a greater number of terminal branches, which correlates to the number of fluorophores which can be substituted on the surface of each dendrimer, thereby increasing the overall absorptivity and number of emitted photons per unit volume and further improving signal intensity.

By providing alternate routes of energy transfer with respect to photoreaction, luminescent lanthanide cations such as Eu^{3+} are hypothesized to partially depopulate the excited state(s) of fluorophores when the donor-acceptor energy levels are sufficiently matched, thereby preventing significant photobleaching from occurring. Polyamidoamine dendrimers (PAMAM) contain numerous binding sites along the alternating amide bond architecture of their arms, a requirement for coordinating metal cations.[136] A lanthanide complex was based on a generation-

3 PAMAM dendrimer, capable of coordinating multiple Eu^{3+} cations within the interior. The thirty-two amino end branches of the generation-3 dendrimer were functionalized with 4-amino-1,8-naphthalimide fluorophores (4A18N) using glycine linkers to yield the functionalized dendrimer: generation-3-PAMAM-(glycine-4-amino-1,8-naphthalimide)32 (G3P4A18N). The complete functionalization of each dendrimer branch was confirmed by ^{1}H-NMR (Figure 3.8) and elemental analysis. Eight Eu^{3+} cations were coordinated within the branches to yield the Eu^{3+} complex Eu-G3P4A18N by following a procedure that we have previously developed for a dendrimer carrying different fluorophores.[104]
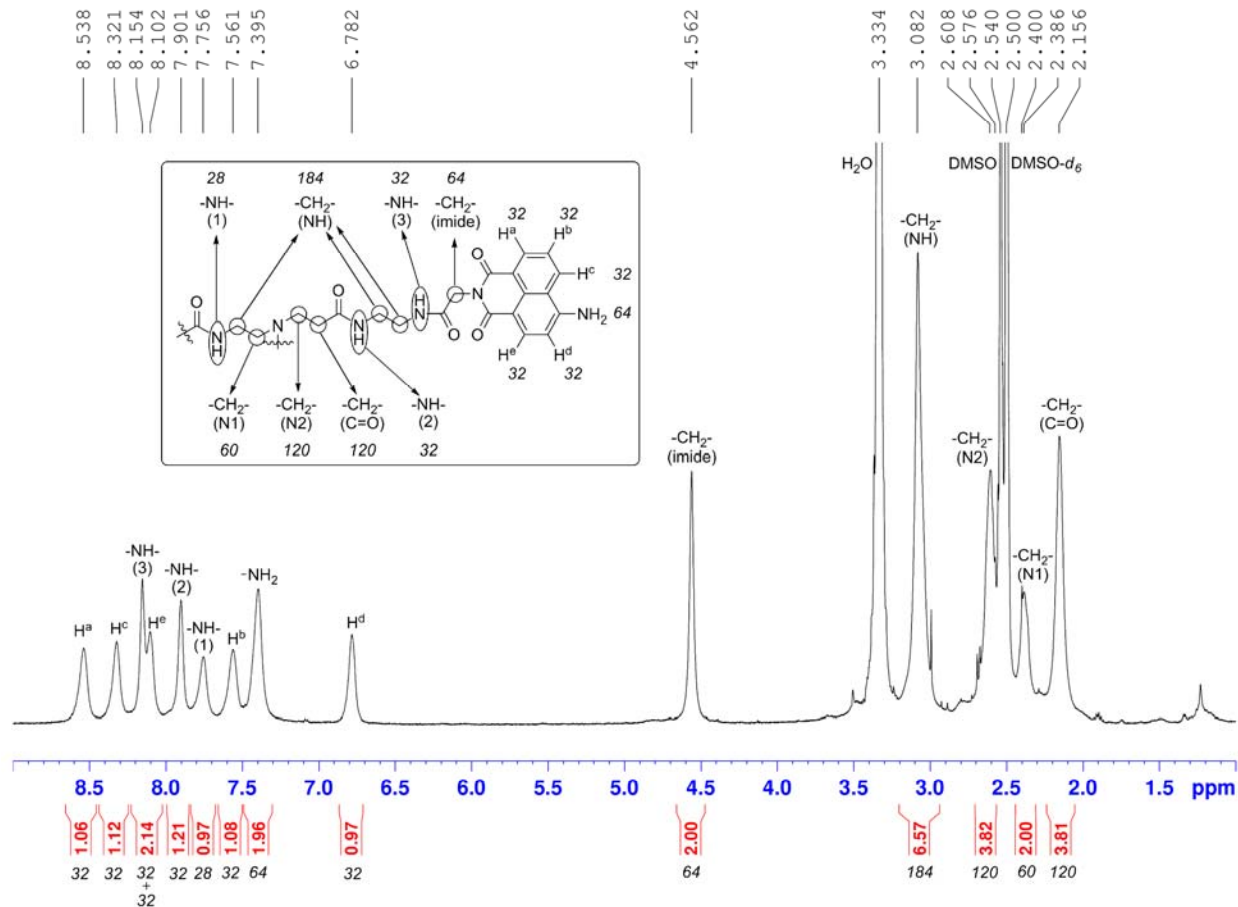
Figure 3.8. ^{1}H-NMR spectrum and peak assignment of G3P4A18N

95

CZE analysis of the Eu-G3P4A18N dendrimer with detection at 450 nm gave rise to one major peak with a cationic electrophoretic mobility of $1.39 \times 10\text{-}4$ cm^2/V s (Figure 3.9). A minor component present in some samples represented no more than 7% by peak area and had a mobility of about 6.8×10^{-5} cm^2/V s. The UV-Vis spectrum obtained from the major peak is consistent with the expected spectrum for the dendrimer. These data are consistent with a well-defined species not showing any significant dispersity. The chemical structure of Eu-G3P4A18N is depicted in Figure 3.10.
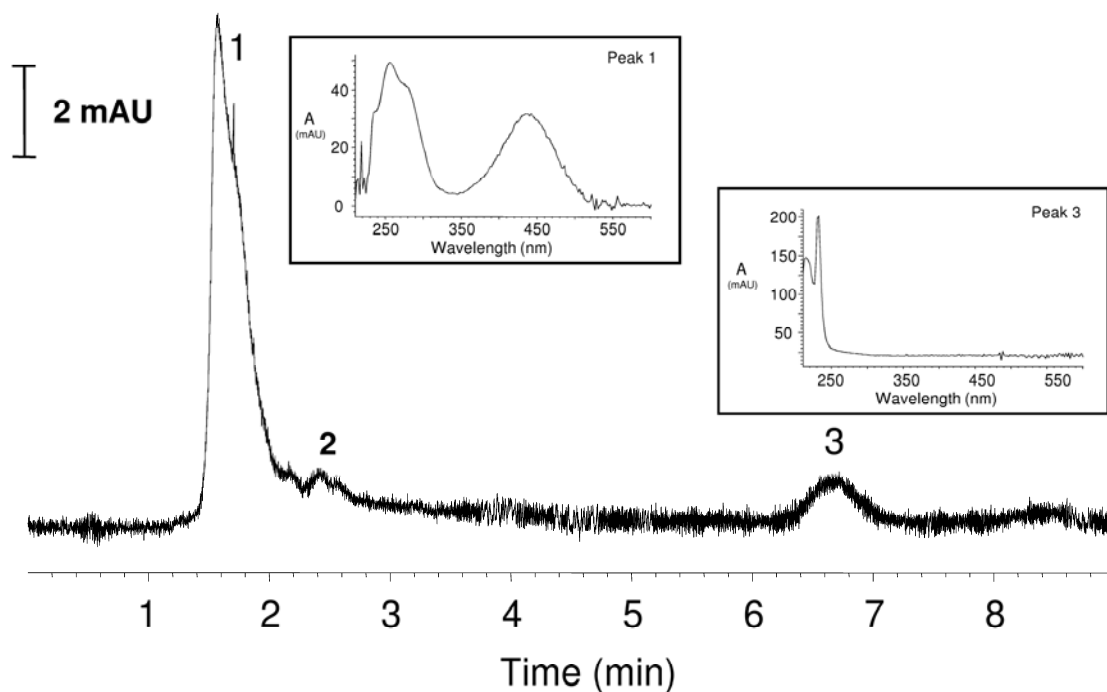
Figure 3.9. Electropherogram of Eu-G3P4A18N. Electropherogram obtained at 450 nm upon CZE analysis of 3 mg/mL (in DMSO) sample of Eu-G3P4A18N. Key: 1. Dendrimer, 2. Impurity, 3. DMSO solvent zone (to mark flow). Insets: UV-Vis spectra collected from peaks 1 and 3. Separation conditions listed in experimental section.
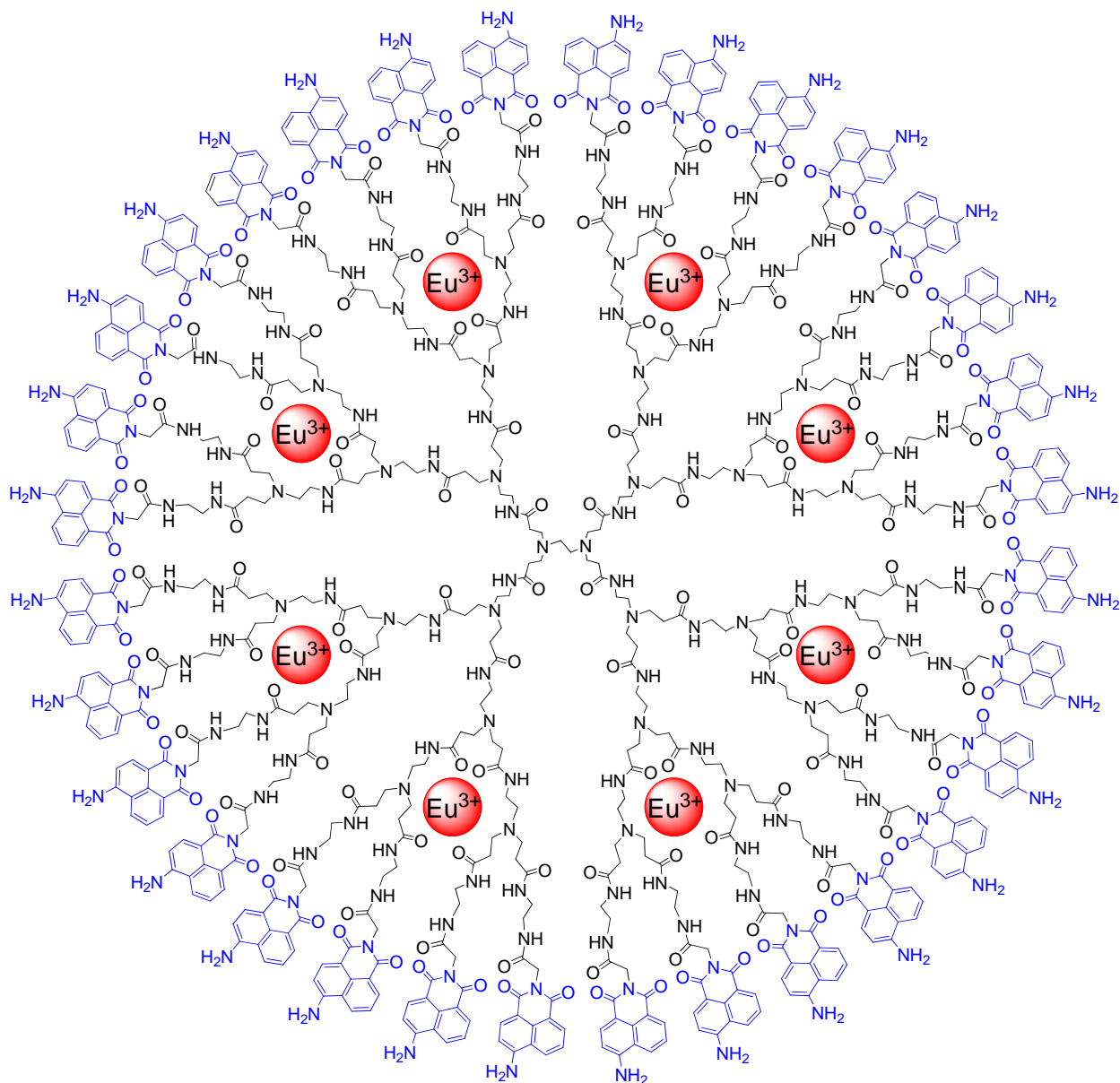
Figure 3.10. The chemical structure of the Eu-G3P4A18N dendrimer. The chromophoric group, 4-amino-1,8-naphthalimide were in blue. The red spheres indicate the coordination of eight lanthanide cations.

The absorption spectrum indicates an apparent maximum at approximately 440 nm; however, it is worth noting that the compound does absorb significantly at longer wavelengths. The molar extinction coefficient is 5,000 $cm^{-1}mol^{-1}L$ at 630 nm, which is almost two times

greater than that of Photofrin at the same wavelength.[137] Absorption at longer wavelengths is attractive for biological imaging since photons at these wavelengths generate very little autofluorescence and since such photons are not harmful to biological systems, preventing any perturbation of the system to be monitored. The luminescence emission spectrum indicates the presence of a prominent broad band with a significant component in the red/NIR part of the electromagnetic spectrum (Figure 3.11, solid line). The collection of luminescence lifetime measurements arising from Eu^{3+}-centered emission was made possible with the help of the spectroscopic resolution of a laser exciting at 354 nm. A monoexponential decay of 1.09 ($\pm$ 0.03) ms was fitted best from the experimental decay curve. This value is in good agreement with comparable systems[104] and provides strong evidence that each of the eight Eu^{3+} cations located within the dendrimer are both well protected and feel a similar coordination environment inside the dendritic architecture. The similar coordination environment around each of the lanthanide cation is a strong indication that only one well defined species is formed in solution. Polydispersity would result in several luminescence lifetimes as these cations are highly sensitive to their environment. The quantum yield of the compound upon excitation at 450 nm is 2.9 ($\pm$0.1)%. This value is relatively low, but the overall sensitivity provided by the imaging agent will be related to the number of emitted photons per unit of volume and, in this case, the small quantum yield will be compensated by the high density of luminescent 4-amino-1,8-naphthalimide groups.
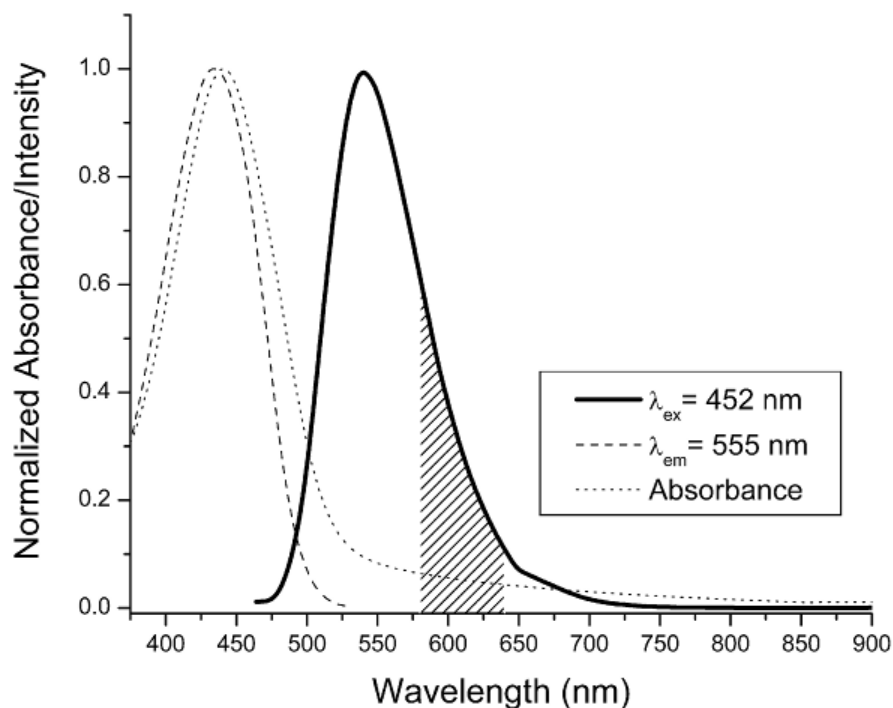
Figure 3.11. The luminescence emission spectrum displays a prominent band with an intensity maximum at 550 nm and a tail extending into the red/NIR part of the spectrum (solid line). The shaded area of the emission spectrum indicates the luminescence signal detected during the confocal microscopy experiments. A steady-state excitation spectrum (dashed line), collected upon monitoring the maximum intensity of the luminescence band (555 nm), overlaps significantly with the absorption spectrum (dotted line).

When specific conditions are met, the electronic structures of lanthanide cations are hypothesized[138] to stabilize the excited states of organic fluorophores against photobleaching. To analyze this hypothesis, the absorbance from the 1,8-naphthalimide derivative was monitored as a function of time upon exposure to white excitation light (Figure 3.12). In the absence of Eu^{3+}, the absorbance of G3P4A18N decreased exponentially. This behavior indicates that the fluorophores are vulnerable to photobleaching. In the presence of Eu^{3+}, the absorbance of Eu-G3P4A18N experienced a modest decrease within the first hour of exposure to white light;

however, the absorbance maintained constant values for the remaining part of the experiment. Indeed, the exciting side-by-side comparison depicted in Figure 3.12 lends an evidence to the idea that the eight Eu^{3+} provide increased stabilization to the electronic structure of the thirty-two 4-amino-1,8-naphthalimide fluorophores (singlet and triplet states). This feature is advantageous for applications, allowing for an extended shelf life, longer exposure time to excitation light, and repeatability of experiments. Such stabilization for a molecular complex in solution has been, to the best of our knowledge, only reported in one article so far.[57]
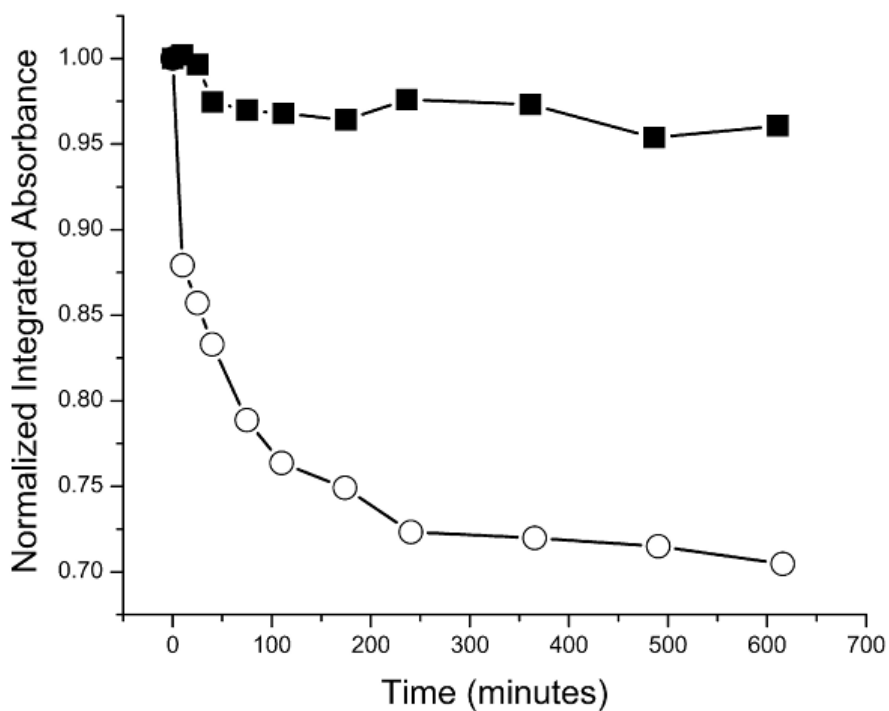
Figure 3.12. The absorbance of G3P4A18N was monitored as a function of time upon exposure to white light. In the absence of Eu^{3+} (open circle), the absorption decreased exponentially for the duration of the experiment, leading to an overall decrease approaching 30%. The trend observed in the presence of Eu^{3+} (filled square) was a modest decrease in absorbance during the first minutes, followed by an impressive level of stability for the same duration.

3.3.2.2 Hepatic arterial infusion of Eu-G3P4A18N

Regional hepatic delivery of Eu-G3P4A18N was made possible by infusion via the gastroduodenal artery (GDA) of 160 – 330 gm WAG/RijHsd rats. This technique involves isolation of the vasculature of the liver by clamping closed the common hepatic artery, portal vein and infra-hepatic inferior vena cava (Figure 3.13). A polyethylene 10 (PE-10) catheter was inserted retrograde into the GDA for a length of approximately 4 mm and secured with two 6-0 silk sutures. Infusion of 7 mL of 100 units/mL of heparinized normal saline was made into the GDA of a live WAG/RijHsd rat to temporarily evacuate the hepatic blood volume prior to delivery of the functionalized dendrimer complex. To demonstrate its preferential accumulation in tumors, Eu-G3P4A18N (0.8 µg/g total body weight) was infused through the GDA followed by 5 mL of normal saline to ensure full distribution of the dendrimer into the liver. The liver was excised following infusion to evaluate the luminescence signal emitted by the Eu-G3P4A18N in the tumor and the background liver parenchyma.

3.3.2.3 *Ex vivo* imaging of Eu-G3P4A18N infusion

Imaging of *ex vivo* rat livers demonstrated that high-intensity luminescence was evident in the tumors only seconds following an *ex vivo* Eu-G3P4A18N infusion (Figure 3.14(a),(b)) when observing emission signal at 610 nm and 740 nm. Although there were some minor uptakes by the non-tumorous portion of the liver, these background signals were negligible in the red/NIR range of imaging. In animals with extra-hepatic intra-abdominal tumor deposits, no luminescence was observed in these tissues. To confirm that Eu-G3P4A18N enhancement is occurring specifically in the tumor tissues, histological evaluation of the luminescent foci demonstrated that they were adenocarcinomas (Figure 3.14(c)).
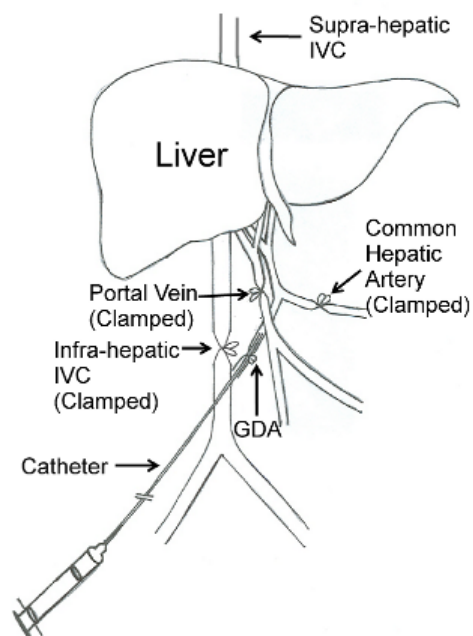
Figure 3.13. Diagram of the GDA cannulation illustrating isolation of the liver with clamping of the major vessels: portal vein, infra-hepatic inferior vena cava, and the common hepatic artery. The cannulation is indicated by a syringe and catheter leading into the site of the GDA.

(a) (b) (c)
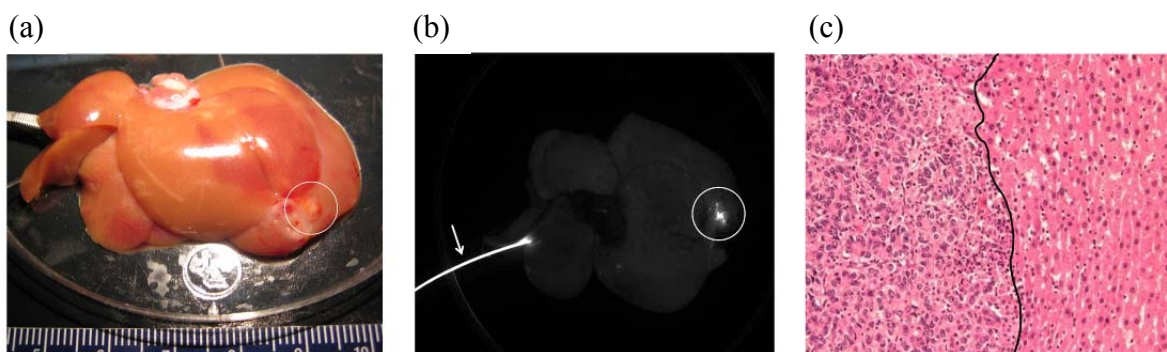
Figure 3.14. (a) White light image of an ex vivo liver with an established tumor implant. The white circle indicates the location of the tumor within the liver. (b) Luminescence image of liver after Eu-G3P4A18N infusion with an excitation wavelength of 450 nm and emission filter of 610 nm with a 30 nm bandpass. The circle shows the luminescence emitted by the tumor area only seconds after infusion of Eu-G3P4A18N. (c) 20x, H&E stained section of the tumor from the same liver showing the transition zone between adenocarcinoma on the left and normal liver parenchyma on the right of the solid black line.

To verify that only Eu-G3P4A18N has the capacity labeling tumors in the liver, rat livers were infused in vivo with Eu^{3+} cations only, dendrimers without Eu^{3+} and naphthalimide (G3P), or Eu-G3P4A18N. Figure 3.15. demonstrates the gross and luminescence images of the livers infused with the three different molecules or cations. The Eu^{3+}-only infusion and the dendrimer-only infusion both show minimal or no luminescence arising from the tumor when compared to the tissue autofluorescence. However, intrahepatic Eu-G3P4A18N infusion demonstrated specific higher-intensity luminescence in the tumor. These data are represented quantitatively in Figure 3.15.
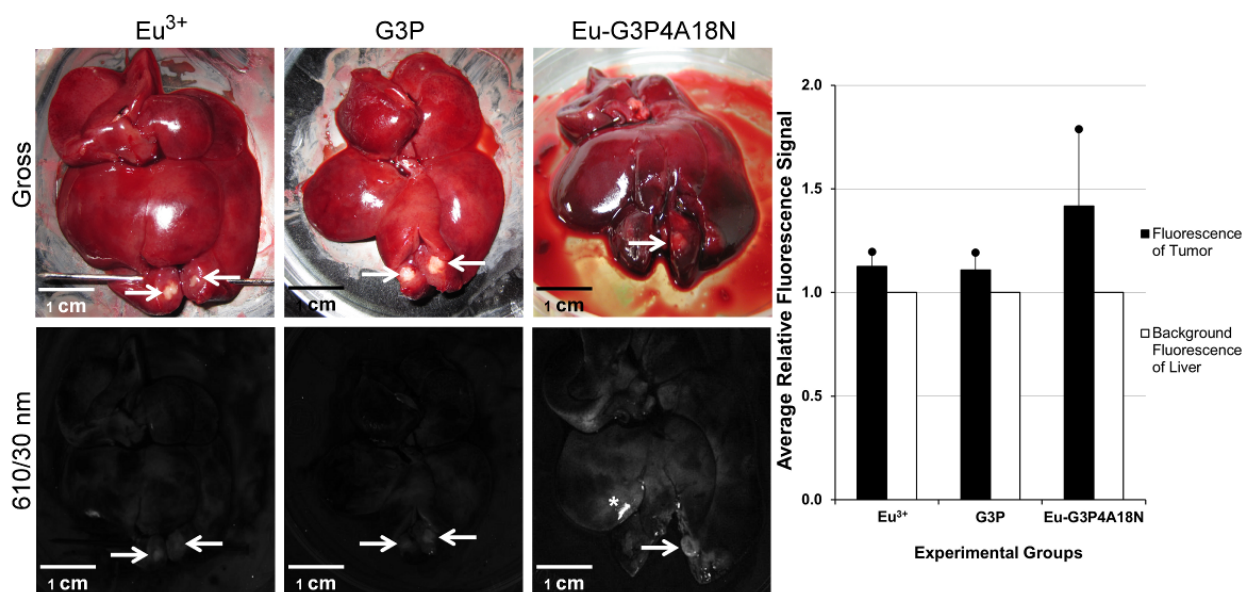
Figure 3.15. Gross photographs (top row) and luminescence images (bottom row) of the livers containing tumors (arrows) that were implanted 20 – 30 days prior to infusion and excised at 0 h time point. Images are from liver infused with Eu3+ only (first column), G3P (non-functionalized dendrimer without Eu^{3+}; second column) or Eu-G3P4A18N (third column). Average tumor luminescence was corrected for background autofluorescence in the resulting graph. Asterisks represent specular reflection of the liver. Scale bars represent 1 cm.

Multiple metastatic tumor nodules were generated in a rat liver via a splenic injection of CC531 colorectal cancer cells. After infusion of Eu-G3P4A18N, the rat liver was excised and imaged by luminescence. Figure 3.16(a) shows the gross and corresponding luminescence photographs of an *ex vivo* liver. This liver was used as a control and was not infused with the dendrimer complex to demonstrate that the metastatic tumor nodules themselves have minimal native fluorescence within the spectral region of detection (595 to 625 nm). Figure 3.16(b) presents the gross and corresponding luminescence photographs of another *ex vivo* rat liver with metastatic lesions. The metastatic nodules display a more intense luminescence signal than the background after infusion of Eu-G3P4A18N.
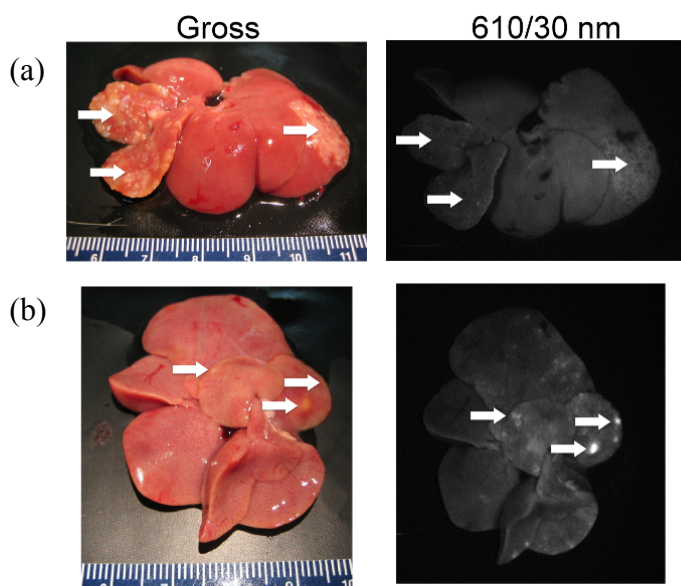
Figure 3.16. Colorectal metastasis to the liver (a) without and (b) with infusion of Eu-G3P4A18N. (a) Arrows show tumor nodules in the liver of a rat generated after a splenic injection of CC531 tumor cells. No dendrimer was infused into this liver. The second image shows the absence of luminescence in the nodules. (b) Arrows show metastatic lesions in another liver of a rat from a splenic injection of CC531 tumor cells. The liver was infused with Eu-G3P4A18N (300 μL of a 60 μM solution in 10%DMSO/H_2O). Luminescence image were taken with a CCD camera (excitation light of 450 nm and emission filter of 610 nm with a 30 nm bandpass filter).

To determine the retention time of the dendrimer in the tumor post infusion, rats were injected intrahepatically with Eu-G3P4A18N and sacrificed at the following time points: 0 h, 4 h, 24 h, and 72 h (Figure 3.17). Sustained luminescence signals from the tumors were observed at all-time points post infusion. Background autofluorescence of the liver was accounted for and the resulting bar graph (Figure 3.17) demonstrates quantitatively that signals from the tumors were present up to 72 h post injection.
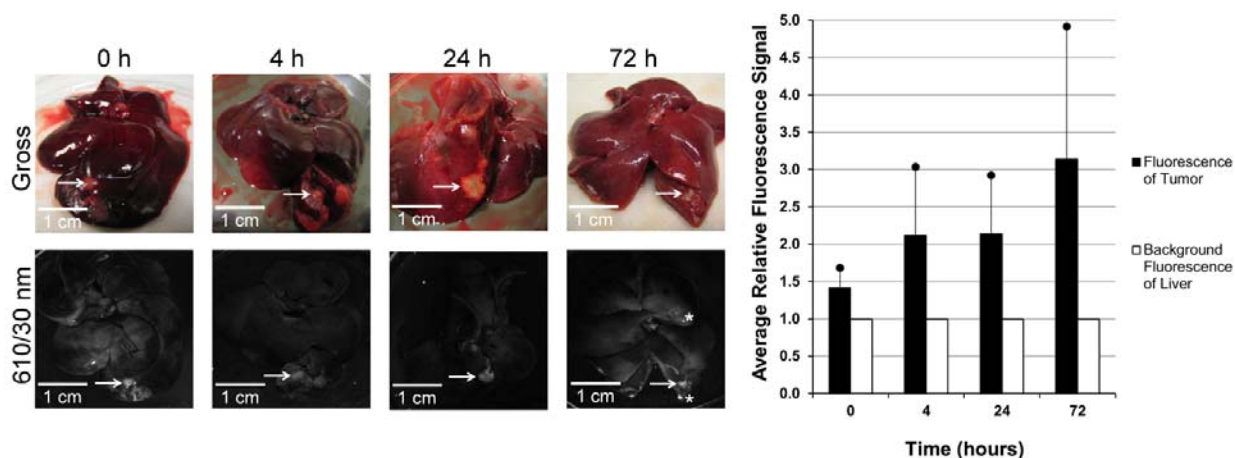
Figure 3.17. Gross and luminescent photographs of tumors in the livers of rats with analysis of the tumor luminescence. Gross (top row) and luminescent (bottom row) images of the livers containing tumors (arrows) that were implanted 20 – 30 days prior to infusion and excised at 0 h, 4 h, 24 h and 72 h time points after hepatic infusion with Eu-G3P4A18N. Average signals obtained from the tumors were compared to that of tissue autofluorescence and displayed in the resulting graph. Asterisks represent specular reflection.

3.3.2.4 *In vivo* imaging of Eu-G3P4A18N infusion

To evaluate the preferential accumulation in tumors of our functionalized dendrimer *in vivo*, *in vivo* intrahepatic infusion of Eu-G3P4A18N in anesthetized rats (Figure 3.18) was performed. Localized luminescence was observed in the tumor tissues within seconds following infusion. This result is consistent with our previous observations in the ex vivo setting. The infused liver

was excised and sectioned for red/NIR microscopy. We found that the signal-to-noise ratio was improved when luminescence was detected at 740 nm/140 nm as compared to 610/30 nm.
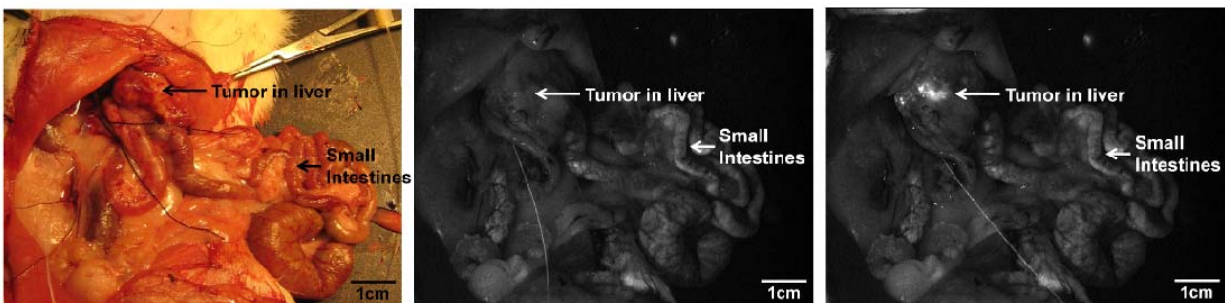
Figure 3.18. *In vivo* colorectal hepatic tumor localization after the infusion of Eu-G3P4A18N and histological imaging using confocal and multi-photon scanning microscopy. (left) White light photograph of an in vivo rat liver containing a tumor; Luminescent images of the abdominal cavity of the rat before (center) and after (right) Eu-G3P4A18N infusion (excitation 450 nm and emission filter of 610 nm with a 30 nm bandpass).

Use of a two-photon excitation scanning confocal microscope allowed us to confirm that the luminescence signal of the dendrimer was present within the vasculature of the liver (Figure 3.19(a)). Higher magnifications of the tissue sections revealed that the luminescence is located outside of the vessels in the perivascular space (Figure 3.19(b)). Figure 3.19(c) and (d) also show a section of tumor from a rat liver that was infused with Eu-G3P4A18N displaying the same association of the dendrimer with the vasculature under confocal microscopy. Tumor vasculature is disorganized and displays widened inter-endothelial junctions and fenestrae that range from 400 – 800 nm in size.[137] Thus, tumor vasculature is often described as "leaky", allowing for larger molecules to extravasate the vascular endothelium into the extravascular space and in the process bypass normal liver parenchyma. The relatively small size of our dendrimer[139] facilitates its exit through the fenestrae and allows it to be trapped in the extravascular spaces of the tumor. The confocal microscopy observations are consistent with the hypothesis that Eu-G3P4A18N has

increased extravasation from the leaky tumor vasculature and therefore is more likely to be trapped in the perivascular spaces of the tumor.
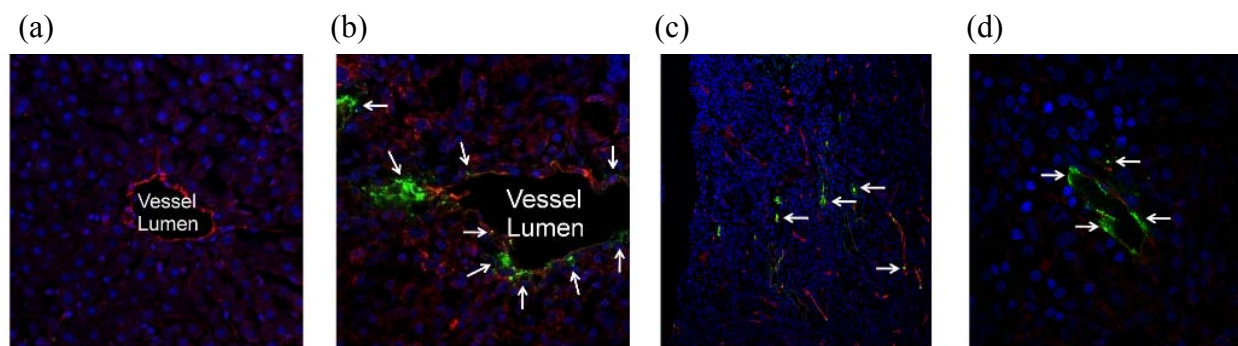
Figure 3.19. (a) 20x confocal microscopic image of a section of liver without the tumor after Eu-G3P4A18N infusion, no luminescence of the dendrimer is seen. The excitation wavelength was 488 nm and emission wavelength was 567 nm. Vessels are labeled with CD-31 (red), nuclei of hepatocytes with dapi (blue) and dendrimer (green); (b) Eu-G3P4A18N can be seen in green (arrows) with the 40x magnification of a confocal microscopic image of tumor in the liver after infusion. The same colored labels are used; (c) 25x magnification of a tumor section in a rat liver after infusion of Eu-G3P4A18N. The two-photon excitation was 820 nm and the luminescence emission was 570 – 625 nm. The nuclei of cancer cells are seen in blue, the aberrant vessels are depicted in red and the dendrimer is designated in green (arrows) to show the association of Eu-G3P4A18N with the tumor vasculature seen in red; (d) 60x magnification of another section of tumor within the same liver also demonstrating the same concept.

3.3.3 Imaging with the generation-3 PAMAM dendrimer with naphthalimide and biotin (G3P-NB)

3.3.3.1 Synthetic strategy of functionalized dendrimer complex

When the dendrimer with 3-isothiocyanato-1,8-naphthalimide was synthesized, ITC group was introduced on the naphthalimide group which was already on the surface of dendrimer. It was confirmed that all the 32 naphthalimide groups on the dendrimer, but this method is not ideal

107

because some of the branches may not be substituted, and there is no practical way to separate the mixture of dendrimers with different number of substituents. The other problem of this approach is that the reaction can be completed only at high temperature. As shown in Figure 3.20, the direct reaction between the terminal amino groups on PAMAM dendrimer and naphthalic anhydride requires high temperature over 90 °C. It is questionable whether the functional groups or their precursors on naphthalic groups remain intact in this reaction condition.
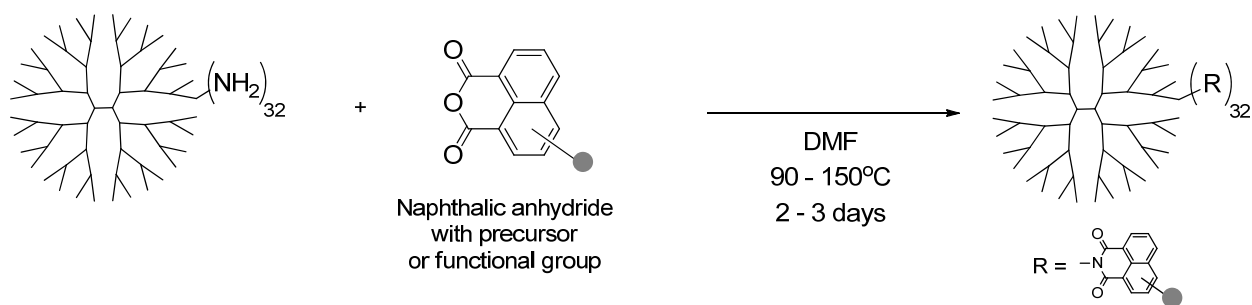
Figure 3.20. Direct attachment of naphthalic anhydride on dendrimer in high temperature

In order to ensure the functionalization of dendrimer branches, a mild condition reaction is required for the attachment of naphthalic moiety with functional groups. Amide coupling reaction condition with coupling reagents is a good candidate for such reaction. The general strategy of the syntheses of functionalized dendrimer is depicted in Figure 3.21. The synthesis of G3P4A18N in the previous section was a proof of concept of this synthetic strategy, adopting glycine as a linker and using HATU as an amide coupling reagent.
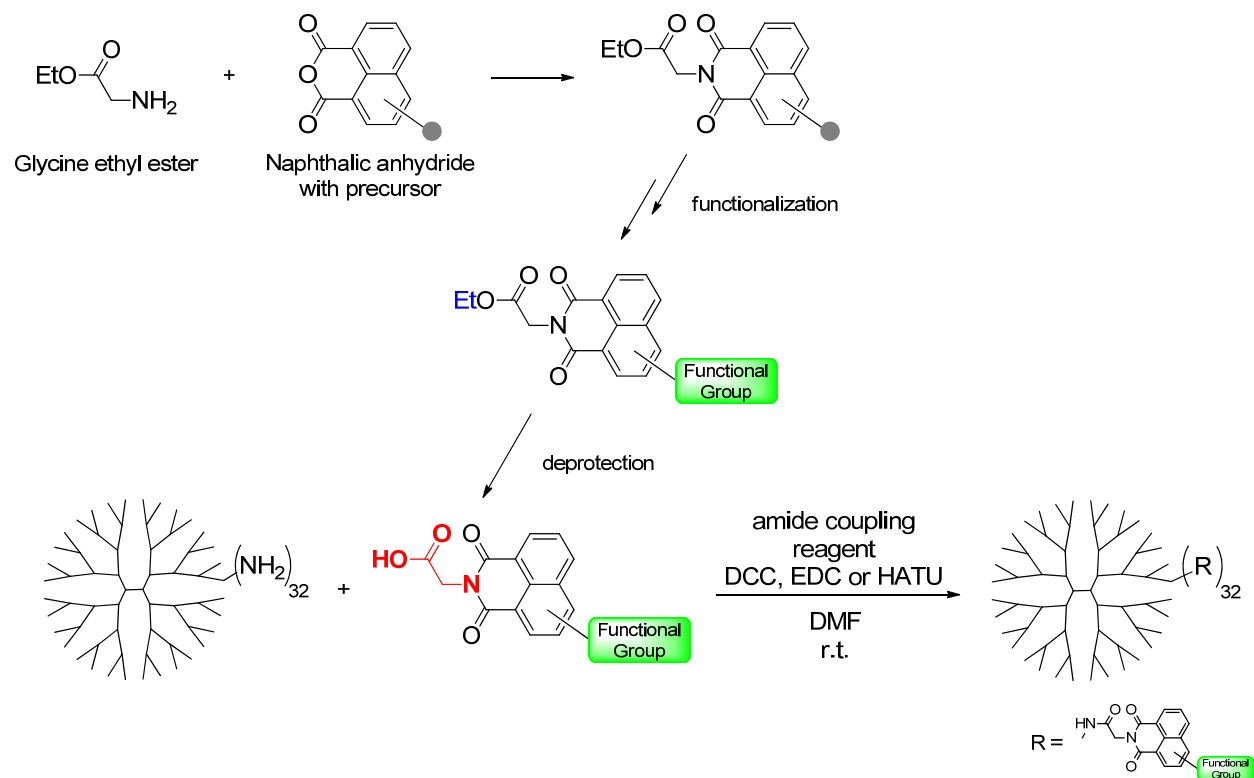
Figure 3.21. Synthetic strategy for synthesis of naphthalimide-attached dendrimer with functional groups

In this work, biotin was conjugated dendrimer was synthesized as a first example of biological functional group on the dendrimer complex. Biotin is a water soluble vitamin, which is also known as vitamin H or coenzyme R. It is important in several biochemical reactions, such as fatty acid synthesis, amino acid catabolism and gluconeogenesis.[140] Biotin binds strongly with protein avidin and streptavidin with a dissociation constant on the order of 10^{-15} M, which is one of the strongest interactions in biological systems.[141] It is expected that the attachment of biotin to the dendrimer can enhance water solubility and biocompatibility of the complex. Due to the strong binding with avidin or streptavidin, it is easy to conjugate the dendrimer complex with many biological molecules such as proteins, oligonucleotides or antibodies

The synthetic protocol for biotinylated dendrimer is summarized in Figure 3.22. Triethylene glycol was used as a linker between naphthalimide and biotin, and glycine linked naphthalimide and dendrimer. Except for the reactions of attachment of glycine and triethylene glycol amine on the naphthalimide, all the reactions were carried out in mild conditions, which can ensure integrity of biotin.
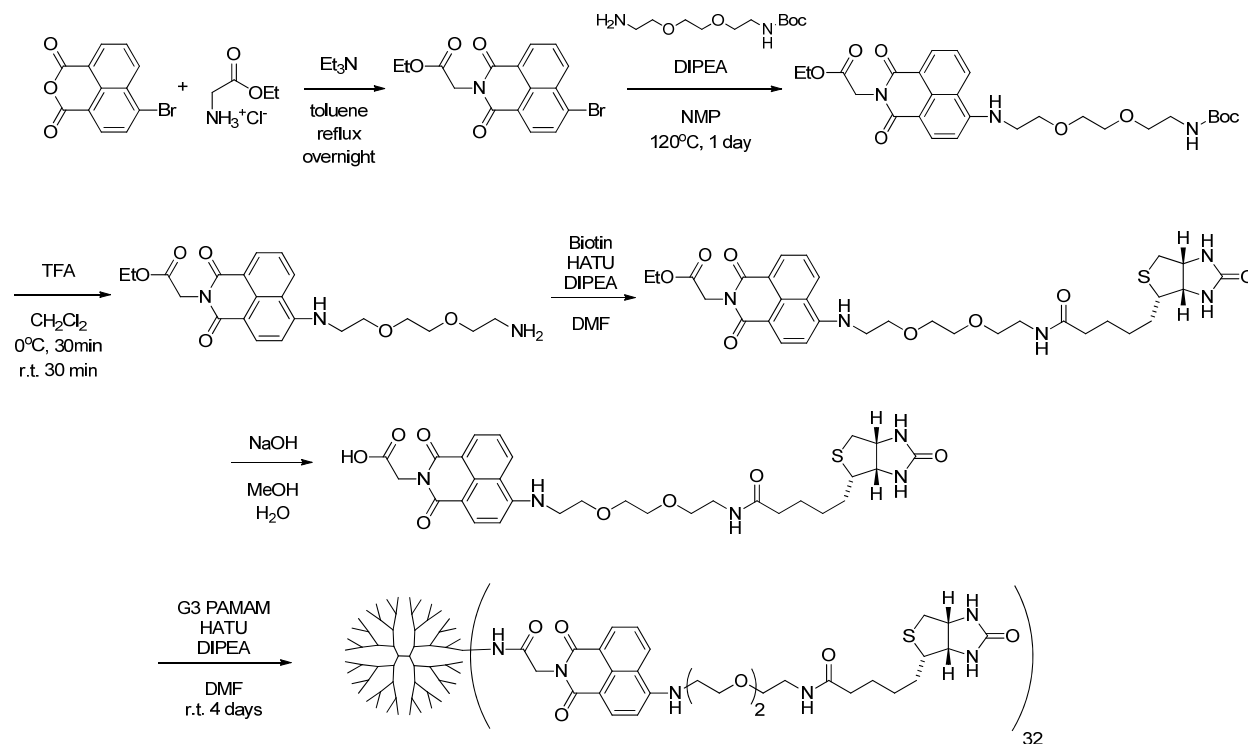
Figure 3.22. Synthetic protocol of generation 3 PAMAM dendrimer conjugated with biotin

3.3.3.2 Cell imaging

Europium, neodymium and ytterbium complexes were made with the generation 3 PAMAM dendrimer with naphthalimide and biotin (Ln-G3P-NB; Ln = Eu, Nd or Yb). The complexation was carried out following the method that we have already established.[104]

In order to evaluate the bio compatibility of these complexes, cytotoxicity test was carried out with HeLa cell. As shown in Figure 3.23, the percentage of viability is around 100% in the concentration range of 1 to 2 μM, indicating these complexes are not toxic to HeLa cells at this range.
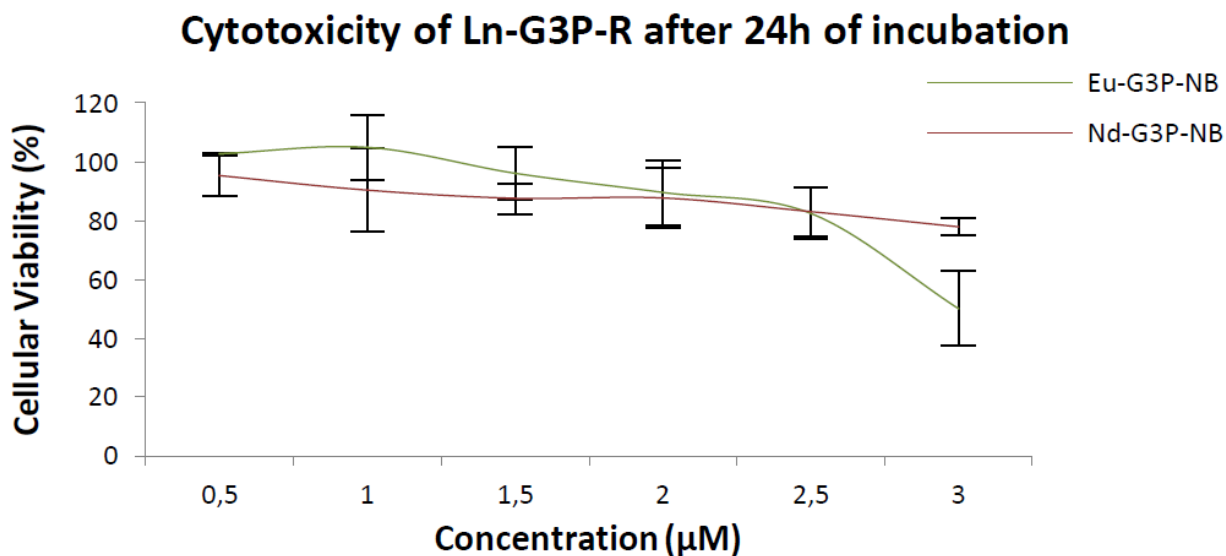
Figure 3.23. Cytotoxicity test of Ln-G3P-NB complexes after 24 h of incubation

The Yb^{3+} complex, Yb-G3P-NB dendrimer was incubated with HeLa cell for 24 h, and the microscopy image was taken under visible and near infrared regions. The Yb-G3P-NB dendrimer was observed inside of the cell, which means the dendrimer could penetrate or be transported without damage to the cell membrane. On the near infrared image, the main signal arises from dendrimer not the autofluorescence from cell as in visible image. This promising dendrimer system is under further investigations, such as other cell imaging, oxygen sensing and interaction with DNA.
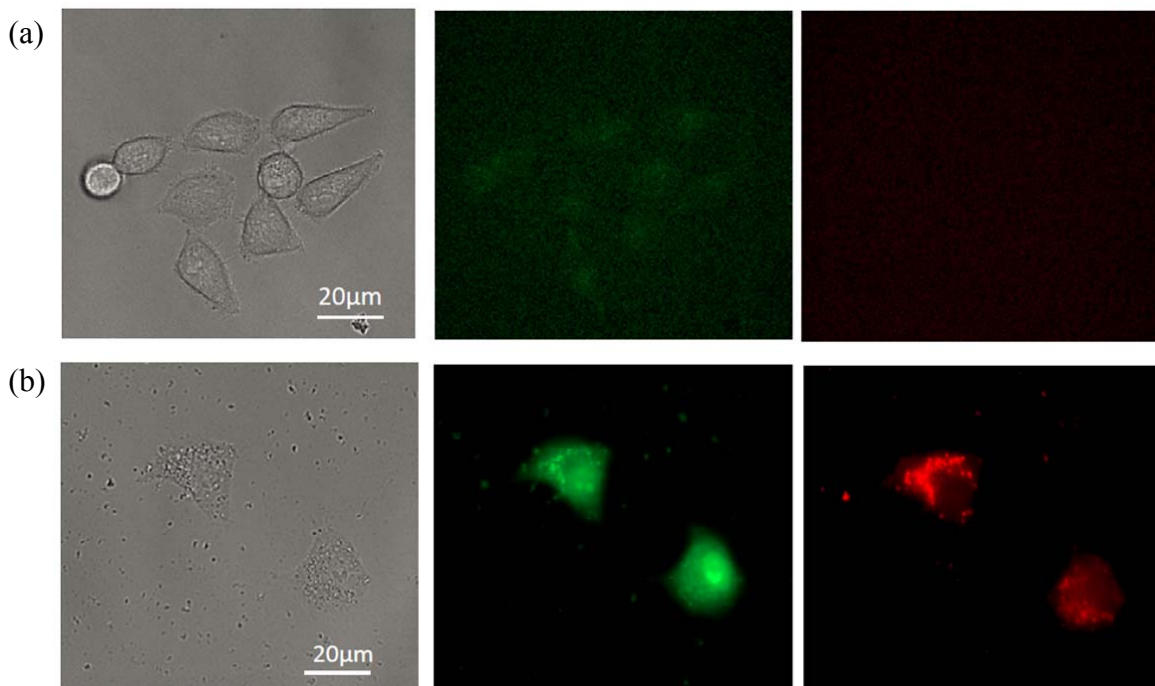
Figure 3.24. Microscopy images of HeLa cell (a) without dendrimer complex and (b) after incubation with Yb-G3P-NB (1μM, 24 h): bright field (left), visible (λ_{ex}:417/60nm; λ_{em}: 525/50nm; center) and near infrared (λ_{ex}: 417/60nm; λ_{em}: > 700nm; right) with

3.4   CONCLUSIONS

Several lanthanide-dendrimer complexes based on a generation-3 dendrimer were designed and synthesized. The versatility of the functionalized dendrimer platform has been proved through these examples.

The lanthanide-dendrimer complex with ITC not only emits photons in the red domain of the spectrum, allowing real-time monitoring of the compound localization, but also can be used as a delivery system for ITC. We demonstrated the uptake of this complex by the cancer cells, most likely through the process of endocytosis, and localized into the lysosomal compartment

112

within the cells. We also showed that the ITC functionalized dendrimer can selectively reduce viability and induce apoptosis in cancer cells, but not in normal cells.

The dendrimer complex with 4-amino-1,8-naphthalimide acts as a robust luminescent marker. Real-time luminescence imaging of hepatic tumors in the WAG/Rij Hsd rat model was possible with this complex. We have observed that the luminescence located in the tumor was visible within seconds following hepatic arterial infusion of the dendrimer. These dendrimers are strongly resistant to photobleaching and preferentially accumulate within liver tumors after hepatic artery infusion. These results suggest that the dendrimer complex has great potential to serve as imaging agent to detect metastatic sites during regional therapy.

The syntheses of functionalized dendrimer need a strategy which can minimize the effect on the functionalized groups. A mild reaction condition – amide coupling with coupling reagent was adopted. Biotin-conjugated dendrimer was designed and synthesized using this strategy. The lanthanide complexes of this dendrimer showed strong bio-compatibility.

4.0   OXYGEN SENSING WITH LANTHANIDE COMPLEXES

Parts of the work presented here have been completed in collaboration with Benedikt Huber, Matthias Bischof (Visiting Students from Philipps-Universität Marburg, Germany), Chad Shade, Jason Cross (Stéphane Petoud Research Group, Department of Chemistry, University of Pittsburgh), Douglas Kauffman (Alex Star Research Group, Department of Chemistry, University of Pittsburgh) and Claudette M. St Croix (Center for Biologic Imaging, University of Pittsburgh). A portion of the results presented here have been published in Nature Chemistry, Vol. 1, No. 6, p 500, 2009: "Decorated carbon nanotubes with unique oxygen sensitivity."[142]

4.1   INTRODUCTION

The determination of the concentration of oxygen in solution or in the gas phase is important in many fields such as industry, military, and medicine. The widely used oxygen sensor technologies, such as solid-state or solution-phase electrochemistry,[143, 144] and resistive metal–oxide semiconductors[144, 145] are based on electrochemical measurement. The current electrochemical oxygen sensors sometimes need high operating temperatures, high power or complicated fabrication,[143-145] and the electrochemical methods cannot be applied in biological applications, especially at cellular level, because it is challenging to make and manipulate tiny

electrode which has comparable size of a cell. In order to overcome the limitation of electrochemical methods, development of simple low-power devices[146, 147] or photochemical sensor is required.[148-151]

In this work, we present oxygen sensor systems based on luminescent lanthanide complexes. These systems have advantages over common organic and inorganic fluorophores such as easiness of spectral discrimination, long luminescence life time and photostability. The oxygen sensitivity was quantified with specially designed device which can measure luminescence spectra and to monitor the amount of oxygen at the same time. The luminescent lanthanide complex successfully showed oxygen sensitivity in cells. The oxygen sensing ability was also demonstrated in solid state in combination with SWNT (single-walled nanotubes). The simple chemiresistor device composed of SWNT networks with an oxygen-sensitive europium complex showed bimodal (optical and electrical) sensitivity to oxygen.

4.2   EXPERIMENTAL

4.2.1   Synthesis of Compounds
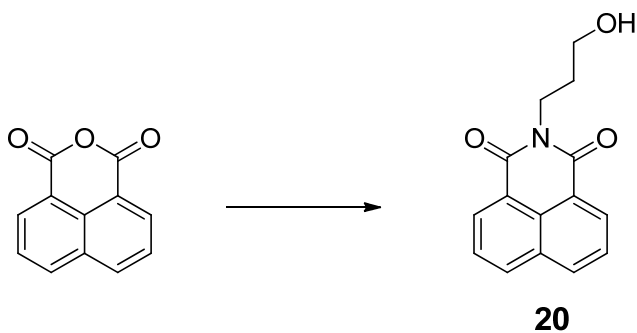
2-(3-Hydroxy-propyl)-benzo[*de*]isoquinoline-1,3-dione (**20**) was synthesized as follows: 1,8-napthalic anhydride (5g, 0.025 mol) and 3-amino-1-propanol (0.01 mol) was suspended in 1,4-dioxane (200 mL) and refluxed under N_2 with stirring for 24 hours. The solution was allowed to cool and the solvent volume reduced to ca. 50 mL. The remaining material was poured into water (100 mL) causing a beige precipitate to form then was filtered off, washed with water (2 × 20 mL) and ether (2 × 20 mL). The crude material was recrystallized from 1,4-dioxane to yield the title compound as a white crystalline solid (4.73 g, 84%); mp 122-124 °C; ^{1}H NMR (300MHz; CDCl$_3$, δ): 2.34 (m, 2H, -CH$_2$*CH$_2$*CH$_2$-), 3.50 (t, *J*=7 Hz, 2H, N(CO)$_2$-*CH$_2$*CH$_2$), 4.33 (t, *J*=7 Hz, 2H, CH$_2$*CH$_2$*OH), 7.77 (t, *J*=8 Hz, 2H, 3-H and 6-H), 8.23 (dd, *J*=1 Hz and 8 Hz, 2H, 2-H and 7-H), 8.60 (dd, *J*=1 Hz and 8 Hz, 2H, 4-H and 5-H); EIMS *m/z*: 255 (M$^+$, 82%).

20   **21**
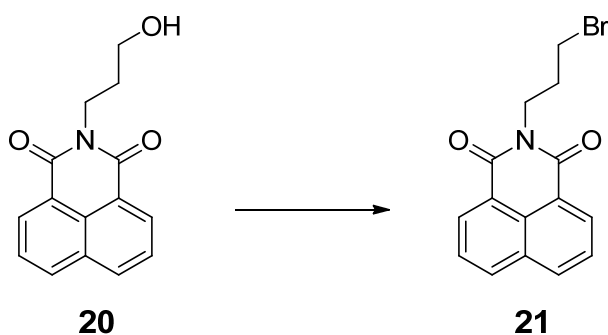
2-(3-Bromopropyl)-benzo[*de*]ioquinoline-1,3-dione (**21**) was synthesized as follows: the hydroxyl naphthalimide **20** (1 g, 7.84 mmol) suspended in phosphorus tribromide (15 mL) was heated at 100 ºC with stirring under an N_2 atmosphere for 24 hours. The solution was allowed to cool and quenched by the slow addition of water, causing a beige precipitate to form. The precipitate was filtered, washed with water (2 × 10 mL) and ether (2 × 10 mL) and recrystallized from ethanol to yield white needles (1.70 g, 68%); mp 142-144°C; ^{1}H NMR (300MHz; CDCl$_3$, δ): 2.34 (m, 2H, -CH$_2$*CH$_2$*CH$_2$-), 3.45 (t, *J*=7 Hz, 2H, N(CO)$_2$-*CH$_2$*CH$_2$), 4.38 (t, *J*=7 Hz, 2H,

CH$_2$CH$_2$OH), 7.77 (t, J=8 Hz, 2H, 3-H and 6-H), 8.23 (dd, J=1 Hz and 8 Hz, 2H, 2-H and 7H), 8.60 (dd, J=1 Hz and 8 Hz, 2H, 4-H and 5-H); EIMS m/z: 317 (M$^+$, ^{79}Br, 83%), 319 (M$^+$, ^{81}Br, 79%).

21   **22**   **23**

1-[(3-propyl)-benzo[*de*]iosoquinoline-1,3-dione]-4,7,10-tris-(*tert*-butoxycarbonylmethyl)-1,4,7,10-tetraazaylododecane (**23**) was synthesized as follows: the ester hydrobromide salt **22**[152] (400 mg, 0.67 mmol) was dissolved in freshly distilled acetonitrile (25 mL) with triethylamine (149 mg, 4.47 mmol) and stirred at 70 ºC under an argon atmosphere. The propyl bromide **21** (234 mg, 0.74 mmol) in acetonitrile (10 mL) was added dropwise over 1 hour and the mixture left to react for 24 hours. After which period, the solvent was removed under reduced pressure and the title compound was isolated by preparative TLC (silica gel) using 10% methanol in dichloromethane as the eluent as a cream colored foam (431 mg, 86%); mp 89-91°C; ^{1}H NMR (300MHz; CDCl$_3$, δ): 1.25 (s, 18H, *tert*-Bu), 1.34 (s, 9H, *tert*-Bu), 1.70 (s, 2H, -CH$_2$CH$_2$CH$_2$-), 2.18-3.78 (broad m, 26H, aza crown ring, bridgehead and C1-CH$_2$), 3.97 (s, 2H, -CH$_2$CH$_2$-N), 7.58 (t, J=7.7 Hz, 2H, 3-H and 6-H), 8.14 (d, J=8 Hz, 2H, 2-H and 7-H), 8.35 (d, J=8 Hz, 2H, 4-H and 5-H); API-ESMS m/z: 752 ([M + H]$^+$,82%).
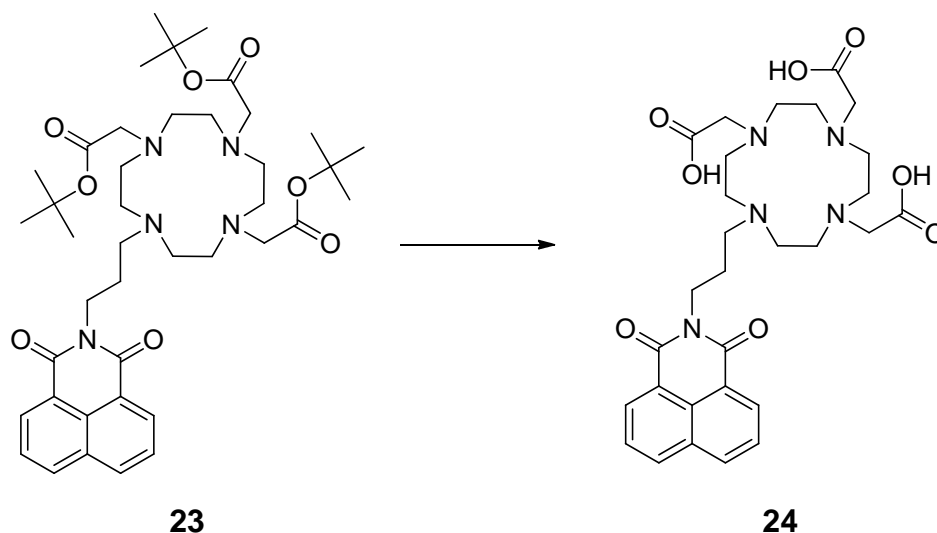
23   **24**

1-[(3-propyl)-benzo[*de*]iosoquinoline-1,3-dione]-4,7,10-tris-(carboxymethyl)-1,4,7,10-

tetraazaylododecane (**24**) was synthesized as follows: the ester **23** (362 mg, 0.48 mmol) was

dissolved in dichloromethane (5 mL) and trifluoroacetic acid (5 mL) was added to the solution.

The solution was allowed to stir at room temperature for 24 hours. The solvents were removed

under reduced pressure and the residue was twice evaporated with dichloromethane (2 × 10 mL)

followed by methanol (2 × 10 mL). The remaining tan solid was dissolved in the minimum

amount of methanol and the title complex isolated by the slow diffusion of ether as a fine, white

microcrystalline solid (244 g, 87%); λ_{max} (H$_2$O)/nm 233 (ε/M^{-1}cm^{-1}, 19,700 cm^{-1}), 344 (6770cm^{-1}

); ^{1}H NMR (300MHz; CDCl$_3$, δ): 2.24 (s, 2H, -CH$_2$*CH$_2$*CH$_2$-), 2.87-3.52 (broad m, 26H, aza

crown ring, bridgehead and C1-CH$_2$), 3.97 (s, 2H, -CH$_2$*CH$_2$*-N), 7.80 (t, *J*=7.7 Hz, 2H, 3-H and

6-H), 8.38 (d, *J*=8 Hz, 2H, 2-H and 7-H), 8.58 (d, *J*=8 Hz, 2H, 4-H and 5-H); API-ESMS *m/z*:

584 ([M + H]$^+$, 100%), 606 ([M + Na]$^+$, 22%).

24 → **25**
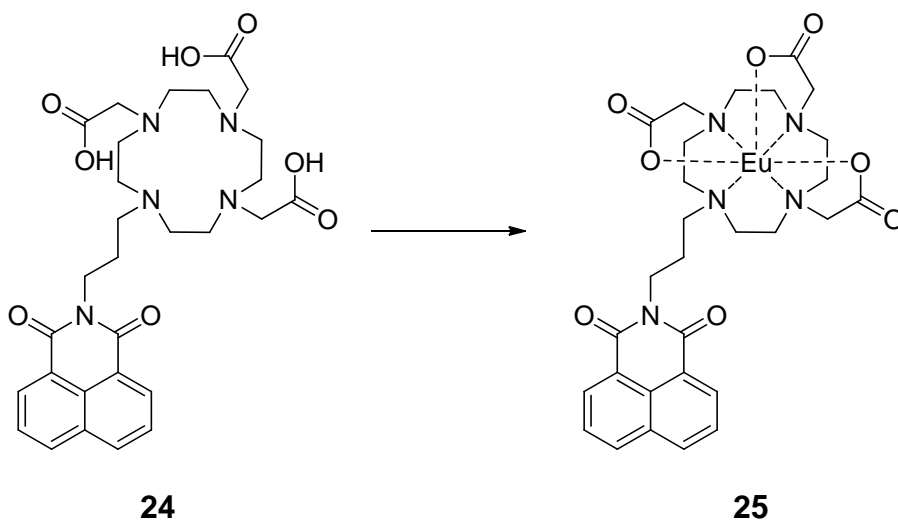
Europium complex of 1-[(3-propyl)-benzo[*de*]iosoquinoline-1,3-dione]-4,7,10-tris-(carboxymethyl)-1,4,7,10-tetraazaylododecane (**25**) was synthesized as follows: the cyclen tris acid **24** (50 mg, 0.086 mmol) and europium triflate hexahydrate (0.1 mmol) was dissolved in anhydrous methanol (2 mL) with a few drops of water. The solution was heated at 50 °C for 14 hours under N_2 with stirring. After which time the solvent was removed under reduced pressure and residue redissolved in water (4 mL). The resulting turbid solution was passed through a celite plug with washing with water (2 × 5 mL). The filtrate was evaporated to dryness, redissolved in methanol (0.5 mL) and the complex isolated as a white microcrystalline solid by the slow diffusion of ether (35 mg, 55%); mp >300°C; λ_{max} (H_2O)/nm 233 (ε/$M^{-1}cm^{-1}$, 17,970 cm^{-1}), 344 (6410 cm^{-1}); APIESMS *m/z*: 734 ([M + H]$^+$ ^{153}Eu, 100%), 732 ([M + H]$^+$ ^{151}Eu, 78%); HRMS (TOF-ES$^+$): [M + H]$^+$ calcd for $C_{29}H_{35}N_5O_8Eu$ 732.1684; found 732.1705.

G3-PAMAM-(1,8-naphthalimide)$_{32}$ was synthesized as follows: generation 3 PAMAM dendrimer with NH_2 terminal groups (390.5 mg, 0.0565 mmol) and 1,8-naphthalic anhydride (447.9 mg, 2.26 mmol) were suspended in DMF (25 mL) and stirred at 95°C for 48 hours under a nitrogen atmosphere, with monitoring for the disappearance of the naphthalic anhydride by TLC.

119

The compound was purified by dialysis using a regenerated cellulose membrane (Fisher; nominal MWCO 12,000-14,000) in DMSO for three days. The solution in the dialysis membrane was dried in a vacuum oven to yield the title product as brown solid (517.6 mg, 72%); ^{1}H NMR (300MHz; CDCl$_3$, δ): 8.23 (br s, 64H, Ar H), 7.97 (br s, 64H, Ar H), 7.69 (m, 60H, -NH), 7.49 (br s, 64H, Ar H), 4.12 (br s, 64H, –N(CO)$_2$CH_2–), 3.51 (br s, 64H, -NHCH_2-), 3.19 (m, 56H, -NHCH_2-), 2.90–2.40 (m, 60H, –NCH_2CH$_2$NH–), 2.27 (m, 120H, –NCH_2CH$_2$CO–), 1.93 (m, 120H, –COCH_2–).

Eu-G3P18N-G3-PAMAM-(1,8-naphthalimide)$_{32}$ was synthesized as follows: G3-PAMAM-(1,8-naphthalimide)$_{32}$ (16.81 mg, 1.326×10^{-6} mol) was dissolved in DMSO (5.0 mL) and 1.397 mM Eu(NO$_3$)$_3$ solution in DMSO (7.593 mL, 1.061×10^{-5} mol) was added. The mixture was incubated for one week. DMSO was evaporated in a vacuum oven, and the residual solid was dissolved in 10.0 mL of DMF to make 1.40×10^{-4} M solution.

4.2.2   Determination of Oxygen Concentration with Clark Electrode

A commercially available oxygen electrode was used, consisting of a lead anode and a platinum cathode, surrounded by an electrolyte solution of 65% 0.1 M NaOH and 35% ethylene glycol. To power the electrode and record the currents, a potentiostat was used, made by Bioanalytical Systems Inc., West Lafayette, IND, model CV-1A-110. The used potential between the electrodes and the running current have been monitored on a computer using a USB-aquisition card and recording software from Dataq Instruments, Akron, OH, model DI-158U. For all measurements, always a potential of 200 mV was used.

Calibration of the electrode was done accordingly to the method of LeFevre,[153] by generating solutions of known oxygen concentrations by mixing air- and nitrogen saturated water in different relations. Information on the absolute solubility of oxygen in water at certain temperatures and pressures was obtained from USGS National Field Manual for the Collection of Water-Quality Data.[154]

4.2.3   Cell Imaging with Eu Complex

An IX81 Olympus microscope was used for microinjection and imaging. Both were done using a 40X oil, UplanFl, 1.3 numerical aperture objectives. Rat aortic endothelial cells (RAECs) were plated at approximately 70% confluence on single chamber Labteks (Nalge Nunce International, Naperville, IL) in phosphate free hepes buffer maintained at 37 °C in an open Harvard microincubator (Harvard Apparatus, Holliston, MA). Individual RAECs were injected using an InjectMan NI2, Femtojet, and Femtotips II (all by Eppendorf North America, Westbury, NY). Injection was done using 100 mg/mL europium complex for 1.2 sec and an injection pressure of 180 hpa. Cells were imaged using MetaMorph 6.2 (Universal Imaging Corp, Downington, PA) using differential interference contrast (dic), and fluorescence was detected using 380 nm excitation filter and BA515IF emission filter. Cells were imaged prior to microinjection to identify any autofluorescence and then were immediately imaged after microinjection and then timelapse imaging was obtained every 2 minutes while hypo- or hyper-oxic gas was bubbled into the media.

121

4.2.4 Dendrimer-SWNT Device

4.2.4.1 SWNT device fabrication

Optically transparent and electrically conductive SWNT network devices were fabricated and measured as described previously. Briefly, commercially available SWNTs (Carbon Solutions, P2 SWNTs; reported purity 70–90%) were suspended in DMF using sonication without further purification. Fused quartz (SiO_2) plates (1 in^2 times 0.0625 in thick; Quartz Scientific; reported specific resistance of 10 Ω 1018 V cm^{-3} at 20 °C) served as the device substrates, and were cleaned prior to SWNT deposition with acetone, rinsed with water and dried under compressed air. After spray casting the SWNT networks with a commercial air brush (Iwata) onto the heated quartz plates, aluminum tape and silver paint were used to form the device electrodes. To create devices with two SWNT networks a cotton-tipped applicator soaked in acetone was used to wipe clean a section of the spray-cast SWNT network. Two devices were created from the bisected SWNT network by Individually connecting electrodes to each section with aluminum tape and silver paint. Quartz plates with additional hydroxyl surface groups were created by soaking overnight in Piranha solution (1:3 H_2SO_4:H_2O_2 v/v; *Warning*: Piranha is a vigorous oxidant and this solution should be handled appropriately). Nanotube field-effect transistor (NTFET) devices consisted of interdigitated gold electrodes (10 μm pitch size) on a Si–SiO_2 substrate, and dilute suspensions of Carbon Solutions P2 SWNTs in DMF were drop cast onto heated devices to form the conduction channel.

4.2.4.2 SWNT device decoration and measurement

SWNT devices were heated to just above the solvent boiling temperature and 200 μL (4 μL for NTFETs) of a particular molecule was drop cast evenly onto the surface of the device. For NTFET devices, all measurements were conducted in ambient conditions with a drain-source bias voltage of 100 mV with two Keithley model 2400 SourceMeters interfaced with LabVIEW 7.1 software.[155] UVVNIR absorption spectra were recorded with a Perkin Elmer Lambda 900 UVVNIR spectrophotometer, and steady-state excitation and emission spectra, as well as the luminescence lifetime measurements, were recorded using a custom-designed JY Horiba Fluorolog-322 spectrofluorimeter and a Tektronix TDS model 754D oscilloscope. At least 1,000 luminescence decay curves, each containing 50,000 points, were averaged and treated to calculate the lifetimes using Origin Pro 7.0 software.[156] The reported lifetime for a particular excited state is the average of at least two independent measurements. For multiexponential fittings, we used the amplitude of the major component as a criterion to isolate the values reported; components with amplitudes less than 1% were discarded. Time-resolved excitation and emission spectra of the dendrimer complex solutions were measured using a Varian Cary Eclipse spectrofluorimeter.

For the optically transparent SWNT devices, the ultraviolet-exposure and gas sensitivity measurements were performed in a custom-built gas-delivery chamber housed within the spectrometers for simultaneous electrical and optical measurements; the device conductance was measured at a bias voltage of 500 mV using a Keithley model 2400 SourceMeter interfaced to LabVIEW 7.1 software. The network conductance of two devices on a single quartz substrate was simultaneously measured at 500 mV with a Keithley 2602 SourceMeter and a Keithley 708A switching matrix using Zephyr data-acquisition software (Zephyr is an open source, Java-

based data acquisition and measurement program freely available for download at http://zephyr.sourceforge.net/). The atmosphere inside the chamber was controlled with flowing research-grade gases at a constant flow rate of 1,000 standard cubic centimetres per minute; all gases were dry unless otherwise noted. Atmospheres of 43% relative humidity were created by passing the gases over the headspace of a sealed container of saturated K_2CO_3 solution (literature relative humidity, 43.2 ± 0.3% at 20 °C[157]). The ultraviolet lamp used for device illumination was a UVP Model UVGL-55 hand-held unit (365 nm; 250 μW cm^{-2}; *Warning*: ultraviolet light can be dangerous and appropriate eye protection should be worn). All measurements were conducted at room temperature and ambient pressure. SEM and EDX spectroscopy were conducted on a Phillips XL30 FEG microscope operated at an accelerating voltage of 10 kV; samples were sputter coated with palladium prior to imaging to prevent charging of the insulating quartz substrate.

4.3   RESULTS AND DISCUSSION

4.3.1   Oxygen Sensing with Europium-Cyclen Complex

4.3.1.1 Novel europium-cyclen complex

The europium complex is depicted in Figure 4.1. The ligand has cyclen derivative DOTA chelator for stable coordination of Eu^{3+} ion, and 1,8-naphthamide chromophore as a sensitizer. 1,8-Naphthalimide was chosen on the basis of the relatively low energy of its triplet state (18 500 cm^{-1}) that can potentially interact with the electronic levels of oxygen. Recently, de Sousa et al reported the use

of a 1,8-naphthalimide chromophore as sensitizer of europium with its emission being sensitive in presence and absence of oxygen.[158] However, this system limited in a practical application due to the complex being formed in situ in acetonitrile at high concentrations and the ligand forming a mixture of species in solution.
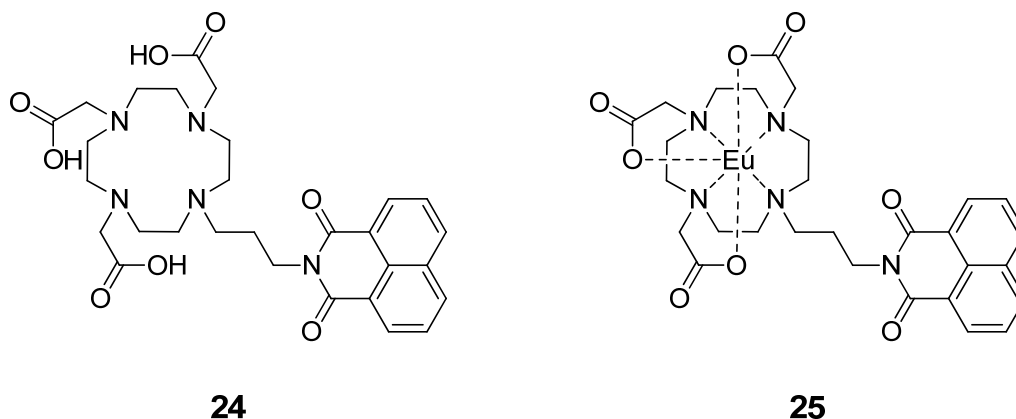
Figure 4.1. Europium complex (**25**) for oxygen sensing and its ligand (**24**)

The luminescence properties are outlined in Table 4.1. Excitation of the **25** in water at 10^{-5} M revealed typical metal centered emission arising from the $^5D_0\ ^7F_{0, 1, 2, 3, 4}$ transitions. Lifetime of the $^5D_0\rightarrow^7F_2$ transition at 615 nm was determined to be 0.36ms. Analogous measurements in D_2O revealed a lifetime of 1.08 ms indicating that the complex has 2.5 water molecules associated with it and is not coordinatively saturated.[15]

Table 4.1. Luminescence lifetime and quantum yield of europium complex **25**

Solvent	H_2O	D_2O	H_2O, deoxygenated
Luminescence lifetime at 300 K (ms)	0.36	1.08	0.43
Luminescence lifetime at 77 K (ms)	0.74 and 4.4	0.66 and 8.8	n/a
Quantum yield (%)	0.18	0.48	0.45

Luminescent lifetimes recorded at 77 K in both H_2O and D_2O indicate that there is a significant degree of thermal deactivation associated with the complex arising from both back energy transfer and solvent oscillations. The luminescent lifetime in both H_2O and D_2O at 77 K produce decays that fit well to a biexponential decay curves with the longer lived components being 4.4 ms and 8.8 ms, respectively. The lifetime in D_2O at 77 K is almost twice as large as the analogous water measurement (Table 4.1). O-D oscillations at 77 K are relatively inefficient along with thermally activated back energy transfer mechanism. This however cannot be deemed an accurate measurement as there is significant emission arising from the triplet state of the naphthalimide chromophore at this temperature due to inefficient energy transfer. Phosphorescence emission from the triplet state significantly overlaps with the emission arising from the sensitized europium and the observed longer lifetime is likely to arise from such emission. A phosphorescence emission spectra at 77 K in water of both ligand **24** and its gadolinium complex show very little change in the relative position of the triplet state of the 1,8-naphthalimide moiety, with both values being 18,300 cm^{-1} taken from the onset of phosphorescence emission and extends to cover the emission region of europium. This indicates that the chromophore has no significant interaction with the paramagnetic metal ion that could possibly affect the triplet state energy of the chromophore.[159] Further evidence for this lack of interaction is given by the near identical UV absorption spectra of **24** and **25**, showing the chromophore is not significantly influenced by the lanthanide ion.[160]

The quantum yield of metal centered emission at 298 K in water was calculated relative to Ru(bipy)$_3$ and was found to be 0.18%.[161] Upon deoxygenating of an aqueous solution of **25** either by displacing the dissolve oxygen with argon or by freeze-pump-thaw cycles, the emission intensity of europium is significantly increased. More importantly, the red emission becomes

126

visible with the naked eye when irradiated with 354 nm light whereas under ambient conditions, only blue fluorescence arising from 1,8-naphthalimide is observed (Figure 4.2). The quantum yield upon degassing rises to 0.45% giving a 2.6 fold increase in europium luminescence output comparison to aerated conditions.
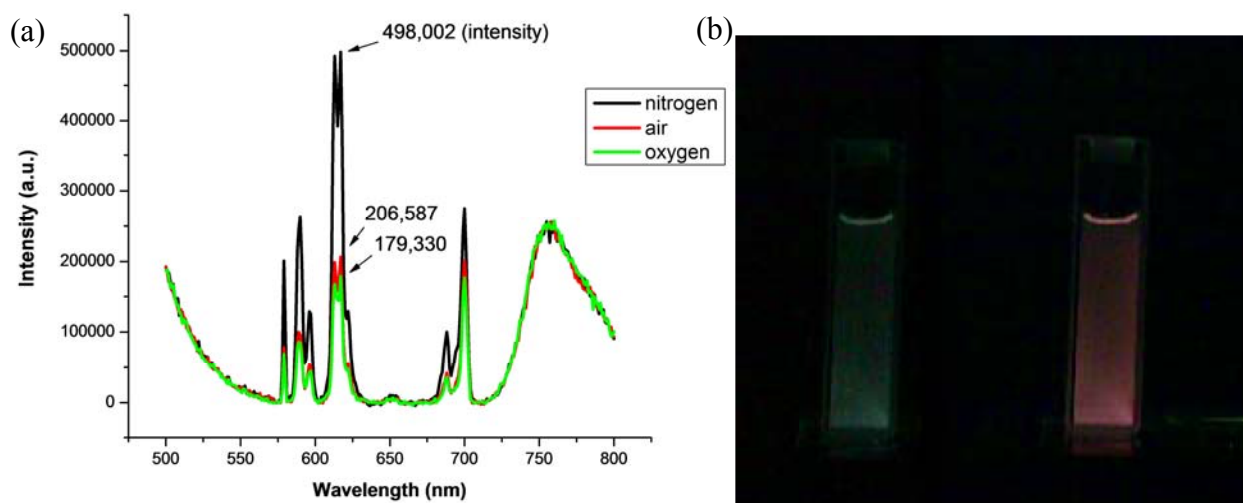
Figure 4.2 (a) Luminescence spectra of **25**; (b) Solution of **25** at 10^{-5} M in aerated water (left) and deoxygenated water (right) irradiated with 354 nm UV light.

The mechanism of oxygen sensitivity of lanthanide complexes was explained by Parker.[162, 163] A typical photochemical sequence of sensitized lanthanide luminescence is shown in Figure 4.3. The first two steps, initial excitation of sensitizer and formation of excited triplet state of sensitizer by intersystem crossing, are generally fast. If the rate of energy transfer to the lanthanide excited state (k_1) is sufficiently slow, then rate processes that lead to deactivation of the triplet state may compete: quenching by molecular oxygen ($k_q'[O_2]$) often occurs in such cases due to the high second-order quenching rate constants (ca. 1×10^9 dm^3 mol^{-1} s^{-1}) typically found with aromatic triplet states.[164, 165]
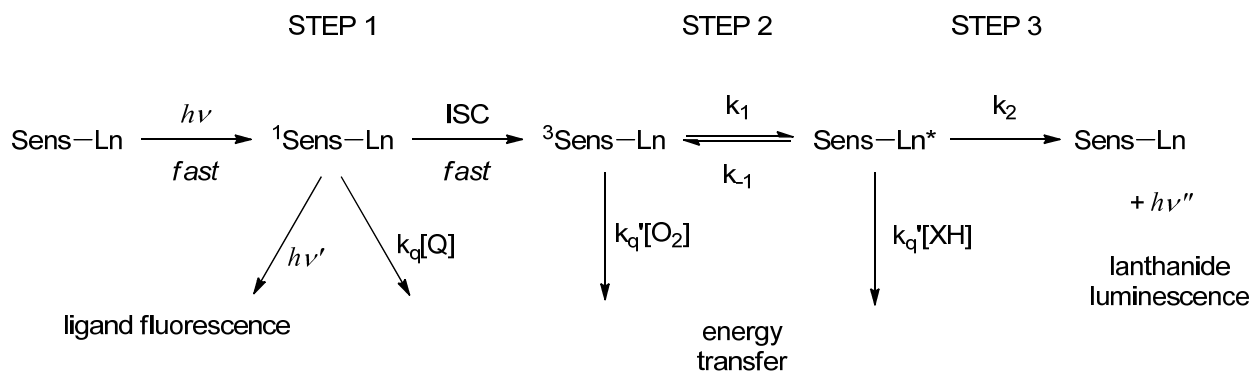
Figure 4.3. Kinetic scheme showing the three key photophysical processes that occur during sensitized lanthanide luminescence. (Sens = sensitizer)[163]

4.3.1.2 Quantification oxygen sensitivity

In order to quantify the oxygen sensitivity of the lanthanide complexes in solution, we designed a specialized apparatus to record luminescence spectra and to monitor the amount of oxygen at the same time. This glassware consists of a luminescence measurement cuvette combined with temperature controlled chamber with vacuum insulation. When mounted in the spectrometer, the sample holder around the cuvette as well as the upper part are heated and cooled with water from the same source. The apparatus is sealed with a Teflon® cap with precise holes for the electrodes and gas tubes for nitrogen and oxygen.

We have found quantitatively that the oxygen concentration can be held constant for at least 20 minutes whereas the temperature can be maintained constant with water circulator for several hours. In order to perform a measurement, the sample chamber was filled with the solution to examine (~10 mL). A little stir bar placed on the bottom of the cuvette to reach the equilibrium. We could generate solutions with various contents of oxygen and nitrogen by bubbling gasses into the solutions. When the gas was bubbled, the tube was always placed on the bottom of the cuvette to ensure the saturation of the solution with bubbled gas, and then the tube

was removed from solution during fluorescence measurement to prevent any interference. Since there was no stir bar in the upper part of the apparatus, the electrode we had to be twisted and moved slightly until a constant signal was obtained.
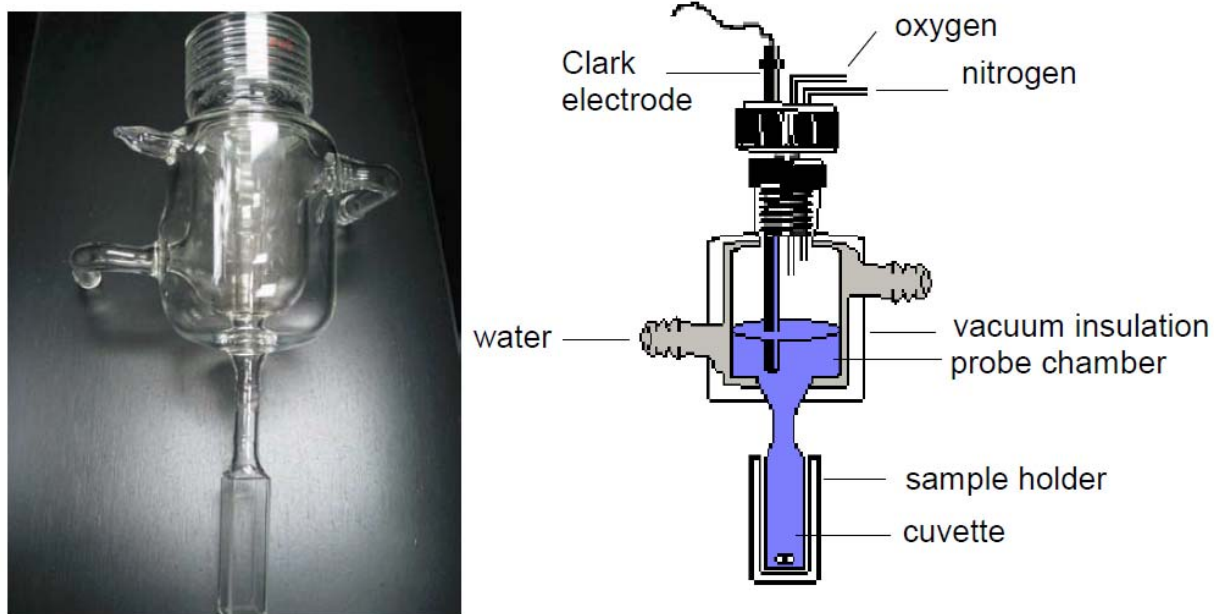
Figure 4.4. Apparatus for measuring luminescence and oxygen concentration

With this apparatus the luminescence spectra of **25** were recorded at 22.5 °C and 37.5 °C varying the concentration of dissolved oxygen (Figure 4.5). The differences of the luminescence intensities between nitrogen and air saturated solutions are 78% and 66%, at 22.5 °C and 37.5 °C, respectively. The changes at both temperatures were high enough to use for actual application. The both data fit well to a biexponential decay curves (red curves in Figure 4.4). The equations for the best-fit curves are $y = 1.46 + 6.58\ e^{-x/0.464} + 2.78\ e^{-x/8.34}$ and $y = 1.14 + 1.12\ e^{-x/0.0684} + 1.05\ e^{-x/1.72}$ for the data at 22.5 °C and 37.5 °C, respectively. This result indicates that there are two luminescent components that were quenched by molecular oxygen. This can be the

europium centered emission along with the emission from the triplet state of the naphthalimide chromophore.
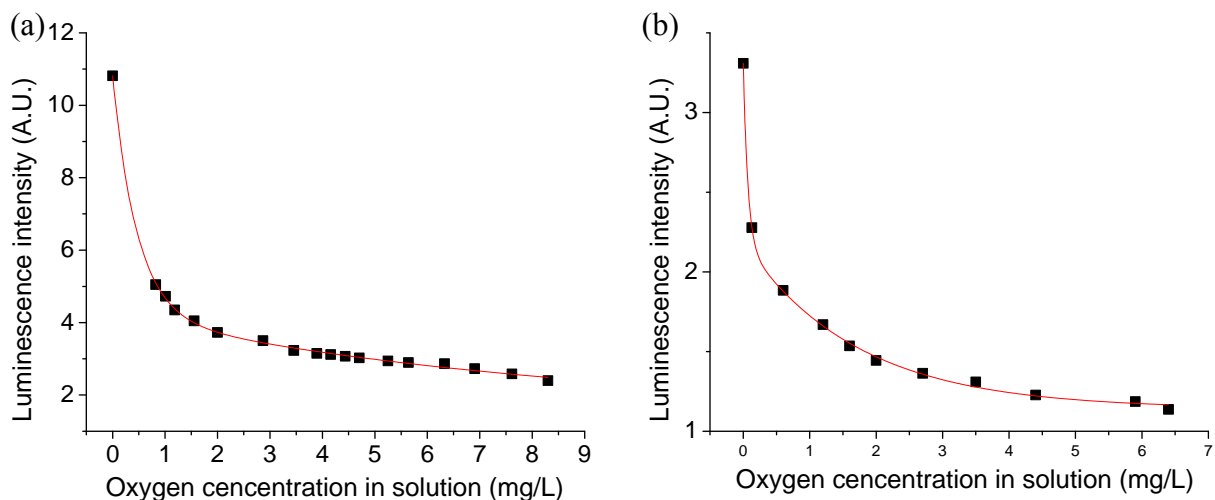
Figure 4.5. Luminescence intensity change versus oxygen concentration at (a) 22.5 °C and (b) 37.5 °C at 980 hPa. [**25**] = 1 × 10^{-5} M, λ_{ex} = 344 nm. The emission signal around 614 nm was integrated for each measurement.

4.3.1.3 Measurement of cellular oxygen contents

In order to investigate the viability of the europium complex **25** in cellar imaging, the complex was microinjected to rat aortic endothelial cells and the luminescence were recorded. Figure 4.6 shows the time-lapse images of at 5 min intervals. As demonstrated in solution, the europium centered emission of the complex **25** decreased upon the addition of O_2 into the cell. Though this cell imaging experiment was a qualitative result, it demonstrated the oxygen sensitivity of the complex along with the sufficient stability and kinetic inertness in biological system.

130
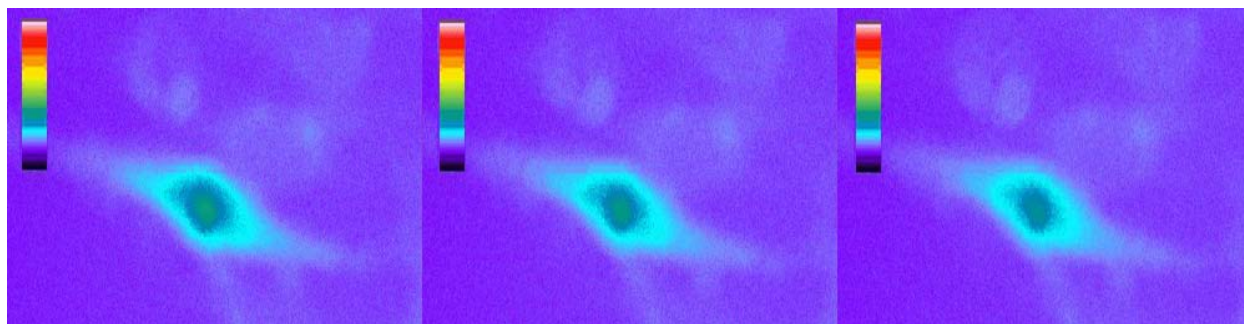
Figure 4.6. Rat aortic endothelial cell microinjected with europium complex 25. Imaged at 40X using 380nm excitation and 515 nm long pass emission. Initially cell in normoxic conditions but gradually subjected to O_2 saturated media by constant bubbling with 95% O_2. Images collected every 5 min.

4.3.2 Oxygen Sensing with Carbon Nanotube decorated with Europium-dendrimer Complex

4.3.2.1 Europium-dendrimer complex Eu-G3P18N and its behavior in solution

In order to establish an understanding of the solid state oxygen sensitivity of naphthalimide-sensitized europium complex system, we have developed a chemiresistor device composed of single-walled nanotube (SWNT) networks decorated with an oxygen-sensitive Eu^{3+}-containing dendrimer complex. The dendrimer complex was synthesized from generation 3 polyamidoamine (PAMAM) dendrimer, 1,8-naphthalimide and europium cations. The structure of this dendrimer complex is depicted in Figure 4.7. As already demonstrated by de Sousa et al[158] and in the previous section, 1,8-naphthalimide shows oxygen sensitivity coupled with lanthanide luminescence. Additionally, the choice of 1,8-naphthalimide as a surface group of dendrimer complex is advantageous in terms of stability of the whole SWNT-dendrimer network, because highly conjugated naphthalimides can link with SWNT through π-stacking interactions.[166]
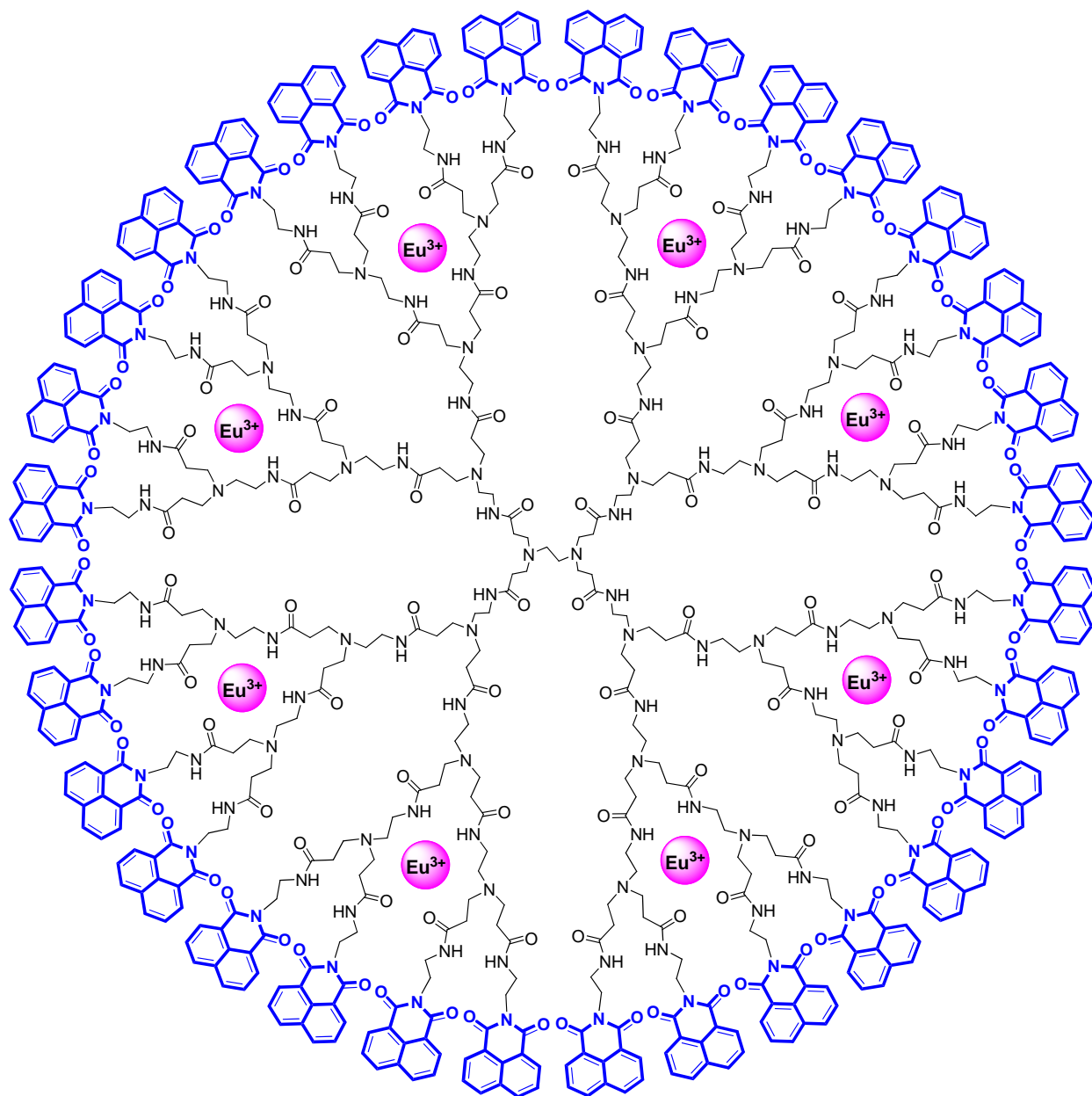
Figure 4.7. Molecular structure of the generation-3 PAMAM dendrimer 1,8-naphthalimide containing europium ions (Eu-G3P18N)

Figure 4.8 presents the emission spectra of a Eu-G3P18N solution in DMF saturated with either argon or oxygen; oxygen saturation results in a decrease of the apparent emission intensity. The emission profile contains a broad band that arises from the excited states of 1,8-

naphthalimide groups centered around 469 nm, and three narrow emission bands located at lower energies characteristic of the Eu^{3+}-centered transitions. The reversible and reproducible quenching effect of oxygen on the solution-phase emission intensity is in accordance with its predicted behavior. However, we find that the Eu^{3+}-centered emission bands show a larger sensitivity to oxygen compared with the 1,8-naphthalimide band. As shown in Figure 4.8(b), the relative emission intensity of the naphthalimide-centered (469 nm, open squares) and Eu^{3+} $^5D_0 \rightarrow ^7F_2$ (615 nm, filled circles) bands in a solution cycled several times between oxygen and argon saturation. The larger relative change in the Eu^{3+} emission spectrum suggests that oxygen deactivates the Eu^{3+} excited state more effectively compared with 1,8-naphthalimide, through the introduction of non-radiative pathways.
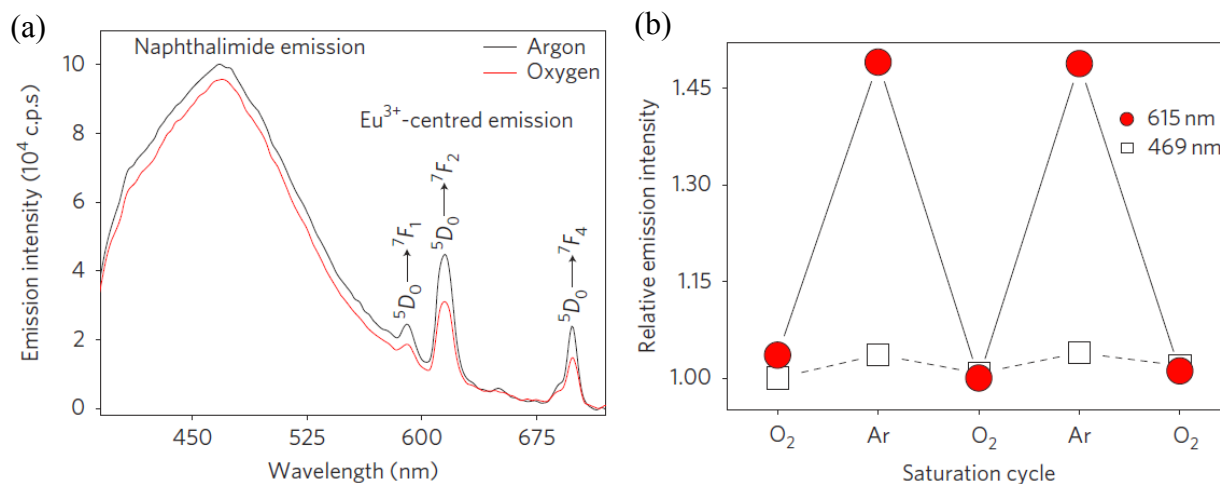
Figure 4.8. Solution-phase oxygen sensitivity of Eu-G3P18N. (a) emission spectrum of a Eu-G3P18N solution (in DMF, 1.45×10^{-5} M; λ_{ex} = 354 nm) saturated with oxygen (black curve) and argon (red curve); (b) Relative emission intensity of the 1,8-naphthalimide-centered (λ_{em} = 469 nm, open squares) and Eu^{3+}-centered (λ_{em} = 615 nm, filled circles) emission bands cycled between argon and oxygen saturation.

In the solid state, the relative intensity of the Eu^{3+}-centered transitions are greatly attenuated, and we could only resolve the $^5D_0 \rightarrow {}^7F_2$ transition. The decreased emission intensity and apparent absence of distinguishable $^5D_0 \rightarrow {}^7F_1$ and $^5D_0 \rightarrow {}^7F_4$ transitions may result from less efficient sensitization through a decrease in the efficiency of energy transfer into the accepting levels of Eu^{3+}. Measurement in a pure O_2 atmosphere did not result in substantial quenching of the intensity of Eu-G3P18N emission. However, the apparent maximum of the naphthalimide emission band undergoes a slight apparent red-shift, as compared to a pure Ar atmosphere (Figure 4.9(a)). Irradiation with UV light (in flowing Ar) decreased the emission intensities of both the naphthalimide and Eu^{3+}-centered bands, and the naphthalimide band showed a slight apparent blue-shift (Figure 4.9(b)). The introduction of pure O_2 in the system results in the partial restoration of the intensity of the emission bands and a red-shift of the naphthalimide centered emission (Figure 4.9(b)).
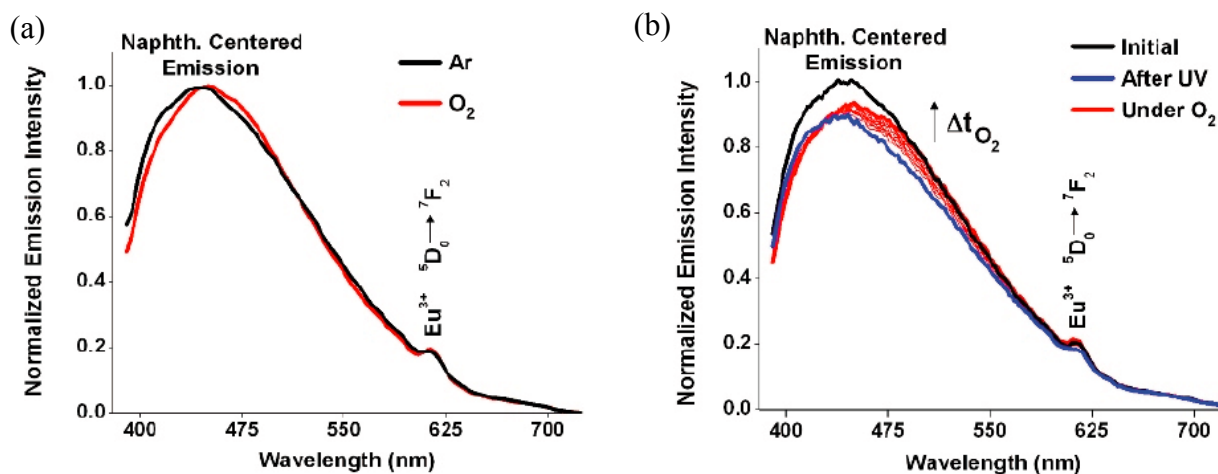
Figure 4.9. (a) Normalized emission spectra of Eu-G3P18N (on quartz) in flowing Ar (black line) and pure O_2 (red line). (b) Emission spectra of Eu-G3P18N before (black line) and after (blue line) UV illumination in flowing Ar, and in flowing O_2 (red lines); spectra in flowing O_2 were recorded every minute.

The similar spectroscopic response of pure Eu-G3P18N films and the Eu-G3P18N-SWNT devices (Figure 4.11(a)) observed after UV illumination suggests this phenomenon was not induced by the underlying SWNT network.

4.3.2.2 Behavior of Eu-G3P18N-SWNT networks

The Eu-G3P18N-SWNT device was composed of a SWNT network with Eu-G3P18N dendrimer complex for simultaneous spectroscopic and electrical conductance measurement. The schematic representation and photograph of the device are depicted in Figure 4.10.
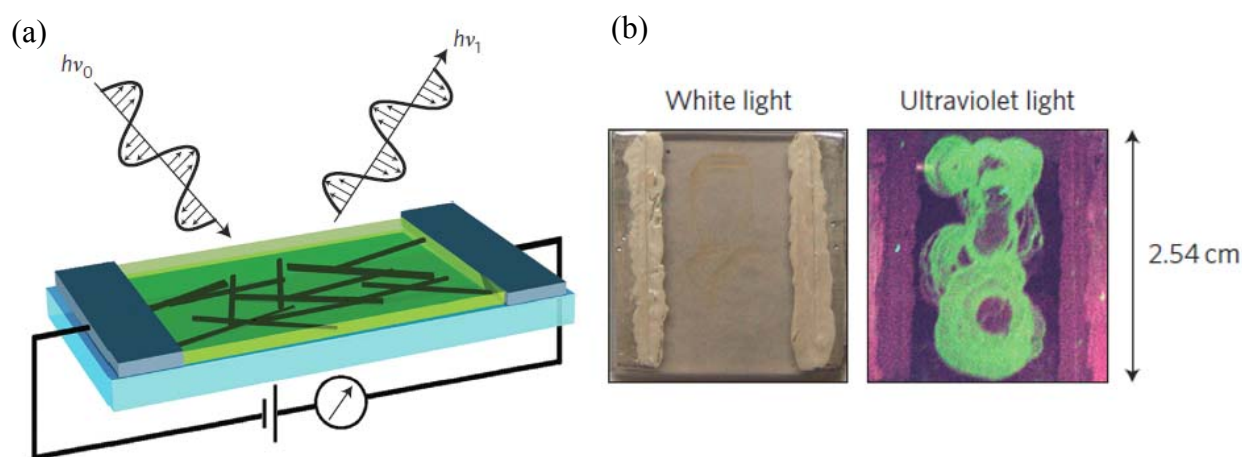
Figure 4.10. (a) Schematic representation of the Eu-G3P18N-SWNT device. SWNT network (black bars) was decorated with Eu-G3P18N (green layer). (b) Digital photographs of Eu-G3P18N-SWNT device under white light (left) and UV light (365 nm, right);. Drop-cast layer of Eu-G3P18N was luminescent in green color under UV light.

Using simultaneous ultraviolet-visible-near infrared (UV-Vis-NIR) absorbance spectroscopy and network conductance measurements on Eu-G3P18N-SWNT devices, we found that the underlying SWNT network was able to transduce changes in the electronic properties of the Eu-G3P18N layer during illumination with 365 nm light and exposure to pure oxygen gas.

135

After an illumination period of 30 minutes the device experienced a decrease in the first semiconducting SWNT absorption band, labelled S_{11} in Figure 4.11(b).[167, 168]
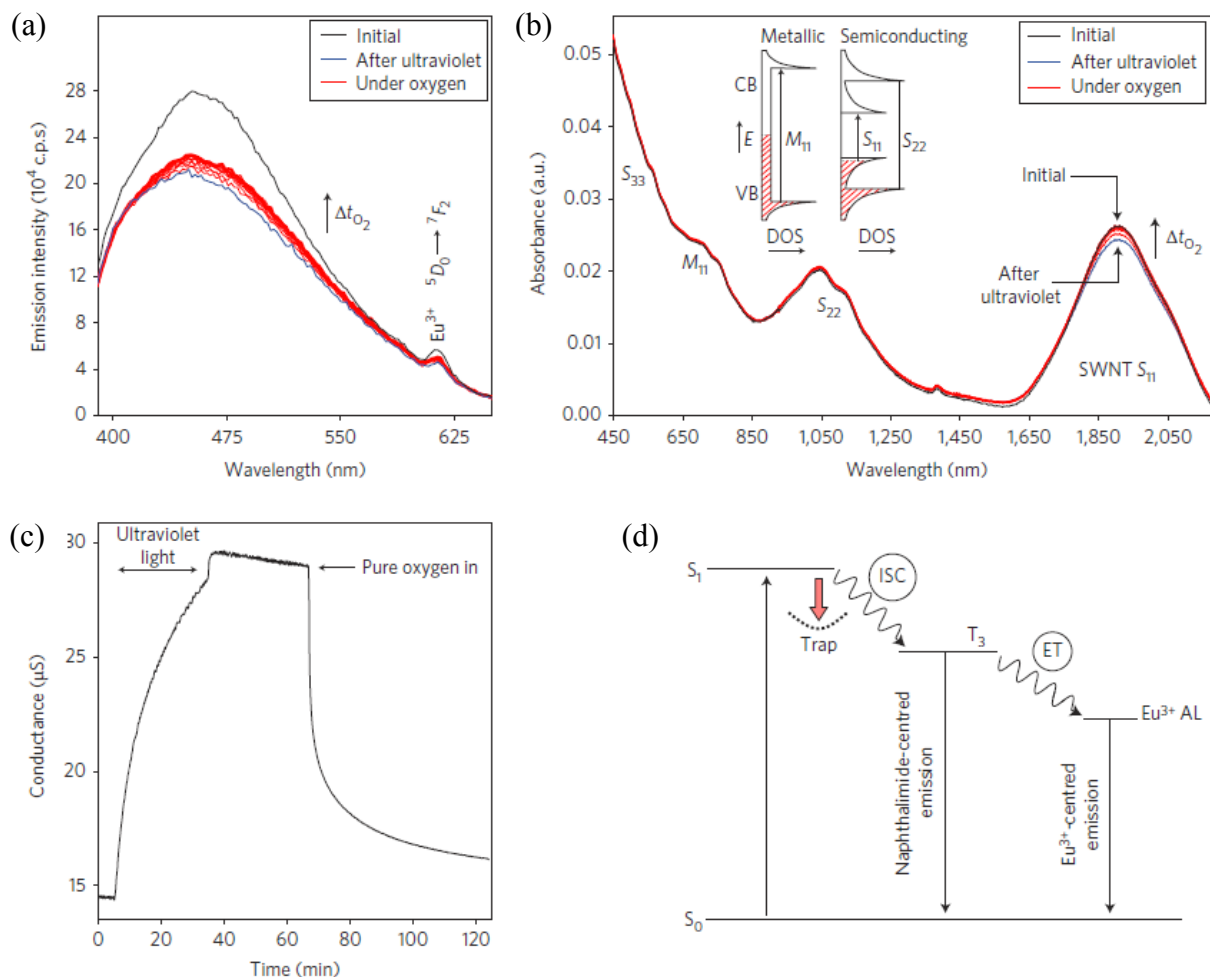
Figure 4.11. Bimodal oxygen sensitivity of the Eu-G3P18N-SWNT devices. (a) Emission (λ_{ex} = 354 nm) spectra of a Eu-G3P18N -SWNT device before (black) and after (blue) 30 minutes of illumination with 365 nm light (in flowing argon) and during one hour of oxygen exposure (red); the ultraviolet- and gas-exposure times are identical in a–c. (b) UV-vis-NIR absorbance spectra of the Eu-G3P18N-SWNT device before and after illumination with 365 nm light (in argon) and during oxygen exposure. (c) Network conductance of the Eu-G3P18N-SWNT device during 365 nm illumination and sustained photogenerated ON-state (in flowing argon), followed by the introduction of pure oxygen. (d) Proposed mechanism to describe the Eu-G3P18N -SWNT oxygen sensitivity in terms of the Eu-G3P18N electronic structure.

Additionally, illumination triggered an increase in the network conductance (Figure 4.11(c)), which we call the photogenerated ON-state. We found that the ON-state conductance abruptly increased after termination of the ultraviolet light and then slowly decayed as a function of time. To test the reproducibility of the Eu-G3P18N-SWNT response to ultraviolet light we exposed nine individual devices to 365 nm light for 30 minutes. Each device's behavior was qualitatively similar, but we found that the magnitude of the response scaled inversely with the initial device conductance. This behavior differs drastically from the response of undecorated SWNTs to ultraviolet light, which show a decrease in the SWNT network conductance and an increase in the S_{11} absorption band.[169, 170]
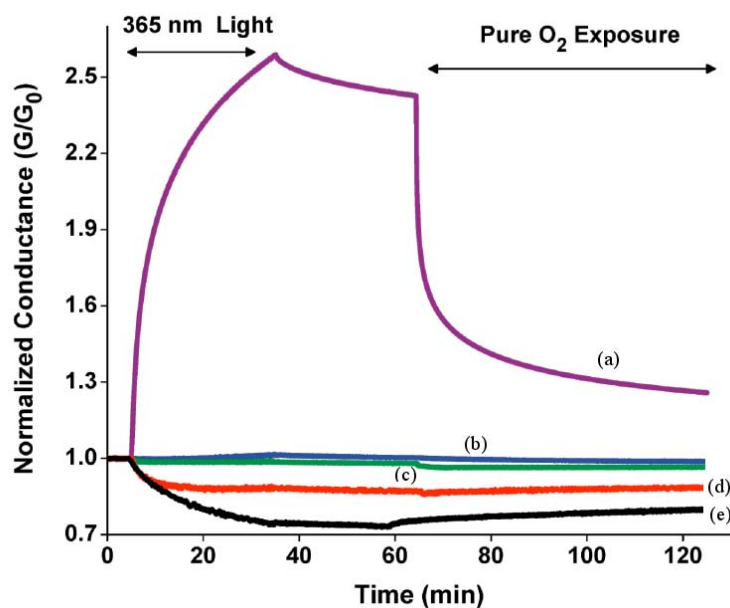
Figure 4.12. Normalized conductance of SWNT networks decorated with (a) G3P18N, (b) G3P, (c)1,8-naphthalimide, (d) tetraphenylporphyrin Fe(III) chloride and (e) without decoration.

Further control experiments were conducted on SWNT networks individually decorated with each component of the Eu-G3P18N complex, including the generation-3 PAMAM

137

dendrimer, generation-3 PAMAM dendrimer with naphthalimide (G318N) and the 1,8-naphthalic anhydride molecule alone. Additionally, SWNT networks were decorated with an iron-containing tetraphenylporphyrin as an analogue to a heme-containing moiety (Figure 4.12). We found that only the SWNT networks decorated with G3P18N demonstrated both a photoresponse and oxygen sensitivity comparable to those of the Eu-G3P18N-SWNT networks, which indicates that the set of 1,8-naphthalimide attached on the dendrimer structure plays a key-role for the observed behavior.

Oxygen has been shown to passivate quartz charge traps, such as SiOH, through the introduction of non-radiative relaxation pathways.[171] Consequently, we suggest that the introduction of oxygen results in adsorption on the device surface and passivation of the electron traps through the addition of non-radiative pathways. The adsorption of oxygen removes the electronic bottleneck, increases ISC and leads to the restoration of both the naphthalimide and Eu^{3+}-centered emission band intensities. The increased lifetime of the Eu^{3+}-centered transition after 365 nm illumination is a consequence of oxygen desorption, which removes any oxygen-induced non-radiative pathways in the Eu^{3+} electronic structure. Finally, exciton recombination in the naphthalimide S_0 state eliminates the Coulombic attraction between the Eu-G3P18N ground-state holes and SWNT valence-band electrons, which decreases the Eu-GP18N-SWNT network conductance and increases the absorption of the SWNT S_{11} band.

To summarize the proposed response mechanism, we suggest that photoexcitation of the Eu-G3P18N-SWNT system promotes Eu-G3P18N ground-state electrons into an excited state, which subsequently fill electron traps at the quartz substrate surface (Figure 4.11(d)). This leads to a Coulombic attraction between SWNT valence-band electrons and the depleted Eu-G3P18N ground-state orbital, effectively p-doping the SWNT valence band. Upon the introduction of

138

oxygen gas, nonradiative relaxation pathways allow electrons to return from the quartz electron traps back into the Eu-G3P18N ground state. This alleviates the Coulombic attraction between the SWNT valence band and Eu-G3P18N ground state and reverses the SWNT p-doping.

4.3.2.3 Oxygen detection

Using the Eu-G3P18N-SWNT devices in a chemiresistor configuration, we found a linear electrical response to oxygen in the concentration range tested (5–27%). By exploiting the stability of the Eu-G3P18N-SWNT photogenerated ON-state conductance we were able to create a baseline for measuring oxygen response. For example, an initial 365 nm illumination in dry argon (left-most blue asterisk in Figure 4.13(a)) established a baseline at an arbitrary network conductance (G_{ON}). Sequential pulses of dry oxygen gas (diluted in argon) produced a concentration-dependent decrease in the network conductance. Oxygen exposure (indicated with dashed lines, Figure 4.13(a)) was followed by short periods of 365 nm illumination (marked with blue asterisks) to return the device to its arbitrarily defined ON-state conductance.

During the oxygen-exposure periods of 200 seconds the device response did not saturate, but we found that the rate of change in the network conductance scaled with the concentration of oxygen. Figure 4.13(b) shows the rate of conductance change (ΔG relative to G_{ON}) during oxygen-exposure cycles. Based on the standard deviation in the ON-state conductance before the first oxygen exposure, we calculated a signal-to-noise ratio of 4.44 for the device response to 5% oxygen. The linear response to oxygen and repeated return to the ON-state conductance indicate that the Eu-G3P18N-SWNT network did not experience any photodegradation or chemical damage during operation. Using a value three times the standard deviation of the ON-state conductance as the minimum detection limit (MDL), we determined that the MDL of our

139

unoptimized devices is approximately 0.8% oxygen for an exposure time of 200 seconds, which is comparable with state-of-the-art, high-temperature metal–oxide semiconductor sensor platforms.[172]
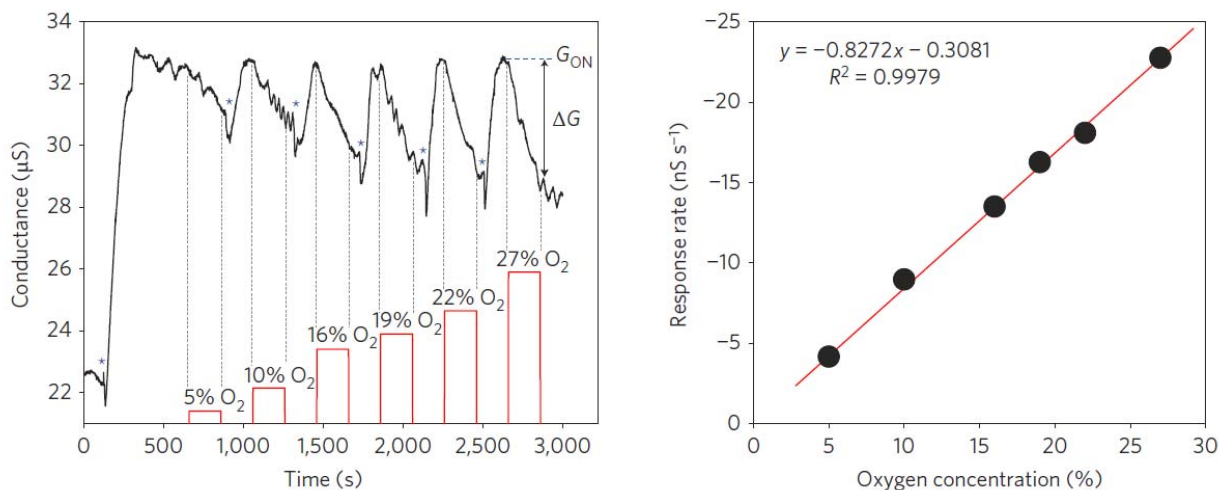
Figure 4.13. (a) Network conductance of the Eu-G3P18N-SWNT device during gas exposure cycles (200 seconds) of pure argon and increasing oxygen concentrations (in argon) at 0% relative humidity. The dotted lines represent the period of oxygen delivery, the red bars represent the delivered oxygen concentration and the blue asterisks represent the initiation of brief ultraviolet illumination periods (365 nm light, flowing argon) that returned the device to a designated ON-state conductance (G_{ON}). (b) Electrical response rate of the Eu-G3P18N –SWNT device to increasing oxygen concentrations during an exposure cycle of 200 seconds; the response rate is defined as the change in network conductance (ΔG as measured from G_{ON}) during an oxygen-exposure period.

The Eu-G3P18N-SWNT devices showed a comparable photoresponse with nitrogen as the carrier gas, demonstrated insignificant response to CO_2 and NH_3, were not affected adversely by relative humidity (0–43%) and retained good oxygen sensitivity, even with storage of the device in ambient conditions up to one week after the initial measurement. Typical of most solid-state oxygen sensors, we observed sensitivity towards NO_2. To identify false positives caused by oxidizing species we created a device that contained both a Eu-G3P18N-SWNT network and a

140

bare SWNT network (Figure 4.14). Bare SWNTs respond to oxidizing gases, such as NO_2,[173] but do not respond to oxygen, so this device design provides an internal reference against the measurement of false positives. By monitoring the simultaneous conductance of both networks during ultraviolet, oxygen and NO_2 exposure we determined the difference between a true oxygen response and a false response caused by NO_2.
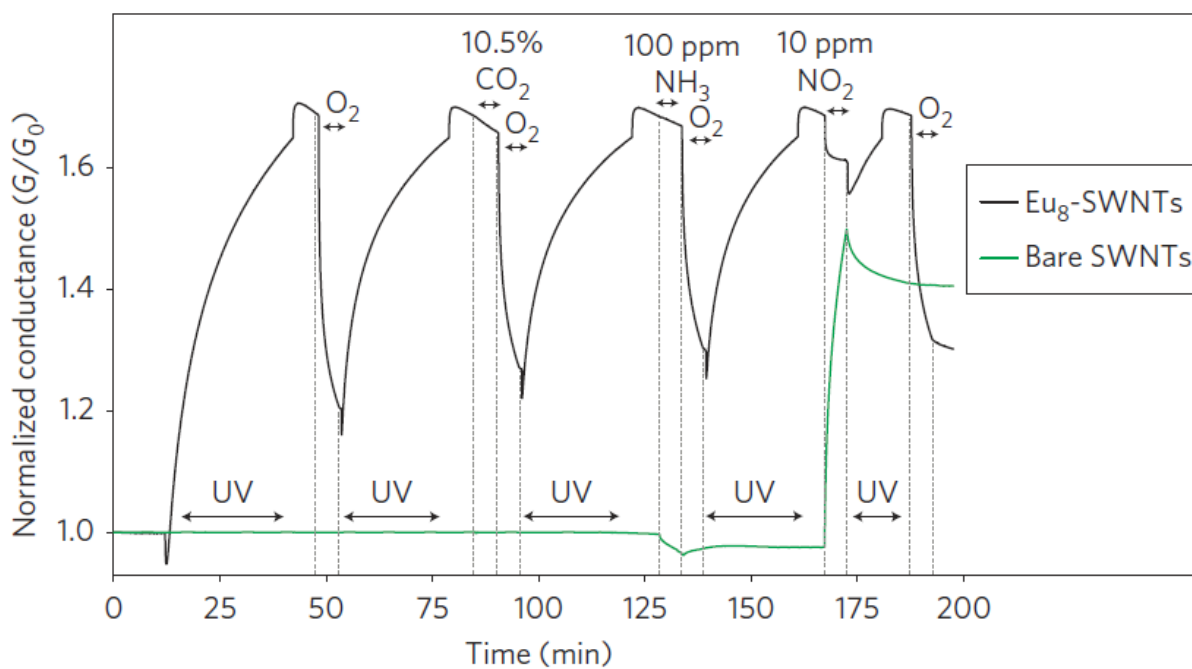
Figure 4.14. Simultaneously recorded conductance of a Eu-G3P18N-SWNT network (black curve) and bare SWNT network (green curve) on a single quartz substrate during illumination with 365 nm UV light (in flowing nitrogen) and exposure to pure oxygen, 10.5% CO_2, 100 ppm NH_3 and 10 ppm NO_2.

The insignificant sensitivity towards CO_2 and NH_3, identifiable response to an oxidizing species (NO_2) and comparable device operation in nitrogen and humid atmospheres indicate that this system holds promise as a low-temperature platform for monitoring oxygen levels under ambient conditions. However, in the design of a field-usable platform we need to take into

consideration the requirement for a small reservoir of inert gas, such as nitrogen or argon, to purge the sample chamber during illumination with a compact ultraviolet light source.

4.4   CONCLUSION

We presented here a novel type of photostable oxygen sensor based on a lanthanide complex that can work in living cells. Even if the quantum yield of the reported europium complex is modest, due in good part to the insufficient protection of the lanthanide cation from non-radiative deactivations, we were able to measure microscopy images for an extended period of time, used on the emission of these lanthanide complexes due to the photophysical robustness of these compounds. The oxygen sensitivity was quantified with newly designed apparatus which can measure luminescence and oxygen concentration through spectroscopic and electrochemical detection at the same time. The microscopy images presented the oxygen sensitivity of the complex along with the sufficient stability and kinetic inertness in biological system. We are currently working on a lanthanide complex that can be loaded into a cell without injection and has higher luminescence intensity.

We have used SWNT networks as a tool to establish a mechanistic understanding of the solid-state oxygen sensitivity observed in the Eu-G3P18N system. When incorporated into electrically conductive and optically transparent devices, the Eu-G3P18N-SWNT system shows bimodal (optical spectroscopic and electrical conductance) sensitivity to oxygen gas at room temperature and ambient pressure. Using Eu-G3P18N-SWNT devices as chemiresistors, we have demonstrated a linear and reversible response to environmentally relevant oxygen concentrations

between 5 and 27%, with a calculated MDL of 0.8% oxygen. The response of Eu-G3P18N-SWNTs towards ultraviolet light and oxygen gas is completely unlike that of bare SWNTs, and allows us to explore the mechanisms of device behavior without the controversy concerning the direct interaction between SWNTs and oxygen.[174]

APPENDIX A

CRYSTALLOGRAPHIC DATA AND STRUCTURE REFINEMENT FOR SALOPHEN-LANTHANIDE COMPLEXES

Table AA.1. Crystal data and structure refinement for $Nd_2(DMSal)_3 \cdot MeOH$

Identification code	hyu404s
Empirical formula	C67 H54 N6 Nd2 O7
Formula weight	1343.64
Temperature	150(2) K
Wavelength	0.71073 Å
Crystal system	Monoclinic
Space group	P2(1)
Unit cell dimensions	a = 14.2974(15) Å $\quad$ α = 90°.
	b = 25.028(3) Å $\quad$ β = 106.392(2)°.
	c = 17.7418(18) Å $\quad$ γ = 90°.
Volume	6090.7(11) Å^3
Z	4
Density (calculated)	1.465 Mg/m^3
Absorption coefficient	1.744 mm^{-1}
F(000)	2696
Crystal size	? × ? × ? mm^3

Theta range for data collection	1.48 to 25.00°.
Index ranges	$-17 \leq h \leq 17$, $-29 \leq k \leq 29$, $-21 \leq l \leq 21$
Reflections collected	48619
Independent reflections	21403 [R(int) = 0.0505]
Completeness to theta = 25.00°	99.9 %
Absorption correction	None
Refinement method	Full-matrix least-squares on F^2
Data / restraints / parameters	21403 / 3 / 1469
Goodness-of-fit on F^2	1.285
Final R indices [I>2sigma(I)]	R1 = 0.0676, wR2 = 0.1643
R indices (all data)	R1 = 0.0813, wR2 = 0.1703
Absolute structure parameter	0.043(17)
Extinction coefficient	0.00000(4)
Largest diff. peak and hole	5.462 and -1.699 e.Å^{-3}

Table AA.2 Atomic coordinates ($\times 10^4$) and equivalent isotropic displacement parameters (Å$^2 \times 10^3$) for

Nd$_2$(DMSal)$_3$·MeOH. U(eq) is defined as one third of the trace of the orthogonalized U^{ij} tensor.

	x	y	z	U(eq)
Nd(1)	1075(1)	8491(1)	1313(1)	23(1)
C(1)	-191(8)	9404(5)	2095(7)	26(3)
O(1)	270(6)	9211(3)	1599(5)	33(2)
N(1)	689(6)	8314(3)	2606(5)	22(2)
Nd(2)	257(1)	7168(1)	77(1)	23(1)
O(2)	2496(6)	8906(3)	1387(5)	32(2)
N(2)	2406(7)	8037(4)	2390(6)	26(2)
C(2)	-582(9)	9915(5)	2000(8)	36(3)
Nd(3)	6409(1)	8469(1)	6186(1)	25(1)
O(3)	-210(6)	7799(3)	931(5)	28(2)

N(3)	26(7)	6689(4)	1311(6)	27(2)
C(3)	-1073(10)	10121(5)	2475(8)	42(3)
Nd(4)	5083(1)	7166(1)	5135(1)	25(1)
O(4)	1573(5)	7790(3)	577(5)	25(2)
N(4)	1790(7)	6705(4)	1096(5)	28(2)
C(4)	-1153(10)	9823(5)	3139(8)	44(3)
O(5)	-1376(6)	6945(4)	-373(5)	40(2)
N(5)	73(9)	6176(4)	-320(6)	41(3)
C(5)	-770(8)	9329(5)	3259(7)	31(3)
O(6)	83(6)	7788(3)	-960(4)	28(2)
N(6)	1220(7)	6826(4)	-853(6)	31(2)
C(6)	-270(8)	9105(5)	2751(7)	30(3)
C(7)	156(7)	8577(5)	2961(7)	26(3)
N(7)	7450(7)	7999(4)	7422(6)	32(2)
O(7)	221(7)	8698(4)	-65(5)	48(3)
O(8)	6049(6)	8842(4)	7216(5)	34(2)
C(8)	1044(8)	7809(5)	2895(7)	26(3)
N(8)	8172(7)	8314(4)	6255(5)	25(2)
O(9)	6998(6)	9224(3)	5766(5)	30(2)
C(9)	586(9)	7449(5)	3251(7)	27(3)
N(9)	6001(6)	6640(4)	6445(6)	30(2)
O(10)	5365(6)	7728(3)	6284(4)	22(2)
N(10)	6812(7)	6743(4)	5252(6)	26(2)
C(10)	962(9)	6947(5)	3527(7)	27(3)
O(11)	6233(6)	7846(3)	5094(5)	25(2)
N(11)	3634(7)	6772(4)	5560(5)	32(2)
C(11)	1884(8)	6807(4)	3406(7)	26(3)
O(12)	3784(6)	7778(3)	4790(5)	27(2)

146

C(12)	2317(8)	7168(7)	3070(7)	38(3)
N(12)	4646(7)	6183(4)	4829(6)	32(2)
O(13)	4987(6)	7011(3)	3839(5)	37(2)
C(13)	1957(8)	7660(4)	2783(6)	21(2)
C(14)	3342(8)	8089(4)	2576(7)	27(3)
O(14)	4838(7)	8703(4)	5258(6)	56(3)
C(15)	3885(7)	8426(5)	2185(6)	21(2)
C(16)	4886(9)	8363(5)	2384(8)	37(3)
C(17)	5468(9)	8638(5)	2032(8)	39(3)
C(18)	5053(10)	9015(6)	1474(8)	45(4)
C(19)	4060(10)	9095(5)	1271(8)	41(3)
C(20)	3445(10)	8807(5)	1610(7)	34(3)
C(21)	419(9)	6571(5)	3892(8)	40(3)
C(22)	2287(9)	6273(5)	3652(7)	32(3)
C(23)	-1008(8)	7768(5)	1165(7)	30(3)
C(24)	-1605(9)	8203(5)	1121(7)	32(3)
C(25)	-2456(10)	8192(6)	1351(8)	45(4)
C(26)	-2717(10)	7710(7)	1640(9)	52(4)
C(27)	-2111(9)	7264(6)	1739(7)	39(3)
C(28)	-1246(9)	7277(5)	1491(7)	34(3)
C(29)	-636(9)	6816(5)	1651(8)	37(3)
C(30)	623(9)	6223(5)	1559(6)	30(3)
C(31)	297(10)	5778(5)	1863(7)	37(3)
C(32)	953(12)	5348(5)	2133(7)	44(4)
C(33)	1876(10)	5360(5)	2051(6)	29(3)
C(34)	2185(10)	5817(5)	1726(7)	38(3)
C(35)	1567(9)	6251(4)	1459(7)	30(3)
C(36)	2679(9)	6834(5)	1186(7)	30(3)

C(37)	3016(8)	7264(5)	764(7)	29(3)
C(38)	3967(9)	7218(6)	686(7)	40(3)
C(39)	4332(11)	7591(6)	260(9)	52(4)
C(40)	3739(10)	8004(6)	-71(8)	43(3)
C(41)	2825(9)	8084(5)	14(7)	31(3)
C(42)	2448(8)	7704(5)	456(7)	24(3)
C(43)	549(11)	4853(6)	2462(8)	52(4)
C(44)	2577(12)	4914(6)	2325(10)	59(4)
C(45)	-1918(10)	6536(6)	-371(8)	47(4)
C(46)	-2840(13)	6627(7)	-323(11)	69(5)
C(47)	-3499(14)	6193(9)	-365(13)	91(7)
C(48)	-3223(18)	5642(11)	-498(17)	136(12)
C(49)	-2301(16)	5576(8)	-488(15)	105(9)
C(50)	-1634(11)	6003(6)	-414(9)	51(4)
C(51)	-654(16)	5874(8)	-398(7)	79(6)
C(52)	997(11)	5968(5)	-352(7)	37(3)
C(53)	1406(15)	5454(6)	-73(8)	64(5)
C(54)	2321(15)	5311(7)	-117(10)	68(6)
C(55)	2874(15)	5648(7)	-370(9)	68(6)
C(56)	2515(11)	6135(6)	-633(7)	48(4)
C(57)	1582(11)	6295(5)	-634(7)	38(3)
C(58)	1412(9)	7051(5)	-1460(7)	34(3)
C(59)	1124(8)	7573(5)	-1773(7)	30(3)
C(60)	1508(9)	7737(5)	-2373(7)	37(3)
C(61)	1327(10)	8236(6)	-2712(7)	45(4)
C(62)	701(9)	8576(5)	-2479(7)	37(3)
C(63)	261(9)	8407(6)	-1902(7)	39(3)
C(64)	483(9)	7906(5)	-1525(6)	23(3)

C(65)	2709(19)	4752(8)	222(12)	105(9)
C(66)	3889(17)	5483(9)	-338(13)	111(9)
C(67)	6082(11)	8732(6)	7956(9)	45(4)
C(68)	5440(9)	9017(6)	8308(8)	42(3)
C(69)	5443(10)	8899(6)	9077(8)	46(4)
C(70)	6064(10)	8501(7)	9513(8)	53(4)
C(71)	6678(11)	8244(6)	9203(8)	42(4)
C(72)	6721(8)	8340(5)	8424(7)	28(3)
C(73)	7391(9)	8007(5)	8129(7)	36(3)
C(74)	8099(8)	7636(5)	7213(6)	26(3)
C(75)	8321(9)	7152(5)	7544(6)	34(3)
C(76)	8936(8)	6798(5)	7282(7)	31(3)
C(77)	9325(8)	6953(5)	6664(7)	33(3)
C(78)	9072(9)	7449(5)	6328(7)	32(3)
C(79)	8462(8)	7791(5)	6583(7)	26(3)
C(80)	8795(8)	8594(5)	5999(6)	26(3)
C(81)	8626(8)	9118(5)	5676(7)	25(3)
C(82)	9429(9)	9369(5)	5493(7)	33(3)
C(83)	9385(9)	9890(5)	5214(7)	36(3)
C(84)	8509(10)	10175(5)	5127(7)	38(3)
C(85)	7715(10)	9961(5)	5313(8)	38(3)
C(86)	7761(9)	9409(5)	5588(7)	30(3)
C(87)	9178(10)	6235(5)	7632(8)	38(3)
C(88)	9953(10)	6586(5)	6343(8)	41(3)
C(89)	5010(9)	7601(5)	6877(7)	31(3)
C(90)	4355(9)	7945(6)	7106(8)	38(3)
C(91)	4014(11)	7835(7)	7740(9)	53(4)
C(92)	4298(11)	7383(7)	8184(9)	57(4)

149

C(93)	4921(12)	7034(6)	7952(8)	54(4)
C(94)	5258(9)	7124(6)	7302(7)	41(3)
C(95)	5911(8)	6725(5)	7139(8)	31(3)
C(96)	6608(10)	6221(5)	6311(9)	44(4)
C(97)	6781(11)	5742(6)	6772(9)	51(4)
C(98)	7331(10)	5330(6)	6605(10)	49(4)
C(99)	7681(10)	5371(6)	5945(10)	52(4)
C(100)	7527(9)	5835(5)	5498(9)	43(3)
C(101)	6987(9)	6267(5)	5682(8)	38(3)
C(102)	7422(9)	6927(5)	4902(7)	33(3)
C(103)	7365(9)	7433(5)	4501(7)	32(3)
C(104)	7961(10)	7508(6)	3987(8)	48(4)
C(105)	8009(11)	7998(7)	3634(9)	55(4)
C(106)	7480(9)	8414(6)	3755(7)	42(3)
C(107)	6864(8)	8359(5)	4246(6)	30(3)
C(108)	6786(9)	7874(5)	4605(7)	30(3)
C(109)	7483(13)	4838(7)	7102(11)	71(5)
C(110)	8280(11)	4914(6)	5736(11)	65(5)
C(111)	2935(8)	7863(5)	4906(7)	28(3)
C(112)	2443(8)	8378(6)	4614(7)	40(3)
C(113)	1546(8)	8485(6)	4763(7)	35(3)
C(114)	1100(10)	8126(6)	5143(8)	41(3)
C(115)	1540(10)	7647(5)	5401(8)	40(3)
C(116)	2445(9)	7510(5)	5297(7)	30(3)
C(117)	2805(9)	6987(5)	5567(7)	31(3)
C(118)	3851(9)	6245(5)	5838(8)	34(3)
C(119)	3626(9)	6043(6)	6487(8)	43(3)
C(120)	3924(11)	5532(7)	6764(9)	56(5)

C(121)	4439(11)	5210(7)	6378(11)	60(5)
C(122)	4648(9)	5422(6)	5713(10)	51(4)
C(123)	4358(9)	5929(5)	5447(8)	36(3)
C(124)	4773(8)	5905(6)	4257(9)	46(4)
C(125)	5011(10)	6085(6)	3565(8)	47(4)
C(126)	5089(13)	5670(7)	3032(11)	67(5)
C(127)	5357(16)	5816(10)	2349(10)	98(8)
C(128)	5537(15)	6357(8)	2215(10)	82(7)
C(129)	5432(12)	6741(7)	2727(9)	61(5)
C(130)	5129(9)	6627(6)	3395(7)	39(3)
C(131)	3745(13)	5326(8)	7484(11)	86(7)
C(132)	4791(15)	4670(7)	6700(14)	93(7)
C(133)	-651(8)	8491(6)	-878(6)	29(2)
C(134)	4117(7)	8498(5)	4281(6)	26(2)

Table AA.3. Bond lengths [Å] and angles [°] for Nd$_2$(DMSal)$_3$·MeOH.

Nd(1)-O(2)	2.253(8)	N(1)-C(8)	1.404(14)
Nd(1)-O(1)	2.271(8)	Nd(2)-O(5)	2.313(8)
Nd(1)-O(4)	2.409(8)	Nd(2)-O(6)	2.365(8)
Nd(1)-O(7)	2.459(10)	Nd(2)-O(3)	2.409(8)
Nd(1)-O(3)	2.476(8)	Nd(2)-O(4)	2.410(8)
Nd(1)-N(1)	2.545(9)	Nd(2)-N(5)	2.573(11)
Nd(1)-N(2)	2.552(10)	Nd(2)-N(6)	2.575(10)
Nd(1)-Nd(2)	3.9605(9)	Nd(2)-N(3)	2.598(10)
C(1)-O(1)	1.330(14)	Nd(2)-N(4)	2.679(10)
C(1)-C(2)	1.386(17)	O(2)-C(20)	1.326(15)
C(1)-C(6)	1.415(17)	N(2)-C(14)	1.292(14)
N(1)-C(7)	1.297(14)	N(2)-C(13)	1.428(14)

C(2)-C(3)	1.344(17)	O(5)-C(45)	1.284(16)
C(2)-H(2A)	0.9500	N(5)-C(51)	1.26(2)
Nd(3)-O(8)	2.237(8)	N(5)-C(52)	1.436(18)
Nd(3)-O(9)	2.279(8)	C(5)-C(6)	1.415(17)
Nd(3)-O(10)	2.418(8)	C(5)-H(5A)	0.9500
Nd(3)-O(11)	2.443(8)	O(6)-C(64)	1.320(14)
Nd(3)-O(14)	2.453(11)	N(6)-C(58)	1.312(16)
Nd(3)-N(8)	2.519(9)	N(6)-C(57)	1.438(16)
Nd(3)-N(7)	2.562(11)	C(6)-C(7)	1.458(16)
Nd(3)-Nd(4)	3.9629(10)	C(7)-H(7A)	0.9500
O(3)-C(23)	1.321(14)	N(7)-C(73)	1.282(15)
N(3)-C(29)	1.297(16)	N(7)-C(74)	1.420(15)
N(3)-C(30)	1.440(15)	O(7)-C(133)	1.700(13)
C(3)-C(4)	1.426(18)	O(8)-C(67)	1.329(16)
C(3)-H(3A)	0.9500	C(8)-C(9)	1.369(17)
Nd(4)-O(13)	2.298(8)	C(8)-C(13)	1.424(15)
Nd(4)-O(12)	2.351(8)	N(8)-C(80)	1.310(14)
Nd(4)-O(11)	2.382(8)	N(8)-C(79)	1.445(14)
Nd(4)-O(10)	2.413(8)	O(9)-C(86)	1.303(15)
Nd(4)-N(12)	2.560(10)	C(9)-C(10)	1.400(16)
Nd(4)-N(11)	2.591(10)	C(9)-H(9A)	0.9500
Nd(4)-N(10)	2.642(9)	N(9)-C(95)	1.290(16)
Nd(4)-N(9)	2.671(10)	N(9)-C(96)	1.424(17)
O(4)-C(42)	1.346(13)	O(10)-C(89)	1.331(14)
N(4)-C(36)	1.277(15)	N(10)-C(102)	1.291(15)
N(4)-C(35)	1.386(15)	N(10)-C(101)	1.399(16)
C(4)-C(5)	1.344(18)	C(10)-C(11)	1.437(16)
C(4)-H(4A)	0.9500	C(10)-C(21)	1.480(16)

O(11)-C(108)	1.331(14)	C(22)-H(22B)	0.9800
N(11)-C(117)	1.305(15)	C(22)-H(22C)	0.9800
N(11)-C(118)	1.412(15)	C(23)-C(24)	1.371(17)
C(11)-C(12)	1.329(18)	C(23)-C(28)	1.441(18)
C(11)-C(22)	1.472(16)	C(24)-C(25)	1.389(17)
O(12)-C(111)	1.304(14)	C(24)-H(24A)	0.9500
C(12)-C(13)	1.376(19)	C(25)-C(26)	1.40(2)
C(12)-H(12A)	0.9500	C(25)-H(25A)	0.9500
N(12)-C(124)	1.283(18)	C(26)-C(27)	1.39(2)
N(12)-C(123)	1.425(16)	C(26)-H(26A)	0.9500
O(13)-C(130)	1.294(15)	C(27)-C(28)	1.425(16)
C(14)-C(15)	1.448(15)	C(27)-H(27A)	0.9500
C(14)-H(14A)	0.9500	C(28)-C(29)	1.426(17)
O(14)-C(134)	1.822(12)	C(29)-H(29A)	0.9500
C(15)-C(16)	1.382(15)	C(30)-C(31)	1.374(17)
C(15)-C(20)	1.409(17)	C(30)-C(35)	1.411(17)
C(16)-C(17)	1.359(17)	C(31)-C(32)	1.421(18)
C(16)-H(16A)	0.9500	C(31)-H(31A)	0.9500
C(17)-C(18)	1.377(19)	C(32)-C(33)	1.37(2)
C(17)-H(17A)	0.9500	C(32)-C(43)	1.549(19)
C(18)-C(19)	1.377(19)	C(33)-C(34)	1.407(17)
C(18)-H(18A)	0.9500	C(33)-C(44)	1.487(19)
C(19)-C(20)	1.396(17)	C(34)-C(35)	1.397(17)
C(19)-H(19A)	0.9500	C(34)-H(34A)	0.9500
C(21)-H(21A)	0.9800	C(36)-C(37)	1.468(17)
C(21)-H(21B)	0.9800	C(36)-H(36A)	0.9500
C(21)-H(21C)	0.9800	C(37)-C(42)	1.387(16)
C(22)-H(22A)	0.9800	C(37)-C(38)	1.410(16)

C(38)-C(39)	1.39(2)	C(53)-C(54)	1.38(3)
C(38)-H(38A)	0.9500	C(53)-H(53A)	0.9500
C(39)-C(40)	1.36(2)	C(54)-C(55)	1.32(3)
C(39)-H(39A)	0.9500	C(54)-C(65)	1.56(2)
C(40)-C(41)	1.371(18)	C(55)-C(56)	1.35(2)
C(40)-H(40A)	0.9500	C(55)-C(66)	1.50(3)
C(41)-C(42)	1.430(17)	C(56)-C(57)	1.393(19)
C(41)-H(41A)	0.9500	C(56)-H(56A)	0.9500
C(43)-H(43A)	0.9800	C(58)-C(59)	1.434(17)
C(43)-H(43B)	0.9800	C(58)-H(58A)	0.9500
C(43)-H(43C)	0.9800	C(59)-C(60)	1.390(17)
C(44)-H(44A)	0.9800	C(59)-C(64)	1.399(16)
C(44)-H(44B)	0.9800	C(60)-C(61)	1.377(19)
C(44)-H(44C)	0.9800	C(60)-H(60A)	0.9500
C(45)-C(46)	1.36(2)	C(61)-C(62)	1.381(18)
C(45)-C(50)	1.40(2)	C(61)-H(61A)	0.9500
C(46)-C(47)	1.43(2)	C(62)-C(63)	1.408(17)
C(46)-H(46A)	0.9500	C(62)-H(62A)	0.9500
C(47)-C(48)	1.47(3)	C(63)-C(64)	1.414(18)
C(47)-H(47A)	0.9500	C(63)-H(63A)	0.9500
C(48)-C(49)	1.32(3)	C(65)-H(65A)	0.9800
C(48)-H(48A)	0.9500	C(65)-H(65B)	0.9800
C(49)-C(50)	1.41(2)	C(65)-H(65C)	0.9800
C(49)-H(49A)	0.9500	C(66)-H(66A)	0.9800
C(50)-C(51)	1.43(2)	C(66)-H(66B)	0.9800
C(51)-H(51A)	0.9500	C(66)-H(66C)	0.9800
C(52)-C(57)	1.36(2)	C(67)-C(72)	1.437(19)
C(52)-C(53)	1.442(19)	C(67)-C(68)	1.436(18)

C(68)-C(69)	1.395(19)	C(84)-C(85)	1.377(18)
C(68)-H(68A)	0.9500	C(84)-H(84A)	0.9500
C(69)-C(70)	1.41(2)	C(85)-C(86)	1.460(18)
C(69)-H(69A)	0.9500	C(85)-H(85A)	0.9500
C(70)-C(71)	1.326(19)	C(87)-H(87A)	0.9800
C(70)-H(70A)	0.9500	C(87)-H(87B)	0.9800
C(71)-C(72)	1.421(17)	C(87)-H(87C)	0.9800
C(71)-H(71A)	0.9500	C(88)-H(88A)	0.9800
C(72)-C(73)	1.470(18)	C(88)-H(88B)	0.9800
C(73)-H(73A)	0.9500	C(88)-H(88C)	0.9800
C(74)-C(75)	1.345(17)	C(89)-C(94)	1.403(19)
C(74)-C(79)	1.414(16)	C(89)-C(90)	1.413(18)
C(75)-C(76)	1.416(18)	C(90)-C(91)	1.38(2)
C(75)-H(75A)	0.9500	C(90)-H(90A)	0.9500
C(76)-C(77)	1.417(18)	C(91)-C(92)	1.37(2)
C(76)-C(87)	1.539(16)	C(91)-H(91A)	0.9500
C(77)-C(78)	1.381(17)	C(92)-C(93)	1.39(2)
C(77)-C(88)	1.504(17)	C(92)-H(92A)	0.9500
C(78)-C(79)	1.385(17)	C(93)-C(94)	1.388(18)
C(78)-H(78A)	0.9500	C(93)-H(93A)	0.9500
C(80)-C(81)	1.425(16)	C(94)-C(95)	1.451(19)
C(80)-H(80A)	0.9500	C(95)-H(95A)	0.9500
C(81)-C(86)	1.405(16)	C(96)-C(101)	1.38(2)
C(81)-C(82)	1.424(16)	C(96)-C(97)	1.434(19)
C(82)-C(83)	1.389(18)	C(97)-C(98)	1.38(2)
C(82)-H(82A)	0.9500	C(97)-H(97A)	0.9500
C(83)-C(84)	1.411(18)	C(98)-C(99)	1.40(2)
C(83)-H(83A)	0.9500	C(98)-C(109)	1.49(2)

C(99)-C(100)	1.39(2)	C(114)-C(115)	1.371(18)
C(99)-C(110)	1.535(19)	C(114)-H(11F)	0.9500
C(100)-C(101)	1.418(19)	C(115)-C(116)	1.401(18)
C(100)-H(10A)	0.9500	C(115)-H(11G)	0.9500
C(102)-C(103)	1.443(17)	C(116)-C(117)	1.439(17)
C(102)-H(10B)	0.9500	C(117)-H(11H)	0.9500
C(103)-C(108)	1.421(17)	C(118)-C(119)	1.376(18)
C(103)-C(104)	1.426(18)	C(118)-C(123)	1.385(19)
C(104)-C(105)	1.39(2)	C(119)-C(120)	1.39(2)
C(104)-H(10C)	0.9500	C(119)-H(11I)	0.9500
C(105)-C(106)	1.34(2)	C(120)-C(121)	1.40(3)
C(105)-H(10D)	0.9500	C(120)-C(131)	1.46(2)
C(106)-C(107)	1.409(16)	C(121)-C(122)	1.40(2)
C(106)-H(10E)	0.9500	C(121)-C(132)	1.50(2)
C(107)-C(108)	1.392(17)	C(122)-C(123)	1.375(18)
C(107)-H(10F)	0.9500	C(122)-H(12B)	0.9500
C(109)-H(10G)	0.9800	C(124)-C(125)	1.44(2)
C(109)-H(10H)	0.9800	C(124)-H(12C)	0.9500
C(109)-H(10I)	0.9800	C(125)-C(130)	1.41(2)
C(110)-H(11A)	0.9800	C(125)-C(126)	1.43(2)
C(110)-H(11B)	0.9800	C(126)-C(127)	1.42(3)
C(110)-H(11C)	0.9800	C(126)-H(12D)	0.9500
C(111)-C(116)	1.424(17)	C(127)-C(128)	1.41(3)
C(111)-C(112)	1.489(18)	C(127)-H(12E)	0.9500
C(112)-C(113)	1.406(16)	C(128)-C(129)	1.36(2)
C(112)-H(11D)	0.9500	C(128)-H(12F)	0.9500
C(113)-C(114)	1.382(18)	C(129)-C(130)	1.40(2)
C(113)-H(11E)	0.9500	C(129)-H(12G)	0.9500

C(131)-H(13A)	0.9800	O(2)-Nd(1)-Nd(2)	122.6(2)
C(131)-H(13B)	0.9800	O(1)-Nd(1)-Nd(2)	134.3(2)
C(131)-H(13C)	0.9800	O(4)-Nd(1)-Nd(2)	34.74(18)
C(132)-H(13D)	0.9800	O(7)-Nd(1)-Nd(2)	68.89(19)
C(132)-H(13E)	0.9800	O(3)-Nd(1)-Nd(2)	35.27(19)
C(132)-H(13F)	0.9800	N(1)-Nd(1)-Nd(2)	104.4(2)
		N(2)-Nd(1)-Nd(2)	94.8(2)
O(2)-Nd(1)-O(1)	97.2(3)	O(1)-C(1)-C(2)	120.9(11)
O(2)-Nd(1)-O(4)	88.2(3)	O(1)-C(1)-C(6)	121.3(11)
O(1)-Nd(1)-O(4)	160.7(3)	C(2)-C(1)-C(6)	117.8(11)
O(2)-Nd(1)-O(7)	98.5(3)	C(1)-O(1)-Nd(1)	144.4(8)
O(1)-Nd(1)-O(7)	85.1(3)	C(7)-N(1)-C(8)	118.8(10)
O(4)-Nd(1)-O(7)	75.8(3)	C(7)-N(1)-Nd(1)	131.0(8)
O(2)-Nd(1)-O(3)	157.8(3)	C(8)-N(1)-Nd(1)	109.8(6)
O(1)-Nd(1)-O(3)	103.5(3)	O(5)-Nd(2)-O(6)	90.9(3)
O(4)-Nd(1)-O(3)	69.7(3)	O(5)-Nd(2)-O(3)	86.7(3)
O(7)-Nd(1)-O(3)	75.8(3)	O(6)-Nd(2)-O(3)	94.2(3)
O(2)-Nd(1)-N(1)	116.7(3)	O(5)-Nd(2)-O(4)	152.9(3)
O(1)-Nd(1)-N(1)	71.6(3)	O(6)-Nd(2)-O(4)	76.3(3)
O(4)-Nd(1)-N(1)	122.3(3)	O(3)-Nd(2)-O(4)	70.8(3)
O(7)-Nd(1)-N(1)	139.4(3)	O(5)-Nd(2)-N(5)	70.0(4)
O(3)-Nd(1)-N(1)	78.0(3)	O(6)-Nd(2)-N(5)	116.1(3)
O(2)-Nd(1)-N(2)	72.1(3)	O(3)-Nd(2)-N(5)	141.1(3)
O(1)-Nd(1)-N(2)	120.2(3)	O(4)-Nd(2)-N(5)	137.2(3)
O(4)-Nd(1)-N(2)	79.0(3)	O(5)-Nd(2)-N(6)	111.7(3)
O(7)-Nd(1)-N(2)	153.4(3)	O(6)-Nd(2)-N(6)	71.2(3)
O(3)-Nd(1)-N(2)	103.4(3)	O(3)-Nd(2)-N(6)	156.1(3)
N(1)-Nd(1)-N(2)	63.4(3)	O(4)-Nd(2)-N(6)	87.1(3)

N(5)-Nd(2)-N(6)	62.3(3)	C(1)-C(2)-H(2A)	118.6
O(5)-Nd(2)-N(3)	79.8(3)	O(8)-Nd(3)-O(9)	96.4(3)
O(6)-Nd(2)-N(3)	161.4(3)	O(8)-Nd(3)-O(10)	88.4(3)
O(3)-Nd(2)-N(3)	69.4(3)	O(9)-Nd(3)-O(10)	162.3(3)
O(4)-Nd(2)-N(3)	105.0(3)	O(8)-Nd(3)-O(11)	156.6(3)
N(5)-Nd(2)-N(3)	76.0(3)	O(9)-Nd(3)-O(11)	103.6(3)
N(6)-Nd(2)-N(3)	127.2(3)	O(10)-Nd(3)-O(11)	68.9(2)
O(5)-Nd(2)-N(4)	133.0(3)	O(8)-Nd(3)-O(14)	94.0(3)
O(6)-Nd(2)-N(4)	134.1(3)	O(9)-Nd(3)-O(14)	86.3(3)
O(3)-Nd(2)-N(4)	100.2(3)	O(10)-Nd(3)-O(14)	76.4(3)
O(4)-Nd(2)-N(4)	68.1(3)	O(11)-Nd(3)-O(14)	75.5(3)
N(5)-Nd(2)-N(4)	76.6(3)	O(8)-Nd(3)-N(8)	118.8(3)
N(6)-Nd(2)-N(4)	78.8(3)	O(9)-Nd(3)-N(8)	71.7(3)
N(3)-Nd(2)-N(4)	60.4(3)	O(10)-Nd(3)-N(8)	120.6(3)
O(5)-Nd(2)-Nd(1)	120.3(2)	O(11)-Nd(3)-N(8)	79.6(3)
O(6)-Nd(2)-Nd(1)	80.35(19)	O(14)-Nd(3)-N(8)	141.6(3)
O(3)-Nd(2)-Nd(1)	36.41(18)	O(8)-Nd(3)-N(7)	72.8(3)
O(4)-Nd(2)-Nd(1)	34.73(18)	O(9)-Nd(3)-N(7)	118.8(3)
N(5)-Nd(2)-Nd(1)	161.7(2)	O(10)-Nd(3)-N(7)	78.9(3)
N(6)-Nd(2)-Nd(1)	120.4(2)	O(11)-Nd(3)-N(7)	106.9(3)
N(3)-Nd(2)-Nd(1)	90.4(2)	O(14)-Nd(3)-N(7)	152.3(3)
N(4)-Nd(2)-Nd(1)	86.0(2)	N(8)-Nd(3)-N(7)	63.6(3)
C(20)-O(2)-Nd(1)	139.6(8)	O(8)-Nd(3)-Nd(4)	122.5(2)
C(14)-N(2)-C(13)	121.3(10)	O(9)-Nd(3)-Nd(4)	134.5(2)
C(14)-N(2)-Nd(1)	130.2(8)	O(10)-Nd(3)-Nd(4)	34.85(18)
C(13)-N(2)-Nd(1)	108.5(7)	O(11)-Nd(3)-Nd(4)	34.27(17)
C(3)-C(2)-C(1)	122.8(12)	O(14)-Nd(3)-Nd(4)	69.8(2)
C(3)-C(2)-H(2A)	118.6	N(8)-Nd(3)-Nd(4)	103.7(2)

158

N(7)-Nd(3)-Nd(4)	96.3(2)	O(10)-Nd(4)-N(10)	103.7(3)
C(23)-O(3)-Nd(2)	125.3(7)	N(12)-Nd(4)-N(10)	78.4(3)
C(23)-O(3)-Nd(1)	126.4(7)	N(11)-Nd(4)-N(10)	129.2(3)
Nd(2)-O(3)-Nd(1)	108.3(3)	O(13)-Nd(4)-N(9)	131.5(3)
C(29)-N(3)-C(30)	120.2(10)	O(12)-Nd(4)-N(9)	134.9(3)
C(29)-N(3)-Nd(2)	124.2(8)	O(11)-Nd(4)-N(9)	101.9(3)
C(30)-N(3)-Nd(2)	115.3(7)	O(10)-Nd(4)-N(9)	68.2(3)
C(2)-C(3)-C(4)	119.7(12)	N(12)-Nd(4)-N(9)	75.0(3)
C(2)-C(3)-H(3A)	120.1	N(11)-Nd(4)-N(9)	78.2(3)
C(4)-C(3)-H(3A)	120.1	N(10)-Nd(4)-N(9)	61.0(3)
O(13)-Nd(4)-O(12)	91.7(3)	O(13)-Nd(4)-Nd(3)	119.7(2)
O(13)-Nd(4)-O(11)	86.4(3)	O(12)-Nd(4)-Nd(3)	79.89(19)
O(12)-Nd(4)-O(11)	91.6(3)	O(11)-Nd(4)-Nd(3)	35.28(18)
O(13)-Nd(4)-O(10)	153.1(3)	O(10)-Nd(4)-Nd(3)	34.92(18)
O(12)-Nd(4)-O(10)	76.8(3)	N(12)-Nd(4)-Nd(3)	161.2(2)
O(11)-Nd(4)-O(10)	70.0(3)	N(11)-Nd(4)-Nd(3)	119.5(2)
O(13)-Nd(4)-N(12)	71.5(3)	N(10)-Nd(4)-Nd(3)	88.9(2)
O(12)-Nd(4)-N(12)	116.3(3)	N(9)-Nd(4)-Nd(3)	86.8(2)
O(11)-Nd(4)-N(12)	144.1(3)	C(42)-O(4)-Nd(1)	129.3(7)
O(10)-Nd(4)-N(12)	135.4(3)	C(42)-O(4)-Nd(2)	120.1(7)
O(13)-Nd(4)-N(11)	113.6(3)	Nd(1)-O(4)-Nd(2)	110.5(3)
O(12)-Nd(4)-N(11)	71.7(3)	C(36)-N(4)-C(35)	119.9(10)
O(11)-Nd(4)-N(11)	153.7(3)	C(36)-N(4)-Nd(2)	124.8(8)
O(10)-Nd(4)-N(11)	86.1(3)	C(35)-N(4)-Nd(2)	114.7(7)
N(12)-Nd(4)-N(11)	61.9(3)	C(5)-C(4)-C(3)	119.2(12)
O(13)-Nd(4)-N(10)	78.5(3)	C(5)-C(4)-H(4A)	120.4
O(12)-Nd(4)-N(10)	159.0(3)	C(3)-C(4)-H(4A)	120.4
O(11)-Nd(4)-N(10)	69.5(3)	C(45)-O(5)-Nd(2)	138.0(9)

C(51)-N(5)-C(52)	121.1(14)	C(8)-C(9)-C(10)	124.5(11)
C(51)-N(5)-Nd(2)	128.7(13)	C(8)-C(9)-H(9A)	117.8
C(52)-N(5)-Nd(2)	109.7(8)	C(10)-C(9)-H(9A)	117.8
C(4)-C(5)-C(6)	121.4(12)	C(95)-N(9)-C(96)	120.7(11)
C(4)-C(5)-H(5A)	119.3	C(95)-N(9)-Nd(4)	126.3(8)
C(6)-C(5)-H(5A)	119.3	C(96)-N(9)-Nd(4)	113.0(8)
C(64)-O(6)-Nd(2)	139.8(7)	C(89)-O(10)-Nd(4)	121.3(7)
C(58)-N(6)-C(57)	118.5(11)	C(89)-O(10)-Nd(3)	128.4(7)
C(58)-N(6)-Nd(2)	131.0(8)	Nd(4)-O(10)-Nd(3)	110.2(3)
C(57)-N(6)-Nd(2)	110.6(8)	C(102)-N(10)-C(101)	121.6(11)
C(1)-C(6)-C(5)	119.0(11)	C(102)-N(10)-Nd(4)	124.4(8)
C(1)-C(6)-C(7)	124.4(11)	C(101)-N(10)-Nd(4)	113.8(8)
C(5)-C(6)-C(7)	116.5(11)	C(9)-C(10)-C(11)	116.4(11)
N(1)-C(7)-C(6)	126.6(11)	C(9)-C(10)-C(21)	121.8(11)
N(1)-C(7)-H(7A)	116.7	C(11)-C(10)-C(21)	121.8(11)
C(6)-C(7)-H(7A)	116.7	C(108)-O(11)-Nd(4)	126.8(7)
C(73)-N(7)-C(74)	119.7(11)	C(108)-O(11)-Nd(3)	122.5(7)
C(73)-N(7)-Nd(3)	130.3(9)	Nd(4)-O(11)-Nd(3)	110.5(3)
C(74)-N(7)-Nd(3)	109.6(7)	C(117)-N(11)-C(118)	119.5(11)
C(133)-O(7)-Nd(1)	144.9(7)	C(117)-N(11)-Nd(4)	130.4(8)
C(67)-O(8)-Nd(3)	140.2(9)	C(118)-N(11)-Nd(4)	110.1(8)
C(9)-C(8)-N(1)	126.2(10)	C(12)-C(11)-C(10)	117.7(11)
C(9)-C(8)-C(13)	118.0(11)	C(12)-C(11)-C(22)	123.9(12)
N(1)-C(8)-C(13)	115.8(10)	C(10)-C(11)-C(22)	118.4(11)
C(80)-N(8)-C(79)	118.5(10)	C(111)-O(12)-Nd(4)	140.1(8)
C(80)-N(8)-Nd(3)	132.1(7)	C(11)-C(12)-C(13)	127.0(10)
C(79)-N(8)-Nd(3)	109.2(7)	C(11)-C(12)-H(12A)	116.5
C(86)-O(9)-Nd(3)	141.8(8)	C(13)-C(12)-H(12A)	116.5

C(124)-N(12)-C(123)	120.2(12)	C(19)-C(20)-C(15)	117.0(12)
C(124)-N(12)-Nd(4)	127.4(10)	C(10)-C(21)-H(21A)	109.5
C(123)-N(12)-Nd(4)	111.8(8)	C(10)-C(21)-H(21B)	109.5
C(130)-O(13)-Nd(4)	139.4(8)	H(21A)-C(21)-H(21B)	109.5
C(12)-C(13)-C(8)	116.4(10)	C(10)-C(21)-H(21C)	109.5
C(12)-C(13)-N(2)	126.8(10)	H(21A)-C(21)-H(21C)	109.5
C(8)-C(13)-N(2)	116.9(10)	H(21B)-C(21)-H(21C)	109.5
N(2)-C(14)-C(15)	126.4(10)	C(11)-C(22)-H(22A)	109.5
N(2)-C(14)-H(14A)	116.8	C(11)-C(22)-H(22B)	109.5
C(15)-C(14)-H(14A)	116.8	H(22A)-C(22)-H(22B)	109.5
C(134)-O(14)-Nd(3)	137.4(7)	C(11)-C(22)-H(22C)	109.5
C(16)-C(15)-C(20)	118.7(11)	H(22A)-C(22)-H(22C)	109.5
C(16)-C(15)-C(14)	117.9(11)	H(22B)-C(22)-H(22C)	109.5
C(20)-C(15)-C(14)	123.4(10)	O(3)-C(23)-C(24)	121.0(12)
C(17)-C(16)-C(15)	123.3(13)	O(3)-C(23)-C(28)	119.9(11)
C(17)-C(16)-H(16A)	118.4	C(24)-C(23)-C(28)	119.1(11)
C(15)-C(16)-H(16A)	118.4	C(23)-C(24)-C(25)	123.4(13)
C(16)-C(17)-C(18)	118.8(12)	C(23)-C(24)-H(24A)	118.3
C(16)-C(17)-H(17A)	120.6	C(25)-C(24)-H(24A)	118.3
C(18)-C(17)-H(17A)	120.6	C(24)-C(25)-C(26)	118.0(13)
C(17)-C(18)-C(19)	119.3(13)	C(24)-C(25)-H(25A)	121.0
C(17)-C(18)-H(18A)	120.3	C(26)-C(25)-H(25A)	121.0
C(19)-C(18)-H(18A)	120.3	C(27)-C(26)-C(25)	121.0(13)
C(18)-C(19)-C(20)	122.8(14)	C(27)-C(26)-H(26A)	119.5
C(18)-C(19)-H(19A)	118.6	C(25)-C(26)-H(26A)	119.5
C(20)-C(19)-H(19A)	118.6	C(26)-C(27)-C(28)	120.4(13)
O(2)-C(20)-C(19)	119.4(13)	C(26)-C(27)-H(27A)	119.8
O(2)-C(20)-C(15)	123.6(11)	C(28)-C(27)-H(27A)	119.8

C(27)-C(28)-C(29)	117.2(12)	C(42)-C(37)-C(36)	123.0(11)
C(27)-C(28)-C(23)	117.9(11)	C(38)-C(37)-C(36)	117.1(11)
C(29)-C(28)-C(23)	124.7(11)	C(39)-C(38)-C(37)	121.3(13)
N(3)-C(29)-C(28)	126.3(12)	C(39)-C(38)-H(38A)	119.3
N(3)-C(29)-H(29A)	116.9	C(37)-C(38)-H(38A)	119.4
C(28)-C(29)-H(29A)	116.9	C(40)-C(39)-C(38)	117.3(13)
C(31)-C(30)-C(35)	122.2(12)	C(40)-C(39)-H(39A)	121.3
C(31)-C(30)-N(3)	122.6(11)	C(38)-C(39)-H(39A)	121.3
C(35)-C(30)-N(3)	115.2(10)	C(39)-C(40)-C(41)	124.0(13)
C(30)-C(31)-C(32)	118.8(13)	C(39)-C(40)-H(40A)	118.0
C(30)-C(31)-H(31A)	120.6	C(41)-C(40)-H(40A)	118.0
C(32)-C(31)-H(31A)	120.6	C(40)-C(41)-C(42)	118.9(12)
C(33)-C(32)-C(31)	120.8(12)	C(40)-C(41)-H(41A)	120.6
C(33)-C(32)-C(43)	122.1(13)	C(42)-C(41)-H(41A)	120.6
C(31)-C(32)-C(43)	116.9(14)	O(4)-C(42)-C(37)	122.1(11)
C(32)-C(33)-C(34)	119.1(12)	O(4)-C(42)-C(41)	119.5(10)
C(32)-C(33)-C(44)	122.0(12)	C(37)-C(42)-C(41)	118.4(11)
C(34)-C(33)-C(44)	118.9(12)	C(32)-C(43)-H(43A)	109.5
C(35)-C(34)-C(33)	122.0(12)	C(32)-C(43)-H(43B)	109.5
C(35)-C(34)-H(34A)	119.0	H(43A)-C(43)-H(43B)	109.5
C(33)-C(34)-H(34A)	119.0	C(32)-C(43)-H(43C)	109.5
N(4)-C(35)-C(34)	126.1(11)	H(43A)-C(43)-H(43C)	109.5
N(4)-C(35)-C(30)	116.9(10)	H(43B)-C(43)-H(43C)	109.5
C(34)-C(35)-C(30)	117.0(11)	C(33)-C(44)-H(44A)	109.5
N(4)-C(36)-C(37)	125.4(11)	C(33)-C(44)-H(44B)	109.5
N(4)-C(36)-H(36A)	117.3	H(44A)-C(44)-H(44B)	109.5
C(37)-C(36)-H(36A)	117.3	C(33)-C(44)-H(44C)	109.5
C(42)-C(37)-C(38)	119.9(12)	H(44A)-C(44)-H(44C)	109.5

H(44B)-C(44)-H(44C)	109.5	C(55)-C(54)-C(53)	121.4(16)
O(5)-C(45)-C(46)	117.6(15)	C(55)-C(54)-C(65)	121.5(18)
O(5)-C(45)-C(50)	125.0(14)	C(53)-C(54)-C(65)	117(2)
C(46)-C(45)-C(50)	117.4(14)	C(54)-C(55)-C(56)	119.3(19)
C(45)-C(46)-C(47)	120.4(18)	C(54)-C(55)-C(66)	118.7(17)
C(45)-C(46)-H(46A)	119.8	C(56)-C(55)-C(66)	122(2)
C(47)-C(46)-H(46A)	119.8	C(55)-C(56)-C(57)	121.9(18)
C(46)-C(47)-C(48)	121.2(19)	C(55)-C(56)-H(56A)	119.1
C(46)-C(47)-H(47A)	119.4	C(57)-C(56)-H(56A)	119.1
C(48)-C(47)-H(47A)	119.4	C(52)-C(57)-C(56)	121.0(14)
C(49)-C(48)-C(47)	115.3(18)	C(52)-C(57)-N(6)	116.2(12)
C(49)-C(48)-H(48A)	122.4	C(56)-C(57)-N(6)	122.5(14)
C(47)-C(48)-H(48A)	122.3	N(6)-C(58)-C(59)	127.4(11)
C(48)-C(49)-C(50)	123(2)	N(6)-C(58)-H(58A)	116.3
C(48)-C(49)-H(49A)	118.4	C(59)-C(58)-H(58A)	116.3
C(50)-C(49)-H(49A)	118.4	C(60)-C(59)-C(64)	120.0(12)
C(45)-C(50)-C(49)	121.8(17)	C(60)-C(59)-C(58)	115.7(11)
C(45)-C(50)-C(51)	120.7(14)	C(64)-C(59)-C(58)	124.2(11)
C(49)-C(50)-C(51)	117.5(18)	C(61)-C(60)-C(59)	122.4(12)
N(5)-C(51)-C(50)	129.7(18)	C(61)-C(60)-H(60A)	118.8
N(5)-C(51)-H(51A)	115.1	C(59)-C(60)-H(60A)	118.8
C(50)-C(51)-H(51A)	115.2	C(60)-C(61)-C(62)	119.0(12)
C(57)-C(52)-N(5)	117.6(11)	C(60)-C(61)-H(61A)	120.5
C(57)-C(52)-C(53)	115.5(14)	C(62)-C(61)-H(61A)	120.5
N(5)-C(52)-C(53)	126.8(14)	C(61)-C(62)-C(63)	119.6(13)
C(54)-C(53)-C(52)	120.8(17)	C(61)-C(62)-H(62A)	120.2
C(54)-C(53)-H(53A)	119.6	C(63)-C(62)-H(62A)	120.2
C(52)-C(53)-H(53A)	119.6	C(62)-C(63)-C(64)	121.6(12)

C(62)-C(63)-H(63A)	119.2	C(69)-C(70)-H(70A)	119.9
C(64)-C(63)-H(63A)	119.2	C(70)-C(71)-C(72)	122.5(14)
O(6)-C(64)-C(59)	124.6(11)	C(70)-C(71)-H(71A)	118.8
O(6)-C(64)-C(63)	118.1(11)	C(72)-C(71)-H(71A)	118.7
C(59)-C(64)-C(63)	117.3(11)	C(71)-C(72)-C(67)	118.8(12)
C(54)-C(65)-H(65A)	109.5	C(71)-C(72)-C(73)	117.5(11)
C(54)-C(65)-H(65B)	109.5	C(67)-C(72)-C(73)	123.6(11)
H(65A)-C(65)-H(65B)	109.5	N(7)-C(73)-C(72)	126.0(11)
C(54)-C(65)-H(65C)	109.5	N(7)-C(73)-H(73A)	117.0
H(65A)-C(65)-H(65C)	109.5	C(72)-C(73)-H(73A)	117.0
H(65B)-C(65)-H(65C)	109.5	C(75)-C(74)-C(79)	120.0(11)
C(55)-C(66)-H(66A)	109.4	C(75)-C(74)-N(7)	123.6(11)
C(55)-C(66)-H(66B)	109.5	C(79)-C(74)-N(7)	116.3(11)
H(66A)-C(66)-H(66B)	109.5	C(74)-C(75)-C(76)	120.8(11)
C(55)-C(66)-H(66C)	109.5	C(74)-C(75)-H(75A)	119.6
H(66A)-C(66)-H(66C)	109.5	C(76)-C(75)-H(75A)	119.6
H(66B)-C(66)-H(66C)	109.5	C(75)-C(76)-C(77)	119.9(11)
O(8)-C(67)-C(72)	123.4(12)	C(75)-C(76)-C(87)	122.0(11)
O(8)-C(67)-C(68)	118.6(14)	C(77)-C(76)-C(87)	118.1(11)
C(72)-C(67)-C(68)	117.9(13)	C(78)-C(77)-C(76)	118.0(12)
C(69)-C(68)-C(67)	119.6(15)	C(78)-C(77)-C(88)	119.8(12)
C(69)-C(68)-H(68A)	120.2	C(76)-C(77)-C(88)	122.1(11)
C(67)-C(68)-H(68A)	120.2	C(77)-C(78)-C(79)	121.8(13)
C(68)-C(69)-C(70)	121.0(13)	C(77)-C(78)-H(78A)	119.1
C(68)-C(69)-H(69A)	119.5	C(79)-C(78)-H(78A)	119.1
C(70)-C(69)-H(69A)	119.5	C(78)-C(79)-C(74)	119.5(11)
C(71)-C(70)-C(69)	120.2(13)	C(78)-C(79)-N(8)	124.4(11)
C(71)-C(70)-H(70A)	119.9	C(74)-C(79)-N(8)	116.1(11)

164

N(8)-C(80)-C(81)	125.2(10)	C(77)-C(88)-H(88B)	109.5
N(8)-C(80)-H(80A)	117.4	H(88A)-C(88)-H(88B)	109.5
C(81)-C(80)-H(80A)	117.4	C(77)-C(88)-H(88C)	109.5
C(86)-C(81)-C(82)	119.1(11)	H(88A)-C(88)-H(88C)	109.5
C(86)-C(81)-C(80)	124.4(11)	H(88B)-C(88)-H(88C)	109.5
C(82)-C(81)-C(80)	116.3(10)	O(10)-C(89)-C(94)	122.2(12)
C(83)-C(82)-C(81)	122.5(11)	O(10)-C(89)-C(90)	120.9(12)
C(83)-C(82)-H(82A)	118.7	C(94)-C(89)-C(90)	116.9(12)
C(81)-C(82)-H(82A)	118.7	C(91)-C(90)-C(89)	121.9(14)
C(82)-C(83)-C(84)	117.5(11)	C(91)-C(90)-H(90A)	119.1
C(82)-C(83)-H(83A)	121.3	C(89)-C(90)-H(90A)	119.0
C(84)-C(83)-H(83A)	121.3	C(92)-C(91)-C(90)	121.3(15)
C(85)-C(84)-C(83)	123.0(12)	C(92)-C(91)-H(91A)	119.4
C(85)-C(84)-H(84A)	118.5	C(90)-C(91)-H(91A)	119.3
C(83)-C(84)-H(84A)	118.5	C(91)-C(92)-C(93)	117.3(14)
C(84)-C(85)-C(86)	119.0(12)	C(91)-C(92)-H(92A)	121.3
C(84)-C(85)-H(85A)	120.5	C(93)-C(92)-H(92A)	121.3
C(86)-C(85)-H(85A)	120.5	C(92)-C(93)-C(94)	123.1(15)
O(9)-C(86)-C(81)	124.0(12)	C(92)-C(93)-H(93A)	118.4
O(9)-C(86)-C(85)	117.0(11)	C(94)-C(93)-H(93A)	118.5
C(81)-C(86)-C(85)	118.9(12)	C(93)-C(94)-C(89)	119.3(14)
C(76)-C(87)-H(87A)	109.5	C(93)-C(94)-C(95)	116.6(13)
C(76)-C(87)-H(87B)	109.5	C(89)-C(94)-C(95)	123.9(11)
H(87A)-C(87)-H(87B)	109.5	N(9)-C(95)-C(94)	123.1(12)
C(76)-C(87)-H(87C)	109.5	N(9)-C(95)-H(95A)	118.4
H(87A)-C(87)-H(87C)	109.5	C(94)-C(95)-H(95A)	118.4
H(87B)-C(87)-H(87C)	109.5	C(101)-C(96)-N(9)	118.2(11)
C(77)-C(88)-H(88A)	109.5	C(101)-C(96)-C(97)	119.3(14)

N(9)-C(96)-C(97)	122.4(14)	C(105)-C(106)-C(107)	120.2(14)
C(98)-C(97)-C(96)	121.3(16)	C(105)-C(106)-H(10E)	119.9
C(98)-C(97)-H(97A)	119.3	C(107)-C(106)-H(10E)	119.9
C(96)-C(97)-H(97A)	119.3	C(108)-C(107)-C(106)	120.9(12)
C(97)-C(98)-C(99)	118.9(14)	C(108)-C(107)-H(10F)	119.6
C(97)-C(98)-C(109)	119.1(17)	C(106)-C(107)-H(10F)	119.6
C(99)-C(98)-C(109)	121.9(15)	O(11)-C(108)-C(107)	118.9(11)
C(100)-C(99)-C(98)	120.2(14)	O(11)-C(108)-C(103)	121.4(11)
C(100)-C(99)-C(110)	119.7(16)	C(107)-C(108)-C(103)	119.5(12)
C(98)-C(99)-C(110)	120.1(14)	C(98)-C(109)-H(10G)	109.5
C(99)-C(100)-C(101)	121.0(14)	C(98)-C(109)-H(10H)	109.5
C(99)-C(100)-H(10A)	119.5	H(10G)-C(109)-H(10H)	109.5
C(101)-C(100)-H(10A)	119.5	C(98)-C(109)-H(10I)	109.5
C(96)-C(101)-N(10)	117.5(12)	H(10G)-C(109)-H(10I)	109.5
C(96)-C(101)-C(100)	119.1(12)	H(10H)-C(109)-H(10I)	109.5
N(10)-C(101)-C(100)	123.3(13)	C(99)-C(110)-H(11A)	109.5
N(10)-C(102)-C(103)	126.7(12)	C(99)-C(110)-H(11B)	109.5
N(10)-C(102)-H(10B)	116.7	H(11A)-C(110)-H(11B)	109.5
C(103)-C(102)-H(10B)	116.7	C(99)-C(110)-H(11C)	109.5
C(108)-C(103)-C(104)	117.2(12)	H(11A)-C(110)-H(11C)	109.5
C(108)-C(103)-C(102)	124.8(11)	H(11B)-C(110)-H(11C)	109.5
C(104)-C(103)-C(102)	118.0(12)	O(12)-C(111)-C(116)	125.7(12)
C(105)-C(104)-C(103)	121.3(14)	O(12)-C(111)-C(112)	117.2(11)
C(105)-C(104)-H(10C)	119.4	C(116)-C(111)-C(112)	117.2(11)
C(103)-C(104)-H(10C)	119.3	C(113)-C(112)-C(111)	117.8(13)
C(106)-C(105)-C(104)	120.8(13)	C(113)-C(112)-H(11D)	121.1
C(106)-C(105)-H(10D)	119.6	C(111)-C(112)-H(11D)	121.1
C(104)-C(105)-H(10D)	119.6	C(114)-C(113)-C(112)	122.6(13)

C(114)-C(113)-H(11E)	118.7	C(121)-C(122)-H(12B)	119.2
C(112)-C(113)-H(11E)	118.7	C(122)-C(123)-C(118)	120.3(13)
C(115)-C(114)-C(113)	120.1(12)	C(122)-C(123)-N(12)	123.4(14)
C(115)-C(114)-H(11F)	120.0	C(118)-C(123)-N(12)	115.9(11)
C(113)-C(114)-H(11F)	120.0	N(12)-C(124)-C(125)	128.9(14)
C(114)-C(115)-C(116)	121.5(12)	N(12)-C(124)-H(12C)	115.6
C(114)-C(115)-H(11G)	119.2	C(125)-C(124)-H(12C)	115.6
C(116)-C(115)-H(11G)	119.3	C(130)-C(125)-C(126)	121.4(15)
C(115)-C(116)-C(111)	120.9(12)	C(130)-C(125)-C(124)	123.7(13)
C(115)-C(116)-C(117)	115.8(11)	C(126)-C(125)-C(124)	114.9(15)
C(111)-C(116)-C(117)	123.2(11)	C(127)-C(126)-C(125)	118.0(18)
N(11)-C(117)-C(116)	127.8(11)	C(127)-C(126)-H(12D)	121.0
N(11)-C(117)-H(11H)	116.1	C(125)-C(126)-H(12D)	121.0
C(116)-C(117)-H(11H)	116.1	C(128)-C(127)-C(126)	119.8(17)
C(119)-C(118)-C(123)	119.2(12)	C(128)-C(127)-H(12E)	120.1
C(119)-C(118)-N(11)	123.8(13)	C(126)-C(127)-H(12E)	120.1
C(123)-C(118)-N(11)	116.9(12)	C(129)-C(128)-C(127)	120.3(18)
C(118)-C(119)-C(120)	120.8(15)	C(129)-C(128)-H(12F)	119.8
C(118)-C(119)-H(11I)	119.6	C(127)-C(128)-H(12F)	119.9
C(120)-C(119)-H(11I)	119.6	C(128)-C(129)-C(130)	122.8(18)
C(119)-C(120)-C(121)	120.6(14)	C(128)-C(129)-H(12G)	118.6
C(119)-C(120)-C(131)	121.3(18)	C(130)-C(129)-H(12G)	118.6
C(121)-C(120)-C(131)	118.1(15)	O(13)-C(130)-C(129)	120.2(14)
C(120)-C(121)-C(122)	117.5(14)	O(13)-C(130)-C(125)	122.4(13)
C(120)-C(121)-C(132)	120.0(16)	C(129)-C(130)-C(125)	117.4(13)
C(122)-C(121)-C(132)	122.4(19)	C(120)-C(131)-H(13A)	109.5
C(123)-C(122)-C(121)	121.6(16)	C(120)-C(131)-H(13B)	109.5
C(123)-C(122)-H(12B)	119.2	H(13A)-C(131)-H(13B)	109.5

C(120)-C(131)-H(13C)	109.5
H(13A)-C(131)-H(13C)	109.5
H(13B)-C(131)-H(13C)	109.5
C(121)-C(132)-H(13D)	109.5
C(121)-C(132)-H(13E)	109.5

H(13D)-C(132)-H(13E)	109.5
C(121)-C(132)-H(13F)	109.5
H(13D)-C(132)-H(13F)	109.5
H(13E)-C(132)-H(13F)	109.5

Table AA.4. Anisotropic displacement parameters ($Å^2 \times 10^3$) for $Nd_2(DMSal)_3 \cdot MeOH$. The anisotropic displacement factor exponent takes the form: $-2p^2[\, h^2 a^{*2}U^{11} + ... + 2\, h\, k\, a^* b^* U^{12}\,]$

	U^{11}	U^{22}	U^{33}	U^{23}	U^{13}	U^{12}
Nd(1)	24(1)	23(1)	22(1)	-1(1)	7(1)	0(1)
C(1)	20(6)	28(7)	26(7)	-2(5)	3(5)	-10(5)
O(1)	39(5)	28(5)	37(5)	-2(4)	19(4)	3(4)
N(1)	19(5)	24(5)	17(5)	2(4)	-3(4)	7(4)
Nd(2)	25(1)	22(1)	21(1)	0(1)	5(1)	0(1)
O(2)	19(5)	36(5)	39(5)	1(4)	1(4)	-2(4)
N(2)	35(6)	14(5)	33(6)	-3(4)	15(5)	1(4)
C(2)	40(8)	32(7)	39(8)	6(6)	16(6)	12(6)
Nd(3)	22(1)	26(1)	28(1)	-1(1)	5(1)	-2(1)
O(3)	19(4)	30(5)	33(5)	-4(4)	6(4)	-6(4)
N(3)	22(5)	31(6)	26(6)	2(4)	3(4)	-9(4)
C(3)	53(9)	33(7)	44(8)	10(6)	22(7)	14(6)
Nd(4)	20(1)	24(1)	27(1)	2(1)	1(1)	-2(1)
O(4)	20(4)	22(4)	37(5)	0(4)	15(4)	-1(3)
N(4)	25(6)	41(6)	21(5)	-4(4)	13(4)	9(5)
C(4)	56(9)	36(8)	49(8)	-6(6)	29(7)	7(7)
O(5)	24(5)	50(6)	38(5)	13(4)	-2(4)	-17(4)
N(5)	69(9)	31(7)	21(6)	7(5)	8(6)	-13(6)
C(5)	29(7)	35(7)	28(7)	5(5)	7(5)	-1(5)

O(6)	33(5)	31(5)	19(4)	1(3)	7(4)	12(4)
N(6)	25(5)	27(6)	31(6)	-1(4)	-8(4)	5(4)
C(6)	18(6)	29(7)	42(8)	-3(5)	7(5)	0(5)
C(7)	14(5)	36(8)	27(6)	-8(5)	2(5)	-2(5)
N(7)	22(5)	30(6)	45(7)	-8(5)	12(5)	-11(4)
O(7)	57(6)	45(6)	53(6)	-50(5)	33(5)	-13(5)
O(8)	33(5)	40(5)	34(5)	-8(4)	16(4)	-1(4)
C(8)	25(6)	35(7)	21(6)	-3(5)	13(5)	4(5)
N(8)	25(5)	25(5)	21(5)	7(4)	0(4)	4(4)
O(9)	26(5)	25(4)	43(5)	2(4)	17(4)	2(4)
C(9)	22(6)	36(7)	22(6)	-7(5)	3(5)	2(5)
N(9)	12(5)	30(6)	44(7)	0(5)	2(4)	-5(4)
O(10)	20(4)	28(4)	22(4)	3(3)	11(3)	2(3)
N(10)	14(5)	31(6)	26(5)	-3(4)	-4(4)	-3(4)
C(10)	30(7)	24(6)	30(7)	-3(5)	11(5)	-1(5)
O(11)	24(4)	29(5)	28(5)	3(3)	16(4)	-2(4)
N(11)	31(6)	36(6)	21(5)	9(4)	-4(4)	-11(5)
C(11)	28(7)	23(6)	22(6)	-3(5)	-1(5)	0(5)
O(12)	20(4)	28(5)	35(5)	6(4)	9(4)	-3(3)
C(12)	12(5)	64(9)	41(7)	-23(8)	16(5)	-4(7)
N(12)	29(6)	22(6)	36(6)	-6(5)	-5(5)	2(4)
O(13)	34(5)	42(6)	32(5)	2(4)	2(4)	9(4)
C(13)	15(5)	21(6)	24(6)	-4(5)	-2(5)	1(4)
C(14)	15(6)	24(6)	33(7)	2(5)	-8(5)	5(5)
O(14)	61(6)	60(7)	54(6)	-34(5)	24(5)	-59(5)
C(15)	20(5)	22(6)	24(5)	-2(5)	11(4)	2(5)
C(16)	24(6)	44(9)	41(7)	-13(6)	7(5)	-5(6)
C(17)	31(7)	46(9)	45(8)	-23(6)	19(6)	-8(6)

169

C(18)	40(8)	61(10)	45(8)	-15(7)	28(7)	-8(7)
C(19)	45(9)	38(8)	48(9)	-2(6)	25(7)	-7(6)
C(20)	39(8)	33(7)	34(7)	-17(6)	15(6)	-17(6)
C(21)	39(8)	42(8)	43(8)	21(6)	16(6)	3(6)
C(22)	31(7)	36(7)	29(7)	-3(5)	8(6)	4(6)
C(23)	15(6)	46(8)	26(7)	-9(6)	1(5)	-3(6)
C(24)	38(7)	35(7)	25(7)	-5(5)	13(6)	2(6)
C(25)	39(8)	68(10)	37(8)	-4(7)	25(7)	7(7)
C(26)	28(8)	73(11)	63(10)	-17(8)	24(7)	-3(7)
C(27)	34(7)	50(9)	41(7)	-6(6)	22(6)	-9(6)
C(28)	24(6)	46(9)	30(7)	-9(6)	5(5)	2(6)
C(29)	34(8)	37(8)	42(8)	16(6)	14(6)	1(6)
C(30)	44(8)	29(7)	15(6)	1(5)	3(5)	-6(6)
C(31)	46(8)	37(8)	25(7)	-2(5)	6(6)	-1(6)
C(32)	73(11)	28(7)	24(7)	0(6)	1(7)	-1(7)
C(33)	43(7)	20(6)	19(6)	-4(5)	3(5)	-3(5)
C(34)	46(8)	42(8)	30(7)	-8(6)	20(6)	-3(6)
C(35)	40(7)	15(6)	33(7)	13(5)	6(6)	2(5)
C(36)	32(7)	29(7)	31(7)	-1(5)	11(6)	10(5)
C(37)	27(6)	32(8)	23(6)	-12(5)	-1(5)	-1(5)
C(38)	31(7)	57(9)	35(7)	-5(7)	16(6)	3(7)
C(39)	38(9)	64(11)	63(11)	-16(8)	29(8)	-6(8)
C(40)	44(8)	48(9)	48(9)	-7(7)	31(7)	-11(7)
C(41)	31(7)	25(7)	37(7)	-7(5)	10(6)	0(5)
C(42)	17(6)	28(7)	29(7)	-7(5)	9(5)	3(5)
C(43)	62(10)	46(9)	45(9)	2(7)	9(8)	-22(8)
C(44)	79(12)	35(9)	71(11)	0(8)	34(10)	9(8)
C(45)	29(8)	58(10)	40(9)	8(7)	-13(6)	-9(7)

170

C(46)	62(12)	59(11)	73(13)	22(9)	-4(9)	-3(9)
C(47)	55(12)	99(17)	116(18)	49(14)	20(12)	-14(12)
C(48)	78(17)	110(20)	190(30)	35(19)	2(17)	-73(16)
C(49)	72(15)	66(14)	160(20)	43(14)	1(14)	-37(11)
C(50)	32(8)	57(10)	54(10)	3(8)	-4(7)	-22(7)
C(51)	141(19)	75(12)	1(6)	-21(7)	-10(8)	-27(13)
C(52)	55(9)	33(8)	16(6)	-6(5)	-3(6)	16(7)
C(53)	122(16)	43(9)	16(7)	-2(6)	1(8)	9(10)
C(54)	99(15)	55(11)	45(10)	6(8)	11(10)	58(11)
C(55)	106(15)	61(12)	27(8)	2(8)	1(9)	44(11)
C(56)	54(9)	53(9)	26(7)	-8(6)	-8(6)	35(8)
C(57)	52(9)	29(8)	24(7)	-16(6)	-3(6)	7(7)
C(58)	30(7)	40(9)	27(7)	-10(6)	0(5)	3(6)
C(59)	19(6)	36(7)	34(7)	-2(5)	7(5)	1(5)
C(60)	34(7)	47(8)	28(7)	-13(6)	8(6)	-2(6)
C(61)	46(8)	68(10)	24(7)	-2(6)	16(6)	-10(7)
C(62)	46(8)	37(8)	25(6)	2(6)	6(6)	4(6)
C(63)	47(8)	35(8)	29(6)	-13(6)	2(6)	8(7)
C(64)	33(7)	23(6)	11(5)	-4(5)	2(5)	-5(5)
C(65)	170(20)	61(13)	92(16)	27(12)	50(16)	68(15)
C(66)	130(20)	107(18)	109(18)	26(14)	56(16)	82(16)
C(67)	52(9)	41(8)	53(9)	-33(7)	30(8)	-31(7)
C(68)	27(7)	48(9)	55(9)	-16(7)	16(6)	-17(6)
C(69)	43(8)	65(10)	44(8)	-23(7)	33(7)	-19(7)
C(70)	52(9)	66(10)	46(8)	-2(9)	23(7)	-19(10)
C(71)	47(9)	54(9)	27(7)	-9(6)	12(6)	-14(7)
C(72)	17(6)	32(7)	29(6)	-1(5)	-1(5)	-6(5)
C(73)	30(7)	42(8)	30(7)	13(6)	-5(6)	-10(6)

171

C(74)	23(6)	35(7)	15(6)	-5(5)	-5(5)	0(5)
C(75)	45(7)	29(6)	18(5)	13(6)	-7(5)	-7(7)
C(76)	22(6)	21(6)	43(8)	5(5)	-1(6)	-1(5)
C(77)	16(6)	35(7)	40(8)	-1(6)	-4(5)	-4(5)
C(78)	26(7)	38(8)	27(7)	-10(6)	-1(5)	-7(6)
C(79)	22(6)	28(7)	22(6)	6(5)	-3(5)	-5(5)
C(80)	20(6)	36(8)	23(6)	-11(5)	6(5)	3(5)
C(81)	21(6)	29(7)	26(6)	0(5)	5(5)	3(5)
C(82)	27(7)	47(8)	26(7)	2(6)	10(5)	7(6)
C(83)	30(7)	32(7)	49(8)	-2(6)	20(6)	-3(6)
C(84)	46(8)	31(7)	34(7)	10(6)	9(6)	-13(6)
C(85)	39(8)	28(7)	42(8)	7(6)	4(6)	-3(6)
C(86)	23(7)	36(8)	26(7)	-10(6)	1(5)	-2(6)
C(87)	41(8)	29(7)	40(8)	14(6)	5(6)	-3(6)
C(88)	40(8)	37(8)	47(8)	5(6)	14(6)	-1(6)
C(89)	24(7)	44(8)	27(7)	-2(6)	9(6)	-14(6)
C(90)	33(7)	40(8)	43(8)	-15(6)	14(6)	-12(6)
C(91)	36(8)	65(11)	65(11)	-22(9)	25(8)	-19(8)
C(92)	50(10)	81(12)	50(10)	-15(9)	31(8)	-21(9)
C(93)	69(11)	47(10)	42(9)	2(7)	6(8)	-26(8)
C(94)	37(7)	49(8)	36(7)	16(7)	9(6)	-15(7)
C(95)	19(6)	37(7)	34(7)	6(6)	2(5)	-14(5)
C(96)	28(7)	22(7)	72(11)	13(7)	-3(7)	-3(6)
C(97)	50(9)	44(9)	45(9)	7(7)	-11(7)	-1(7)
C(98)	24(7)	32(8)	80(12)	7(7)	-5(7)	-8(6)
C(99)	25(7)	33(8)	88(13)	3(8)	1(8)	10(6)
C(100)	23(7)	38(8)	61(9)	6(7)	0(6)	-1(6)
C(101)	17(6)	41(8)	46(8)	9(6)	-9(6)	0(6)

C(102)	31(7)	38(7)	29(7)	1(6)	4(6)	5(6)
C(103)	25(7)	42(7)	28(7)	-7(6)	5(5)	-5(6)
C(104)	37(8)	68(11)	42(9)	2(7)	18(7)	2(7)
C(105)	45(9)	81(12)	45(9)	8(8)	24(7)	-13(8)
C(106)	36(7)	45(8)	42(7)	-3(7)	6(6)	-8(7)
C(107)	23(6)	44(9)	21(6)	6(5)	3(5)	-2(5)
C(108)	19(6)	39(8)	31(7)	-8(6)	3(5)	0(6)
C(109)	71(12)	54(10)	79(13)	41(10)	5(10)	15(9)
C(110)	34(9)	39(9)	120(16)	-4(9)	16(9)	19(7)
C(111)	16(6)	44(8)	24(7)	-4(6)	4(5)	0(6)
C(112)	25(6)	48(9)	42(8)	-5(6)	2(5)	0(6)
C(113)	28(6)	41(7)	36(7)	2(7)	10(5)	6(7)
C(114)	31(7)	56(9)	43(8)	-11(7)	23(6)	13(6)
C(115)	41(8)	41(8)	49(9)	3(6)	30(7)	11(6)
C(116)	34(7)	32(7)	25(7)	-1(5)	9(6)	-5(6)
C(117)	27(7)	42(8)	24(6)	0(5)	6(5)	-8(5)
C(118)	22(7)	29(7)	40(8)	4(6)	-7(6)	-9(6)
C(119)	31(8)	49(9)	43(8)	16(7)	2(6)	-12(6)
C(120)	38(9)	62(11)	54(10)	36(8)	-12(7)	-19(8)
C(121)	27(8)	55(10)	78(12)	49(9)	-16(8)	-8(7)
C(122)	21(7)	41(9)	78(12)	12(8)	-9(7)	1(6)
C(123)	23(7)	27(7)	48(8)	20(6)	-7(6)	-10(5)
C(124)	3(6)	48(9)	74(11)	1(8)	-9(6)	3(5)
C(125)	32(8)	57(10)	43(9)	-13(7)	-3(6)	11(7)
C(126)	69(12)	55(11)	75(13)	-14(9)	17(10)	16(9)
C(127)	117(18)	140(20)	37(10)	-15(12)	19(11)	65(16)
C(128)	116(17)	85(15)	40(10)	13(9)	17(10)	69(13)
C(129)	74(12)	78(12)	34(9)	-5(8)	18(8)	25(10)

C(130)	30(7)	48(9)	27(7)	0(6)	-11(6)	25(6)
C(131)	48(10)	100(15)	102(16)	48(13)	11(10)	-11(10)
C(132)	84(15)	55(12)	150(20)	36(12)	42(14)	-8(10)

Table AA.5. Hydrogen coordinates ($\times 10^4$) and isotropic displacement parameters ($\text{Å}^2 \times 10^3$) for

$Nd_2(DMSal)_3 \cdot MeOH$.

	x	y	z	U(eq)
H(2A)	-499	10128	1580	43
H(3A)	-1366	10464	2369	50
H(4A)	-1472	9972	3493	53
H(5A)	-838	9126	3693	37
H(7A)	30	8409	3402	32
H(9A)	-29	7546	3315	33
H(12A)	2943	7077	3023	45
H(14A)	3711	7887	3012	32
H(16A)	5182	8115	2786	44
H(17A)	6149	8570	2169	47
H(18A)	5448	9219	1230	54
H(19A)	3781	9356	885	50
H(21A)	-186	6740	3926	61
H(21B)	821	6477	4421	61
H(21C)	264	6247	3571	61
H(22A)	2910	6232	3530	48
H(22B)	1829	6000	3370	48
H(22C)	2388	6231	4218	48
H(24A)	-1427	8528	922	38
H(25A)	-2850	8502	1313	54
H(26A)	-3316	7686	1771	63

174

H(27A)	-2275	6950	1974	47
H(29A)	-722	6579	2044	44
H(31A)	-356	5760	1892	44
H(34A)	2834	5830	1686	45
H(36A)	3163	6634	1557	36
H(38A)	4366	6928	929	48
H(39A)	4970	7559	202	62
H(40A)	3971	8253	-381	52
H(41A)	2449	8386	-216	37
H(43A)	-129	4919	2455	78
H(43B)	942	4786	3003	78
H(43C)	578	4540	2136	78
H(44A)	3199	5003	2226	89
H(44B)	2314	4586	2040	89
H(44C)	2680	4858	2889	89
H(46A)	-3045	6981	-261	83
H(47A)	-4128	6260	-305	109
H(48A)	-3674	5355	-585	163
H(49A)	-2076	5224	-533	127
H(51A)	-533	5505	-454	94
H(53A)	1040	5211	143	77
H(56A)	2911	6375	-824	58
H(58A)	1785	6846	-1721	41
H(60A)	1911	7497	-2555	44
H(61A)	1628	8344	-3101	54
H(62A)	568	8921	-2705	44
H(63A)	-195	8635	-1763	47
H(65A)	3358	4693	154	158

H(65B)	2263	4473	-59	158
H(65C)	2748	4738	782	158
H(66A)	4003	5116	-141	167
H(66B)	4355	5723	14	167
H(66C)	3975	5502	-866	167
H(68A)	5015	9284	8019	51
H(69A)	5022	9089	9310	55
H(70A)	6042	8417	10030	63
H(71A)	7106	7987	9514	51
H(73A)	7818	7778	8497	44
H(75A)	8063	7046	7960	40
H(78A)	9324	7559	5911	38
H(80A)	9408	8434	6031	32
H(82A)	10016	9173	5563	40
H(83A)	9925	10049	5087	43
H(84A)	8465	10530	4932	45
H(85A)	7145	10169	5263	46
H(87A)	9610	6054	7372	58
H(87B)	8574	6029	7551	58
H(87C)	9504	6263	8196	58
H(88A)	10141	6766	5918	61
H(88B)	9587	6261	6141	61
H(88C)	10540	6492	6763	61
H(90A)	4145	8263	6813	46
H(91A)	3572	8075	7874	64
H(92A)	4078	7312	8632	69
H(93A)	5126	6720	8253	65
H(95A)	6292	6517	7563	37

H(97A)	6511	5707	7201	62
H(10A)	7788	5864	5063	51
H(10B)	7966	6707	4908	40
H(10C)	8334	7217	3884	57
H(10D)	8422	8040	3302	66
H(10E)	7521	8747	3510	50
H(10F)	6497	8658	4332	36
H(10G)	7198	4890	7539	107
H(10H)	8183	4767	7311	107
H(10I)	7167	4533	6783	107
H(11A)	8445	5003	5251	98
H(11B)	7896	4584	5659	98
H(11C)	8880	4865	6164	98
H(11D)	2725	8626	4336	48
H(11E)	1234	8817	4597	42
H(11F)	489	8211	5225	49
H(11G)	1223	7402	5656	48
H(11H)	2389	6772	5775	37
H(11I)	3264	6254	6750	51
H(12B)	4998	5212	5439	62
H(12C)	4698	5530	4298	55
H(12D)	4966	5308	3132	81
H(12E)	5415	5550	1983	117
H(12F)	5732	6454	1764	98
H(12G)	5569	7101	2628	74
H(13A)	4001	4962	7581	128
H(13B)	3043	5324	7424	128
H(13C)	4073	5556	7928	128

H(13D)	5139	4499	6362	139
H(13E)	4232	4448	6718	139
H(13F)	5232	4708	7232	139
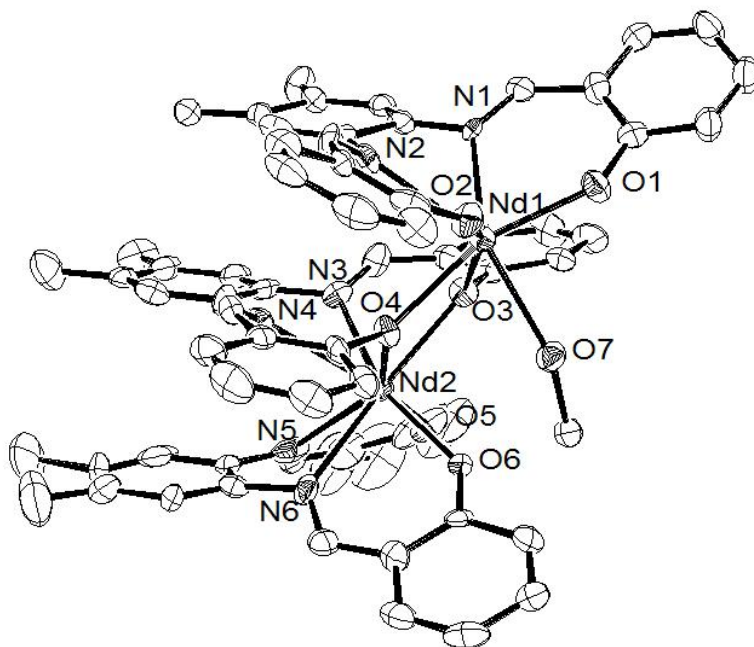
Figure AA.1. Molecular structure of $Nd_2(DMSal)_3$. All atoms represented by thermal ellipsoids drawn at the 30% probability level. All hydrogen atoms were omitted for clarity.
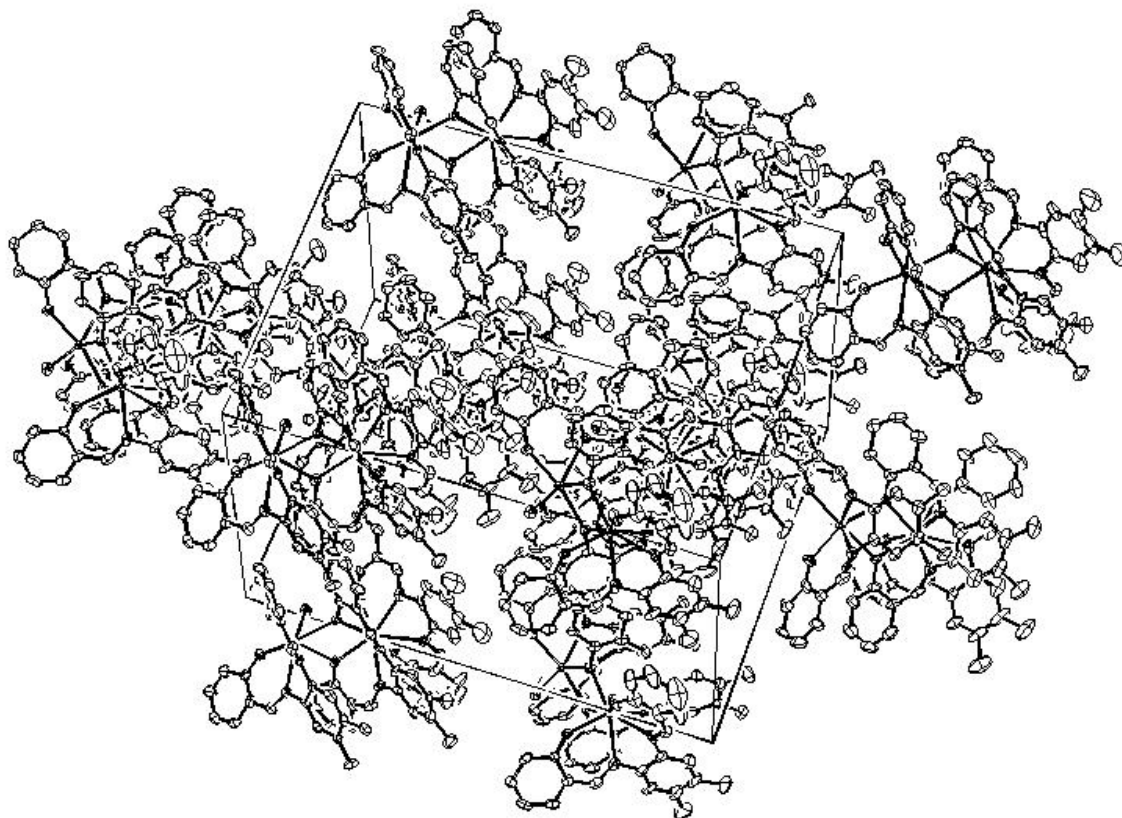
Figure AA.2. Unit cell structure of $Nd_2(DMSal)_3$

Table AA.6. Crystal data and structure refinement for $Et_3NH[Nd(TBDMSal)_2]$.

Identification code	hu0414s	
Empirical formula	C50 H43 Br8 N5 Nd O4	
Formula weight	1561.41	
Temperature	273(2) K	
Wavelength	0.71073 Å	
Crystal system	Monoclinic	
Space group	P2(1)/n	
Unit cell dimensions	a = 8.2612(3) Å	$\alpha = 90°$.
	b = 14.1640(5) Å	$\beta = 93.2130(10)°$.
	c = 46.8454(18) Å	$\gamma = 90°$.

179

Volume	5472.8(3) Å^3
Z	4
Density (calculated)	1.895 Mg/m^3
Absorption coefficient	6.836 mm^{-1}
F(000)	3000
Crystal size	$0.35 \times 0.08 \times 0.08 \text{ mm}^3$
Theta range for data collection	1.50 to 25.00°.
Index ranges	$-9 \le h \le 9, -16 \le k \le 16, -55 \le l \le 55$
Reflections collected	43476
Independent reflections	9639 [R(int) = 0.1284]
Completeness to theta = 25.00°	100.0 %
Absorption correction	None
Max. and min. transmission	0.6108 and 0.1982
Refinement method	Full-matrix least-squares on F^2
Data / restraints / parameters	9639 / 0 / 613
Goodness-of-fit on F^2	0.854
Final R indices [I>2sigma(I)]	R1 = 0.0634, wR2 = 0.1314
R indices (all data)	R1 = 0.1359, wR2 = 0.1585
Largest diff. peak and hole	0.927 and -0.795 e.Å^{-3}

Table AA.7. Atomic coordinates ($\times 10^4$) and equivalent isotropic displacement parameters ($\text{Å}^2 \times 10^3$) for

Et$_3$NH[Nd(TBDMSal)$_2$]. U(eq) is defined as one third of the trace of the orthogonalized U^{ij} tensor.

	x	y	z	U(eq)
Nd	6845(1)	7663(1)	1176(1)	41(1)
Br(1)	8195(2)	10913(1)	776(1)	84(1)
Br(2)	10628(2)	12471(1)	1818(1)	128(1)
Br(3)	11810(2)	3167(1)	651(1)	99(1)
Br(4)	8867(2)	6493(1)	225(1)	81(1)

Br(5)	6550(2)	9205(1)	236(1)	80(1)
Br(6)	3417(2)	6261(1)	-390(1)	99(1)
Br(7)	1962(2)	9129(1)	2545(1)	110(1)
Br(8)	4866(2)	10708(1)	1596(1)	79(1)
O(1)	8150(8)	9108(4)	1135(1)	50(2)
O(2)	8491(8)	6862(5)	861(1)	53(2)
O(3)	5462(8)	8050(4)	736(1)	48(2)
O(4)	5133(8)	8646(4)	1426(1)	50(2)
N(1)	8450(9)	8098(6)	1659(2)	48(2)
N(2)	8701(10)	6356(6)	1445(2)	49(2)
N(3)	5075(9)	6208(5)	969(2)	41(2)
N(4)	4940(10)	6710(5)	1523(2)	46(2)
N(5)	2498(12)	9110(7)	704(2)	74(3)
C(1)	8640(12)	9821(7)	1292(2)	55(3)
C(2)	8801(12)	10735(7)	1166(3)	64(3)
C(3)	9376(14)	11487(8)	1322(3)	74(4)
C(4)	9822(14)	11414(8)	1600(4)	79(4)
C(5)	9672(14)	10565(9)	1738(3)	76(4)
C(6)	9127(12)	9747(7)	1586(2)	55(3)
C(7)	9042(12)	8890(7)	1747(2)	58(3)
C(8)	8407(12)	7328(8)	1857(2)	53(3)
C(9)	8153(15)	7436(9)	2143(2)	75(4)
C(10)	8079(16)	6650(10)	2321(2)	79(4)
C(11)	8308(13)	5756(8)	2212(2)	61(3)
C(12)	8529(13)	5654(7)	1924(2)	59(3)
C(13)	8604(12)	6437(8)	1744(2)	54(3)
C(14)	9565(14)	5703(8)	1346(2)	60(3)
C(15)	9769(12)	5467(7)	1048(2)	54(3)

181

C(16)	10581(13)	4632(8)	992(2)	63(3)
C(17)	10818(13)	4340(8)	721(3)	63(3)
C(18)	10310(13)	4912(8)	496(2)	63(3)
C(19)	9571(12)	5755(7)	542(2)	53(3)
C(20)	9224(11)	6071(7)	822(2)	46(2)
C(21)	8163(17)	4866(9)	2395(2)	92(4)
C(22)	7690(20)	6784(10)	2636(2)	134(7)
C(23)	5183(11)	7594(7)	497(2)	48(3)
C(24)	5490(13)	8032(8)	234(2)	58(3)
C(25)	5002(13)	7648(8)	-33(2)	62(3)
C(26)	4238(13)	6774(9)	-37(2)	65(3)
C(27)	4041(13)	6290(8)	211(2)	59(3)
C(28)	4542(11)	6676(7)	472(2)	47(2)
C(29)	4423(12)	6076(7)	719(2)	49(3)
C(30)	5035(11)	5477(6)	1176(2)	38(2)
C(31)	5180(12)	4531(7)	1104(2)	54(3)
C(32)	5240(12)	3839(6)	1311(2)	53(3)
C(33)	5153(12)	4076(7)	1596(2)	51(3)
C(34)	5009(12)	5021(7)	1667(2)	51(3)
C(35)	4967(11)	5725(6)	1465(2)	42(2)
C(36)	4105(12)	6995(7)	1731(2)	53(3)
C(37)	3933(12)	7948(7)	1828(2)	48(3)
C(38)	3176(13)	8076(8)	2088(2)	65(3)
C(39)	2977(14)	8960(9)	2192(2)	63(3)
C(40)	3466(14)	9734(8)	2049(2)	66(3)
C(41)	4189(11)	9638(7)	1792(2)	49(3)
C(42)	4475(11)	8736(7)	1672(2)	45(2)
C(43)	5404(18)	2802(7)	1220(2)	89(4)

C(44)	5329(14)	3328(7)	1828(2)	66(3)
C(45)	1650(30)	9230(20)	452(5)	310(30)
C(46)	1338(19)	8810(13)	205(4)	136(6)
C(47)	1500(30)	8590(20)	870(8)	400(30)
C(48)	1786(13)	8012(8)	1091(3)	80(4)
C(49)	2860(30)	9921(16)	820(8)	340(30)
C(50)	3660(30)	10663(14)	783(4)	184(10)

Table AA.8. Bond lengths [Å] and angles [°] for Et$_3$NH[Nd(TBDMSal)$_2$].

Nd-O(1)	2.327(6)	O(4)-C(42)	1.307(10)
Nd-O(4)	2.345(6)	N(1)-C(7)	1.284(12)
Nd-O(2)	2.353(6)	N(1)-C(8)	1.432(12)
Nd-O(3)	2.367(6)	N(2)-C(14)	1.271(12)
Nd-N(1)	2.629(7)	N(2)-C(13)	1.415(12)
Nd-N(2)	2.672(8)	N(3)-C(29)	1.275(11)
Nd-N(3)	2.678(7)	N(3)-C(30)	1.422(10)
Nd-N(4)	2.689(8)	N(4)-C(36)	1.291(11)
Br(1)-C(2)	1.881(13)	N(4)-C(35)	1.420(11)
Br(2)-C(4)	1.911(11)	N(5)-C(49)	1.299(19)
Br(3)-C(17)	1.890(10)	N(5)-C(45)	1.35(2)
Br(4)-C(19)	1.880(10)	N(5)-C(47)	1.38(2)
Br(5)-C(24)	1.878(10)	C(1)-C(6)	1.419(14)
Br(6)-C(26)	1.897(11)	C(1)-C(2)	1.432(14)
Br(7)-C(39)	1.910(10)	C(2)-C(3)	1.364(15)
Br(8)-C(41)	1.874(10)	C(3)-C(4)	1.338(17)
O(1)-C(1)	1.300(11)	C(3)-H(3A)	0.9300
O(2)-C(20)	1.291(11)	C(4)-C(5)	1.373(16)
O(3)-C(23)	1.300(11)	C(5)-C(6)	1.419(14)

C(5)-H(5A)	0.9300	C(22)-H(22C)	0.9600
C(6)-C(7)	1.431(14)	C(23)-C(28)	1.406(13)
C(7)-H(7A)	0.9300	C(23)-C(24)	1.416(13)
C(8)-C(9)	1.380(14)	C(24)-C(25)	1.399(14)
C(8)-C(13)	1.381(13)	C(25)-C(26)	1.389(15)
C(9)-C(10)	1.393(16)	C(25)-H(25A)	0.9300
C(9)-H(9A)	0.9300	C(26)-C(27)	1.369(14)
C(10)-C(11)	1.384(16)	C(27)-C(28)	1.380(13)
C(10)-C(22)	1.537(15)	C(27)-H(27A)	0.9300
C(11)-C(12)	1.377(13)	C(28)-C(29)	1.443(13)
C(11)-C(21)	1.534(15)	C(29)-H(29A)	0.9300
C(12)-C(13)	1.396(14)	C(30)-C(31)	1.388(12)
C(12)-H(12A)	0.9300	C(30)-C(35)	1.403(11)
C(14)-C(15)	1.457(14)	C(31)-C(32)	1.377(13)
C(14)-H(14A)	0.9300	C(31)-H(31A)	0.9300
C(15)-C(16)	1.392(14)	C(32)-C(33)	1.382(13)
C(15)-C(20)	1.414(13)	C(32)-C(43)	1.537(13)
C(16)-C(17)	1.359(14)	C(33)-C(34)	1.386(13)
C(16)-H(16A)	0.9300	C(33)-C(44)	1.518(12)
C(17)-C(18)	1.376(15)	C(34)-C(35)	1.373(12)
C(18)-C(19)	1.363(13)	C(34)-H(34A)	0.9300
C(18)-H(18A)	0.9300	C(36)-C(37)	1.433(13)
C(19)-C(20)	1.432(13)	C(36)-H(36A)	0.9300
C(21)-H(21A)	0.9600	C(37)-C(38)	1.412(13)
C(21)-H(21B)	0.9600	C(37)-C(42)	1.419(13)
C(21)-H(21C)	0.9600	C(38)-C(39)	1.357(14)
C(22)-H(22A)	0.9600	C(38)-H(38A)	0.9300
C(22)-H(22B)	0.9600	C(39)-C(40)	1.357(14)

184

C(40)-C(41)	1.380(13)	O(1)-Nd-O(4)	79.3(2)
C(40)-H(40A)	0.9300	O(1)-Nd-O(2)	94.9(2)
C(41)-C(42)	1.422(13)	O(4)-Nd-O(2)	170.2(2)
C(43)-H(43A)	0.9600	O(1)-Nd-O(3)	85.8(2)
C(43)-H(43B)	0.9600	O(4)-Nd-O(3)	91.3(2)
C(43)-H(43C)	0.9600	O(2)-Nd-O(3)	80.4(2)
C(44)-H(44A)	0.9600	O(1)-Nd-N(1)	69.6(2)
C(44)-H(44B)	0.9600	O(4)-Nd-N(1)	73.8(2)
C(44)-H(44C)	0.9600	O(2)-Nd-N(1)	111.8(2)
C(45)-C(46)	1.32(2)	O(3)-Nd-N(1)	153.0(2)
C(45)-H(45A)	0.9700	O(1)-Nd-N(2)	113.1(2)
C(45)-H(45B)	0.9700	O(4)-Nd-N(2)	121.5(2)
C(46)-H(46A)	0.9600	O(2)-Nd-N(2)	68.0(2)
C(46)-H(46B)	0.9600	O(3)-Nd-N(2)	143.8(2)
C(46)-H(46C)	0.9600	N(1)-Nd-N(2)	60.6(2)
C(47)-C(48)	1.33(2)	O(1)-Nd-N(3)	153.2(2)
C(47)-H(47A)	0.9700	O(4)-Nd-N(3)	107.8(2)
C(47)-H(47B)	0.9700	O(2)-Nd-N(3)	74.0(2)
C(48)-H(48A)	0.9600	O(3)-Nd-N(3)	68.6(2)
C(48)-H(48B)	0.9600	N(1)-Nd-N(3)	137.0(2)
C(48)-H(48C)	0.9600	N(2)-Nd-N(3)	85.7(2)
C(49)-C(50)	1.26(3)	O(1)-Nd-N(4)	141.4(2)
C(49)-H(49A)	0.9700	O(4)-Nd-N(4)	66.8(2)
C(49)-H(49B)	0.9700	O(2)-Nd-N(4)	121.0(2)
C(50)-H(50A)	0.9600	O(3)-Nd-N(4)	111.9(2)
C(50)-H(50B)	0.9600	N(1)-Nd-N(4)	83.2(2)
C(50)-H(50C)	0.9600	N(2)-Nd-N(4)	73.0(2)
		N(3)-Nd-N(4)	60.4(2)

C(1)-O(1)-Nd	140.1(6)	C(3)-C(4)-C(5)	119.8(11)
C(20)-O(2)-Nd	143.0(6)	C(3)-C(4)-Br(2)	121.9(11)
C(23)-O(3)-Nd	133.5(6)	C(5)-C(4)-Br(2)	118.3(12)
C(42)-O(4)-Nd	142.3(6)	C(4)-C(5)-C(6)	121.0(12)
C(7)-N(1)-C(8)	118.7(8)	C(4)-C(5)-H(5A)	119.5
C(7)-N(1)-Nd	130.2(7)	C(6)-C(5)-H(5A)	119.5
C(8)-N(1)-Nd	110.4(6)	C(5)-C(6)-C(1)	119.4(11)
C(14)-N(2)-C(13)	118.8(9)	C(5)-C(6)-C(7)	116.9(11)
C(14)-N(2)-Nd	130.8(7)	C(1)-C(6)-C(7)	123.6(9)
C(13)-N(2)-Nd	110.4(6)	N(1)-C(7)-C(6)	127.0(10)
C(29)-N(3)-C(30)	119.8(8)	N(1)-C(7)-H(7A)	116.5
C(29)-N(3)-Nd	129.8(6)	C(6)-C(7)-H(7A)	116.5
C(30)-N(3)-Nd	110.2(5)	C(9)-C(8)-C(13)	120.0(10)
C(36)-N(4)-C(35)	117.8(8)	C(9)-C(8)-N(1)	123.9(10)
C(36)-N(4)-Nd	130.9(6)	C(13)-C(8)-N(1)	116.2(9)
C(35)-N(4)-Nd	111.2(6)	C(8)-C(9)-C(10)	120.6(11)
C(49)-N(5)-C(45)	110(2)	C(8)-C(9)-H(9A)	119.7
C(49)-N(5)-C(47)	111(2)	C(10)-C(9)-H(9A)	119.7
C(45)-N(5)-C(47)	105(2)	C(11)-C(10)-C(9)	119.8(10)
O(1)-C(1)-C(6)	123.7(9)	C(11)-C(10)-C(22)	120.6(12)
O(1)-C(1)-C(2)	120.2(10)	C(9)-C(10)-C(22)	119.6(12)
C(6)-C(1)-C(2)	116.0(10)	C(12)-C(11)-C(10)	119.2(11)
C(3)-C(2)-C(1)	121.5(12)	C(12)-C(11)-C(21)	118.8(11)
C(3)-C(2)-Br(1)	118.8(10)	C(10)-C(11)-C(21)	121.8(10)
C(1)-C(2)-Br(1)	119.7(8)	C(11)-C(12)-C(13)	121.3(10)
C(4)-C(3)-C(2)	122.1(12)	C(11)-C(12)-H(12A)	119.3
C(4)-C(3)-H(3A)	118.9	C(13)-C(12)-H(12A)	119.3
C(2)-C(3)-H(3A)	118.9	C(8)-C(13)-C(12)	119.0(9)

C(8)-C(13)-N(2)	117.8(9)	H(21B)-C(21)-H(21C)	109.5
C(12)-C(13)-N(2)	122.8(9)	C(10)-C(22)-H(22A)	109.5
N(2)-C(14)-C(15)	127.7(10)	C(10)-C(22)-H(22B)	109.5
N(2)-C(14)-H(14A)	116.1	H(22A)-C(22)-H(22B)	109.5
C(15)-C(14)-H(14A)	116.1	C(10)-C(22)-H(22C)	109.5
C(16)-C(15)-C(20)	120.7(10)	H(22A)-C(22)-H(22C)	109.5
C(16)-C(15)-C(14)	117.3(10)	H(22B)-C(22)-H(22C)	109.5
C(20)-C(15)-C(14)	122.0(9)	O(3)-C(23)-C(28)	125.4(9)
C(17)-C(16)-C(15)	122.0(11)	O(3)-C(23)-C(24)	120.0(9)
C(17)-C(16)-H(16A)	119.0	C(28)-C(23)-C(24)	114.7(10)
C(15)-C(16)-H(16A)	119.0	C(25)-C(24)-C(23)	123.3(10)
C(16)-C(17)-C(18)	118.9(10)	C(25)-C(24)-Br(5)	117.4(8)
C(16)-C(17)-Br(3)	121.1(10)	C(23)-C(24)-Br(5)	119.2(8)
C(18)-C(17)-Br(3)	120.1(8)	C(26)-C(25)-C(24)	117.9(10)
C(19)-C(18)-C(17)	121.0(10)	C(26)-C(25)-H(25A)	121.0
C(19)-C(18)-H(18A)	119.5	C(24)-C(25)-H(25A)	121.0
C(17)-C(18)-H(18A)	119.5	C(27)-C(26)-C(25)	120.5(10)
C(18)-C(19)-C(20)	122.2(10)	C(27)-C(26)-Br(6)	119.8(9)
C(18)-C(19)-Br(4)	119.0(8)	C(25)-C(26)-Br(6)	119.7(9)
C(20)-C(19)-Br(4)	118.7(8)	C(26)-C(27)-C(28)	120.7(10)
O(2)-C(20)-C(15)	123.5(9)	C(26)-C(27)-H(27A)	119.7
O(2)-C(20)-C(19)	121.4(9)	C(28)-C(27)-H(27A)	119.7
C(15)-C(20)-C(19)	115.1(9)	C(27)-C(28)-C(23)	122.2(9)
C(11)-C(21)-H(21A)	109.5	C(27)-C(28)-C(29)	116.4(9)
C(11)-C(21)-H(21B)	109.5	C(23)-C(28)-C(29)	121.4(9)
H(21A)-C(21)-H(21B)	109.5	N(3)-C(29)-C(28)	127.2(9)
C(11)-C(21)-H(21C)	109.5	N(3)-C(29)-H(29A)	116.4
H(21A)-C(21)-H(21C)	109.5	C(28)-C(29)-H(29A)	116.4

C(31)-C(30)-C(35)	119.0(8)	C(38)-C(39)-Br(7)	119.6(9)
C(31)-C(30)-N(3)	122.1(8)	C(40)-C(39)-Br(7)	118.8(9)
C(35)-C(30)-N(3)	118.7(8)	C(39)-C(40)-C(41)	120.4(10)
C(32)-C(31)-C(30)	121.1(9)	C(39)-C(40)-H(40A)	119.8
C(32)-C(31)-H(31A)	119.5	C(41)-C(40)-H(40A)	119.8
C(30)-C(31)-H(31A)	119.5	C(40)-C(41)-C(42)	121.6(9)
C(31)-C(32)-C(33)	120.3(9)	C(40)-C(41)-Br(8)	120.3(8)
C(31)-C(32)-C(43)	119.1(10)	C(42)-C(41)-Br(8)	118.1(7)
C(33)-C(32)-C(43)	120.6(9)	O(4)-C(42)-C(41)	121.6(9)
C(34)-C(33)-C(32)	118.5(9)	O(4)-C(42)-C(37)	122.4(8)
C(34)-C(33)-C(44)	120.6(9)	C(41)-C(42)-C(37)	116.0(9)
C(32)-C(33)-C(44)	120.8(9)	C(32)-C(43)-H(43A)	109.5
C(35)-C(34)-C(33)	122.3(9)	C(32)-C(43)-H(43B)	109.5
C(35)-C(34)-H(34A)	118.8	H(43A)-C(43)-H(43B)	109.5
C(33)-C(34)-H(34A)	118.8	C(32)-C(43)-H(43C)	109.5
C(34)-C(35)-C(30)	118.8(8)	H(43A)-C(43)-H(43C)	109.5
C(34)-C(35)-N(4)	125.5(8)	H(43B)-C(43)-H(43C)	109.5
C(30)-C(35)-N(4)	115.6(8)	C(33)-C(44)-H(44A)	109.5
N(4)-C(36)-C(37)	126.9(9)	C(33)-C(44)-H(44B)	109.5
N(4)-C(36)-H(36A)	116.6	H(44A)-C(44)-H(44B)	109.5
C(37)-C(36)-H(36A)	116.6	C(33)-C(44)-H(44C)	109.5
C(38)-C(37)-C(42)	120.7(9)	H(44A)-C(44)-H(44C)	109.5
C(38)-C(37)-C(36)	116.7(9)	H(44B)-C(44)-H(44C)	109.5
C(42)-C(37)-C(36)	122.6(8)	C(46)-C(45)-N(5)	141(2)
C(39)-C(38)-C(37)	119.8(10)	C(46)-C(45)-H(45A)	101.8
C(39)-C(38)-H(38A)	120.1	N(5)-C(45)-H(45A)	101.8
C(37)-C(38)-H(38A)	120.1	C(46)-C(45)-H(45B)	101.8
C(38)-C(39)-C(40)	121.5(10)	N(5)-C(45)-H(45B)	101.8

H(45A)-C(45)-H(45B)	104.7	C(47)-C(48)-H(48C)	109.5
C(45)-C(46)-H(46A)	109.5	H(48A)-C(48)-H(48C)	109.5
C(45)-C(46)-H(46B)	109.5	H(48B)-C(48)-H(48C)	109.5
H(46A)-C(46)-H(46B)	109.5	C(50)-C(49)-N(5)	142(4)
C(45)-C(46)-H(46C)	109.5	C(50)-C(49)-H(49A)	101.4
H(46A)-C(46)-H(46C)	109.5	N(5)-C(49)-H(49A)	101.4
H(46B)-C(46)-H(46C)	109.5	C(50)-C(49)-H(49B)	101.4
C(48)-C(47)-N(5)	133(2)	N(5)-C(49)-H(49B)	101.4
C(48)-C(47)-H(47A)	104.0	H(49A)-C(49)-H(49B)	104.6
N(5)-C(47)-H(47A)	104.0	C(49)-C(50)-H(50A)	109.5
C(48)-C(47)-H(47B)	104.0	C(49)-C(50)-H(50B)	109.5
N(5)-C(47)-H(47B)	104.0	H(50A)-C(50)-H(50B)	109.5
H(47A)-C(47)-H(47B)	105.4	C(49)-C(50)-H(50C)	109.5
C(47)-C(48)-H(48A)	109.5	H(50A)-C(50)-H(50C)	109.5
C(47)-C(48)-H(48B)	109.5	H(50B)-C(50)-H(50C)	109.5
H(48A)-C(48)-H(48B)	109.5		

Table AA.9. Anisotropic displacement parameters ($\text{Å}^2 \times 10^3$) $Et_3NH[Nd(TBDMSal)_2]$. The anisotropic

displacement factor exponent takes the form: $-2p^2[\, h^2\, a^{*2}U^{11} + ... + 2\, h\, k\, a^*\, b^*\, U^{12}]$

	U^{11}	U^{22}	U^{33}	U^{23}	U^{13}	U^{12}
Nd	50(1)	36(1)	37(1)	-1(1)	6(1)	-2(1)
Br(1)	94(1)	59(1)	101(1)	14(1)	13(1)	1(1)
Br(2)	133(1)	78(1)	173(2)	-58(1)	24(1)	-43(1)
Br(3)	117(1)	70(1)	110(1)	-24(1)	11(1)	34(1)
Br(4)	106(1)	89(1)	49(1)	-3(1)	10(1)	30(1)
Br(5)	96(1)	75(1)	70(1)	24(1)	9(1)	-21(1)
Br(6)	117(1)	136(1)	44(1)	-12(1)	-9(1)	-22(1)
Br(7)	151(2)	112(1)	72(1)	-18(1)	56(1)	13(1)
Br(8)	111(1)	40(1)	88(1)	-2(1)	27(1)	2(1)

O(1)	53(4)	39(4)	59(4)	-8(3)	11(3)	-12(3)
O(2)	58(4)	53(4)	49(4)	0(3)	16(3)	6(4)
O(3)	71(5)	39(4)	35(4)	1(3)	1(3)	-5(3)
O(4)	62(4)	42(4)	47(4)	0(3)	12(4)	3(3)
N(1)	58(6)	46(5)	37(5)	0(4)	-7(4)	-1(4)
N(2)	59(6)	41(5)	46(5)	-6(4)	6(4)	2(4)
N(3)	38(5)	42(5)	44(5)	1(4)	11(4)	-7(4)
N(4)	64(6)	37(5)	37(5)	-7(4)	3(4)	-8(4)
N(5)	74(7)	61(7)	87(8)	13(6)	9(6)	-10(5)
C(1)	46(7)	47(7)	74(8)	-3(6)	9(6)	-8(5)
C(2)	47(7)	49(7)	97(9)	-20(7)	22(6)	-6(5)
C(3)	64(8)	58(8)	102(11)	-13(8)	7(8)	-14(6)
C(4)	62(8)	46(7)	128(13)	-38(8)	15(9)	-26(6)
C(5)	71(8)	75(9)	83(9)	-20(7)	20(7)	-16(7)
C(6)	56(7)	44(6)	64(8)	-19(6)	7(6)	6(5)
C(7)	59(7)	55(7)	58(7)	-2(6)	2(6)	-2(6)
C(8)	62(7)	62(7)	35(6)	0(6)	-7(5)	2(6)
C(9)	111(11)	70(8)	44(7)	-12(6)	-3(7)	-13(7)
C(10)	107(11)	105(11)	26(6)	-19(7)	2(6)	-20(8)
C(11)	67(8)	79(8)	34(6)	-2(6)	-18(6)	3(6)
C(12)	81(8)	51(7)	42(6)	-5(5)	-8(6)	5(6)
C(13)	61(7)	64(7)	36(6)	-12(6)	3(5)	5(6)
C(14)	76(8)	57(7)	47(7)	-1(6)	-5(6)	-1(6)
C(15)	63(7)	45(6)	55(7)	-14(5)	8(6)	4(5)
C(16)	73(8)	55(7)	61(8)	2(6)	3(6)	0(6)
C(17)	67(8)	51(7)	73(8)	-22(6)	20(7)	13(6)
C(18)	58(7)	65(8)	66(8)	-17(7)	14(6)	8(6)
C(19)	41(6)	64(7)	53(7)	-8(6)	2(5)	0(5)
C(20)	39(6)	58(7)	42(6)	-1(5)	9(5)	0(5)
C(21)	129(12)	92(10)	51(8)	21(7)	-25(8)	-17(8)
C(22)	260(20)	105(12)	40(8)	-18(8)	8(10)	-25(13)
C(23)	44(6)	54(7)	48(6)	20(5)	11(5)	11(5)
C(24)	56(7)	62(7)	56(7)	13(6)	5(6)	-10(5)

C(25)	63(7)	80(8)	43(7)	17(6)	8(6)	1(7)
C(26)	61(8)	98(10)	37(6)	-7(7)	4(6)	2(7)
C(27)	65(7)	78(8)	32(6)	-9(6)	-9(5)	-13(6)
C(28)	44(6)	42(6)	53(7)	9(5)	-3(5)	-5(5)
C(29)	60(7)	40(6)	45(6)	-12(5)	-6(5)	-3(5)
C(30)	55(6)	26(5)	32(5)	7(4)	-2(5)	-3(4)
C(31)	77(8)	41(6)	43(6)	0(5)	-5(6)	2(5)
C(32)	70(8)	31(6)	58(7)	4(5)	7(6)	4(5)
C(33)	67(7)	41(6)	45(6)	9(5)	11(5)	-1(5)
C(34)	78(8)	46(6)	28(5)	12(5)	4(5)	-1(5)
C(35)	59(6)	39(6)	28(5)	-9(4)	9(5)	-7(5)
C(36)	70(7)	48(6)	43(6)	-3(5)	20(5)	3(5)
C(37)	59(7)	48(6)	40(6)	-2(5)	16(5)	-6(5)
C(38)	80(8)	69(8)	47(7)	-3(6)	25(6)	-7(6)
C(39)	78(8)	70(8)	44(7)	-14(6)	19(6)	2(6)
C(40)	83(9)	51(7)	63(8)	-19(6)	10(7)	4(6)
C(41)	49(6)	41(6)	58(7)	-2(5)	6(5)	3(5)
C(42)	49(6)	46(6)	41(6)	-6(5)	7(5)	6(5)
C(43)	164(14)	42(7)	62(8)	-9(6)	16(8)	13(7)
C(44)	109(10)	55(7)	33(6)	9(5)	6(6)	-6(6)
C(45)	310(40)	450(50)	160(20)	-200(30)	-120(30)	230(40)
C(46)	109(13)	166(18)	136(16)	33(14)	33(12)	-1(12)
C(47)	240(30)	450(50)	530(60)	400(50)	300(40)	230(30)
C(48)	66(8)	67(8)	108(11)	24(8)	22(8)	-19(6)
C(49)	260(30)	110(20)	630(70)	-180(30)	-150(40)	-20(20)
C(50)	270(30)	158(19)	134(16)	0(14)	71(17)	-123(19)

Table AA.10. Hydrogen coordinates ($\times 10^4$) and isotropic displacement parameters ($\text{Å}^2 \times 10^3$) for

Et$_3$NH[Nd(TBDMSal)$_2$].

	x	y	z	U(eq)
H(3A)	9462	12070	1233	89
H(5A)	9932	10525	1933	91

H(7A)	9461	8910	1935	69
H(9A)	8031	8037	2219	90
H(12A)	8631	5051	1848	70
H(14A)	10136	5331	1481	72
H(16A)	10972	4262	1144	76
H(18A)	10472	4720	310	75
H(21A)	8356	4318	2282	138
H(21B)	7093	4833	2465	138
H(21C)	8948	4892	2554	138
H(22A)	7686	6181	2729	200
H(22B)	6645	7074	2645	200
H(22C)	8499	7181	2729	200
H(25A)	5184	7967	-201	74
H(27A)	3563	5695	205	71
H(29A)	3802	5532	692	58
H(31A)	5237	4362	913	65
H(34A)	4939	5184	1858	61
H(36A)	3557	6534	1829	63
H(38A)	2815	7556	2187	77
H(40A)	3312	10332	2125	79
H(43A)	5451	2767	1016	133
H(43B)	4484	2451	1279	133
H(43C)	6377	2540	1310	133
H(44A)	5411	2717	1741	98
H(44B)	4398	3343	1941	98
H(44C)	6288	3450	1947	98
H(45A)	564	9350	514	376
H(45B)	2029	9846	392	376

H(46A)	669	9211	82	204
H(46B)	783	8226	235	204
H(46C)	2338	8685	117	204
H(47A)	755	9054	940	476
H(47B)	860	8212	733	476
H(48A)	778	7766	1151	120
H(48B)	2324	8353	1246	120
H(48C)	2462	7500	1035	120
H(49A)	1786	10178	847	410
H(49B)	3257	9732	1010	410
H(50A)	3501	11095	937	277
H(50B)	3307	10950	605	277
H(50C)	4792	10508	780	277
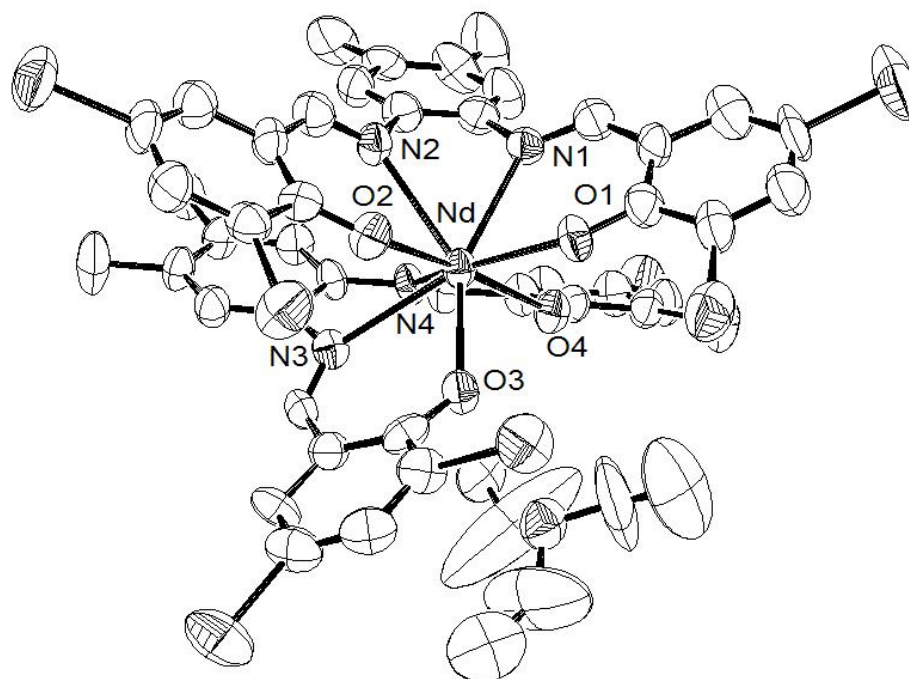
Figure AA.3. Molecular structure of Et$_3$NH[Nd(TBDMSal)$_2$]. All atoms represented by thermal ellipsoids drawn at

the 30% probability level. All hydrogen atoms were omitted for clarity.

193
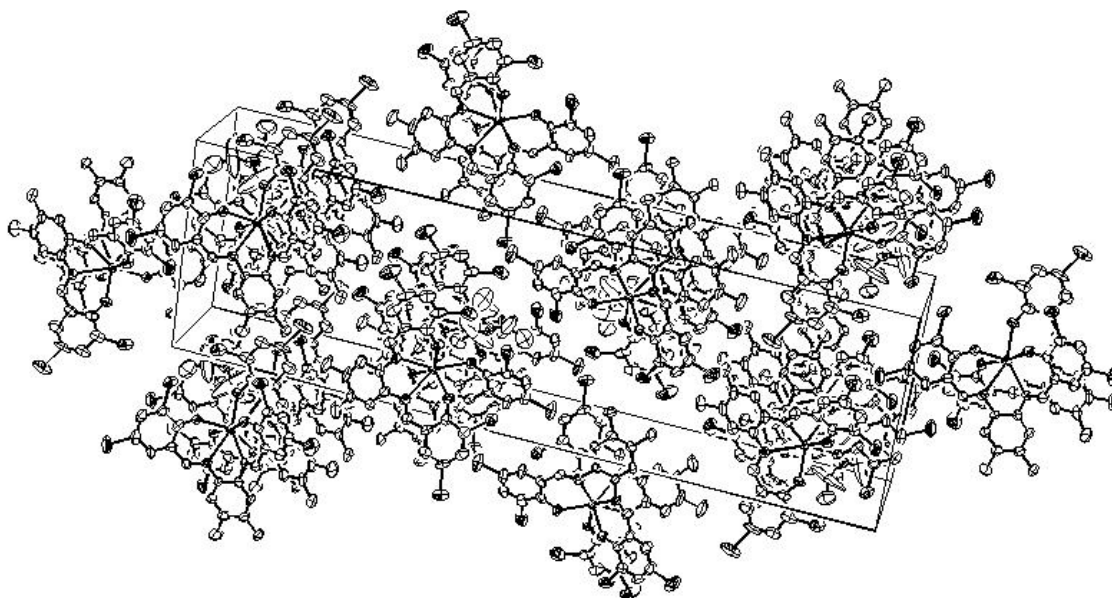
Figure AA.4. Unit cell structure of Et$_3$NH[Nd(TBDMSal)$_2$]

Table AA.11. Crystal data and structure refinement for Et$_3$NH[Yb(3BDMSal)$_2$].

Identification code	hyu531s
Empirical formula	C50 H46 Br4 N5 O4 Yb
Formula weight	1273.60
Temperature	200(2) K
Wavelength	0.71073 Å
Crystal system	Triclinic
Space group	P-1
Unit cell dimensions	a = 14.0444(7) Å $\quad$ α= 71.8530(10)°.
	b = 19.0529(10) Å $\quad$ β= 74.1520(10)°.
	c = 23.0176(12) Å $\quad$ γ = 68.7990(10)°.
Volume	5366.5(5) Å^3
Z	4
Density (calculated)	1.576 Mg/m^3

Absorption coefficient	4.765 mm^{-1}
F(000)	2492
Crystal size	$0.27 \times 0.26 \times 0.17$ mm^3
Theta range for data collection	1.58 to 27.50°.
Index ranges	-18 ≤ h ≤ 18, -24 ≤ k ≤ 24, -29 ≤ l ≤ 29
Reflections collected	52525
Independent reflections	24537 [R(int) = 0.0645]
Completeness to theta = 27.50°	99.6 %
Absorption correction	None
Max. and min. transmission	0.4980 and 0.3594
Refinement method	Full-matrix least-squares on F^2
Data / restraints / parameters	24537 / 0 / 1153
Goodness-of-fit on F^2	0.937
Final R indices [I>2sigma(I)]	R1 = 0.0587, wR2 = 0.1445
R indices (all data)	R1 = 0.1250, wR2 = 0.1632
Largest diff. peak and hole	1.635 and -1.044 e.Å^{-3}

Table AA.12. Atomic coordinates ($\times 10^4$) and equivalent isotropic displacement parameters (Å$^2 \times 10^3$) for

Et$_3$NH[Yb(3BDMSal)$_2$]. U(eq) is defined as one third of the trace of the orthogonalized U^{ij} tensor.

	x	y	z	U(eq)
Yb(1)	7471(1)	1057(1)	3348(1)	35(1)
Br(1)	5846(1)	1366(1)	5460(1)	58(1)
O(1)	7398(4)	830(3)	4358(2)	40(1)
N(1)	9289(5)	672(4)	3518(3)	38(2)
C(1)	7834(6)	1014(5)	4683(4)	39(2)
N(2)	8760(5)	1155(4)	2368(3)	37(2)
C(2)	7291(7)	1265(5)	5232(4)	48(2)
Br(2)	4552(1)	1971(1)	2160(1)	86(1)

O(2)	6636(4)	1396(4)	2560(3)	53(2)
Yb(2)	17093(1)	-3115(1)	1153(1)	35(1)
Br(3)	9585(1)	2690(1)	3159(1)	82(1)
O(3)	7749(4)	2171(3)	3226(3)	45(1)
N(3)	5785(5)	2002(4)	3704(3)	37(2)
C(3)	7734(8)	1476(6)	5595(4)	63(3)
Br(4)	10042(1)	-1474(1)	3222(1)	58(1)
O(4)	8009(4)	-198(3)	3299(2)	42(1)
N(4)	6013(5)	496(4)	3858(3)	39(2)
C(4)	8768(8)	1404(7)	5442(5)	74(3)
C(5)	9350(7)	1146(6)	4911(4)	62(3)
N(5)	18545(5)	-4344(4)	1056(3)	37(2)
O(5)	16418(4)	-4024(3)	1123(2)	34(1)
Br(5)	14535(1)	-3953(1)	689(1)	50(1)
C(6)	8902(6)	967(5)	4535(4)	40(2)
Br(6)	15561(1)	-326(1)	754(1)	72(1)
O(6)	16979(4)	-1933(3)	1174(3)	47(2)
N(6)	18882(5)	-3106(4)	1167(3)	43(2)
C(7)	9556(6)	762(5)	3970(4)	41(2)
N(7)	15714(5)	-2304(4)	499(3)	37(2)
O(7)	17883(4)	-2915(3)	186(3)	40(1)
Br(7)	19954(1)	-3187(1)	-644(1)	65(1)
C(8)	10094(6)	485(5)	3005(4)	38(2)
Br(8)	18656(1)	-4627(1)	3046(1)	72(1)
O(8)	17207(4)	-3680(3)	2140(3)	46(1)
N(8)	15344(5)	-2643(4)	1774(3)	43(2)
C(9)	11117(6)	43(5)	3076(4)	46(2)
N(9)	7490(7)	-638(6)	2383(4)	70(2)

C(10)	11877(6)	-131(5)	2560(5)	54(2)
N(10)	16082(5)	-5140(4)	2158(3)	47(2)
C(11)	11616(6)	90(5)	1967(4)	49(2)
C(12)	10587(7)	525(5)	1910(4)	48(2)
C(13)	9816(6)	720(5)	2423(4)	40(2)
C(14)	8573(6)	1652(5)	1846(4)	44(2)
C(15)	7588(7)	2040(5)	1662(4)	47(2)
C(16)	7576(8)	2557(6)	1092(4)	63(3)
C(17)	6696(9)	2907(6)	844(5)	78(3)
C(18)	5804(8)	2708(6)	1169(5)	67(3)
C(19)	5788(7)	2212(6)	1728(4)	55(3)
C(20)	6670(6)	1860(5)	2014(4)	44(2)
C(21)	12995(7)	-602(7)	2665(5)	79(3)
C(22)	12420(7)	-103(6)	1399(5)	70(3)
C(23)	7490(6)	2649(5)	3571(4)	40(2)
C(24)	8219(8)	2972(6)	3600(5)	61(3)
C(25)	7972(10)	3509(7)	3930(6)	83(4)
C(26)	6975(12)	3760(7)	4258(6)	92(4)
C(27)	6247(9)	3414(6)	4250(5)	71(3)
C(28)	6493(7)	2870(5)	3921(4)	45(2)
C(29)	5684(6)	2559(5)	3947(4)	47(2)
C(30)	4881(6)	1807(5)	3753(4)	42(2)
C(31)	3912(6)	2341(5)	3684(4)	47(2)
C(32)	3061(6)	2121(6)	3700(4)	57(3)
C(33)	3177(7)	1337(6)	3800(5)	60(3)
C(34)	4130(6)	806(5)	3867(4)	51(2)
C(35)	4994(6)	1030(5)	3831(4)	40(2)
C(36)	6088(6)	-180(5)	4224(4)	45(2)

197

C(37)	7061(7)	-826(5)	4246(4)	46(2)
C(38)	7047(9)	-1487(6)	4705(5)	74(3)
C(39)	7915(9)	-2135(6)	4733(5)	83(4)
C(40)	8801(9)	-2128(6)	4320(5)	74(3)
C(41)	8831(7)	-1483(5)	3848(4)	49(2)
C(42)	7984(6)	-797(5)	3777(4)	42(2)
C(43)	2040(7)	2747(6)	3578(5)	81(4)
C(44)	2302(8)	1060(7)	3806(6)	99(4)
C(45)	16686(6)	-4350(4)	658(4)	34(2)
C(46)	15961(6)	-4399(5)	369(4)	41(2)
C(47)	16224(7)	-4736(5)	-116(4)	49(2)
C(48)	17253(7)	-5080(6)	-345(5)	62(3)
C(49)	18021(7)	-5066(5)	-71(4)	53(2)
C(50)	17771(6)	-4705(4)	409(4)	36(2)
C(51)	18618(6)	-4732(5)	669(4)	38(2)
C(52)	19437(6)	-4481(5)	1299(4)	40(2)
C(53)	20124(6)	-5204(5)	1467(4)	46(2)
C(54)	20985(6)	-5309(5)	1713(5)	56(3)
C(55)	21136(6)	-4669(6)	1800(4)	57(3)
C(56)	20476(6)	-3955(5)	1614(4)	52(2)
C(57)	19623(6)	-3845(5)	1360(4)	43(2)
C(58)	19240(7)	-2529(5)	872(4)	50(2)
C(59)	18639(7)	-1739(5)	642(5)	52(2)
C(60)	19147(8)	-1214(6)	264(5)	70(3)
C(61)	18651(9)	-454(6)	40(5)	74(3)
C(62)	17562(9)	-192(6)	192(5)	68(3)
C(63)	17020(8)	-674(5)	553(5)	55(2)
C(64)	17516(8)	-1475(5)	809(4)	53(2)

C(65)	21704(8)	-6100(6)	1892(5)	78(3)
C(66)	22041(7)	-4741(6)	2061(5)	75(3)
C(67)	17794(6)	-2527(5)	-362(4)	38(2)
C(68)	18662(6)	-2551(5)	-850(4)	41(2)
C(69)	18564(8)	-2161(6)	-1448(5)	61(3)
C(70)	16745(7)	-1607(5)	-1149(4)	53(2)
C(70')	17601(8)	-1675(6)	-1616(4)	60(3)
C(71)	16813(6)	-2010(5)	-530(4)	42(2)
C(72)	15855(6)	-1934(5)	-77(4)	44(2)
C(74)	14670(5)	-2195(4)	817(4)	38(2)
C(75)	13846(6)	-2002(5)	511(4)	47(2)
C(76)	12853(6)	-1968(5)	840(5)	52(2)
C(77)	12649(6)	-2115(5)	1491(5)	54(2)
C(78)	13472(7)	-2317(5)	1770(5)	53(2)
C(79)	14494(6)	-2359(5)	1453(4)	41(2)
C(80)	15175(7)	-2544(5)	2332(5)	53(2)
C(81)	15872(8)	-2893(6)	2779(5)	58(3)
C(82)	15526(9)	-2694(7)	3323(5)	88(4)
C(83)	16126(12)	-3047(9)	3795(6)	113(5)
C(84)	17025(11)	-3629(8)	3713(5)	103(4)
C(85)	17384(7)	-3848(6)	3167(4)	61(3)
C(86)	16843(7)	-3476(5)	2662(4)	50(2)
C(87)	12002(7)	-1788(6)	476(5)	67(3)
C(88)	11594(7)	-2124(7)	1859(6)	91(4)
C(89)	7971(15)	-1445(9)	2263(7)	131(7)
C(90)	8049(18)	-2051(13)	2714(11)	215(12)
C(91)	6351(12)	-422(11)	2691(7)	145(7)
C(92)	5588(14)	-459(12)	2428(9)	186(9)

C(93)	7640(11)	-55(8)	1810(6)	98(4)
C(94)	8788(11)	-129(9)	1525(6)	115(5)
C(95)	15394(7)	-4761(6)	2666(5)	61(3)
C(96)	14310(9)	-4270(7)	2518(6)	92(4)
C(97)	17143(7)	-5600(5)	2365(5)	59(3)
C(98)	17851(7)	-6116(6)	1943(5)	68(3)
C(99)	15603(7)	-5624(5)	1977(4)	52(2)
C(100)	15360(8)	-6282(6)	2511(5)	67(3)

Table AA.13. Bond lengths [Å] and angles [°] for Et$_3$NH[Yb(3BDMSal)$_2$].

Yb(1)-O(1)	2.208(5)	O(2)-C(20)	1.292(9)
Yb(1)-O(3)	2.216(5)	Yb(2)-O(7)	2.181(5)
Yb(1)-O(2)	2.228(5)	Yb(2)-O(8)	2.213(6)
Yb(1)-O(4)	2.261(6)	Yb(2)-O(6)	2.215(5)
Yb(1)-N(2)	2.480(6)	Yb(2)-O(5)	2.280(5)
Yb(1)-N(4)	2.491(6)	Yb(2)-N(8)	2.484(7)
Yb(1)-N(1)	2.495(6)	Yb(2)-N(5)	2.514(6)
Yb(1)-N(3)	2.509(6)	Yb(2)-N(7)	2.525(6)
Br(1)-C(2)	1.906(9)	Yb(2)-N(6)	2.529(6)
O(1)-C(1)	1.276(9)	Yb(2)-C(45)	3.187(8)
N(1)-C(7)	1.274(9)	Yb(2)-C(64)	3.208(9)
N(1)-C(8)	1.428(10)	Br(3)-C(24)	1.878(11)
C(1)-C(2)	1.412(11)	O(3)-C(23)	1.283(9)
C(1)-C(6)	1.421(11)	N(3)-C(29)	1.294(10)
N(2)-C(14)	1.300(10)	N(3)-C(30)	1.415(9)
N(2)-C(13)	1.432(10)	C(3)-C(4)	1.363(13)
C(2)-C(3)	1.384(12)	C(3)-H(3A)	0.9500
Br(2)-C(19)	1.887(10)	Br(4)-C(41)	1.907(9)

O(4)-C(42)	1.320(10)	C(9)-H(9A)	0.9500
N(4)-C(36)	1.286(10)	N(9)-C(93)	1.456(14)
N(4)-C(35)	1.429(10)	N(9)-C(89)	1.520(18)
C(4)-C(5)	1.393(13)	N(9)-C(91)	1.522(17)
C(4)-H(4A)	0.9500	C(10)-C(11)	1.407(13)
C(5)-C(6)	1.377(11)	C(10)-C(21)	1.543(12)
C(5)-H(5A)	0.9500	N(10)-C(95)	1.492(11)
N(5)-C(51)	1.285(9)	N(10)-C(99)	1.521(10)
N(5)-C(52)	1.417(9)	N(10)-C(97)	1.549(11)
O(5)-C(45)	1.302(9)	C(11)-C(12)	1.401(12)
Br(5)-C(46)	1.904(8)	C(11)-C(22)	1.521(12)
C(6)-C(7)	1.447(11)	C(12)-C(13)	1.409(11)
Br(6)-C(63)	1.882(10)	C(12)-H(12A)	0.9500
O(6)-C(64)	1.308(10)	C(14)-C(15)	1.423(11)
N(6)-C(58)	1.291(10)	C(14)-H(14A)	0.9500
N(6)-C(57)	1.437(10)	C(15)-C(16)	1.372(12)
C(7)-H(7A)	0.9500	C(15)-C(20)	1.419(11)
N(7)-C(72)	1.293(10)	C(16)-C(17)	1.361(13)
N(7)-C(74)	1.421(9)	C(16)-H(16A)	0.9500
O(7)-C(67)	1.261(9)	C(17)-C(18)	1.389(14)
Br(7)-C(68)	1.873(8)	C(17)-H(17A)	0.9500
C(8)-C(13)	1.392(11)	C(18)-C(19)	1.340(13)
C(8)-C(9)	1.403(10)	C(18)-H(18A)	0.9500
Br(8)-C(85)	1.881(10)	C(19)-C(20)	1.409(11)
O(8)-C(86)	1.291(10)	C(21)-H(21A)	0.9800
N(8)-C(80)	1.303(11)	C(21)-H(21B)	0.9800
N(8)-C(79)	1.423(10)	C(21)-H(21C)	0.9800
C(9)-C(10)	1.399(12)	C(22)-H(22A)	0.9800

C(22)-H(22B)	0.9800	C(38)-H(38A)	0.9500
C(22)-H(22C)	0.9800	C(39)-C(40)	1.345(14)
C(23)-C(24)	1.396(11)	C(39)-H(39A)	0.9500
C(23)-C(28)	1.398(12)	C(40)-C(41)	1.369(13)
C(24)-C(25)	1.352(15)	C(40)-H(40A)	0.9500
C(25)-C(26)	1.387(16)	C(41)-C(42)	1.413(12)
C(25)-H(25A)	0.9500	C(43)-H(43A)	0.9800
C(26)-C(27)	1.409(14)	C(43)-H(43B)	0.9800
C(26)-H(26A)	0.9500	C(43)-H(43C)	0.9800
C(27)-C(28)	1.362(12)	C(44)-H(44A)	0.9800
C(27)-H(27A)	0.9500	C(44)-H(44B)	0.9800
C(28)-C(29)	1.440(11)	C(44)-H(44C)	0.9800
C(29)-H(29A)	0.9500	C(45)-C(46)	1.402(10)
C(30)-C(31)	1.388(11)	C(45)-C(50)	1.459(10)
C(30)-C(35)	1.388(11)	C(46)-C(47)	1.358(11)
C(31)-C(32)	1.392(11)	C(47)-C(48)	1.383(12)
C(31)-H(31A)	0.9500	C(47)-H(47A)	0.9500
C(32)-C(33)	1.394(13)	C(48)-C(49)	1.401(12)
C(32)-C(43)	1.527(12)	C(48)-H(48A)	0.9500
C(33)-C(34)	1.369(12)	C(49)-C(50)	1.379(11)
C(33)-C(44)	1.497(12)	C(49)-H(49A)	0.9500
C(34)-C(35)	1.399(10)	C(50)-C(51)	1.451(10)
C(34)-H(34A)	0.9500	C(51)-H(51A)	0.9500
C(36)-C(37)	1.472(11)	C(52)-C(53)	1.375(11)
C(36)-H(36A)	0.9500	C(52)-C(57)	1.382(11)
C(37)-C(38)	1.372(12)	C(53)-C(54)	1.396(11)
C(37)-C(42)	1.449(11)	C(53)-H(53A)	0.9500
C(38)-C(39)	1.385(14)	C(54)-C(55)	1.391(13)

C(54)-C(65)	1.484(12)	C(70)-C(71)	1.404(12)
C(55)-C(56)	1.354(12)	C(70)-H(70A)	0.9500
C(55)-C(66)	1.496(12)	C(70')-H(70B)	0.9500
C(56)-C(57)	1.396(11)	C(71)-C(72)	1.450(11)
C(56)-H(56A)	0.9500	C(72)-H(72A)	0.9500
C(58)-C(59)	1.445(12)	C(74)-C(79)	1.370(11)
C(58)-H(58A)	0.9500	C(74)-C(75)	1.394(11)
C(59)-C(60)	1.380(12)	C(75)-C(76)	1.382(11)
C(59)-C(64)	1.449(12)	C(75)-H(75A)	0.9500
C(60)-C(61)	1.360(14)	C(76)-C(77)	1.403(13)
C(60)-H(60A)	0.9500	C(76)-C(87)	1.522(12)
C(61)-C(62)	1.405(14)	C(77)-C(78)	1.351(12)
C(61)-H(61A)	0.9500	C(77)-C(88)	1.496(12)
C(62)-C(63)	1.341(13)	C(78)-C(79)	1.407(11)
C(62)-H(62A)	0.9500	C(78)-H(78A)	0.9500
C(63)-C(64)	1.434(12)	C(80)-C(81)	1.453(13)
C(65)-H(65A)	0.9800	C(80)-H(80A)	0.9500
C(65)-H(65B)	0.9800	C(81)-C(82)	1.333(12)
C(65)-H(65C)	0.9800	C(81)-C(86)	1.434(12)
C(66)-H(66A)	0.9800	C(82)-C(83)	1.406(16)
C(66)-H(66B)	0.9800	C(82)-H(82A)	0.9500
C(66)-H(66C)	0.9800	C(83)-C(84)	1.359(16)
C(67)-C(68)	1.413(11)	C(83)-H(83A)	0.9500
C(67)-C(71)	1.446(11)	C(84)-C(85)	1.356(14)
C(68)-C(69)	1.362(12)	C(84)-H(84A)	0.9500
C(69)-C(70')	1.412(13)	C(85)-C(86)	1.418(12)
C(69)-H(69A)	0.9500	C(87)-H(87A)	0.9800
C(70)-C(70')	1.374(12)	C(87)-H(87B)	0.9800

C(87)-H(87C)	0.9800	C(97)-H(97B)	0.9900
C(88)-H(88A)	0.9800	C(98)-H(98A)	0.9800
C(88)-H(88B)	0.9800	C(98)-H(98B)	0.9800
C(88)-H(88C)	0.9800	C(98)-H(98C)	0.9800
C(89)-C(90)	1.28(2)	C(99)-C(100)	1.524(12)
C(89)-H(89A)	0.9500	C(99)-H(99A)	0.9900
C(90)-H(90A)	0.9800	C(99)-H(99B)	0.9900
C(90)-H(90B)	0.9800	C(100)-H(10A)	0.9800
C(90)-H(90C)	0.9800	C(100)-H(10B)	0.9800
C(91)-C(92)	1.399(18)	C(100)-H(10C)	0.9800
C(91)-H(91A)	0.9500		
C(92)-H(92A)	0.9800	O(1)-Yb(1)-O(3)	89.1(2)
C(92)-H(92B)	0.9800	O(1)-Yb(1)-O(2)	148.5(2)
C(92)-H(92C)	0.9800	O(3)-Yb(1)-O(2)	98.6(2)
C(93)-C(94)	1.538(16)	O(1)-Yb(1)-O(4)	96.6(2)
C(93)-H(93A)	0.9900	O(3)-Yb(1)-O(4)	152.50(19)
C(93)-H(93B)	0.9900	O(2)-Yb(1)-O(4)	90.5(2)
C(94)-H(94A)	0.9800	O(1)-Yb(1)-N(2)	139.25(19)
C(94)-H(94B)	0.9800	O(3)-Yb(1)-N(2)	76.7(2)
C(94)-H(94C)	0.9800	O(2)-Yb(1)-N(2)	72.1(2)
C(95)-C(96)	1.537(14)	O(4)-Yb(1)-N(2)	81.7(2)
C(95)-H(95A)	0.9900	O(1)-Yb(1)-N(4)	74.2(2)
C(95)-H(95B)	0.9900	O(3)-Yb(1)-N(4)	136.0(2)
C(96)-H(96A)	0.9800	O(2)-Yb(1)-N(4)	79.3(2)
C(96)-H(96B)	0.9800	O(4)-Yb(1)-N(4)	71.1(2)
C(96)-H(96C)	0.9800	N(2)-Yb(1)-N(4)	140.0(2)
C(97)-C(98)	1.504(13)	O(1)-Yb(1)-N(1)	72.9(2)
C(97)-H(97A)	0.9900	O(3)-Yb(1)-N(1)	75.8(2)

O(2)-Yb(1)-N(1)	138.6(2)	O(7)-Yb(2)-O(5)	97.37(19)
O(4)-Yb(1)-N(1)	80.1(2)	O(8)-Yb(2)-O(5)	89.64(19)
N(2)-Yb(1)-N(1)	66.7(2)	O(6)-Yb(2)-O(5)	153.23(18)
N(4)-Yb(1)-N(1)	132.9(2)	O(7)-Yb(2)-N(8)	138.7(2)
O(1)-Yb(1)-N(3)	76.0(2)	O(8)-Yb(2)-N(8)	73.2(2)
O(3)-Yb(1)-N(3)	71.5(2)	O(6)-Yb(2)-N(8)	75.7(2)
O(2)-Yb(1)-N(3)	77.7(2)	O(5)-Yb(2)-N(8)	82.00(19)
O(4)-Yb(1)-N(3)	135.93(19)	O(7)-Yb(2)-N(5)	74.1(2)
N(2)-Yb(1)-N(3)	131.6(2)	O(8)-Yb(2)-N(5)	78.7(2)
N(4)-Yb(1)-N(3)	65.0(2)	O(6)-Yb(2)-N(5)	135.52(19)
N(1)-Yb(1)-N(3)	134.7(2)	O(5)-Yb(2)-N(5)	71.12(18)
C(1)-O(1)-Yb(1)	133.5(5)	N(8)-Yb(2)-N(5)	141.0(2)
C(7)-N(1)-C(8)	116.9(7)	O(7)-Yb(2)-N(7)	73.0(2)
C(7)-N(1)-Yb(1)	125.5(6)	O(8)-Yb(2)-N(7)	139.0(2)
C(8)-N(1)-Yb(1)	116.3(5)	O(6)-Yb(2)-N(7)	79.1(2)
O(1)-C(1)-C(2)	122.3(7)	O(5)-Yb(2)-N(7)	78.46(18)
O(1)-C(1)-C(6)	123.3(7)	N(8)-Yb(2)-N(7)	66.4(2)
C(2)-C(1)-C(6)	114.4(7)	N(5)-Yb(2)-N(7)	131.2(2)
C(14)-N(2)-C(13)	118.5(6)	O(7)-Yb(2)-N(6)	73.6(2)
C(14)-N(2)-Yb(1)	124.9(5)	O(8)-Yb(2)-N(6)	79.3(2)
C(13)-N(2)-Yb(1)	115.7(5)	O(6)-Yb(2)-N(6)	71.9(2)
C(3)-C(2)-C(1)	124.0(8)	O(5)-Yb(2)-N(6)	134.87(19)
C(3)-C(2)-Br(1)	118.5(7)	N(8)-Yb(2)-N(6)	133.6(2)
C(1)-C(2)-Br(1)	117.5(6)	N(5)-Yb(2)-N(6)	63.8(2)
C(20)-O(2)-Yb(1)	135.7(5)	N(7)-Yb(2)-N(6)	135.3(2)
O(7)-Yb(2)-O(8)	147.92(19)	O(7)-Yb(2)-C(45)	77.74(19)
O(7)-Yb(2)-O(6)	89.9(2)	O(8)-Yb(2)-C(45)	104.3(2)
O(8)-Yb(2)-O(6)	97.8(2)	O(6)-Yb(2)-C(45)	154.8(2)

O(5)-Yb(2)-C(45)	19.97(18)	C(6)-C(5)-C(4)	121.4(9)
N(8)-Yb(2)-C(45)	99.2(2)	C(6)-C(5)-H(5A)	119.3
N(5)-Yb(2)-C(45)	62.2(2)	C(4)-C(5)-H(5A)	119.3
N(7)-Yb(2)-C(45)	76.30(19)	C(51)-N(5)-C(52)	118.5(7)
N(6)-Yb(2)-C(45)	123.7(2)	C(51)-N(5)-Yb(2)	121.8(5)
O(7)-Yb(2)-C(64)	72.6(2)	C(52)-N(5)-Yb(2)	117.3(5)
O(8)-Yb(2)-C(64)	109.0(2)	C(45)-O(5)-Yb(2)	123.3(4)
O(6)-Yb(2)-C(64)	18.4(2)	C(5)-C(6)-C(1)	121.4(8)
O(5)-Yb(2)-C(64)	158.6(2)	C(5)-C(6)-C(7)	117.1(8)
N(8)-Yb(2)-C(64)	93.1(2)	C(1)-C(6)-C(7)	121.5(7)
N(5)-Yb(2)-C(64)	121.8(2)	C(64)-O(6)-Yb(2)	129.4(5)
N(7)-Yb(2)-C(64)	80.5(2)	C(58)-N(6)-C(57)	117.3(7)
N(6)-Yb(2)-C(64)	61.6(2)	C(58)-N(6)-Yb(2)	123.6(5)
C(45)-Yb(2)-C(64)	146.6(2)	C(57)-N(6)-Yb(2)	116.7(5)
C(23)-O(3)-Yb(1)	134.0(5)	N(1)-C(7)-C(6)	128.2(7)
C(29)-N(3)-C(30)	117.5(7)	N(1)-C(7)-H(7A)	115.9
C(29)-N(3)-Yb(1)	125.7(5)	C(6)-C(7)-H(7A)	115.9
C(30)-N(3)-Yb(1)	115.6(5)	C(72)-N(7)-C(74)	116.8(7)
C(4)-C(3)-C(2)	119.4(9)	C(72)-N(7)-Yb(2)	127.1(5)
C(4)-C(3)-H(3A)	120.3	C(74)-N(7)-Yb(2)	115.9(5)
C(2)-C(3)-H(3A)	120.3	C(67)-O(7)-Yb(2)	145.2(5)
C(42)-O(4)-Yb(1)	125.8(5)	C(13)-C(8)-C(9)	119.9(8)
C(36)-N(4)-C(35)	117.5(6)	C(13)-C(8)-N(1)	117.3(7)
C(36)-N(4)-Yb(1)	125.8(5)	C(9)-C(8)-N(1)	122.6(7)
C(35)-N(4)-Yb(1)	115.6(5)	C(86)-O(8)-Yb(2)	136.1(6)
C(3)-C(4)-C(5)	119.3(9)	C(80)-N(8)-C(79)	118.6(7)
C(3)-C(4)-H(4A)	120.4	C(80)-N(8)-Yb(2)	124.5(6)
C(5)-C(4)-H(4A)	120.4	C(79)-N(8)-Yb(2)	116.1(5)

C(10)-C(9)-C(8)	120.6(8)	C(17)-C(16)-H(16A)	119.1
C(10)-C(9)-H(9A)	119.7	C(15)-C(16)-H(16A)	119.1
C(8)-C(9)-H(9A)	119.7	C(16)-C(17)-C(18)	118.4(9)
C(93)-N(9)-C(89)	110.4(10)	C(16)-C(17)-H(17A)	120.8
C(93)-N(9)-C(91)	109.3(11)	C(18)-C(17)-H(17A)	120.8
C(89)-N(9)-C(91)	116.8(11)	C(19)-C(18)-C(17)	121.3(9)
C(9)-C(10)-C(11)	120.6(8)	C(19)-C(18)-H(18A)	119.4
C(9)-C(10)-C(21)	118.3(9)	C(17)-C(18)-H(18A)	119.4
C(11)-C(10)-C(21)	121.1(9)	C(18)-C(19)-C(20)	122.1(9)
C(95)-N(10)-C(99)	113.1(7)	C(18)-C(19)-Br(2)	119.8(7)
C(95)-N(10)-C(97)	107.2(7)	C(20)-C(19)-Br(2)	118.1(7)
C(99)-N(10)-C(97)	114.0(7)	O(2)-C(20)-C(19)	121.4(8)
C(12)-C(11)-C(10)	117.6(8)	O(2)-C(20)-C(15)	122.7(8)
C(12)-C(11)-C(22)	120.5(9)	C(19)-C(20)-C(15)	115.9(8)
C(10)-C(11)-C(22)	121.9(8)	C(10)-C(21)-H(21A)	109.5
C(11)-C(12)-C(13)	122.5(8)	C(10)-C(21)-H(21B)	109.5
C(11)-C(12)-H(12A)	118.8	H(21A)-C(21)-H(21B)	109.5
C(13)-C(12)-H(12A)	118.8	C(10)-C(21)-H(21C)	109.5
C(8)-C(13)-C(12)	118.7(8)	H(21A)-C(21)-H(21C)	109.5
C(8)-C(13)-N(2)	118.7(7)	H(21B)-C(21)-H(21C)	109.5
C(12)-C(13)-N(2)	122.7(7)	C(11)-C(22)-H(22A)	109.5
N(2)-C(14)-C(15)	126.9(7)	C(11)-C(22)-H(22B)	109.5
N(2)-C(14)-H(14A)	116.5	H(22A)-C(22)-H(22B)	109.5
C(15)-C(14)-H(14A)	116.5	C(11)-C(22)-H(22C)	109.5
C(16)-C(15)-C(20)	120.5(8)	H(22A)-C(22)-H(22C)	109.5
C(16)-C(15)-C(14)	116.7(8)	H(22B)-C(22)-H(22C)	109.5
C(20)-C(15)-C(14)	122.6(8)	O(3)-C(23)-C(24)	119.5(8)
C(17)-C(16)-C(15)	121.7(9)	O(3)-C(23)-C(28)	122.5(7)

C(24)-C(23)-C(28)	118.0(9)	C(34)-C(33)-C(32)	119.1(8)
C(25)-C(24)-C(23)	121.9(10)	C(34)-C(33)-C(44)	119.0(10)
C(25)-C(24)-Br(3)	117.3(8)	C(32)-C(33)-C(44)	121.9(9)
C(23)-C(24)-Br(3)	120.8(8)	C(33)-C(34)-C(35)	121.9(9)
C(24)-C(25)-C(26)	120.9(10)	C(33)-C(34)-H(34A)	119.1
C(24)-C(25)-H(25A)	119.6	C(35)-C(34)-H(34A)	119.1
C(26)-C(25)-H(25A)	119.6	C(30)-C(35)-C(34)	119.6(8)
C(25)-C(26)-C(27)	117.4(11)	C(30)-C(35)-N(4)	117.3(7)
C(25)-C(26)-H(26A)	121.3	C(34)-C(35)-N(4)	123.1(8)
C(27)-C(26)-H(26A)	121.3	N(4)-C(36)-C(37)	124.1(7)
C(28)-C(27)-C(26)	121.9(11)	N(4)-C(36)-H(36A)	118.0
C(28)-C(27)-H(27A)	119.0	C(37)-C(36)-H(36A)	118.0
C(26)-C(27)-H(27A)	119.0	C(38)-C(37)-C(42)	120.4(9)
C(27)-C(28)-C(23)	119.8(9)	C(38)-C(37)-C(36)	117.5(8)
C(27)-C(28)-C(29)	116.9(9)	C(42)-C(37)-C(36)	122.0(8)
C(23)-C(28)-C(29)	123.2(8)	C(37)-C(38)-C(39)	120.7(10)
N(3)-C(29)-C(28)	126.1(8)	C(37)-C(38)-H(38A)	119.6
N(3)-C(29)-H(29A)	116.9	C(39)-C(38)-H(38A)	119.6
C(28)-C(29)-H(29A)	116.9	C(40)-C(39)-C(38)	121.1(10)
C(31)-C(30)-C(35)	118.1(7)	C(40)-C(39)-H(39A)	119.4
C(31)-C(30)-N(3)	124.6(8)	C(38)-C(39)-H(39A)	119.4
C(35)-C(30)-N(3)	117.1(7)	C(39)-C(40)-C(41)	119.4(10)
C(30)-C(31)-C(32)	122.2(9)	C(39)-C(40)-H(40A)	120.3
C(30)-C(31)-H(31A)	118.9	C(41)-C(40)-H(40A)	120.3
C(32)-C(31)-H(31A)	118.9	C(40)-C(41)-C(42)	123.6(9)
C(31)-C(32)-C(33)	119.0(8)	C(40)-C(41)-Br(4)	120.8(7)
C(31)-C(32)-C(43)	119.1(9)	C(42)-C(41)-Br(4)	115.6(7)
C(33)-C(32)-C(43)	121.8(9)	O(4)-C(42)-C(41)	122.6(7)

O(4)-C(42)-C(37)	122.6(8)	C(49)-C(48)-H(48A)	120.7
C(41)-C(42)-C(37)	114.7(8)	C(50)-C(49)-C(48)	121.5(8)
C(32)-C(43)-H(43A)	109.5	C(50)-C(49)-H(49A)	119.3
C(32)-C(43)-H(43B)	109.5	C(48)-C(49)-H(49A)	119.3
H(43A)-C(43)-H(43B)	109.5	C(49)-C(50)-C(51)	117.5(7)
C(32)-C(43)-H(43C)	109.5	C(49)-C(50)-C(45)	120.2(7)
H(43A)-C(43)-H(43C)	109.5	C(51)-C(50)-C(45)	122.2(7)
H(43B)-C(43)-H(43C)	109.5	N(5)-C(51)-C(50)	125.8(7)
C(33)-C(44)-H(44A)	109.5	N(5)-C(51)-H(51A)	117.1
C(33)-C(44)-H(44B)	109.5	C(50)-C(51)-H(51A)	117.1
H(44A)-C(44)-H(44B)	109.5	C(53)-C(52)-C(57)	119.0(8)
C(33)-C(44)-H(44C)	109.5	C(53)-C(52)-N(5)	123.5(8)
H(44A)-C(44)-H(44C)	109.5	C(57)-C(52)-N(5)	117.4(7)
H(44B)-C(44)-H(44C)	109.5	C(52)-C(53)-C(54)	121.3(8)
O(5)-C(45)-C(46)	122.9(7)	C(52)-C(53)-H(53A)	119.3
O(5)-C(45)-C(50)	122.0(7)	C(54)-C(53)-H(53A)	119.3
C(46)-C(45)-C(50)	115.1(7)	C(55)-C(54)-C(53)	119.1(8)
O(5)-C(45)-Yb(2)	36.7(3)	C(55)-C(54)-C(65)	121.2(9)
C(46)-C(45)-Yb(2)	139.3(5)	C(53)-C(54)-C(65)	119.6(9)
C(50)-C(45)-Yb(2)	96.1(4)	C(56)-C(55)-C(54)	119.2(8)
C(47)-C(46)-C(45)	123.8(8)	C(56)-C(55)-C(66)	118.9(9)
C(47)-C(46)-Br(5)	119.8(6)	C(54)-C(55)-C(66)	121.8(9)
C(45)-C(46)-Br(5)	116.4(6)	C(55)-C(56)-C(57)	121.9(9)
C(46)-C(47)-C(48)	120.8(8)	C(55)-C(56)-H(56A)	119.1
C(46)-C(47)-H(47A)	119.6	C(57)-C(56)-H(56A)	119.1
C(48)-C(47)-H(47A)	119.6	C(52)-C(57)-C(56)	119.3(8)
C(47)-C(48)-C(49)	118.6(9)	C(52)-C(57)-N(6)	116.1(7)
C(47)-C(48)-H(48A)	120.7	C(56)-C(57)-N(6)	124.6(8)

N(6)-C(58)-C(59)	126.6(8)	H(65A)-C(65)-H(65C)	109.5
N(6)-C(58)-H(58A)	116.7	H(65B)-C(65)-H(65C)	109.5
C(59)-C(58)-H(58A)	116.7	C(55)-C(66)-H(66A)	109.5
C(60)-C(59)-C(58)	119.2(9)	C(55)-C(66)-H(66B)	109.5
C(60)-C(59)-C(64)	118.8(9)	H(66A)-C(66)-H(66B)	109.5
C(58)-C(59)-C(64)	122.0(8)	C(55)-C(66)-H(66C)	109.5
C(61)-C(60)-C(59)	123.4(10)	H(66A)-C(66)-H(66C)	109.5
C(61)-C(60)-H(60A)	118.3	H(66B)-C(66)-H(66C)	109.5
C(59)-C(60)-H(60A)	118.3	O(7)-C(67)-C(68)	121.8(8)
C(60)-C(61)-C(62)	118.3(9)	O(7)-C(67)-C(71)	122.8(7)
C(60)-C(61)-H(61A)	120.8	C(68)-C(67)-C(71)	115.4(8)
C(62)-C(61)-H(61A)	120.8	C(69)-C(68)-C(67)	122.0(8)
C(63)-C(62)-C(61)	121.3(9)	C(69)-C(68)-Br(7)	121.3(7)
C(63)-C(62)-H(62A)	119.4	C(67)-C(68)-Br(7)	116.7(6)
C(61)-C(62)-H(62A)	119.4	C(68)-C(69)-C(70')	122.5(9)
C(62)-C(63)-C(64)	122.0(10)	C(68)-C(69)-H(69A)	118.7
C(62)-C(63)-Br(6)	121.3(8)	C(70')-C(69)-H(69A)	118.7
C(64)-C(63)-Br(6)	116.7(7)	C(70')-C(70)-C(71)	121.8(9)
O(6)-C(64)-C(63)	121.3(9)	C(70')-C(70)-H(70A)	119.1
O(6)-C(64)-C(59)	122.5(8)	C(71)-C(70)-H(70A)	119.1
C(63)-C(64)-C(59)	116.1(8)	C(70)-C(70')-C(69)	117.2(9)
O(6)-C(64)-Yb(2)	32.2(4)	C(70)-C(70')-H(70B)	121.4
C(63)-C(64)-Yb(2)	138.9(6)	C(69)-C(70')-H(70B)	121.4
C(59)-C(64)-Yb(2)	98.5(5)	C(70)-C(71)-C(67)	120.8(8)
C(54)-C(65)-H(65A)	109.5	C(70)-C(71)-C(72)	117.6(8)
C(54)-C(65)-H(65B)	109.5	C(67)-C(71)-C(72)	121.4(8)
H(65A)-C(65)-H(65B)	109.5	N(7)-C(72)-C(71)	128.5(7)
C(54)-C(65)-H(65C)	109.5	N(7)-C(72)-H(72A)	115.8

C(71)-C(72)-H(72A)	115.8	C(84)-C(83)-C(82)	120.0(11)
C(79)-C(74)-C(75)	119.5(7)	C(84)-C(83)-H(83A)	120.0
C(79)-C(74)-N(7)	117.6(7)	C(82)-C(83)-H(83A)	120.0
C(75)-C(74)-N(7)	122.5(8)	C(85)-C(84)-C(83)	120.8(11)
C(76)-C(75)-C(74)	121.1(9)	C(85)-C(84)-H(84A)	119.6
C(76)-C(75)-H(75A)	119.5	C(83)-C(84)-H(84A)	119.6
C(74)-C(75)-H(75A)	119.5	C(84)-C(85)-C(86)	121.3(10)
C(75)-C(76)-C(77)	120.4(8)	C(84)-C(85)-Br(8)	120.5(8)
C(75)-C(76)-C(87)	118.1(9)	C(86)-C(85)-Br(8)	118.1(7)
C(77)-C(76)-C(87)	121.4(8)	O(8)-C(86)-C(85)	120.6(8)
C(78)-C(77)-C(76)	116.6(8)	O(8)-C(86)-C(81)	123.4(8)
C(78)-C(77)-C(88)	121.7(10)	C(85)-C(86)-C(81)	115.9(8)
C(76)-C(77)-C(88)	121.5(9)	C(76)-C(87)-H(87A)	109.5
C(77)-C(78)-C(79)	124.7(9)	C(76)-C(87)-H(87B)	109.5
C(77)-C(78)-H(78A)	117.6	H(87A)-C(87)-H(87B)	109.5
C(79)-C(78)-H(78A)	117.6	C(76)-C(87)-H(87C)	109.5
C(74)-C(79)-C(78)	117.6(8)	H(87A)-C(87)-H(87C)	109.5
C(74)-C(79)-N(8)	120.1(7)	H(87B)-C(87)-H(87C)	109.5
C(78)-C(79)-N(8)	122.0(8)	C(77)-C(88)-H(88A)	109.5
N(8)-C(80)-C(81)	127.8(8)	C(77)-C(88)-H(88B)	109.5
N(8)-C(80)-H(80A)	116.1	H(88A)-C(88)-H(88B)	109.5
C(81)-C(80)-H(80A)	116.1	C(77)-C(88)-H(88C)	109.5
C(82)-C(81)-C(86)	121.6(10)	H(88A)-C(88)-H(88C)	109.5
C(82)-C(81)-C(80)	116.7(9)	H(88B)-C(88)-H(88C)	109.5
C(86)-C(81)-C(80)	121.4(9)	C(90)-C(89)-N(9)	121.1(17)
C(81)-C(82)-C(83)	120.1(11)	C(90)-C(89)-H(89A)	119.4
C(81)-C(82)-H(82A)	120.0	N(9)-C(89)-H(89A)	119.4
C(83)-C(82)-H(82A)	120.0	C(89)-C(90)-H(90A)	109.5

211

C(89)-C(90)-H(90B)	109.5	C(96)-C(95)-H(95A)	109.0
H(90A)-C(90)-H(90B)	109.5	N(10)-C(95)-H(95B)	109.0
C(89)-C(90)-H(90C)	109.5	C(96)-C(95)-H(95B)	109.0
H(90A)-C(90)-H(90C)	109.5	H(95A)-C(95)-H(95B)	107.8
H(90B)-C(90)-H(90C)	109.5	C(95)-C(96)-H(96A)	109.5
C(92)-C(91)-N(9)	121.1(14)	C(95)-C(96)-H(96B)	109.5
C(92)-C(91)-H(91A)	119.5	H(96A)-C(96)-H(96B)	109.5
N(9)-C(91)-H(91A)	119.5	C(95)-C(96)-H(96C)	109.5
C(91)-C(92)-H(92A)	109.5	H(96A)-C(96)-H(96C)	109.5
C(91)-C(92)-H(92B)	109.5	H(96B)-C(96)-H(96C)	109.5
H(92A)-C(92)-H(92B)	109.5	C(98)-C(97)-N(10)	112.5(8)
C(91)-C(92)-H(92C)	109.5	C(98)-C(97)-H(97A)	109.1
H(92A)-C(92)-H(92C)	109.5	N(10)-C(97)-H(97A)	109.1
H(92B)-C(92)-H(92C)	109.5	C(98)-C(97)-H(97B)	109.1
N(9)-C(93)-C(94)	113.6(11)	N(10)-C(97)-H(97B)	109.1
N(9)-C(93)-H(93A)	108.8	H(97A)-C(97)-H(97B)	107.8
C(94)-C(93)-H(93A)	108.8	C(97)-C(98)-H(98A)	109.5
N(9)-C(93)-H(93B)	108.8	C(97)-C(98)-H(98B)	109.5
C(94)-C(93)-H(93B)	108.8	H(98A)-C(98)-H(98B)	109.5
H(93A)-C(93)-H(93B)	107.7	C(97)-C(98)-H(98C)	109.5
C(93)-C(94)-H(94A)	109.5	H(98A)-C(98)-H(98C)	109.5
C(93)-C(94)-H(94B)	109.5	H(98B)-C(98)-H(98C)	109.5
H(94A)-C(94)-H(94B)	109.5	N(10)-C(99)-C(100)	113.3(7)
C(93)-C(94)-H(94C)	109.5	N(10)-C(99)-H(99A)	108.9
H(94A)-C(94)-H(94C)	109.5	C(100)-C(99)-H(99A)	108.9
H(94B)-C(94)-H(94C)	109.5	N(10)-C(99)-H(99B)	108.9
N(10)-C(95)-C(96)	112.9(8)	C(100)-C(99)-H(99B)	108.9
N(10)-C(95)-H(95A)	109.0	H(99A)-C(99)-H(99B)	107.7

C(99)-C(100)-H(10A)	109.5	C(99)-C(100)-H(10C)	109.5
C(99)-C(100)-H(10B)	109.5	H(10A)-C(100)-H(10C)	109.5
H(10A)-C(100)-H(10B)	109.5	H(10B)-C(100)-H(10C)	109.5

Table AA.14. Anisotropic displacement parameters ($Å^2 \times 10^3$) for $Et_3NH[Yb(3BDMSal)_2]$. The anisotropic displacement factor exponent takes the form: $-2p^2[\ h^2\ a^{*2}U^{11} + ... + 2\ h\ k\ a^*\ b^*\ U^{12}\ ]$.

	U^{11}	U^{22}	U^{33}	U^{23}	U^{13}	U^{12}
Yb(1)	28(1)	46(1)	34(1)	-7(1)	-7(1)	-16(1)
Br(1)	53(1)	74(1)	48(1)	-19(1)	7(1)	-28(1)
O(1)	38(3)	54(4)	34(3)	-12(3)	-6(2)	-19(3)
N(1)	32(4)	47(4)	41(4)	-3(3)	-14(3)	-18(3)
C(1)	43(5)	43(5)	31(5)	-3(4)	-13(4)	-13(4)
N(2)	29(3)	56(4)	27(4)	-5(3)	-4(3)	-18(3)
C(2)	52(5)	52(6)	43(5)	-6(4)	-5(4)	-24(4)
Br(2)	48(1)	149(1)	70(1)	-16(1)	-26(1)	-39(1)
O(2)	39(3)	81(5)	43(4)	2(3)	-22(3)	-27(3)
Yb(2)	28(1)	37(1)	44(1)	-9(1)	-10(1)	-10(1)
Br(3)	54(1)	87(1)	112(1)	10(1)	-36(1)	-43(1)
O(3)	40(3)	49(4)	51(4)	-1(3)	-8(3)	-27(3)
N(3)	32(4)	42(4)	37(4)	-4(3)	-7(3)	-15(3)
C(3)	75(7)	90(8)	40(6)	-25(5)	-2(5)	-42(6)
Br(4)	43(1)	67(1)	65(1)	-27(1)	-7(1)	-9(1)
O(4)	39(3)	55(4)	34(3)	-12(3)	1(2)	-20(3)
N(4)	30(4)	46(4)	44(4)	-13(4)	-5(3)	-15(3)
C(4)	67(7)	125(10)	48(6)	-20(6)	-19(5)	-47(7)
C(5)	52(6)	99(8)	48(6)	-7(6)	-21(5)	-38(6)
N(5)	26(3)	39(4)	45(4)	-3(3)	-9(3)	-11(3)

O(5)	30(3)	35(3)	37(3)	-6(3)	-8(2)	-11(2)
Br(5)	35(1)	53(1)	69(1)	-22(1)	-20(1)	-8(1)
C(6)	42(5)	52(5)	27(4)	-4(4)	-11(4)	-14(4)
Br(6)	70(1)	53(1)	85(1)	-20(1)	-28(1)	5(1)
O(6)	39(3)	40(3)	67(4)	-15(3)	-18(3)	-10(3)
N(6)	37(4)	40(4)	56(5)	-8(4)	-17(3)	-12(3)
C(7)	30(4)	57(6)	42(5)	-9(4)	-9(4)	-19(4)
N(7)	32(4)	36(4)	47(4)	-10(3)	-11(3)	-14(3)
O(7)	30(3)	43(3)	42(3)	-3(3)	-9(2)	-7(2)
Br(7)	35(1)	65(1)	80(1)	-14(1)	3(1)	-10(1)
C(8)	31(4)	49(5)	41(5)	-8(4)	-5(4)	-23(4)
Br(8)	68(1)	84(1)	63(1)	-9(1)	-32(1)	-14(1)
O(8)	40(3)	50(4)	46(4)	-5(3)	-10(3)	-14(3)
N(8)	43(4)	36(4)	50(5)	-10(4)	-7(3)	-14(3)
C(9)	24(4)	53(5)	62(6)	-19(5)	-9(4)	-8(4)
N(9)	80(6)	97(7)	53(6)	-24(5)	-9(5)	-46(6)
C(10)	33(5)	53(6)	81(7)	-16(5)	-14(5)	-19(4)
N(10)	46(4)	52(5)	43(4)	-14(4)	-4(3)	-15(4)
C(11)	37(5)	56(6)	61(6)	-24(5)	4(4)	-21(4)
C(12)	49(5)	53(6)	46(5)	-10(5)	-6(4)	-23(4)
C(13)	35(4)	48(5)	44(5)	-10(4)	-6(4)	-23(4)
C(14)	42(5)	58(6)	37(5)	-12(4)	-3(4)	-24(4)
C(15)	51(5)	58(6)	32(5)	-2(4)	-12(4)	-21(5)
C(16)	69(7)	82(8)	39(6)	5(5)	-22(5)	-33(6)
C(17)	92(9)	80(8)	43(6)	18(6)	-30(6)	-21(7)
C(18)	51(6)	83(8)	63(7)	-18(6)	-25(5)	-4(5)
C(19)	43(5)	81(7)	41(5)	-17(5)	-22(4)	-6(5)
C(20)	44(5)	62(6)	31(5)	-10(4)	-6(4)	-22(4)

C(21)	35(5)	102(9)	86(8)	-39(7)	2(5)	1(5)
C(22)	56(6)	86(8)	70(7)	-32(6)	7(5)	-26(6)
C(23)	43(5)	43(5)	39(5)	4(4)	-20(4)	-21(4)
C(24)	69(7)	61(6)	71(7)	3(6)	-41(6)	-33(5)
C(25)	81(9)	84(9)	105(10)	-13(8)	-34(8)	-44(7)
C(26)	130(12)	78(9)	107(11)	-37(8)	-48(9)	-42(8)
C(27)	76(8)	64(7)	80(8)	-18(6)	-17(6)	-27(6)
C(28)	57(6)	38(5)	45(5)	-7(4)	-19(4)	-16(4)
C(29)	38(5)	49(6)	47(5)	-2(5)	-10(4)	-13(4)
C(30)	22(4)	53(5)	41(5)	1(4)	-4(3)	-12(4)
C(31)	35(5)	46(5)	50(6)	0(4)	-7(4)	-11(4)
C(32)	27(4)	82(7)	53(6)	1(5)	-5(4)	-21(5)
C(33)	45(6)	75(7)	65(7)	-5(6)	-11(5)	-35(5)
C(34)	33(5)	58(6)	67(6)	-15(5)	-5(4)	-21(4)
C(35)	34(4)	51(5)	37(5)	-1(4)	-5(4)	-22(4)
C(36)	36(5)	54(6)	45(5)	-16(5)	6(4)	-22(4)
C(37)	52(5)	44(5)	38(5)	-4(4)	-7(4)	-17(4)
C(38)	86(8)	53(7)	55(7)	5(5)	9(6)	-21(6)
C(39)	95(9)	55(7)	69(8)	5(6)	3(7)	-17(6)
C(40)	78(8)	70(8)	54(7)	-7(6)	-10(6)	-7(6)
C(41)	60(6)	51(6)	29(5)	-11(4)	-11(4)	-7(5)
C(42)	42(5)	58(6)	37(5)	-26(5)	-2(4)	-18(4)
C(43)	35(5)	96(9)	101(9)	-5(7)	-19(6)	-17(5)
C(44)	54(7)	103(10)	146(12)	1(9)	-36(7)	-43(7)
C(45)	39(4)	32(4)	32(4)	-1(4)	-9(4)	-14(4)
C(46)	42(5)	34(5)	44(5)	-3(4)	-16(4)	-9(4)
C(47)	42(5)	68(6)	49(6)	-21(5)	-16(4)	-18(4)
C(48)	55(6)	83(8)	67(7)	-46(6)	-2(5)	-26(5)

215

C(49)	44(5)	63(6)	56(6)	-26(5)	-2(4)	-18(4)
C(50)	35(4)	35(4)	38(5)	-9(4)	-5(4)	-11(3)
C(51)	26(4)	40(5)	46(5)	-12(4)	-4(4)	-9(3)
C(52)	27(4)	49(5)	42(5)	-5(4)	-12(4)	-10(4)
C(53)	35(5)	48(5)	50(6)	-2(4)	-12(4)	-8(4)
C(54)	31(5)	48(6)	78(7)	-6(5)	-16(5)	-2(4)
C(55)	33(5)	74(7)	56(6)	5(5)	-23(4)	-15(5)
C(56)	39(5)	56(6)	65(6)	-8(5)	-17(5)	-17(4)
C(57)	31(4)	54(6)	46(5)	-10(4)	-9(4)	-15(4)
C(58)	43(5)	54(6)	64(6)	-11(5)	-23(4)	-19(4)
C(59)	50(5)	45(5)	67(6)	-5(5)	-23(5)	-20(4)
C(60)	71(7)	62(7)	83(8)	8(6)	-36(6)	-33(6)
C(61)	90(9)	64(7)	73(8)	18(6)	-31(6)	-47(7)
C(62)	94(9)	40(6)	71(7)	-4(5)	-30(6)	-20(6)
C(63)	73(7)	41(6)	59(6)	-14(5)	-28(5)	-12(5)
C(64)	69(6)	50(6)	60(6)	-19(5)	-27(5)	-26(5)
C(65)	64(7)	75(8)	97(9)	-5(7)	-46(6)	-15(6)
C(66)	54(6)	94(8)	79(8)	-12(7)	-43(6)	-9(6)
C(67)	41(5)	38(5)	40(5)	-10(4)	-4(4)	-20(4)
C(68)	36(5)	45(5)	44(5)	-13(4)	0(4)	-20(4)
C(69)	53(6)	74(7)	59(7)	-26(6)	13(5)	-33(5)
C(70)	49(6)	51(6)	59(6)	-6(5)	-16(5)	-17(4)
C(70')	76(7)	69(7)	43(6)	-10(5)	-9(5)	-37(6)
C(71)	39(5)	44(5)	46(5)	-5(4)	-13(4)	-18(4)
C(72)	27(4)	45(5)	58(6)	-15(5)	-17(4)	-2(4)
C(74)	19(4)	36(5)	54(6)	-12(4)	-6(4)	-2(3)
C(75)	37(5)	42(5)	62(6)	-14(5)	-14(4)	-8(4)
C(76)	24(4)	43(5)	93(8)	-23(5)	-17(5)	-3(4)

216

C(77)	26(5)	58(6)	72(7)	-18(5)	3(4)	-10(4)
C(78)	39(5)	57(6)	64(6)	-29(5)	-1(5)	-10(4)
C(79)	29(4)	38(5)	60(6)	-14(4)	-13(4)	-9(4)
C(80)	44(5)	45(6)	69(7)	-24(5)	1(5)	-12(4)
C(81)	67(7)	60(6)	49(6)	-21(5)	-16(5)	-12(5)
C(82)	79(8)	123(11)	62(8)	-63(8)	-7(6)	-1(7)
C(83)	127(12)	140(13)	73(9)	-69(9)	-37(9)	10(10)
C(84)	124(12)	131(12)	51(8)	-31(8)	-37(7)	-13(10)
C(85)	60(6)	80(7)	46(6)	-19(5)	-20(5)	-13(5)
C(86)	49(5)	59(6)	47(6)	-23(5)	-2(4)	-21(5)
C(87)	39(5)	61(6)	109(9)	-22(6)	-26(5)	-13(5)
C(88)	31(5)	128(11)	118(10)	-56(9)	1(6)	-15(6)
C(89)	220(20)	83(11)	70(10)	3(9)	-26(11)	-45(12)
C(90)	270(30)	200(20)	270(30)	-100(20)	-170(20)	-60(20)
C(91)	120(13)	280(20)	101(12)	-77(13)	-9(10)	-118(15)
C(92)	165(18)	280(30)	190(20)	-59(18)	-67(15)	-118(18)
C(93)	137(13)	120(11)	72(9)	-38(9)	-39(8)	-52(10)
C(94)	119(12)	163(14)	111(11)	-79(11)	23(9)	-90(11)
C(95)	69(7)	60(7)	63(7)	-13(5)	-10(5)	-31(5)
C(96)	86(9)	89(9)	89(9)	-26(8)	7(7)	-25(7)
C(97)	52(6)	54(6)	71(7)	4(5)	-25(5)	-21(5)
C(98)	56(6)	53(6)	80(8)	-6(6)	-13(6)	-6(5)
C(99)	63(6)	54(6)	49(6)	-13(5)	-13(5)	-25(5)
C(100)	84(8)	63(7)	66(7)	-9(6)	-5(6)	-49(6)

Table AA.15. Hydrogen coordinates ($\times 10^4$) and isotropic displacement parameters ($Å^2 \times 10^3$) for

Et$_3$NH[Yb(3BDMSal)$_2$].
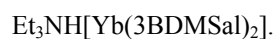
	x	y	z	U(eq)
H(3A)	7322	1669	5946	75
H(4A)	9088	1528	5695	88
H(5A)	10072	1093	4806	74
H(7A)	10276	686	3930	50
H(9A)	11295	-141	3478	55
H(12A)	10401	696	1511	58
H(14A)	9155	1769	1558	52
H(16A)	8198	2673	866	75
H(17A)	6692	3280	457	93
H(18A)	5194	2928	991	80
H(21A)	13028	-702	3104	119
H(21B)	13472	-307	2408	119
H(21C)	13195	-1096	2548	119
H(22A)	12086	102	1033	105
H(22B)	12723	-666	1465	105
H(22C)	12968	133	1333	105
H(25A)	8488	3717	3937	100
H(26A)	6790	4150	4479	111
H(27A)	5564	3565	4481	85
H(29A)	5013	2783	4163	56
H(31A)	3828	2875	3623	56
H(34A)	4208	272	3939	62
H(36A)	5478	-267	4498	54
H(38A)	6435	-1501	5008	88
H(39A)	7883	-2591	5048	100

H(40A)	9401	-2568	4357	89
H(43A)	1519	2503	3603	122
H(43B)	2150	3085	3162	122
H(43C)	1796	3055	3890	122
H(44A)	2537	493	3885	149
H(44B)	2075	1283	3403	149
H(44C)	1721	1222	4135	149
H(47A)	15694	-4735	-300	59
H(48A)	17436	-5321	-681	75
H(49A)	18730	-5311	-220	63
H(51A)	19286	-5065	543	45
H(53A)	20011	-5641	1415	56
H(56A)	20598	-3516	1658	63
H(58A)	19971	-2635	799	60
H(60A)	19883	-1392	155	83
H(61A)	19031	-109	-214	88
H(62A)	17204	336	37	81
H(65A)	22267	-6073	2050	116
H(65B)	21996	-6323	1527	116
H(65C)	21325	-6426	2215	116
H(66A)	22003	-4230	2092	112
H(66B)	22688	-4946	1787	112
H(66C)	22025	-5094	2475	112
H(69A)	19167	-2218	-1763	73
H(70A)	16089	-1279	-1248	63
H(70B)	17548	-1407	-2036	72
H(72A)	15253	-1565	-224	53
H(75A)	13970	-1893	70	56

H(78A)	13351	-2438	2211	64
H(80A)	14517	-2203	2463	64
H(82A)	14874	-2314	3392	105
H(83A)	15904	-2878	4171	136
H(84A)	17407	-3885	4042	123
H(87A)	12294	-1708	31	101
H(87B)	11450	-1318	557	101
H(87C)	11715	-2223	607	101
H(88A)	11604	-2232	2303	137
H(88B)	11399	-2527	1782	137
H(88C)	11088	-1618	1733	137
H(89A)	8219	-1502	1848	157
H(90A)	8383	-2515	2548	323
H(90B)	7355	-2058	2950	323
H(90C)	8469	-2042	2988	323
H(91A)	6156	-259	3068	175
H(92A)	4908	-304	2692	279
H(92B)	5741	-990	2394	279
H(92C)	5582	-108	2013	279
H(93A)	7291	466	1895	118
H(93B)	7302	-97	1502	118
H(94A)	8834	279	1143	173
H(94B)	9135	-637	1428	173
H(94C)	9126	-76	1823	173
H(95A)	15726	-4425	2738	74
H(95B)	15319	-5165	3054	74
H(96A)	13892	-4035	2865	138
H(96B)	13970	-4601	2454	138

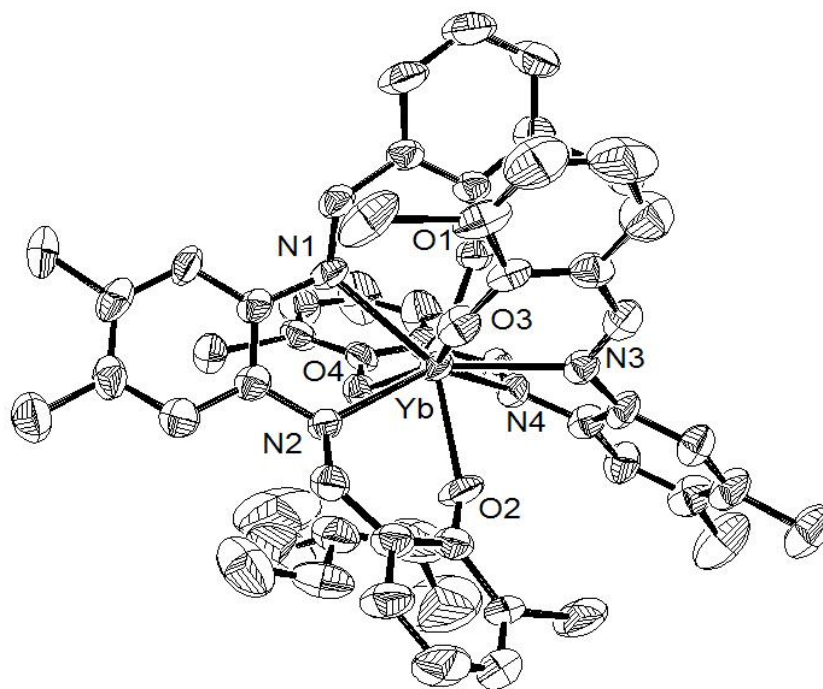|				
H(96C)	14377	-3861	2139	138
H(97A)	17485	-5230	2371	71
H(97B)	17026	-5920	2793	71
H(98A)	18513	-6389	2089	103
H(98B)	17976	-5802	1519	103
H(98C)	17527	-6495	1946	103
H(99A)	16088	-5844	1631	63
H(99B)	14954	-5282	1825	63
H(10A)	15060	-6574	2365	100
H(10B)	14863	-6068	2851	100
H(10C)	16001	-6628	2660	100

Figure AA.5. Molecular structure of Et$_3$NH[Yb(3BDMSal)$_2$]. All atoms represented by thermal ellipsoids drawn at

the 30% probability level. All hydrogen atoms were omitted for clarity.

221
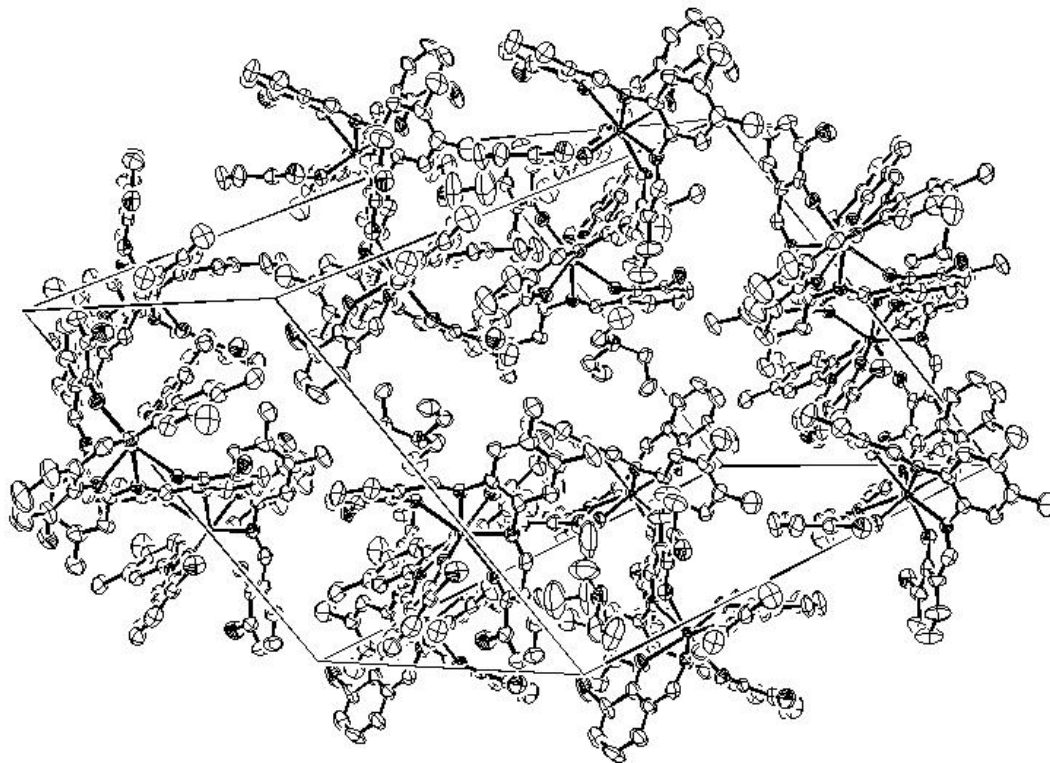
Figure AA.6. Unit cell structure of Et$_3$NH[Yb(3BDMSal)$_2$]

BIBLIOGRAPHY

1.   Derfus, A. M.; Chan, W. C. W.; Bhatia, S. N., Probing the Cytotoxicity of Semiconductor Quantum Dots. *Nano Lett.* 2003, 4, 11-18.

2.   Bünzli, J.-C. G.; Piguet, C., Taking advantage of luminescent lanthanide ions. *Chem. Soc. Rev.* 2005, 34, 1048-1077.

3.   Eliseeva, S. V.; Bünzli, J.-C. G., Lanthanide luminescence for functional materials and bio-sciences. *Chem. Soc. Rev.* 2010, 39, 189-227.

4.   Petoud, S.; Cohen, S. M.; Bünzli, J.-C. G.; Raymond, K. N., Stable Lanthanide Luminescence Agents Highly Emissive in Aqueous Solution: Multidentate 2-Hydroxyisophthalamide Complexes of Sm^{3+}, Eu^{3+}, Tb^{3+}, Dy^{3+}. *J. Am. Chem. Soc.* 2003, 125, 13324-13325.

5.   Zhang, J.; Badger, P. D.; Geib, S. J.; Petoud, S., Sensitization of Near-Infrared-Emitting Lanthanide Cations in Solution by Tropolonate Ligands. *Angew. Chem. Int. Ed.* 2005, 44, 2508-2512.

6.   Weiss, S., Fluorescence Spectroscopy of Single Biomolecules. *Science* 1999, 283, 1676-1683.

7.   Alivisatos, A. P.; Gu, W.; Larabell, C., Quantum Dots as Cellular Probes. *Annu. Rev. Biomed. Eng.* 2005, 7, 55-76.

8.   Bruchez, M.; Moronne, M.; Gin, P.; Weiss, S.; Alivisatos, A. P., Semiconductor Nanocrystals as Fluorescent Biological Labels. *Science* 1998, 281, 2013-2016.

9.   Medintz, I. L.; Uyeda, H. T.; Goldman, E. R.; Mattoussi, H., Quantum dot bioconjugates for imaging, labelling and sensing. *Nat Mater* 2005, 4, 435-446.

10.   Michalet, X.; Pinaud, F. F.; Bentolila, L. A.; Tsay, J. M.; Doose, S.; Li, J. J.; Sundaresan, G.; Wu, A. M.; Gambhir, S. S.; Weiss, S., Quantum Dots for Live Cells, in Vivo Imaging, and Diagnostics. *Science* 2005, 307, 538-544.

11.   O'Connell, M. J.; Bachilo, S. M.; Huffman, C. B.; Moore, V. C.; Strano, M. S.; Haroz, E. H.; Rialon, K. L.; Boul, P. J.; Noon, W. H.; Kittrell, C.; Ma, J.; Hauge, R. H.; Weisman,

R. B.; Smalley, R. E., Band Gap Fluorescence from Individual Single-Walled Carbon Nanotubes. *Science* 2002, 297, 593-596.

12. Liu, Z.; Li, X.; Tabakman, S. M.; Jiang, K.; Fan, S.; Dai, H., Multiplexed Multicolor Raman Imaging of Live Cells with Isotopically Modified Single Walled Carbon Nanotubes. *J. Am. Chem. Soc.* 2008, 130, 13540-13541.

13. Ye, Z.; Tan, M.; Wang, G.; Yuan, J., Preparation, Characterization, and Time-Resolved Fluorometric Application of Silica-Coated Terbium(III) Fluorescent Nanoparticles. *Anal. Chem.* 2004, 76, 513-518.

14. Horrocks, W. D.; Sudnick, D. R., Lanthanide ion luminescence probes of the structure of biological macromolecules. *Acc. Chem. Res.* 1981, 14, 384-392.

15. Beeby, A.; M. Clarkson, I.; S. Dickins, R.; Faulkner, S.; Parker, D.; Royle, L.; S. de Sousa, A.; A. Gareth Williams, J.; Woods, M., Non-radiative deactivation of the excited states of europium, terbium and ytterbium complexes by proximate energy-matched OH, NH and CH oscillators: an improved luminescence method for establishing solution hydration states. *J. Chem. Soc., Perkin Trans. 2* 1999, 493-504.

16. Mathis, G., HTRF® Technology. *J. Biomol. Screen.* 1999, 4, 309-313.

17. Moore, E. G.; Samuel, A. P. S.; Raymond, K. N., From Antenna to Assay: Lessons Learned in Lanthanide Luminescence. *Acc. Chem. Res.* 2009, 42, 542-552.

18. Hemmilá, I.; Mukkala, V.-M., Time-Resolution in Fluorometry Technologies, Labels, and Applications in Bioanalytical Assays. *Crit. Rev. Clin. Lab. Sci.* 2001, 38, 441-519.

19. Cotton, S., *Lanthanide and Actinide Chemistry*. John Wiley & Sons: West Sussex, England, 2007.

20. Weissman, S. I., Intramolecular Energy Transfer The Fluorescence of Complexes of Europium. *J. Chem. Phys.* 1942, 10, 214-217.

21. Petoud, S.; Bünzli, J.-C. G.; Glanzman, T.; Piguet, C.; Xiang, Q.; Thummel, R. P., Influence of charge-transfer states on the Eu(III) luminescence in mononuclear triple helical complexes with tridentate aromatic ligands. *J. Lumin.* 1999, 82, 69-79.

22. Förster, T., Zwischenmolekulare Energiewanderung und Fluoreszenz. *Ann. Phys. (Berlin)* 1948, 437, 55-75.

23. Dexter, D. L., A Theory of Sensitized Luminescence in Solids. *J. Chem. Phys.* 1953, 21, 836-850.

24. Horrocks, W. D.; Bolender, J. P.; Smith, W. D.; Supkowski, R. M., Photosensitized Near Infrared Luminescence of Ytterbium(III) in Proteins and Complexes Occurs via an Internal Redox Process. *J. Am. Chem. Soc.* 1997, 119, 5972-5973.

25. Faulkner, S.; Beeby, A.; Carrié, M.-C.; Dadabhoy, A.; Kenwright, A. M.; Sammes, P. G., Time-resolved near-IR luminescence from ytterbium and neodymium complexes of the Lehn cryptand. *Inorg. Chem. Commun.* 2001, 4, 187-190.

26. Beeby, A.; Burton-Pye, B. P.; Faulkner, S.; Motson, G. R.; Jeffery, J. C.; McCleverty, J. A.; Ward, M. D., Synthesis and near-IR luminescence properties of neodymium(III) and ytterbium(III) complexes with poly(pyrazolyl)borate ligands. *J. Chem. Soc., Dalton Trans.* 2002, 1923-1928.

27. Faulkner, S.; Burton-Pye, B. P.; Khan, T.; Martin, L. R.; Wray, S. D.; Skabara, P. J., Interaction between tetrathiafulvalene carboxylic acid and ytterbium DO3A: solution state self-assembly of a ternary complex which is luminescent in the near IR. *Chem. Commun.* 2002, 1668-1669.

28. Hebbink, G. A.; Grave, L.; Woldering, L. A.; Reinhoudt, D. N.; van Veggel, F. C. J. M., Unexpected Sensitization Efficiency of the Near-Infrared Nd^{3+}, Er^{3+}, and Yb^{3+} Emission by Fluorescein Compared to Eosin and Erythrosin. *J. Phys. Chem. A* 2003, 107, 2483-2491.

29. Lazarides, T.; Alamiry, M. A. H.; Adams, H.; Pope, S. J. A.; Faulkner, S.; Weinstein, J. A.; Ward, M. D., Anthracene as a sensitiser for near-infrared luminescence in complexes of Nd(iii), Er(iii) and Yb(iii): an unexpected sensitisation mechanism based on electron transfer. *Dalton Trans.* 2007, 1484-1491.

30. Weissleder, R.; Ntziachristos, V., Shedding light onto live molecular targets. *Nat. Med.* 2003, 9, 123-128.

31. Müller, M. G.; Georgakoudi, I.; Zhang, Q.; Wu, J.; Feld, M. S., Intrinsic fluorescence spectroscopy in turbid media: disentangling effects of scattering and absorption. *Appl. Opt.* 2001, 40, 4633-4646.

32. Kim, S.; Lim, Y. T.; Soltesz, E. G.; De Grand, A. M.; Lee, J.; Nakayama, A.; Parker, J. A.; Mihaljevic, T.; Laurence, R. G.; Dor, D. M.; Cohn, L. H.; Bawendi, M. G.; Frangioni, J. V., Near-infrared fluorescent type II quantum dots for sentinel lymph node mapping. *Nat Biotech* 2004, 22, 93-97.

33. Jüstel, T.; Wiechert, D. U.; Lau, C.; Sendor, D.; Kynast, U., Optically Functional Zeolites: Evaluation of UV and VUV Stimulated Photoluminescence Properties of Ce^{3+}- and Tb^{3+}-doped Zeolite X. *Adv. Funct. Mater.* 2001, 11, 105-110.

34. Kang, T. S.; Harrison, B. S.; Foley, T. J.; Knefely, A. S.; Boncella, J. M.; Reynolds, J. R.; Schanze, K. S., Near-Infrared Electroluminescence from Lanthanide Tetraphenylporphyrin:Polystyrene Blends. *Adv. Mater.* 2003, 15, 1093-1097.

35. Slooff, L. H.; Polman, A.; Wolbers, M. P. O.; van Veggel, F. C. J. M.; Reinhoudt, D. N.; Hofstraat, J. W., Optical properties of erbium-doped organic polydentate cage complexes. *J. Appl. Phys.* 1998, 83, 497-503.

36. Slooff, L. H.; van Blaaderen, A.; Polman, A.; Hebbink, G. A.; Klink, S. I.; Van Veggel, F. C. J. M.; Reinhoudt, D. N.; Hofstraat, J. W., Rare-earth doped polymers for planar optical amplifiers. *J. Appl. Phys.* 2002, 91, 3955-3980.

37. White, K. A.; Chengelis, D. A.; Gogick, K. A.; Stehman, J.; Rosi, N. L.; Petoud, S., Near-Infrared Luminescent Lanthanide MOF Barcodes. *J. Am. Chem. Soc.* 2009, 131, 18069-18071.

38. Imbert, D.; Cantuel, M.; Bünzli, J.-C. G.; Bernardinelli, G.; Piguet, C., Extending Lifetimes of Lanthanide-Based Near-Infrared Emitters (Nd, Yb) in the Millisecond Range through Cr(III) Sensitization in Discrete Bimetallic Edifices. *J. Am. Chem. Soc.* 2003, 125, 15698-15699.

39. Bünzli, J.-C. G., Benefiting from the Unique Properties of Lanthanide Ions. *Acc. Chem. Res.* 2006, 39, 53-61.

40. Comby, S.; Imbert, D.; Chauvin, A.-S.; Bünzli, J.-C. G., Stable 8-Hydroxyquinolinate-Based Podates as Efficient Sensitizers of Lanthanide Near-Infrared Luminescence. *Inorg. Chem.* 2006, 45, 732-743.

41. Ziessel, R. F.; Ulrich, G.; Charbonnière, L.; Imbert, D.; Scopelliti, R.; Bünzli, J.-C. G., NIR Lanthanide Luminescence by Energy Transfer from Appended Terpyridine–Boradiazaindacene Dyes. *Chem. Eur. J.* 2006, 12, 5060-5067.

42. Comby, S.; Imbert, D.; Vandevyver, C.; Bünzli, J.-C. G., A Novel Strategy for the Design of 8-Hydroxyquinolinate-Based Lanthanide Bioprobes That Emit in the Near Infrared Range. *Chem. Eur. J.* 2007, 13, 936-944.

43. Shavaleev, N. M.; Scopelliti, R.; Gumy, F. d. r.; Bünzli, J.-C. G., Near-Infrared Luminescence of Nine-Coordinate Neodymium Complexes with Benzimidazole-Substituted 8-Hydroxyquinolines. *Inorg. Chem.* 2008, 47, 9055-9068.

44. Shavaleev, N. M.; Scopelliti, R.; Gumy, F. d. r.; Bünzli, J.-C. G., Modulating the Near-Infrared Luminescence of Neodymium and Ytterbium Complexes with Tridentate Ligands Based on Benzoxazole-Substituted 8-Hydroxyquinolines. *Inorg. Chem.* 2009, 48, 2908-2918.

45. Beeby, A.; S. Dickins, R.; Faulkner, S.; Parker, D.; A. Gareth Williams, J., Luminescence from ytterbium(iii) and its complexes in solution. *Chem. Commun.* 1997, 1401-1402.

46. Maupin, C. L.; Parker, D.; Williams, J. A. G.; Riehl, J. P., Circularly Polarized Luminescence from Chiral Octadentate Complexes of Yb(III) in the Near-Infrared. *J. Am. Chem. Soc.* 1998, 120, 10563-10564.

47. Beeby, A.; Dickins, R. S.; FitzGerald, S.; Govenlock, L. J.; Maupin, C. L.; Parker, D.; Riehl, J. P.; Siligardi, G.; Williams, J. A. G., Porphyrin sensitization of circularly polarised near-IR lanthanide luminescence: enhanced emission with nucleic acid binding. *Chem. Commun.* 2000, 1183-1184.

48. Pope, S. J. A.; Coe, B. J.; Faulkner, S.; Bichenkova, E. V.; Yu, X.; Douglas, K. T., Self-Assembly of Heterobimetallic d−f Hybrid Complexes: Sensitization of Lanthanide Luminescence by d-Block Metal-to-Ligand Charge-Transfer Excited States. *J. Am. Chem. Soc.* 2004, 126, 9490-9491.

49. Pope, S. J. A.; Coe, B. J.; Faulkner, S.; Laye, R. H., Metal-to-ligand charge-transfer sensitisation of near-infrared emitting lanthanides in trimetallic arrays M_2Ln (M = Ru, Re or Os; Ln = Nd, Er or Yb). *Dalton Trans.* 2005, 1482-1490.

50. Ronson, T. K.; Lazarides, T.; Adams, H.; Pope, S. J. A.; Sykes, D.; Faulkner, S.; Coles, S. J.; Hursthouse, M. B.; Clegg, W.; Harrington, R. W.; Ward, M. D., Luminescent Pt^{II}(bipyridyl)(diacetylide) Chromophores with Pendant Binding Sites as Energy Donors for Sensitised Near-Infrared Emission from Lanthanides: Structures and Photophysics of Pt^{II}/Ln^{III} Assemblies. *Chem. Eur. J.* 2006, 12, 9299-9313.

51. Sénéchal-David, K.; Pope, S. J. A.; Quinn, S.; Faulkner, S.; Gunnlaugsson, T., Sensitized Near-Infrared Lanthanide Luminescence from Nd(III)- and Yb(III)-Based Cyclen−Ruthenium Coordination Conjugates. *Inorg. Chem.* 2006, 45, 10040-10042.

52. P. Oude Wolbers, M.; C. J. M. van Veggel, F.; H. M. Snellink-Ruel, B.; W. Hofstraat, J.; A. J. Geurts, F.; N. Reinhoudt, D., Photophysical studies of m-terphenyl-sensitized visible and near-infrared emission from organic 1: 1 lanthanide ion complexes in methanol solutions. *J. Chem. Soc., Perkin Trans. 2* 1998, 2141-2150.

53. Klink, Stephen I.; Hebbink, Gerald A.; Grave, L.; Peters, Frank G. A.; Van Veggel, Frank C. J. M.; Reinhoudt, David N.; Hofstraat, Johannes W., Near-Infrared and Visible Luminescence from Terphenyl-Based Lanthanide(III) Complexes Bearing Amido and Sulfonamido Pendant Arms. *Eur. J. Org. Chem.* 2000, 2000, 1923-1931.

54. Werts, M. H. V.; Woudenberg, R. H.; Emmerink, P. G.; van Gassel, R.; Hofstraat, J. W.; Verhoeven, J. W., A Near-Infrared Luminescent Label Based on YbIII Ions and Its Application in a Fluoroimmunoassay. *Angew. Chem. Int. Ed.* 2000, 39, 4542-4544.

55. Werts, M. H. V.; Verhoeven, J. W.; Hofstraat, J. W., Efficient visible light sensitisation of water-soluble near-infrared luminescent lanthanide complexes. *J. Chem. Soc., Perkin Trans. 2* 2000, 433-439.

56. Van Deun, R.; Fias, P.; Nockemann, P.; Schepers, A.; Parac-Vogt, T. N.; Van Hecke, K.; Van Meervelt, L.; Binnemans, K., Rare-Earth Quinolinates: Infrared-Emitting Molecular Materials with a Rich Structural Chemistry. *Inorg. Chem.* 2004, 43, 8461-8469.

57. Bassett, A. P.; Van Deun, R.; Nockemann, P.; Glover, P. B.; Kariuki, B. M.; Van Hecke, K.; Van Meervelt, L.; Pikramenou, Z., Long-Lived Near-Infrared Luminescent Lanthanide Complexes of Imidodiphosphinate "Shell" Ligands. *Inorg. Chem.* 2005, 44, 6140-6142.

58. Van Deun, R.; Fias, P.; Nockemann, P.; Van Hecke, K.; Van Meervelt, L.; Binnemans, K., Visible-Light-Sensitized Near-Infrared Luminescence from Rare-Earth Complexes of the 9-Hydroxyphenalen-1-one Ligand. *Inorg. Chem.* 2006, 45, 10416-10418.

59. Van Deun, R.; Nockemann, P.; Parac-Vogt, T. N.; Van Hecke, K.; Van Meervelt, L.; Görller-Walrand, C.; Binnemans, K., Near-infrared photoluminescence of lanthanide complexes containing the hemicyanine chromophore. *Polyhedron* 2007, 26, 5441-5447.

60. Yanagida, S.; Hasegawa, Y.; Murakoshi, K.; Wada, Y.; Nakashima, N.; Yamanaka, T., Strategies for enhancing photoluminescence of Nd3+ in liquid media. *Coord. Chem. Rev.* 1998, 171, 461-480.

61. Iwamuro, M.; Adachi, T.; Wada, Y.; Kitamura, T.; Nakashima, N.; Yanagida, S., Photosensitized Luminescence of Neodymium(III) Coordinated with 8-Quinolinolates in DMSO-d_6. *Bull. Chem. Soc. Jpn.* 2000, 73, 1359-1363.

62. Hasegawa, Y.; Ohkubo, T.; Sogabe, K.; Kawamura, Y.; Wada, Y.; Nakashima, N.; Yanagida, S., Luminescence of Novel Neodymium Sulfonylaminate Complexes in Organic Media. *Angew. Chem. Int. Ed.* 2000, 39, 357-360.

63. Zhang, Z.-H.; Song, Y.; Okamura, T.-a.; Hasegawa, Y.; Sun, W.-Y.; Ueyama, N., Syntheses, Structures, Near-Infrared and Visible Luminescence, and Magnetic Properties of Lanthanide-Organic Frameworks with an Imidazole-Containing Flexible Ligand. *Inorg. Chem.* 2006, 45, 2896-2902.

64. Hasegawa, Y.; Yasuda, T.; Nakamura, K.; Kawai, T., Photosensitized Near-Infrared Luminescence of Yb(III) Complexes Containing Phenanthroline Derivatives. *Jpn. J. Appl. Phys.* 2008, 47, 1192.

65. Foley, T. J.; Harrison, B. S.; Knefely, A. S.; Abboud, K. A.; Reynolds, J. R.; Schanze, K. S.; Boncella, J. M., Facile Preparation and Photophysics of Near-Infrared Luminescent Lanthanide(III) Monoporphyrinate Complexes. *Inorg. Chem.* 2003, 42, 5023-5032.

66. Banerjee, S.; Huebner, L.; Romanelli, M. D.; Kumar, G. A.; Riman, R. E.; Emge, T. J.; Brennan, J. G., Oxoselenido Clusters of the Lanthanides: Rational Introduction of Oxo Ligands and Near-IR Emission from Nd(III). *J. Am. Chem. Soc.* 2005, 127, 15900-15906.

67. Bertolo, L.; Tamburini, S.; Vigato, P. A.; Porzio, W.; Macchi, G.; Meinardi, F., Tris(tropolonato)phenanthroline Lanthanide(III) Complexes as Photochemical Devices. *Eur. J. Inorg. Chem.* 2006, 2006, 2370-2376.

68. Sun, L.-N.; Yu, J.-B.; Zheng, G.-L.; Zhang, H.-J.; Meng, Q.-G.; Peng, C.-Y.; Fu, L.-S.; Liu, F.-Y.; Yu, Y.-N., Syntheses, Structures and Near-IR Luminescent Studies on Ternary Lanthanide (Er[III], Ho[III], Yb[III], Nd[III]) Complexes Containing 4,4,5,5,6,6,6-Heptafluoro-1-(2-thienyl)hexane-1,3-dionate. *Eur. J. Inorg. Chem.* 2006, 2006, 3962-3973.

69. Lo, W.-K.; Wong, W.-K.; Wong, W.-Y.; Guo, J.; Yeung, K.-T.; Cheng, Y.-K.; Yang, X.; Jones, R. A., Heterobimetallic Zn(II)−Ln(III) Phenylene-Bridged Schiff Base Complexes, Computational Studies, and Evidence for Singlet Energy Transfer as the Main Pathway in the Sensitization of Near-Infrared Nd^{3+} Luminescence. *Inorg. Chem.* 2006, 45, 9315-9325.

70. Moore, E. G.; Szigethy, G.; Xu, J.; Pålsson, L.-O.; Beeby, A.; Raymond, K. N., 3-Hydroxypyridin-2-one Complexes of Near-Infrared (NIR) Emitting Lanthanides: Sensitization of Holmium(III) and Praseodymium(III) in Aqueous Solution. *Angew. Chem. Int. Ed.* 2008, 47, 9500-9503.

71. Giraud, M.; Andreiadis, E. S.; Fisyuk, A. S.; Demadrille, R.; Pécaut, J.; Imbert, D.; Mazzanti, M., Efficient Sensitization of Lanthanide Luminescence by Tetrazole-Based Polydentate Ligands. *Inorg. Chem.* 2008, 47, 3952-3954.

72. Quici, S.; Cavazzini, M.; Marzanni, G.; Accorsi, G.; Armaroli, N.; Ventura, B.; Barigelletti, F., Visible and Near-Infrared Intense Luminescence from Water-Soluble Lanthanide [Tb(III), Eu(III), Sm(III), Dy(III), Pr(III), Ho(III), Yb(III), Nd(III), Er(III)] Complexes. *Inorg. Chem.* 2005, 44, 529-537.

73. Tsukube, H.; Suzuki, Y.; Paul, D.; Kataoka, Y.; Shinoda, S., Dendrimer container for anion-responsive lanthanide complexation and "on-off" switchable near-infrared luminescence. *Chem. Commun.* 2007, 2533-2535.

74. Pellegatti, L.; Zhang, J.; Drahos, B.; Villette, S.; Suzenet, F.; Guillaumet, G.; Petoud, S.; Toth, E., Pyridine-based lanthanide complexes: towards bimodal agents operating as near infrared luminescent and MRI reporters. *Chem. Commun.* 2008, 6591-6593.

75. Zhang, J.; Badger, P. D.; Geib, S. J.; Petoud, S., Synthesis and Structural Properties of Lanthanide Complexes Formed with Tropolonate Ligands. *Inorg. Chem.* 2007, 46, 6473-6482.

76. Zhang, J.; Petoud, S., Azulene-Moiety-Based Ligand for the Efficient Sensitization of Four Near-Infrared Luminescent Lanthanide Cations: Nd^{3+}, Er^{3+}, Tm^{3+}, and Yb^{3+}. *Chem. Eur. J.* 2008, 14, 1264-1272.

77. Zhang, J.; Shade, C. M.; Chengelis, D. A.; Petoud, S., A Strategy to Protect and Sensitize Near-Infrared Luminescent Nd^{3+} and Yb^{3+}: Organic Tropolonate Ligands for the Sensitization of Ln^{3+}-Doped $NaYF_4$ Nanocrystals. *J. Am. Chem. Soc.* 2007, 129, 14834-14835.

78.	Uh, H.; Badger, P. D.; Geib, S. J.; Petoud, S., Synthesis and Solid-State, Solution, and Luminescence Properties of Near-Infrared-Emitting Neodymium(3+) Complexes Formed with Ligands Derived from Salophen. *Helv. Chim. Acta* 2009, 92, 2313-2329.

79.	Vigato, P. A.; Tamburini, S., The challenge of cyclic and acyclic schiff bases and related derivatives. *Coord. Chem. Rev.* 2004, 248, 1717-2128.

80.	Archer, R. D.; Chen, H.; Thompson, L. C., Synthesis, Characterization, and Luminescence of Europium(III) Schiff Base Complexes. *Inorg. Chem.* 1998, 37, 2089-2095.

81.	Sheldrick, G. M. *SHELX-97*, University of Göttingen: Göttingen, Germany, 1997.

82.	Farrugia, L. J., ORTEP-3 for Windows - a version of ORTEP-III with a Graphical User Interface (GUI). *J. Appl. Crystallogr.* 1997, 30, 565-565.

83.	Bruno, I. J.; Cole, J. C.; Edgington, P. R.; Kessler, M.; Macrae, C. F.; McCabe, P.; Pearson, J.; Taylor, R., New software for searching the Cambridge Structural Database and visualizing crystal structures. *Acta Crystallogr. Sect. B: Struct. Sci.* 2002, 58, 389-397.

84.	Byrom, P. G.; Lucas, B. W., PARSET and PARSYM - production of files for neutron powder structure refinement program MORGUE and solution/refinement program PARAM. *J. Appl. Crystallogr.* 1995, 28, 65-66.

85.	Verner, E.; Katz, B. A.; Spencer, J. R.; Allen, D.; Hataye, J.; Hruzewicz, W.; Hui, H. C.; Kolesnikov, A.; Li, Y.; Luong, C.; Martelli, A.; Radika, K.; Rai, R.; She, M.; Shrader, W.; Sprengeler, P. A.; Trapp, S.; Wang, J.; Young, W. B.; Mackman, R. L., Development of Serine Protease Inhibitors Displaying a Multicentered Short (<2.3 Å) Hydrogen Bond Binding Mode: Inhibitors of Urokinase-Type Plasminogen Activator and Factor Xa. *J. Med. Chem.* 2001, 44, 2753-2771.

86.	Badger, P. D. Novel Ligands for Sensitization and Protection of Near–infrared Luminescent Lanthanide Cations and Synthesis and Protonation of $[W(\eta^4\text{-anthracene})(CO)_3]^{2-}$. University of Pittsburgh, Pittsburgh, PA, 2004.

87.	Gallant, A. J.; Hui, J. K. H.; Zahariev, F. E.; Wang, Y. A.; MacLachlan, M. J., Synthesis, Structure, and Computational Studies of Soluble Conjugated Multidentate Macrocycles. *J. Org. Chem.* 2005, 70, 7936-7946.

88.	Gallant, A. J.; Patrick, B. O.; MacLachlan, M. J., Mild and Selective Reduction of Imines: Formation of an Unsymmetrical Macrocycle. *J. Org. Chem.* 2004, 69, 8739-8744.

89.	Binstead, R. A.; Zuberbühler, A. D.; Jung, B. *SPECFIT/32*, 3.0.36; Spectrum Software Associates: Marlborough, MA, USA, 1993.

90. Wright, J. B., The Chemistry of the Benzimidazoles. *Chem. Rev.* 1951, 48, 397-541.

91. Hinsberg, O., Ueber die Einwirkung einwerthiger Aldehyde der Fettreihe auf m-p-Toluylendiamin. *Ber. Dtsch. Chem. Ges.* 1887, 20, 1585-1591.

92. Terzis, A.; Mentzafos, D.; Tajmir-Riahi, H. A., Eight-coordination. Synthesis and structure of the schiff-base chelate bis(*N,N* ′ -disalicylidene-1,2-phenylenediamino)cerium(IV). *Inorg. Chim. Acta* 1984, 84, 187-193.

93. Shannon, R. D., Revised effective ionic radii and systematic studies of interatomic distances in halides and chalcogenides. *Acta Crystallogr. Sect. A: Found. Crystallogr.* 1976, 32, 751-767.

94. Chen, H.; Archer, R. D., Synthesis and Characterization of Lanthanide(III) (La, Gd, Yb, Y) Disalicylidene-1,2-phenylenediamine (H2dsp) Schiff-Base Complexes. *Inorg. Chem.* 1994, 33, 5195-5202.

95. Yang, X.; Jones, R. A., Anion Dependent Self-Assembly of "Tetra-Decker" and "Triple-Decker" Luminescent Tb(III) Salen Complexes. *J. Am. Chem. Soc.* 2005, 127, 7686-7687.

96. Yang, X.-P.; Jones, R. A.; Oye, M. M.; Holmes, A. L.; Wong, W.-K., Near Infrared Luminescence and Supramolecular Structure of a Helical Triple-Decker Yb(III) Schiff Base Cluster. *Cryst. Growth Des.* 2006, 6, 2122-2125.

97. Yang, X.; Jones, R. A.; Wong, W.-K., Pentanuclear tetra-decker luminescent lanthanide Schiff base complexes. *Dalton Trans.* 2008, 1676-1678.

98. Serjeant, E. P.; Dempsey, B., *Ionisation constants of organic acids in aqueous solution*. Pergamon Press: New York, 1979.

99. Kepert, D. L., Aspects of the Stereochemistry of Eight-Coordination. In *Prog. Inorg. Chem.*, John Wiley & Sons, Inc.: 1978; pp 179-249.

100. Kubono, K.; Hirayama, N.; Kokusen, H.; Yokoi, K., X-Ray Crystallographic Approach to the Design of Phenolic Schiff Base Reagents for the Mutual Separation of Lanthanoids. *Anal. Sci.* 2001, 17, 193-197.

101. McGlynn, S. P.; Azumi, T., *Molecular spectroscopy of the triplet state*. Prentice-Hall: Englewood Cliffs, NJ, 1969.

102. Alcala, M. A.; Kwan, S. Y.; Shade, C. M.; Lang, M.; Uh, H.; Wang, M.; Weber, S. G.; Bartlett, D. L.; Petoud, S.; Lee, Y. J., Luminescence targeting and imaging using a nanoscale generation 3 dendrimer in an in vivo colorectal metastatic rat model. *Nanomed. Nanotechnol. Biol. Med.* 2011, 7, 249-258.

103. Alcala, M. A.; Shade, C. M.; Uh, H.; Kwan, S. Y.; Bischof, M.; Thompson, Z. P.; Gogick, K. A.; Meier, A. R.; Strein, T. G.; Bartlett, D. L.; Modzelewski, R. A.; Lee, Y. J.; Petoud, S.; Brown, C. K., Preferential accumulation within tumors and in vivo imaging by functionalized luminescent dendrimer lanthanide complexes. *Biomaterials* 2011, 32, 9343-9352.

104. Cross, J. P.; Lauz, M.; Badger, P. D.; Petoud, S., Polymetallic lanthanide complexes with PAMAM-naphthalimide dendritic ligands: luminescent lanthanide complexes formed in solution. *J. Am. Chem. Soc.* 2004, 126, 16278-16279.

105. Li, Z.; Yang, Q.; Qian, X., Novel 2-aminothiazonaphthalimides as visible light activatable photonucleases: effects of intercalation, heterocyclic-fused area and side chains. *Bioorg. Med. Chem. Lett.* 2005, 15, 1769-1772.

106. Yuan, D.; Brown, R. G.; Hepworth, J. D.; Alexiou, M. S.; Tyman, J. H. P., The synthesis and fluorescence of novel *N*-substituted-1,8-naphthylimides. *J. Heterocycl. Chem.* 2008, 45, 397-404.

107. Song, H. Y.; Ngai, M. H.; Song, Z. Y.; MacAry, P. A.; Hobley, J.; Lear, M. J., Practical synthesis of maleimides and coumarin-linked probes for protein and antibody labelling via reduction of native disulfides. *Org. Biomol. Chem.* 2009, 7, 3400-3406.

108. Aebischer, A.; Gumy, F.; Bünzli, J.-C. G., Intrinsic quantum yields and radiative lifetimes of lanthanide tris(dipicolinates). *PCCP* 2009, 11, 1346-1353.

109. Wittmer, A.; Khazaie, K.; Berger, M. R., Quantitative detection of lac-Z-transfected CC531 colon carcinoma cells in an orthotopic rat liver metastasis model. *Clin. Exp. Metastasis* 1999, 17, 369-376.

110. Bouvet, M.; Tsuji, K.; Yang, M.; Jiang, P.; Moossa, A. R.; Hoffman, R. M., In vivo color-coded imaging of the interaction of colon cancer cells and splenocytes in the formation of liver metastases. *Cancer Res.* 2006, 66, 11293-11297.

111. Kollmar, O.; Schilling, M. K.; Menger, M. D., Experimental liver metastasis: standards for local cell implantation to study isolated tumor growth in mice. *Clin. Exp. Metastasis* 2004, 21, 453-460.

112. Hagenaars, M.; Ensink, N. G.; Basse, P. H.; Hokland, M.; Nannmark, U.; Eggermont, A. M. M.; van de Velde, C. J. H.; Fleuren, G. J.; Kuppen, P. J. K., The microscopic anatomy of experimental rat CC531 colon tumour metastases: consequences for immunotherapy? *Clin. Exp. Metastasis* 2000, 18, 189-196.

113. Fahey, J. W.; Zalcmann, A. T.; Talalay, P., The chemical diversity and distribution of glucosinolates and isothiocyanates among plants. *Phytochemistry* 2001, 56, 5-51.

114. Leoni, O.; Iori, R.; Palmieri, S.; Esposito, E.; Menegatti, E.; Cortesi, R.; Nastruzzi, C., Myrosinase-generated isothiocyanate from glucosinolates: Isolation, characterization and in vitro antiproliferative studies. *Bioorg. Med. Chem.* 1997, 5, 1799-1806.

115. Kolonel, L. N.; Hankin, J. H.; Whittemore, A. S.; Wu, A. H.; Gallagher, R. P.; Wilkens, L. R.; John, E. M.; Howe, G. R.; Dreon, D. M.; West, D. W.; Paffenbarger, R. S., Vegetables, Fruits, Legumes and Prostate Cancer: A Multiethnic Case-Control Study. *Cancer Epidemiol. Biomarkers Prev.* 2000, 9, 795-804.

116. Ambrosone, C. B.; McCann, S. E.; Freudenheim, J. L.; Marshall, J. R.; Zhang, Y.; Shields, P. G., Breast Cancer Risk in Premenopausal Women Is Inversely Associated with Consumption of Broccoli, a Source of Isothiocyanates, but Is Not Modified by GST Genotype. *J. Nutr.* 2004, 134, 1134-1138.

117. Tang, L.; Zirpoli, G. R.; Guru, K.; Moysich, K. B.; Zhang, Y.; Ambrosone, C. B.; McCann, S. E., Consumption of Raw Cruciferous Vegetables is Inversely Associated with Bladder Cancer Risk. *Cancer Epidemiol. Biomarkers Prev.* 2008, 17, 938-944.

118. Fowke, J. H.; Chung, F.-L.; Jin, F.; Qi, D.; Cai, Q.; Conaway, C.; Cheng, J.-R.; Shu, X.-O.; Gao, Y.-T.; Zheng, W., Urinary Isothiocyanate Levels, Brassica, and Human Breast Cancer. *Cancer Res.* 2003, 63, 3980-3986.

119. Moy, K. A.; Yuan, J.-M.; Chung, F.-L.; Van Den Berg, D.; Wang, R.; Gao, Y.-T.; Yu, M. C., Urinary Total Isothiocyanates and Colorectal Cancer: A Prospective Study of Men in Shanghai, China. *Cancer Epidemiol. Biomarkers Prev.* 2008, 17, 1354-1359.

120. Carpenter, C. L.; Yu, M. C.; London, S. J., Dietary Isothiocyanates, Glutathione S-Transferase M1 (GSTM1), and Lung Cancer Risk in African Americans and Caucasians from Los Angeles County, California. *Nutr. Cancer* 2009, 61, 492-499.

121. Li, Y.; Zhang, T.; Korkaya, H.; Liu, S.; Lee, H.-F.; Newman, B.; Yu, Y.; Clouthier, S. G.; Schwartz, S. J.; Wicha, M. S.; Sun, D., Sulforaphane, a Dietary Component of Broccoli/Broccoli Sprouts, Inhibits Breast Cancer Stem Cells. *Clin. Cancer. Res.* 2010, 16, 2580-2590.

122. Xiao, D.; Vogel, V.; Singh, S. V., Benzyl isothiocyanate–induced apoptosis in human breast cancer cells is initiated by reactive oxygen species and regulated by Bax and Bak. *Mol. Cancer Ther.* 2006, 5, 2931-2945.

123. Singh, S. V.; Warin, R.; Xiao, D.; Powolny, A. A.; Stan, S. D.; Arlotti, J. A.; Zeng, Y.; Hahm, E.-R.; Marynowski, S. W.; Bommareddy, A.; Desai, D.; Amin, S.; Parise, R. A.; Beumer, J. H.; Chambers, W. H., Sulforaphane Inhibits Prostate Carcinogenesis and Pulmonary Metastasis in TRAMP Mice in Association with Increased Cytotoxicity of Natural Killer Cells. *Cancer Res.* 2009, 69, 2117-2125.

124. Warin, R.; Chambers, W. H.; Potter, D. M.; Singh, S. V., Prevention of Mammary Carcinogenesis in MMTV-neu Mice by Cruciferous Vegetable Constituent Benzyl Isothiocyanate. *Cancer Res.* 2009, 69, 9473-9480.

125. Pledgie-Tracy, A.; Sobolewski, M. D.; Davidson, N. E., Sulforaphane induces cell type–specific apoptosis in human breast cancer cell lines. *Mol. Cancer Ther.* 2007, 6, 1013-1021.

126. Kristensen, M.; Krogholm, K.; Frederiksen, H.; Bügel, S.; Rasmussen, S., Urinary excretion of total isothiocyanates from cruciferous vegetables shows high dose–response relationship and may be a useful biomarker for isothiocyanate exposure. *Eur. J. Nutr.* 2007, 46, 377-382.

127. Ji, Y.; Morris, M. E., Determination of phenethyl isothiocyanate in human plasma and urine by ammonia derivatization and liquid chromatography–tandem mass spectrometry. *Anal. Biochem.* 2003, 323, 39-47.

128. Liebes, L.; Conaway, C. C.; Hochster, H.; Mendoza, S.; Hecht, S. S.; Crowell, J.; Chung, F.-L., High-Performance Liquid Chromatography-Based Determination of Total Isothiocyanate Levels in Human Plasma: Application to Studies with 2-Phenethyl Isothiocyanate. *Anal. Biochem.* 2001, 291, 279-289.

129. Xiao, D.; Lew, K. L.; Zeng, Y.; Xiao, H.; Marynowski, S. W.; Dhir, R.; Singh, S. V., Phenethyl isothiocyanate-induced apoptosis in PC-3 human prostate cancer cells is mediated by reactive oxygen species-dependent disruption of the mitochondrial membrane potential. *Carcinogenesis* 2006, 27, 2223-2234.

130. Xiao, D.; Powolny, A. A.; Singh, S. V., Benzyl Isothiocyanate Targets Mitochondrial Respiratory Chain to Trigger Reactive Oxygen Species-dependent Apoptosis in Human Breast Cancer Cells. *J. Biol. Chem.* 2008, 283, 30151-30163.

131. Hu, J.; Straub, J.; Xiao, D.; Singh, S. V.; Yang, H.-S.; Sonenberg, N.; Vatsyayan, J., Phenethyl Isothiocyanate, a Cancer Chemopreventive Constituent of Cruciferous Vegetables, Inhibits Cap-Dependent Translation by Regulating the Level and Phosphorylation of 4E-BP1. *Cancer Res.* 2007, 67, 3569-3573.

132. Hanlon, N.; Coldham, N.; Gielbert, A.; Kuhnert, N.; Sauer, M. J.; King, L. J.; Ioannides, C., Absolute bioavailability and dose-dependent pharmacokinetic behaviour of dietary doses of the chemopreventive isothiocyanate sulforaphane in rat. *Brit. J. Nutr.* 2008, 99, 559-564.

133. Ottaviani, M. F.; Favuzza, P.; Sacchi, B.; Turro, N. J.; Jockusch, S.; Tomalia, D. A., Interactions between Starburst Dendrimers and Mixed DMPC/DMPA-Na Vesicles Studied by the Spin Label and the Spin Probe Techniques, Supported by Transmission Electron Microscopy. *Langmuir* 2002, 18, 2347-2357.

134.   Bottini, M.; Cerignoli, F.; Mills, D. M.; D'Annibale, F.; Leone, M.; Rosato, N.; Magrini, A.; Pellecchia, M.; Bergamaschi, A.; Mustelin, T., Luminescent Silica Nanobeads: Characterization and Evaluation as Efficient Cytoplasmatic Transporters for T-Lymphocytes. *J. Am. Chem. Soc.* 2007, 129, 7814-7823.

135.   Dufès, C.; Uchegbu, I. F.; Schätzlein, A. G., Dendrimers in gene delivery. *Adv. Drug Del. Rev.* 2005, 57, 2177-2202.

136.   Imaoka, T.; Horiguchi, H.; Yamamoto, K., Metal assembly in novel dendrimers with porphyrin cores. *J. Am. Chem. Soc.* 2003, 125, 340-341.

137.   Dougherty, T. J., Photosensitizers: therapy and detection of malignant tumors. *Photochem. Photobiol.* 1987, 45, 879-889.

138.   Nockemann, P.; Beurer, E.; Driesen, K.; Van Deun, R.; Van Hecke, K.; Van Meervelt, L.; Binnemans, K., Photostability of a highly luminescent europium β-diketonate complex in imidazolium ionic liquids. *Chem. Commun.* 2005, 4354-4356.

139.   Svenson, S.; Tomalia, D. A., Dendrimers in biomedical applications-reflections on the field. *Adv. Drug Del. Rev.* 2005, 57, 2106-2129.

140.   Zempleni, J.; Wijeratne, S. S. K.; Hassan, Y. I., Biotin. *BioFactors* 2009, 35, 36-46.

141.   Laitinen, O.; Hytönen, V.; Nordlund, H.; Kulomaa, M., Genetically engineered avidins and streptavidins. *Cell. Mol. Life Sci.* 2006, 63, 2992-3017.

142.   Kauffman, D. R.; Shade, C. M.; Uh, H.; Petoud, S.; Star, A., Decorated carbon nanotubes with unique oxygen sensitivity. *Nat. Chem.* 2009, 1, 500-506.

143.   Janata, J.; Josowicz, M.; Vanýsek, P.; DeVaney, D. M., Chemical Sensors. *Anal. Chem.* 1998, 70, 179-208.

144.   Madou, M. J.; Morrison, S. R., *Chemical sensing with solid state devices*. Academic Press: 1989.

145.   Ramamoorthy, R.; Dutta, P. K.; Akbar, S. A., Oxygen sensors: Materials, methods, designs and applications. *J. Mater. Sci.* 2003, 38, 4271-4282.

146.   Neri, G.; Bonavita, A.; Micali, G.; Rizzo, G.; Galvagno, S.; Niederberger, M.; Pinna, N., A highly sensitive oxygen sensor operating at room temperature based on platinum-doped In2O3 nanocrystals. *Chem. Commun.* 2005, 6032-6034.

147.   Wang, D.; Hao, C.; Zheng, W.; Peng, Q.; Wang, T.; Liao, Z.; Yu, D.; Li, Y., Ultralong Single-Crystalline Ag$_2$S Nanowires: Promising Candidates for Photoswitches and Room-Temperature Oxygen Sensors. *Adv. Mater.* 2008, 20, 2628-2632.

148. Carraway, E. R.; Demas, J. N.; DeGraff, B. A.; Bacon, J. R., Photophysics and photochemistry of oxygen sensors based on luminescent transition-metal complexes. *Anal. Chem.* 1991, 63, 337-342.

149. Wu, C.; Bull, B.; Christensen, K.; McNeill, J., Ratiometric Single-Nanoparticle Oxygen Sensors for Biological Imaging. *Angew. Chem. Int. Ed.* 2009, 48, 2741-2745.

150. Khatua, S.; Samanta, D.; Bats, J. W.; Schmittel, M., Rapid and Highly Sensitive Dual-Channel Detection of Cyanide by Bis-heteroleptic Ruthenium(II) Complexes. *Inorg. Chem.* 2012, 51, 7075-7086.

151. Dmitriev, R. I.; Zhdanov, A. V.; Jasionek, G.; Papkovsky, D. B., Assessment of Cellular Oxygen Gradients with a Panel of Phosphorescent Oxygen-Sensitive Probes. *Anal. Chem.* 2012, 84, 2930-2938.

152. Dadabhoy, A.; Faulkner, S.; Sammes, P. G., Long wavelength sensitizers for europium(iii) luminescence based on acridone derivatives. *J. Chem. Soc., Perkin Trans. 2* 2002, 348-357.

153. LeFevre, M. E., Calibration of Clark oxygen electrode for use in aqueous solutions. *J. Appl. Physiol.* 1969, 26, 844-846.

154. Radtke, D. B.; White, A. F.; Davis, J. V.; Wilde, F. D., Dissolved Oxygen (version 2.1): U.S. Geological Survey Techniques of Water-Resources Investigations, book 9, chap. A6., section 6.2, June. accessed February, 19th, 2009 from http://pubs.water.usgs.gov/twri9A6/.

155. *LabVIEW*, 7.1; National Instruments Corporation: Austin, TX, 2004.

156. *OriginPro*, 7.0; OriginLab Corporation: Northampton, MA, 2002.

157. Lide, D. R., *CRC Handbook of Chemistry and Physics*. 85th ed.; CRC Press: 2005.

158. de Sousa, M.; Kluciar, M.; Abad, S.; Miranda, M. A.; de Castro, B.; Pischel, U., An inhibit (INH) molecular logic gate based on 1,8-naphthalimide-sensitised europium luminescence. *Photochem. Photobiol. Sci.* 2004, 3, 639-642.

159. Buono-core, G. E.; Li, H.; Marciniak, B., Quenching of excited states by lanthanide ions and chelates in solution. *Coord. Chem. Rev.* 1990, 99, 55-87.

160. Gutierrez, F.; Tedeschi, C.; Maron, L.; Daudey, J.-P.; Poteau, R.; Azema, J.; Tisnes, P.; Picard, C., Quantum chemistry-based interpretations on the lowest triplet state of luminescent lanthanides complexes. Part 1. Relation between the triplet state energy of hydroxamate complexes and their luminescence properties. *Dalton Trans.* 2004, 1334-1347.

161. Haas, Y.; Stein, G., Pathways of radiative and radiationless transitions in europium(III) solutions. Role of solvents and anions. *J. Phys. Chem.* 1971, 75, 3668-3677.

162. Parker, D., Taking advantage of the pH and pO2 sensitivity of a luminescent macrocyclic terbium phenanthridyl complex. *Chem. Commun.* 1998, 245-246.

163. Parker, D., Luminescent lanthanide sensors for pH, pO2 and selected anions. *Coord. Chem. Rev.* 2000, 205, 109-130.

164. Beeby, A.; Parker, D.; Williams, J. A. G., Photochemical investigations of functionalised 1,4,7,10-tetraazacyclododecane ligands incorporating naphthyl chromophores. *J. Chem. Soc., Perkin Trans. 2* 1996, 1565-1579.

165. Parker, D.; Williams, J. A. G., Modest effectiveness of carbostyril 124 as a sensitising chromophore in europium and terbium amide complexes based on 1,4,7,10-tetraazacyclododecane. *J. Chem. Soc., Perkin Trans. 2* 1996, 1581-1586.

166. Valentini, L.; Mengoni, F.; Armentano, I.; Kenny, J. M.; Ricco, L.; Alongi, J.; Trentini, M.; Russo, S.; Mariani, A., Enhancement of photoelectrical properties in polymer nanocomposites containing modified single-walled carbon nanotubes by conducting dendrimer. *J. Appl. Phys.* 2006, 99, 114305-5.

167. Saito, R.; Fujita, M.; Dresselhaus, G.; Dresselhaus, M. S., Electronic structure of chiral graphene tubules. *Appl. Phys. Lett.* 1992, 60, 2204-2206.

168. Kataura, H.; Kumazawa, Y.; Maniwa, Y.; Umezu, I.; Suzuki, S.; Ohtsuka, Y.; Achiba, Y., Optical properties of single-wall carbon nanotubes. *Synth. Met.* 1999, 103, 2555-2558.

169. Chen, R. J.; Franklin, N. R.; Kong, J.; Cao, J.; Tombler, T. W.; Zhang, Y.; Dai, H., Molecular photodesorption from single-walled carbon nanotubes. *Appl. Phys. Lett.* 2001, 79, 2258-2260.

170. Shim, M.; Back, J. H.; Ozel, T.; Kwon, K.-W., Effects of oxygen on the electron transport properties of carbon nanotubes: Ultraviolet desorption and thermally induced processes. *Phys. Rev. B: Condens. Matter* 2005, 71, 205411.

171. Kajihara, K.; Kamioka, H.; Hirano, M.; Miura, T.; Skuja, L.; Hosono, H., Interstitial oxygen molecules in amorphous SiO_2. II. The influence of common dopants (SiOH, SiF, and SiCl groups) and fictive temperature on the decay of singlet photoluminescence. *J. Appl. Phys.* 2005, 98, 013528-5.

172. Aroutiounian, V., Metal oxide hydrogen, oxygen, and carbon monoxide sensors for hydrogen setups and cells. *Int. J. Hydrogen Energy* 2007, 32, 1145-1158.

173. Kong, J.; Franklin, N. R.; Zhou, C.; Chapline, M. G.; Peng, S.; Cho, K.; Dai, H., Nanotube Molecular Wires as Chemical Sensors. *Science* 2000, 287, 622-625.

174. Sorescu, D. C.; Jordan, K. D.; Avouris, P., Theoretical Study of Oxygen Adsorption on Graphite and the (8,0) Single-walled Carbon Nanotube. *J. Phys. Chem. B* 2001, 105, 11227-11232.